Oil And Gas
Geoscience Reports 2009

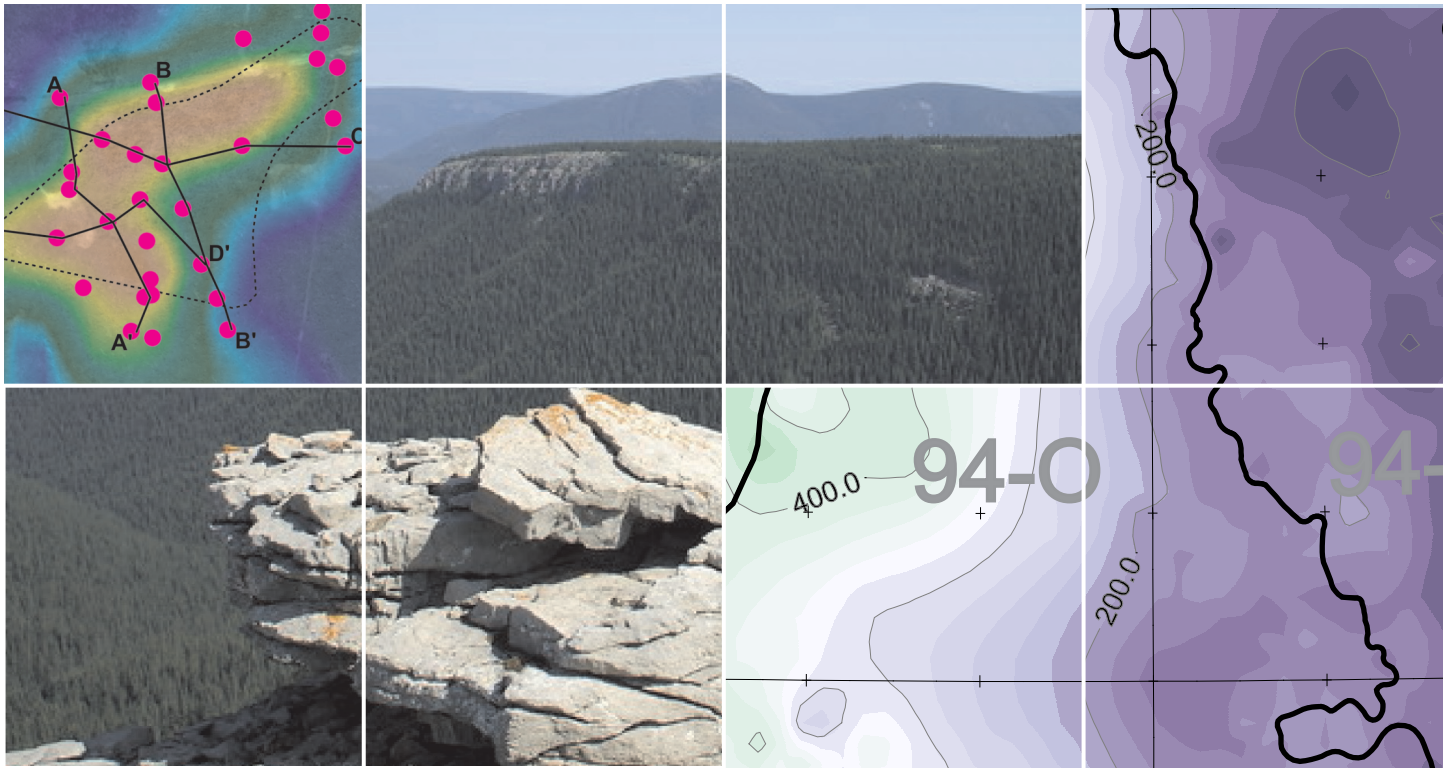

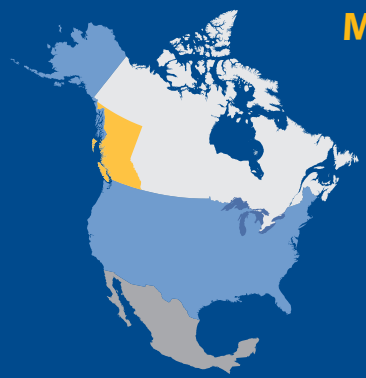

Ministry of Energy, Mines and Petroleum Resources
Resource Development and Geoscience Branch

BRITISH COLUMBIA
The Best Place on Earth

Oil and Gas Division
Resource Development and Geoscience Branch
Victoria, British Columbia, April 2009

Please use the following citation format when quoting or reproducing parts of this document:

Crockford, P. and Telmer, K. (2009): Exploring the Fate of CO_2 at British Columbia's planned Fort Nelson Carbon Capture and Storage Project; Geoscience Reports 2009, *BC Ministry of Energy, Mines and Petroleum Resources,* pages 1-4.

Colour digital copies of this publication in Adobe Acrobat PDF format are available, free of charge, from the BC Ministry of Energy, Mines and Petroleum Resources website at:
http://www.em.gov.bc.ca/subwebs/oilandgas/pub/reports.htm

Front cover images:
Left side: 150 kHz depth slice from airborne resistivity survey with test pit locations and cross-section locations (see Hickin, this publication, for more details).

Centre: Typical beige weathering, wavy to planar bedded calcareous, fine sandstone of the Liard Formation (see Ferri, this publication, for more details).

Right side: Isopach map for thickness (in metres) from the top of the Debolt formation to the top of the Banff Formation (i.e. Rundle Group) (see Johnson, this publication, for more details).

Back cover image:
Close to tight chevron fold defined by Liard Formation sandstones (see Ferri, this publication, for more details).

FOREWORD

Geoscience Reports is published by the Resource Development and Geoscience Branch of the Oil and Gas Division, British Columbia Ministry of Energy, Mines and Petroleum Resources. Like its predecessor, Summary of Activities, Geoscience Reports is an annual publication highlighting petroleum-related geological activities carried out by staff of the Resource Development and Geoscience Branch.

Articles in this volume cover a wide range of topics, including: 1) CO_2 sequestration; 2) geology and geophysics within the Nechako Basin; 3) organic-rich siltstones along northern Vancouver Island; 4) coal and coal bed gas; 5) studies in northeast BC, including Triassic porosity trends and well disposal; 6) the history of oil and gas exploration in BC and 7) water sampling guidelines.

This year's volume has benefited from an editorial review by Justine Pearson and the excellent services of Tetrad Communications.

Vic Levson
Executive Director
Resource Development and Geoscience Branch

TABLE OF CONTENTS

Geoscience Reports 2009

EXPLORING THE FATE OF CO_2 AT BRITISH COLUMBIA'S PLANNED FORT NELSON CARBON CAPTURE AND STORAGE PROJECT

Peter Crockford[1] and Kevin Telmer[1]

ABSTRACT

The geochemical reactions involved in injecting fluids into reservoirs remain poorly understood, yet this information is critical to the success of carbon capture and storage (CCS) projects. Remarkably, no standard methodology exists to estimate storage capacity for CCS, largely because of the inadequacy of thermo-kinetic databases needed to model geochemical processes at the pressures, temperatures, and salinities of deep reservoir conditions. Thermodynamic and kinetic constants and coefficients, reactive surface area estimates, and understanding of pore-scale physical processes that control geochemical reactivity are particularly lacking. This information is required to predict long-term CO_2 trapping. The University of Victoria is aiming to develop this information by performing high-quality research on a case-by-case basis.

In collaboration with the Ministry of Energy, Mines and Petroleum Resources and Spectra Energy, researchers at the University of Victoria are performing laboratory experimental work to measure empirical and site-specific thermo-kinetic properties of reservoir materials from the planned Fort Nelson CCS project. These results and a conceptual model based on field data will be integrated into the project to produce a reactive transport simulation to predict the fate of the injected CO_2.

Crockford, P. and Telmer, K. (2009): Exploring the Fate of CO_2 at British Columbia's planned Fort Nelson Carbon Capture and Storage Project; Geoscience Reports 2009, *BC Ministry of Energy, Mines and Petroleum Resources,* pages 1–4.

[1]University of Victoria

CCS IN BRITISH COLUMBIA: A VIABLE OPTION TO REDUCE CO_2 EMISSIONS

There is broad understanding in the scientific community that rising concentrations of anthropogenic greenhouse gases will change our climate and produce an estimated warming of the planet up to 4°C this century (IPCC 2007). CO_2 is the most abundant greenhouse gas and is thought to be responsible for 76.6% of the enhanced greenhouse effect (IPCC 2007). In 2008, the province of British Columbia emitted an estimated 70.3 Mt of CO_2 (Figure 1), representing nearly 9% of the 780 Mt of CO_2 estimated to have been emitted by Canadians (Environment Canada 2005). While the global energy market waits for development of renewable energy forms, CCS is a technology available to British Columbia that can help the province to achieve it's goal of reducing emissions to 46.4 Mton CO_2 per year (Figure 1).

CCS lowers greenhouse gas emissions by capturing CO_2 and other gases from point-source emitters such as gas-fired power plants and injecting them into the subsurface, where they remain for millennia. CCS is not new—it has been used for a different purpose and at a smaller scale for decades by the oil and gas industry to enhance oil recovery (a technology called EOR) and for the disposal of acid gas (CO_2 and H_2S). Because it is already available and is cost effective, CCS has become an important component to emission reduction strategies of governments and the private sector all around the world. For British Columbia, CCS has great potential to lower emissions because of the presence of several large CO_2 point sources near its numerous potentially good geological storage sites (Figure 2). In particular, British Columbia's natural gas industry, which is expected to grow 50% to 200% over the next 10 to 15 years, is a good candidate for CCS because of its large and relatively pure point sources of CO_2, which are co-located with suitable storage reservoirs (principally deep saline formations).

Government, industry, and academia are cooperating to take advantage of British Columbia's CCS opportunities. A large CCS project at Fort Nelson is in the feasibility stage. It is a collaborative effort involving mainly the British Columbia Ministry of Energy, Mines and Petroleum Resources and Spectra Energy, a natural gas producer. The Plains CO_2 Reduction Partnership (PCOR) and the University of Victoria are also involved, bringing needed institutional capacity and research expertise to the project. The target for the CCS project is Spectra's Fort Nelson sour-gas H_2S processing plant (Figure 2), which emits significant volumes of CO_2 during the processing of raw gas.

The Fort Nelson area is an ideal location for CCS. This area has a large number of candidate CCS sites with suitable stratigraphy—thick shaly aquitards, ideal for sealing in CO_2 for the long term. Northeast British Columbia is also

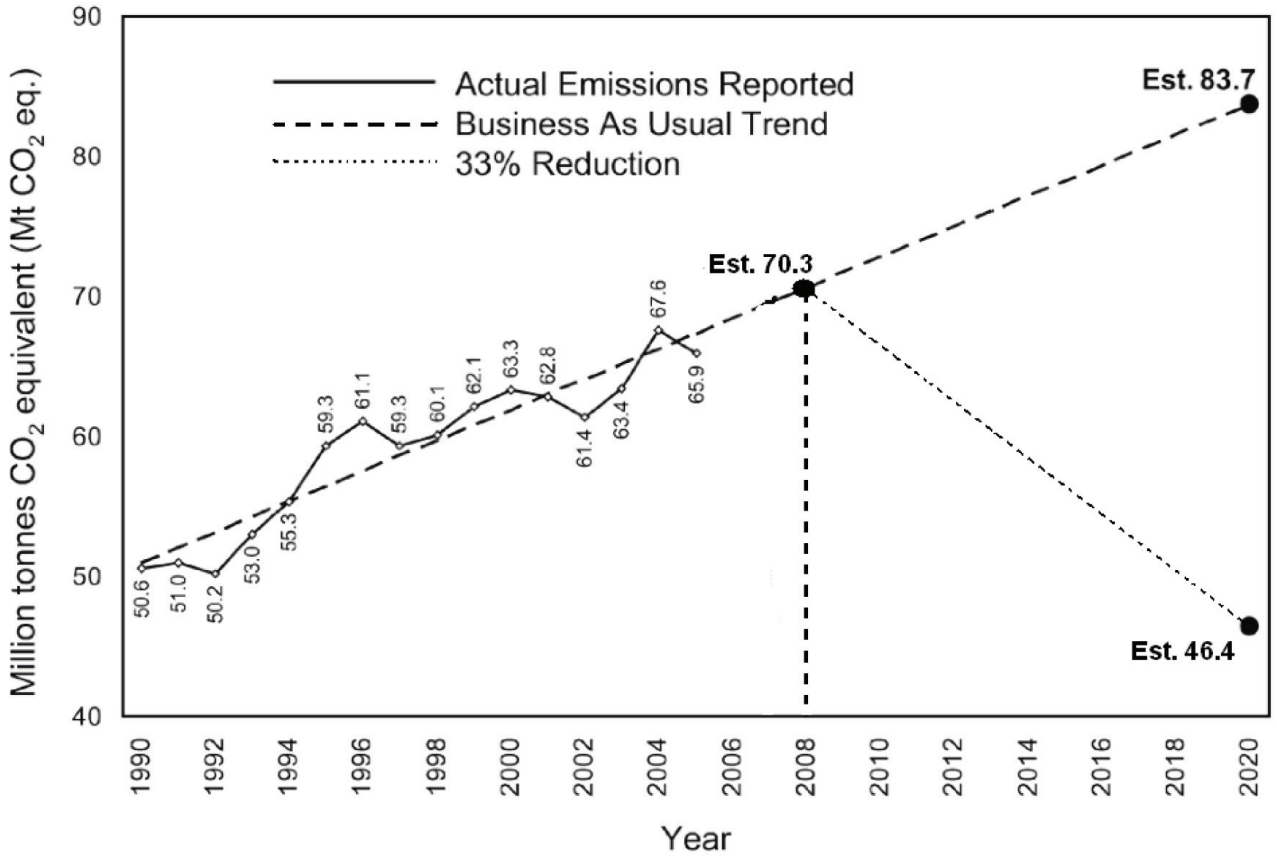

Figure 1. Global measured CO_2 values up to 2003 along with the "Business As Usual" trend to 2020 and British Columbia's 2020 reduction target. Figure adapted from Hartling 2008.

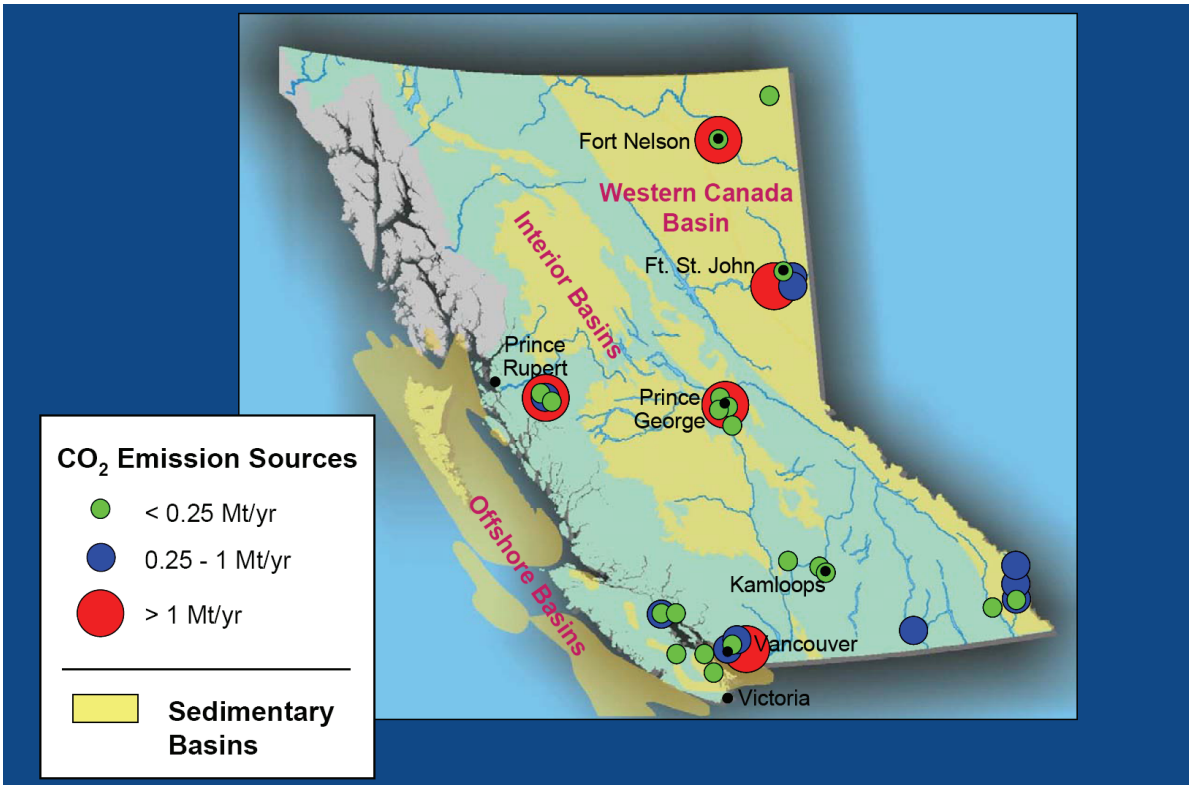

Figure 2. Map of British Columbia showing the largest point source emitters. (Hartling 2008).

a tectonically stable area with a low probability of earthquakes that could fracture rocks and cause leakage.

If successful, the Fort Nelson project will inject about 1 Mt of CO_2 into the subsurface every year and become one of the world's largest CCS operation. This single project could reduce British Columbia's CO_2 emissions by a significant 2.5% and play a pivotal role in British Columbia's reduction goal of 33% by 2020.

THE FORT NELSON CCS PROJECT: RESEARCHING THE GEOCHEMISTRY OF CO_2 IN THE DEEP AQUEOUS ENVIRONMENT

Geochemical knowledge will assist in estimating the storage capacity, limitations on injection rates and injection methods, and contamination risks associated with leakage. Storage capacity is controlled by porosity, permeability, and the pressure and temperature field of the reservoir. These, however, are affected by geochemical reactions that cause mineral precipitation and dissolution and shifts in gas solubility that feedback on the pressure and temperature and ultimately the potential CO_2 injection rate.

University of Victoria research is focusing on the geochemistry of the saline formation environment during and after CO_2 injection to determine which geochemical reactions will occur and at what rates. This information will be coupled with reservoir flow dynamics to estimate where in the aquifer these reactions will be occurring. Both experimental and computer modeling approaches will be taken. Laboratory experiments will be performed at the pressure and temperature range of the proposed CCS location in the Fort Nelson area. These experiments will be performed on brine and rock samples from the proposed reservoir. The laboratory results will also be used to create and refine physical constants in thermodynamic and kinetic databases, which will dictate the accuracy of a mathematical model of the reservoir system.

Fieldwork will be performed at the drill site to collect samples and perform measurements of parameters such as temperature, pressure, and alkalinity of the formation brine. These data can be used in follow-up studies that will track the evolution of these parameters of the saline aquifer.

Samples will be analyzed and experiments run at the School of Earth and Ocean Sciences, University of Victoria. Using the new state-of-the-art laboratories, samples of brine and rock will be placed under aquifer conditions. An acid-gas mixture of supercritical CO_2 and H_2S will be introduced in a reaction vessel at the P-T conditions of the Fort Nelson aquifer. The system will be sampled through ports over a 90-day period to detect the rates of changes in brine chemistry and alterations in the aquifer rock. The rock will be analyzed for changes in porosity and permeability, and the brine composition will be compared to the initial composition before CO_2 introduction. Changes in brine composition combined with petrological work on rock materials will allow mineral precipitation and dissolution rates to be determined. By measuring samples over several intervals, kinetic information will also be generated. Some of this work will address some of the deficiencies in this field today, such as quantification of reactive surface area and geochemical interactions.

More research is required to gain information about the reactivity of the CO_2 phase of the system. The injected CO_2 does not always immediately dissolve into solution or precipitate into minerals—for at least the injection period (25 to 50 years). The majority of CO_2 may reside as a separate phase on top of the formation brine because of its lower density (Figure 3). The reactions that occur in this part of the system are also very important to investigate. Processes such as brine desiccation, where the H_2O of the brine evaporates into the CO_2 layer, and reactions between the CO_2 phase and the rocks may also be important in estimating the overall storage capacity of the reservoir. The university will be performing experiments to look at these reactions as well.

To extrapolate results from the laboratory to the reservoir and from short time scales to long, reactive transport modeling will be performed. Results from the laboratory will be used to replace thermodynamic and kinetic terms in modeling databases with site-specific data. This is essential for developing a realistic and practical model. However, not all reactions that will occur in the aquifer can be observed in the laboratory because of the slow kinetics of

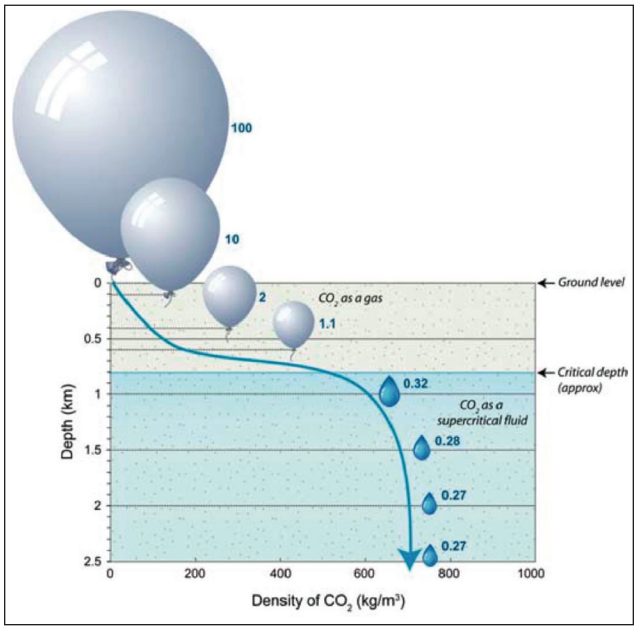

Figure 3. Graphic depiction of CO_2 density changes with depth. Figure taken from CO_2 CRC (2008).

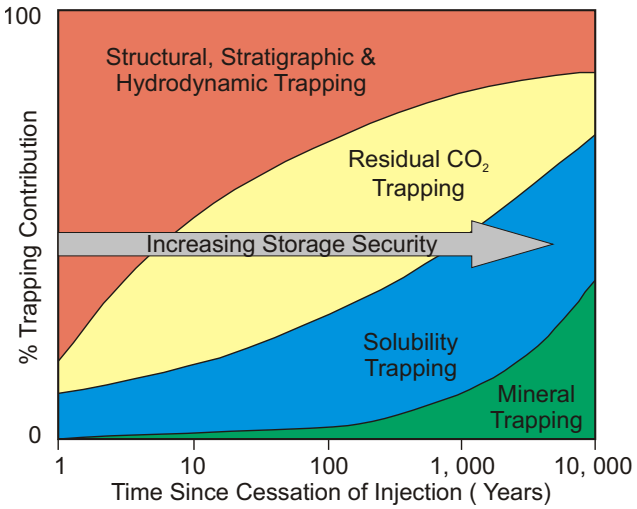

Figure 4. Dominant CO_2 trapping mechanisms over 1- to 10,000-year timescales. Figure from Benson and Cook (2005).

some reactions (Figure 4). Modeling software will be used to predict long-term products as they may be reasonably estimated by chemical equilibrium—a task that software is fairly good at, given the proper initial input chemistry. Fluid dynamics at the aquifer scale are also not replicable in the laboratory, and so scaling factors will be researched.

As well, when CO_2 is injected into the aquifer, gradients of CO_2 concentration and pH will be created around the injection site. Such a chemical distribution cannot directly be emulated in a laboratory reaction vessel and therefore will require computer modeling. By using a model to determine where in the aquifer reactions will be occurring, we will be able to better predict the long-term distribution of CO_2 and the geochemical reactions participating in trapping it in long-term storage.

Predicting the long-term fate of the injected CO_2 will help the Fort Nelson CCS project transition from the planning stages to implementation. As well, the data collected will be useful to the CCS community in implementing projects globally.

CONCLUSIONS

CCS is a rapidly expanding technology that will be a major player in the 21st century as a transitional solution in one of our greatest environmental challenges—the reduction in greenhouse gases emitted into the atmosphere. If implemented in the near future, the Fort Nelson CCS project will be the largest of its kind globally and make a significant contribution to British Columbia's efforts at reducing carbon emissions. However, in order to ensure the long-term viability of the project, it is important to characterize the geochemical environment that will be used for CO_2 storage to be able to estimate potential injection rates and storage capacity. Laboratory and modeling work at the University of Victoria has been designed to help quantify these parameters.

REFERENCES

Hartling, A. (2008): Carbon Capture and Storage in British Columbia. *Oil and Gas Geoscience Reports* BC Ministry of Energy, Mines and Petroleum Resources.

IPCC (2007): Climate Change 2007: Synthesis Report; Allali, A., Bojariu, R., Diaz, S., Elgizouli, I., Griggs, D., Hawkins, D., Hohmeyer, O., Jallow, B.P., Kajfez-Bogataj, L., Leary, N., Lee, H., Wratt, D. (editors), IPCC, 52 pages.

Hartling, A. (2008): Geological Aspects of CO2 Sequestration Northeast British Columbia, Canada. *Search and Discovery Article #80010.*

CO_2 CRC (2008): Geologic storage of carbon dioxide staying safely underground: *IEA Greenhouse Gas R&D Program Special Issue*, 34 pages.

Benson, S. and Cook, P. *Coordinating Lead Authors* (2005) Underground geological storage. *IPCC Special Reports on Carbon dioxide Capture and Storage.*

GEOLOGY OF THE JONES PEAK AREA (NTS 94B/02 AND 07), HALFWAY RIVER MAP SHEET (94B)

Filippo Ferri[1]

ABSTRACT

During the summer of 2008, an area in the Jones Peak region (94B/02 and 07) of northeastern British Columbia was mapped at a scale of 1:50 000. Digital data were collected at the outcrop using hand-held computers running GanFeld software. Over 4000 m of Carboniferous, Permian, Triassic, Jurassic, and Cretaceous rocks were delineated in the map area. Triassic stratigraphy is by far the most areally extensive and covers over three-quarters of the map area. Sedimentary rocks have been shortened through a combination of folding and lesser thrust faulting. Mapping and structural cross-sections suggest the lower Toad and Grayling formations and the Stoddart Group probably acted as detachment horizons above the thick Prophet carbonates. Detrital zircon geochronology of lowermost Liard Formation sandstones returned ages as young as middle Mississippian, together with Early to Middle Devonian, Silurian, Early Ordovician, Cambrian, Proterozoic and Archean ages. Thermal maturation of Pardonet carbonates reached the middle to upper oil window, and the base of the Grayling Formation records upper gas window conditions. Exploration has historically targeted structural plays within the Mississippian Prophet Formation and its subsurface equivalent, the Debolt Formation. Recent efforts tested the thick Devonian carbonates west of the Brewster Thrust Fault.

Ferri, F. (2009): Geology of the Jones Peak area (NTS 94B/02 and 07), Halfway River map sheet (94B); Geoscience Reports 2009, *BC Ministry of Energy, Mines and Petroleum Resources*, pages 5–23.

[1]British Columbia Ministry of Energy, Mines and Petroleum Resources, 1810 Blanshard Street, Victoria, British Columbia

Key Words: Northeast British Columbia, Foothills, Halfway River, regional mapping, Triassic stratigraphy, structure, hydrocarbons, maturation, detrital zircons

INTRODUCTION

The foothills of northeastern British Columbia are believed to contain an undiscovered gas-in-place resource of 349.8 x 10^9 m^3 (12.4 trillion cubic feet, Tcf[1]). Although the exploration for these structural plays is challenging from a geological and logistical perspective, the prizes can be quite large, with some pools containing several hundred Bcf (billion cubic feet of gas).

Surface geological control is important in the proper interpretation of seismic data acquired during exploration efforts in the foothills. Detailed geological maps are available over most of the southern foothills (south of Peace Arm, Figure 1; see Pell et al. 1992; Legun 1987a, 2003; Jahans 1993; Hunter and Cunningham 1991; Kilby and Wrightson 1987a, b; McMechan 1986, 1996a, b; McMechan and Thompson 1995a–d). Although the surface geological database has recently been updated for large areas of the northern foothills (see Lane 2005 and references therein), there are still parts of this region where detailed geological mapping is lacking. These areas include the Halfway River and Toad River (94B and 94N, respectively) map sheets.

The Halfway River map area was chosen as the start of a new 1:50 000-scale regional multi-year mapping program because it is adjacent to the area with the greatest exploration activity, it builds on previous detailed mapping by the Ministry (Legun 1984), and it is the site of past and ongoing exploration. The northern portions of Jones Peak map sheet (94B/02) and southern parts of the Hackney Hills (94B/07) define the initial map area for this project. Current project planning envisions a three to four field season program covering the foothills belt of the Halfway River map area. Collaborators include the Geological Survey of Canada (laboratory services, data collection software) and researchers at the University of Alberta and the University of Victoria. Triassic rocks represent some three-quarters of the study area at surface, allowing for detailed examination of these rocks, which contain an economically significant gas resource in the subsurface to the east. Data were collected digitally at the outcrop with hand-held digital assistants using GanFeld software running on Microsoft Mobile 6® (Buller 2004).

[1]Northeast British Columbia's ultimate potential for conventional natural gas; National Energy Board & BC Ministry of Energy, Mines and Petroleum Resources; Energy Market Assessment Report 2006-A.

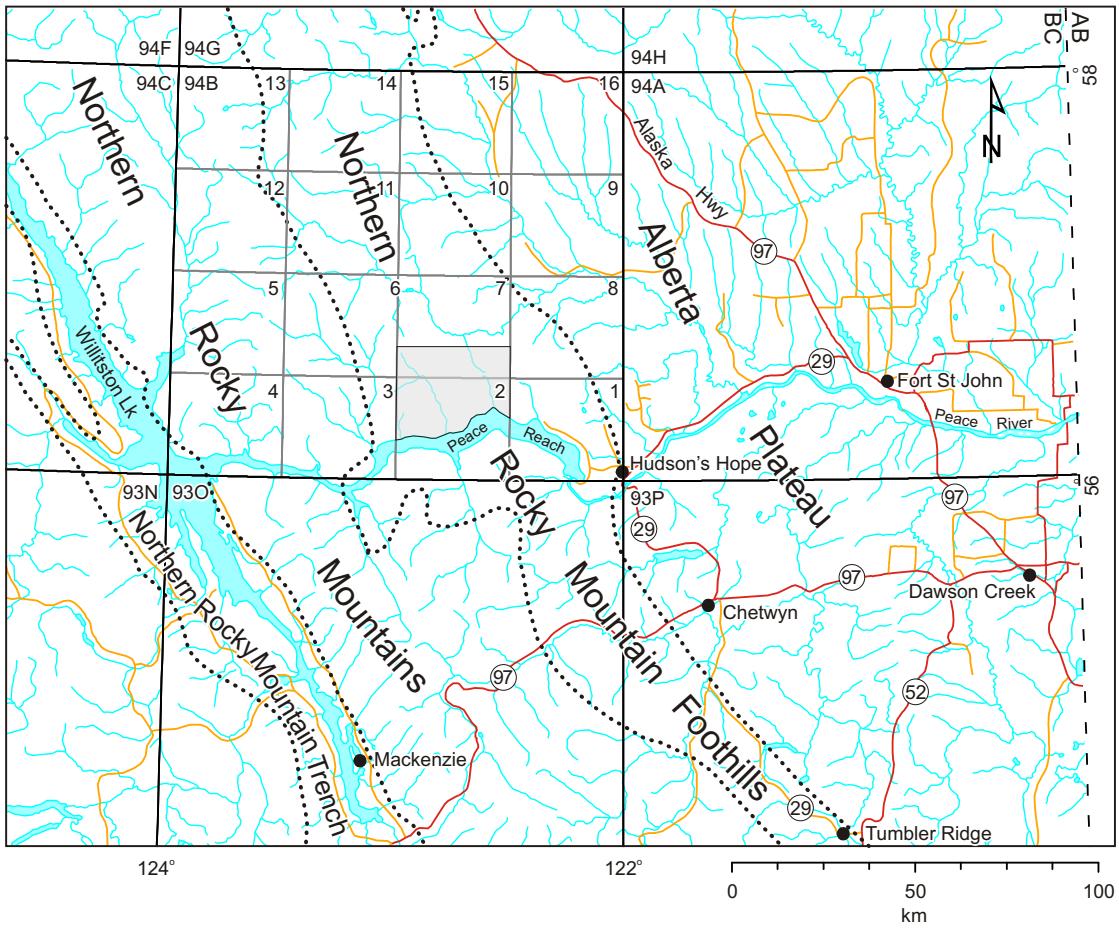

Figure 1. General location of the map area (grey box) with respect to main physiographic features, cities, towns, and access routes.

A total of two months were spent collecting data during the summer of 2008. Approximately 450 km^2 were covered by 61 traverses. Base camps were set up at the Wicked River Lodge and at a hunters' camp on the north side of Graham River. The main products will be a 1:50 000-scale map and several cross-sections, both in hard copy and digital format (ESRI ArcInfo® format), and a digital copy of the field data.

The project area lies within the southeast part of Halfway River (94B) map area north of the Peace Arm of Williston Lake. It is bordered to the south by the Peace Arm of Williston Lake, to the east by "Twenty Mile Ridge", to the west by Black Bear Ridge, and to the north by Graham River (Figure 2). Parts of the eastern and northern regions of the study area are accessible via logging and petroleum development roads, and the southern part is easily reached by boat. The remaining parts of the map area were accessed by helicopter. The closest community is Hudson's Hope, located some 40 km east of the study area. Fort St. John is located approximately 180 km to the east. The nearest permanent dwellings (with airstrips) are Wicked River Lodge, found along Williston Lake at the south end of Black Bear Ridge, and Torwood Lodge, located at the south end of Twenty Mile Ridge.

The Halfway River sheet was originally mapped by Irish (1970) at a 4-mile scale and later by Thompson (1989), who released the entire map sheet at a scale of 1:250 000 and the western parts at a scale of 1:50 000. Although this mapping greatly increased our understanding of this area, particularly the western part of the Rocky Mountains, much of the mapping covering the foothills was based on air photo interpretation. Stott et al. (1983) produced a 1:250 000-scale geology map of the Pine Pass (93O) sheet to the south, and Taylor (1979) covered the Trutch (94G) and eastern half of the Ware (94F) sheet. McMechan (2000) also recompiled the northern parts of the Pine Pass and southern Halfway River sheets, releasing this with an interpretive cross-section. Legun (1982, 1983, 1984, 1985, 1986, 1987a, b) produced geological maps of the Butler Ridge (94B/01) and Carbon Creek (93O/15) map areas, which delineate the northern limit of significant coal resources within the Deep Basin of northeastern British Columbia.

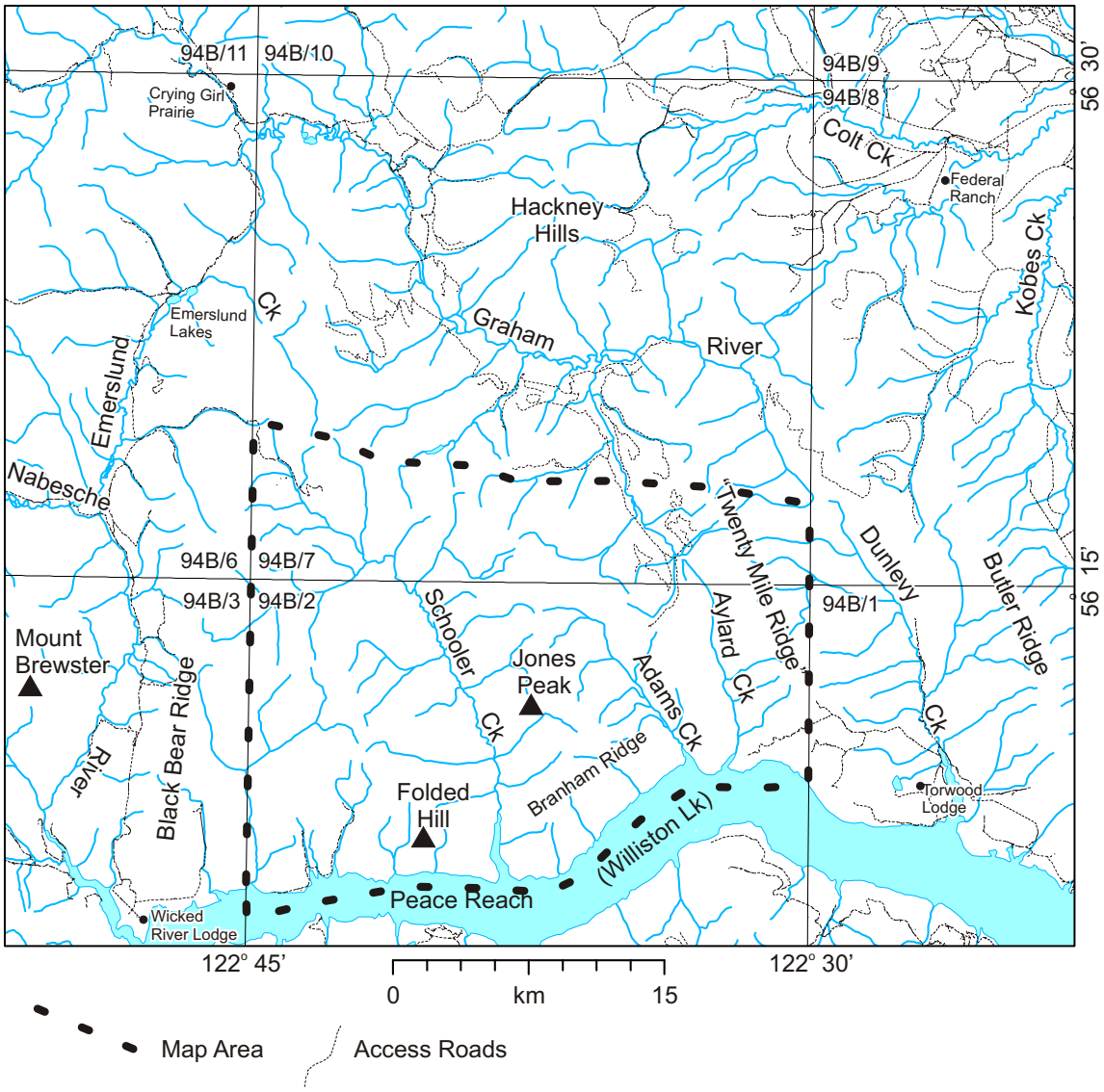

Figure 2. Main geographic elements within and around the study area.

GENERAL GEOLOGY

The study area lies within the northern foothills of the Rocky Mountains; the Rocky Mountains are represented by the Hart Ranges south of Peace Arm and the Muskwa Ranges to the west and north (Mathews 1986). Geomorphologically, the area falls within the Foreland Belt of the Canadian Cordillera, a region representing Proterozoic to Triassic miogeoclinal and Jura-Cretaceous foreland deposits that have been thrusted and folded during the Mesozoic to Cenozoic Orogeny (Wheeler and McFeely 1991; Figure 1, inset; Figure 3). Polydeformed and metamorphosed rocks of the Omineca Belt bound the Foreland Belt to the west, across the Northern Rocky Mountain Trench, and undisturbed sediments of the Western Canada Sedimentary Basin define its eastern limit. The map area lies at the northern termination of the thick Jura-Cretaceous clastic wedge that comprises the Deep Basin. This basin, which extends southward to the Alberta–Montana border, was produced in response to concurrent uplift and shortening within the Cordillera to the west. The disappearance of the north of Peace Arm is a reflection of decreased shortening within the Cordillera at this latitude. This reduction in shortening corroborated by mapping and structural cross-sections, which suggest only a quarter of the 200 km of shortening incurred in the central part of the Canadian southern Rocky Mountains (McMechan et al. 1991). Furthermore, folding is the principal means of shortening in the northern Rocky Mountains, which contrasts with the thrust-dominated structural style of the southern Rocky Mountains. This difference is an expression of the decrease in thick Paleozoic carbonate successions in the northern Rocky Mountains and a greater abundance of fine clastic sequences.

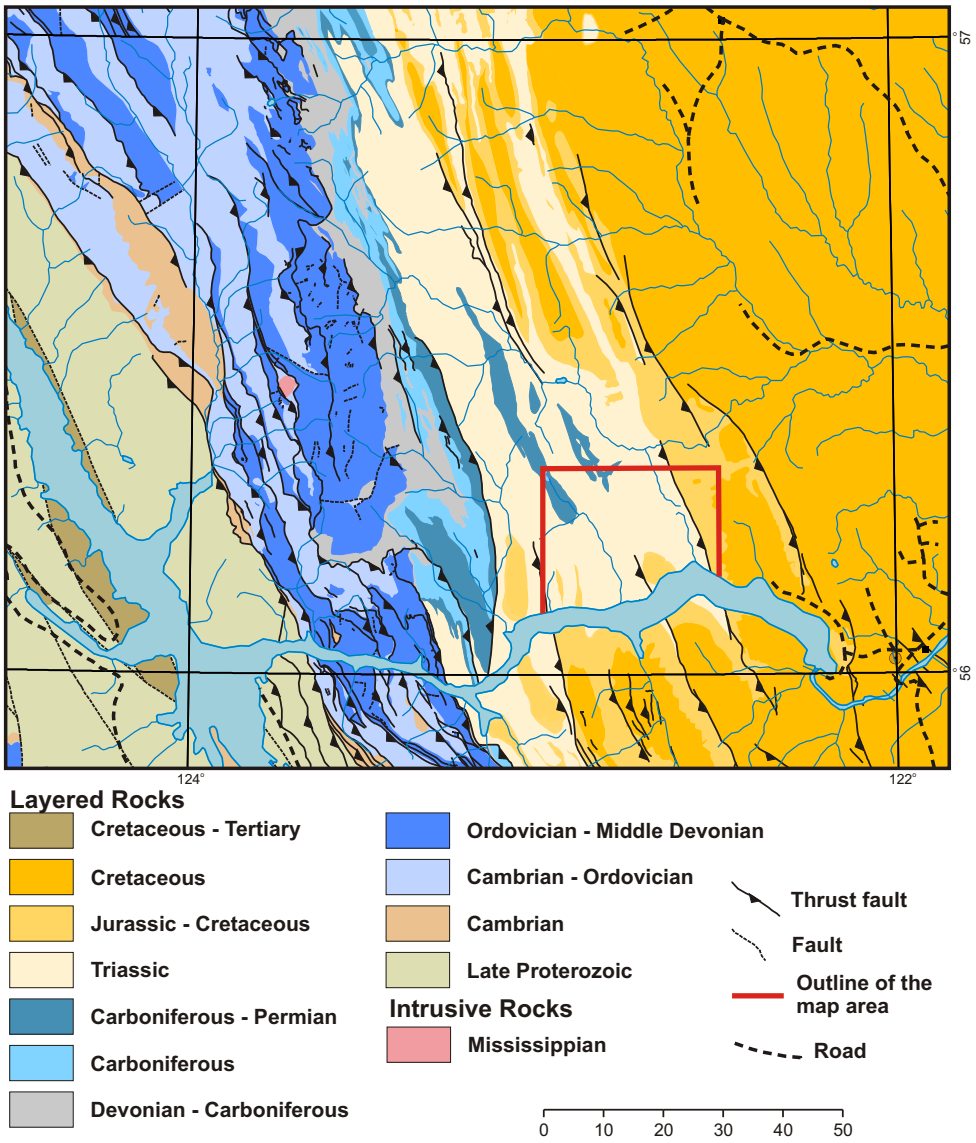

Figure 3. General geology in the vicinity of the Halfway River map area. Halfway River map area is the outlined quadrangle and the study area is shown in the red outline. Adapted from data on the BC Ministry of Energy, Mines and Petroleum Resources Map Place web site (www.mapplace.ca).

STRATIGRAPHY

Stratigraphy within the Foreland Belt of the Halfway River map area spans the Late Proterozoic to Eocene time periods. The oldest rocks are represented by rift-related clastics and minor carbonates of Proterozoic and Early Cambrian age, which are followed by a thick, dominantly carbonate miogeoclinal to platform succession that persisted until mid-Paleozoic times. The Late Paleozoic sequence is a mixed package of clastic and lesser carbonate rocks deposited in an extensional setting (i.e., Fort St. John Graben system; Barclay et al. 1990). Clastic facies dominated much of the Triassic, although carbonate deposition was re-established by Late Triassic times. This was the end of carbonate sedimentation within the Cordillera, as Jurassic and Cretaceous clastics flooded eastward in response to uplift and deformation in the west related to amalgamation of volcanic arc terranes.

Approximately 4000 m of stratigraphy are exposed in the map area and encompass the Mississippian Prophet to Early Cretaceous Cadomin formations (Figure 4). Triassic rocks make up over three-quarters of surface exposures in the map area, with the remainder belonging to Jura-Cretaceous and Late Paleozoic sequences. Stratigraphic nomenclature used in this report follows that used within the foothills of the Halfway River area. Surface and subsurface nomenclature of the Triassic, Jurassic, and Cretaceous units described in the text can be found in Figures 4, 5, and 6.

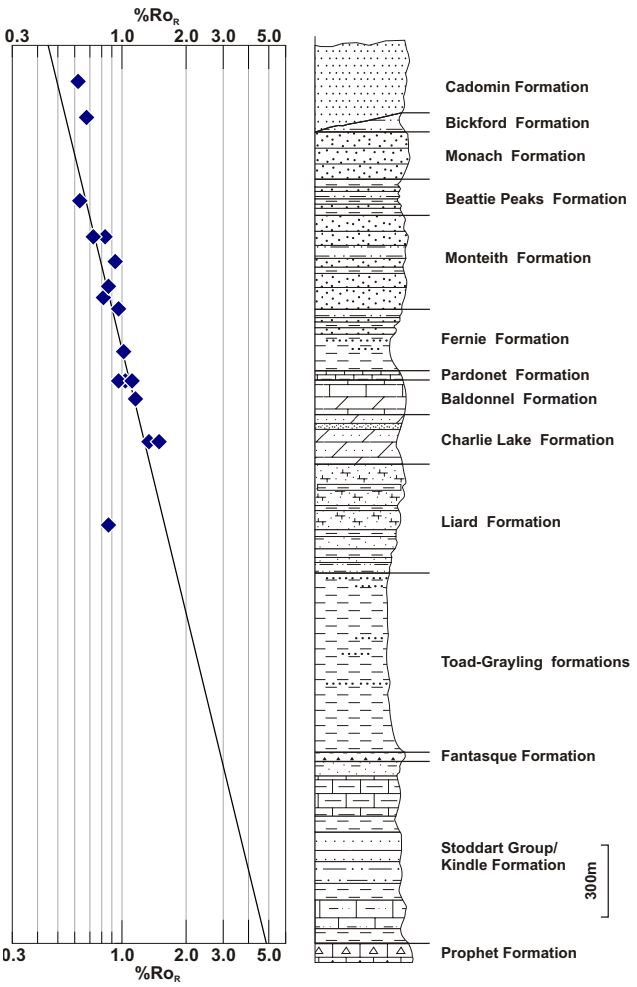

Figure 4. (a) Stylized stratigraphic column of units exposed in the map area. (b) Vitrinite reflectance data values from Table 1 plotted in rough stratigraphic position. The trend line indicates that the base of the Triassic succession is at the top of the dry gas window.

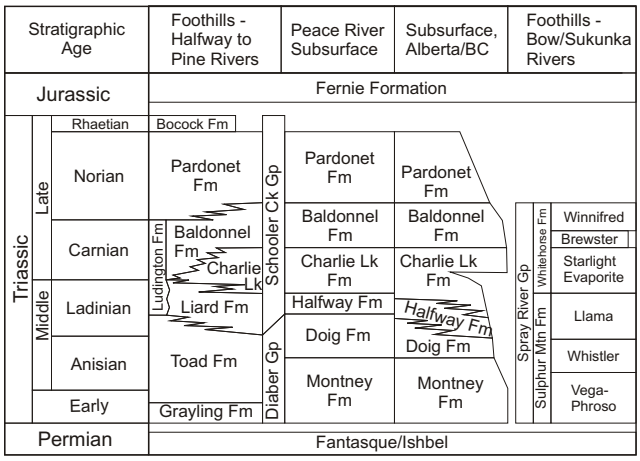

Figure 5. Correlation chart of Triassic nomenclature and general relationships within Halfway River area and with other areas in northeastern British Columbia. Modified from Davies (1997).

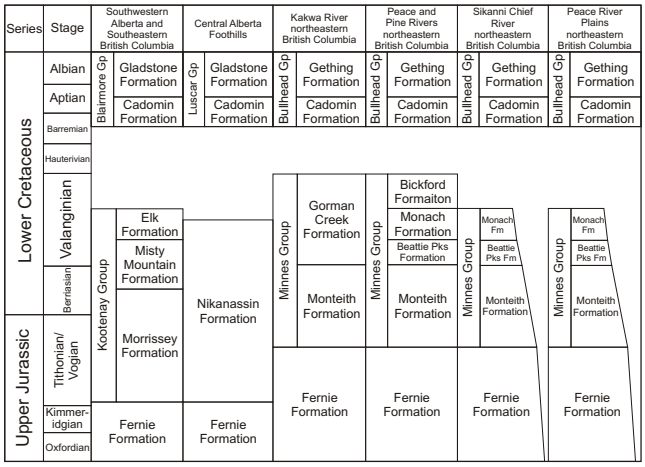

Figure 6. Correlation chart of Jurassic and Cretaceous stratigraphy in northeastern British Columbia. Modified from Stott (1998).

Prophet Formation(?)

Slope to off-shelf carbonate deposits of the Early Mississippian Prophet Formation comprise the oldest unit exposed in the map area. This thick (1000 to 1200 m) succession reflects re-establishment of carbonate deposition in the area following the widespread regression represented by shales of the Besa River Formation.

Large boulders of dark, laminated lime mudstone containing recrystallized fossil debris were encountered along the headwaters of Schooler Creek (Figures 2, 7). Although the boulders have been transported, their large size and angularity suggest they have not travelled far. Thompson (1989) has outlined a region in this area that is underlain by limestone, dolomite, and chert (nodules to discontinuous beds) of the Prophet Formation. In the vicinity of the study area, this unit can be up to 1850 m thick, as seen to the west along the Nabesche River (Thompson 1989). Over 1000 m of limestone, dolomitic limestone, chert, and minor shale and siltstone were penetrated by the Canadian Natural Resources Ltd. (CNRL) Dunlevy a-40-L/94-B-1 well along the southeast margin of the map area. The age of this unit is Early to Middle Mississippian in the map area (late Tournaisian to early Visean; Thompson 1989).

Stoddart Group and Kindle Formation(?)

Approximately 700 to 800 m of sandstone, siltstone, shale, and limestone comprise the Carboniferous to Permian Stoddart Group and Kindle Formation. This highly variable package thins to the north and south of Halfway River map area (Thompson 1989), and its deposition within the western extension of the Peace River Embayment is believed to have occurred in a graben system similar to that documented in the subsurface of the Fort St. John area (Barclay et al. 1990).

The Stoddart Group is found in the core of a large southeast-plunging anticline on the west side of upper Schooler Creek (Figures 7 and 8). The exposure of this unit

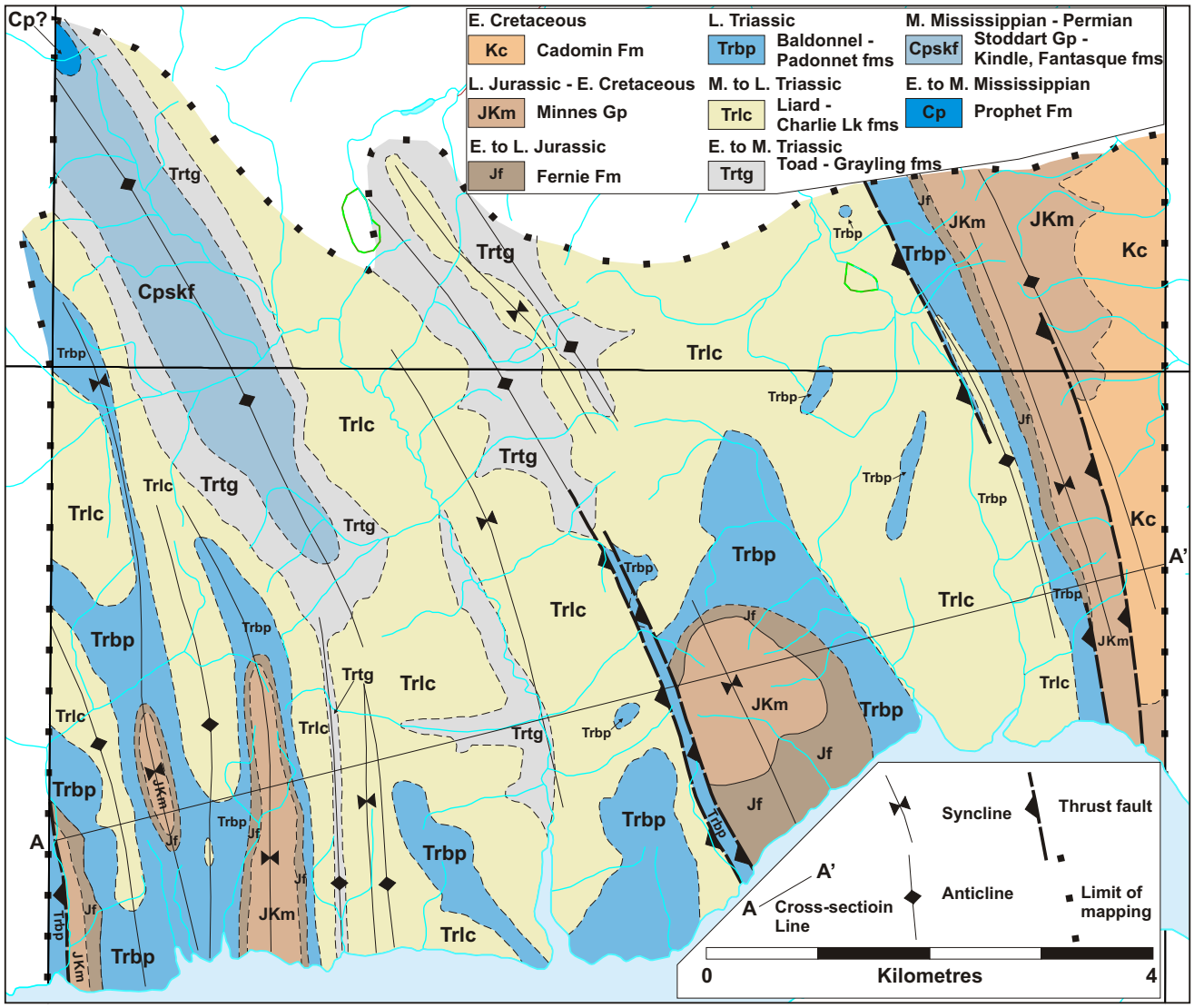

Figure 7. General geology map of the study area.

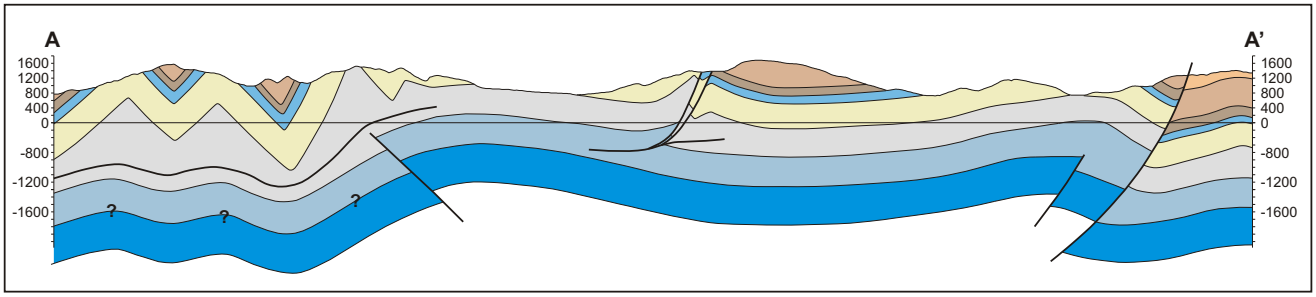

Figure 8. Structural cross-section across the southern part of the map area. See Figure 7 for location.

has been extended further south than originally shown by Thompson (1989). Considering the poor exposure of units below Fantasque Formation cherts and the difficulty in distinguishing Kindle Formation clastics and carbonates from those of the Stoddart Group (Thompson 1989; Bamber et al. 1997), these successions have been grouped together as one map unit. Consequently, no attempt could be made at subdividing Stoddart Group rocks into the various formations recognized in the subsurface to the east (in ascending order, Golata, Kiskatinaw, and Taylor Flat formations).

Structural sections in the map area, together with data from the CNRL Dunlevy a-40-L/94-B-1 well, indicate a thickness of approximately 750 m, although it is not known how much of this could be attributed to structural thickening, particularly within the lower shaly sequence. Thompson (1989) describes more that 500 m of Stoddart Group in the Nabesche River area, and Bamber et al. (1968) describe over 100 m of the Kindle Formation in the Halfway River area. The thickness of these units is quite variable, as shown by their absence below the Permian Fantasque Formation at the north end of Halfway River map area (Thompson, 1989). The age of the Stoddart Group varies between Middle and Late Mississippian (Late Visean to Serpukhovian; Barclay et al. 1990), and the Kindle Formation is Early Permian in age (Asselian to Sakmarian); Thompson 1989).

The bulk of Stoddart–Kindle exposures encountered consisted of light grey to beige fine- to medium-grained calcareous quartz arenite to quartzite. These are typically medium to thickly bedded or massive with planar or cross-bedding and may have thin interbeds of papery, beige shale. These cross-bedded calcareous sandstones have many similarities to sandstones in the Charlie Lake Formation. Lesser lithologies include dark grey argillaceous lime mudstone and beige, papery, silty shale. Some limestone sections are medium-brown–weathered massive limestone, and along Schooler Creek, grey-brown planar-bedded lime mudstone containing chert nodules up to 7 cm thick.

The upper part of this map unit consists of dark grey to black blocky argillaceous chert along its southern extent. This lithology was originally assumed to be part of the Fantasque Formation, but structural considerations, together with the relative thinness of the Fantasque Formation, suggest it is within the upper part of Stoddart-Kindle map unit. These rocks may be part of the Kindle Formation, as it has been described as containing dark grey siliceous mudstone, shale, and chert (Bamber et al. 1997).

Fantasque Formation

The top of the Paleozoic is represented by a thin section of grey chert belonging to the Fantasque Formation. Although thin, this unit forms an easily recognized resistive marker horizon between recessive units of the Stoddart–Kindle succession and Toad and Grayling formations. The Fantasque Formation is Early to Middle Permian in age (Artinskian to Wordian; Thompson 1989).

The Fantasque Formation consists of 20 to 50 m of grey to dark grey blocky chert. It is typically medium to thickly bedded and forms crumbly outcrops that produce abundant talus. The contact between Fantasque cherts and Grayling siltstones is described as an unconformity (Thompson 1989).

Triassic Stratigraphy

Triassic stratigraphy within the map area represents a westward prograding shelf succession up to 1600 m thick. Although fine siliciclastics dominate this succession, limestone and dolomite are abundant in the upper 400 to 500 m of this sequence. There is a general shallowing trend up-section as Early to Middle Triassic turbidites (Toad and Grayling formations) in the lower part give way to shoreface deposits (Liard Formation) in the middle of the succession; these are followed by Late Triassic evaporitic and carbonate shelf deposits (Charlie Lake and Baldonnel formations; Zonneveld 2008; Zonneveld et al. 2004). The evaporitic sequence (Charlie Lake Formation) occupies an intertidal to supratidal setting (sabkha) bounded to the west by either barrier bars and shoreface deposits of the Liard Formation or later by carbonate and clastic shoal deposits (Baldonnel Formation) that grade into deeper-water mid-ramp and outer-ramp deposits represented by the Pardonet Formation (Zonneveld et al. 2004).

Although not present within the map area, Middle to Late Triassic rocks of the Baldonnel, Charlie Lake, and Liard(?) formations transition westward into deeper-water dolomitic to calcareous siltstone and sandstone and silty to sandy bioclastic limestone of the Luddington Formation (Thompson 1989; Gibson 1993). The deposits of the Luddington Formation represent debris flows that originated along the shallow shelf edge of either the Baldonnel or Liard formations. This transition occurs rather abruptly, with the first Luddington lithologies seen on the west flank of Black Bear Ridge, some 2 to 3 km west of the last occurrence of Baldonnel carbonates.

Most workers in this area (see Gibson 1993) have indicated that the Liard Formation also transitions westward into thinner Luddington Formation lithologies, but Zonneveld (2008) infers from stratigraphic and conodont biostratigraphy that a geographic high may have existed to the west, in the Ursula Creek area, during Liard deposition.

TOAD AND GRAYLING FORMATIONS

The Toad and Grayling formations form a recessive sequence some 650 to 750 m thick. The recessive Grayling Formation was not observed. It was originally defined by

Kindle (1944) in the Liard River area as consisting of some 35 m of dark grey silty shale to calcareous siltstone, shale, and minor fine-grained sandstone. Interestingly, Pelletier (1960, 1961) describes over 400 m of Grayling sediments in the Liard River area. Pelletier (1963) describes up to 125 m of this unit in the vicinity of the current map area, and Zonneveld (2008) delineates approximately 37 m at the mouth of Ursula Creek, some 10 km west of the western map boundary. At this locality, Zonneveld (*ibid.*) defines the beginning of the Toad Formation as occurring where the dominantly shale succession of the Grayling Formation gives way to shale with abundant lenses and concretions of fine sandstone.

The Grayling Formation is Early Triassic in age (Griesbachian to Smithian), and the overlying Toad Formation is believed to range up to the Middle Triassic (early Ladinian; Zonneveld 2008).

Only a few dozen outcrops of the Toad Formation were observed during the summer of 2008. Features observed in some of the better exposures are consistent with these sediments having formed through deposition of distal turbidites (Figure 9). At Ursula Creek, the Grayling Formation has also been described as containing turbiditic deposits in its lower part (Zonneveld 2008). Paleocurrent directions measured by Pelletier (1960, 1961, and 1963) indicate easterly, northeasterly, and northwesterly sources for the turbidite flows in the Toad and Grayling formations.

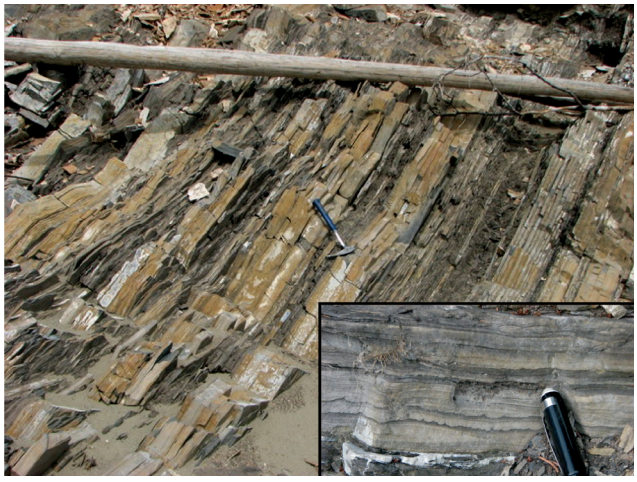

Figure 9. Thinly bedded dark siltstones and very fine sandstones of the Toad Formation along Williston Lake. Inset shows graded beds and flame structures developed within turbidites of this unit.

In the study area, the Toad–Grayling unit is assumed to underlie large parts of the central and southern portions of the Schooler Creek valley and large areas covering the lower slopes in the northern and northeastern parts of the map area. In these areas, the contact with overlying Liard sandstones is commonly inferred to occur where there is a gentler break in slope below the last observed Liard Formation sandstone (Figure 10). The best observed sections of the Toad Formation were seen along the west shore of Williston Lake: in the core of an anticline on the west side of Folded Hill Creek and west of the mouth of Aylard Creek. The contact with the Liard Formation is conformable; sandstone becomes more abundant in the upper part of the Toad Formation, and the contact is placed at the base of the first thick continuous sandstone section, which typically contains large cross-beds or hummocky to swaley cross-beds.

Figure 10. Looking southwest from the north-central part of the map area at a section of Liard sandstone outcropping on the upper slopes of a ridge. Toad Formation siltstones and shales occur in the lower, wooded parts of this ridge, probably close to the break in slope. Jones Peak is in the distance, at the far right.

At these localities, lithologies consist of interbedded, wavy to planar, thin to thick bedded, very fine to fine grey-brown calcareous sandstone and dark grey siltstone to calcareous siltstone or shale. Sandstone displays excellent grading and basal flame structures at the contact with underlying siltstone. Slump folds are also observed. Although fine sandstone to coarser siltstone beds can be up to 50 cm thick, they can form discontinuous horizons resulting in flaser bedding. Siltstone and shale can sometimes form massive horizons several metres thick.

West of the mouth of Folded Hill Creek, the Toad Formation contains at its base several 1 to 3 m thick sandstone sections, which are massive and display basal scouring consistent with turbidite channel deposits. In this area, a 5 m thick massive sandstone bed is found towards the top of the unit. Its base appears to cut into the underlying fine turbidites, and it is succeeded by similar fine turbidites. It appears featureless, but does contain fossil debris layers and large cross-bedsets in the upper part. The basal part of this thick sandstone body suggests it represents a channel in a turbidite fan system, but Zonneveld (2008) has shown through the presence of shallow-water features in the upper part of the unit (interference ripples, possible raindrops, and fossil associations) that it may have been deposited in shallow water and/or been exposed.

LIARD FORMATION

The Liard Formation in the map area is dominated by fine grained calcareous sandstone, lesser interbeds of bioclastic limestone, and sections of siltstone and shale similar to those in the underlying Toad Formation. Sedi-

mentological features and abundant fossil remains suggest deposition in a shallow shelf environment represented by storm influenced barrier bars forming oceanward of sabkha environments represented by the Charlie Lake Formation (Zonneveld 2008; Zonneveld et al. 1997, 2001).

The Liard Formation is some 450 m thick in the eastern part of the map area and thickens to over 500 m in the west. Sandstones and bioclastic sections are reasonably well exposed along ridge tops, although many outcrops consist of isolated exposures consisting of several to tens of metres of section. Due to its resistive nature, sandstone is probably over-represented in exposures. The age of the Liard Formation is Middle to Late Triassic (Ladinian to early Carnian; Thompson 1989; Zonneveld 2008).

The Liard Formation is characterized by beige to brown weathering, grey, fine grained calcareous lithic to quartz arenites (Figure 11). Bedding can be massive to thinly planar or wavy and commonly shows cross-bedding tens of centimetres thick. In addition, swaley to hummocky cross-bedding was observed. Although the formation is typically fine grained, medium to thick grained sections are not uncommon, and occasionally chert-bearing granule conglomerate with abundant bioclastic shelly debris is sometimes present near the base of the unit. Sections showing wavy, interbedded limestone to sandy limestone and calcareous sandstone are another characteristic of the Liard Formation (Figure 12). Skeletal packstone to wackestone sequences up to several metres thick may be present, and these commonly contain abundant shelly (brachiopod and pelecypod) material.

Sections of thin to thick planar bedded, beige to brown weathering, very fine sandstone to siltstone and interbedded dark grey siltstone to shale form a minority of Liard exposures in the map area. The relative under-representation of these lithologies may be directly related to their recessive nature. The upper part of the Liard Formation can contain a 10 to 20 m thick section of Charlie Lake lithologies (Zonneveld, 2008). This can be observed on Williston Lake at the western end of Folded Hill and on the north shore of Aylard Creek inlet.

Figure 11. Typical beige weathering, wavy to planar bedded calcareous, fine sandstone of the Liard Formation. This photo is from the north-central part of the map area looking northeast and shows how these more resistive, flat lying sandstones comprise the tops of ridges in this area.

Figure 12. Wavy to flaser, interbedded limestone and calcareous sandstone within the Liard Formation as seen along the north side of Williston Lake, near Folded Hill.

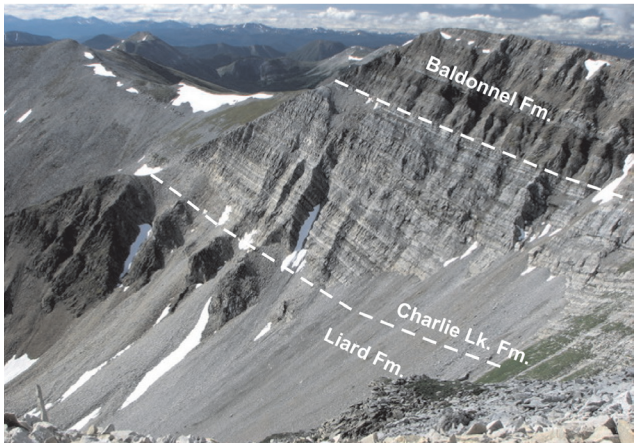

Figure 13. Looking southwest at a section of light coloured Charlie Lake Formation dolomite, dolomitic sandstone, and sandstone sitting on Liard Formation sandstones and followed by darker limestone and dolomitic limestone of the Baldonnel Formation. This section occurs west of the headwaters of Schooler Creek, along the northwestern boundary of the map area.

CHARLIE LAKE FORMATION

The Charlie Lake Formation is characterized by light coloured dolomite to dolomitic limestone and dolomitic sandstone (Figure 13). The unit is some 200 m thick in the east and thickens to near 250 m in the west. This unit represents an intertidal to supratidal (sabkha) evaporitic depositional setting (Zonneveld 2008; Zonneveld et al. 2004; Arnold 1994; Moslow and Davies 1992). It is bounded oceanward by barrier bars of the Liard or Baldonnel formations and landward by aeolian deposits; as such this unit hosts incursions of these other environments, which results in a varied stratigraphic section. The unit sits conformably above Liard sandstones, although locally there are erosion

surfaces (Zonneveld 2008). The age of the unit has been shown to be Late Triassic (Carnian; Thompson 1989); this is based primarily on the age of bounding units, as fossils are rarely preserved within the unit.

Charlie Lake lithologies tend to be lighter weathering and more dolomitic than underlying and succeeding rocks (Figure 13), and the unit generates conspicuous light coloured talus or sections throughout the map area. These are best observed on hill tops west of the headwaters of Aylard Creek and in the far northwestern part of the map area. The formation is one of the easiest to recognize in the field because of the unique lithologies of its depositional environment. The unit is characterized by light grey to cream weathering light grey dolomite, sandy dolomite, or dolomitic sandstone. Interbedded with these sections are yellow, beige to orange or brown weathering sections of medium to coarse grained, highly porous sandstone horizons up to a few metres thick, commonly displaying cross-beds up to 1 m thick. These sandstones can sometimes contain bitumen staining. It is postulated that these cross-beds (Figure 14) represent aeolian dune incursions into the intratidal environment (Zonneveld 2008). These sandstones are probably outcrop equivalents of the Inga, Artex, and other members seen in the subsurface to the east. Another distinctive lithology is grey, finely laminated dolomite to dolomitic limestone that probably represents algal deposits (Figure 14). Although evaporitic horizons (anhydrite) were not observed due to their recessive nature, indications of evaporates are very common within the sequence and are displayed in the form of carbonate solution breccia (Figure 15). Large vugs in a buff weathering, grey, highly porous dolomitic limestone with associated solution breccia found in the northwest corner of the map area may be attributed to dissolution of evaporates.

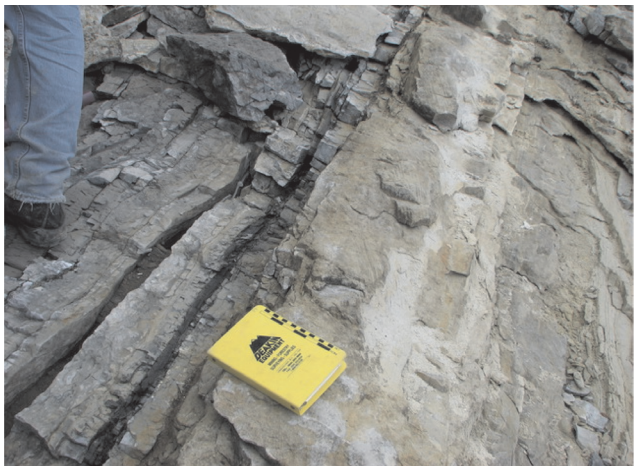

Figure 14. Large cross-beds, possibly of aeolian origin, within the Charlie Lake Formation on Williston Lake, near Brown Hill. The note book is lying on the sandstone horizon, which is about 1 m thick. Algal laminations are found in the dolomite above the sandstone.

Figure 15. Solution collapse breccia in Charlie Lake dolomites, on Williston Lake, near Brown Hill.

BALDONNEL FORMATION

The Baldonnel Formation is composed of fetid limestone and lesser sandstone to siltstone; it is approximately 150 m thick in the east and appears to thicken to about 200 m in the west. The unit is well exposed and forms an excellent structural and stratigraphic marker throughout the map area. Generally, due to the southward plunge of structures, the Baldonnel Formation is best exposed in the southern part of the map area, where it forms cliff exposures along some of the ridge tops and excellent exposures along Williston Lake. It is also well exposed along ridges within the western and northwestern part of the map area. The unit is, in part, the western, marine time-equivalent of the Charlie Lake Formation and represents a bioclastic to siliciclastic barrier bar that transitioned oceanward into distal offshore deposits and finally into deep-water carbonate deposits typical of the Pardonet Formation. The age of the Baldonnel Formation is Late Triassic (Carnian to early Norian; Zonneveld et al. 2004). It is conformable with Charlie Lake and Pardonet formations over relatively sharp but gradational contacts.

The Baldonnel Formation is characterized by its very fetid nature on breakage. Limestone is massive to thickly bedded, grey-brown to grey weathering and commonly contains 1 to 10 cm or larger vugs rimmed with calcite, quartz, and less commonly bitumen. These can sometimes be completely infilled by quartz and carbonate locally. Ovoid to circular, dark grey to black chert nodules up to 15 cm in size can also be observed locally. Limestone varies from a lime mudstone to lime wackestone to grainstone to packstone. Lime grainstone to packstone (Figure 16) is characterized by being almost always composed of crinoidal debris. Furthermore, crinoid ossicles are distinguished by a five-pointed radial symmetry (Figure 17). Sandstone grains can constitute a few percent of lithologies and increase in abundance locally, forming calcareous, fossiliferous sandstone horizons several metres thick. Fossil material is abundant, either as debris or whole pelecypod or bivalve shells.

Figure 16. Skeletal packstone to grainstone of the Baldonnel Formation, west of Aylard Creek.

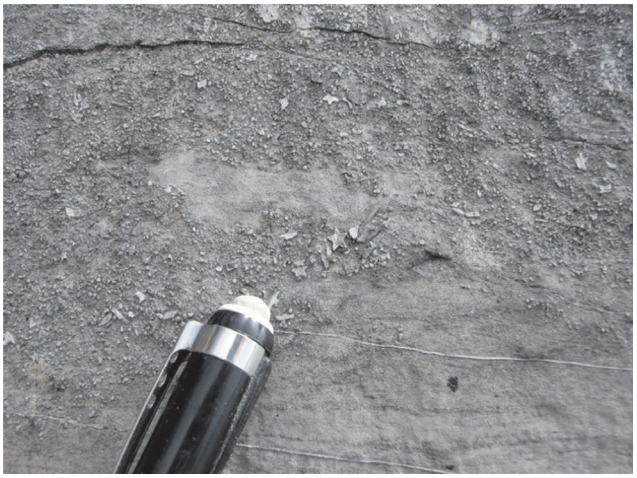

Figure 17. Star-shaped crinoid ossicles within the Baldonnel Formation, on Williston Lake, on the west side of Schooler Creek inlet.

South of Williston Lake, the Baldonnel Formation contains a 50 m thick section of grey-brown weathering, carbonaceous to argillaceous siltstone, very fine grained sandstone, limestone, and dolomite referred to as the Doucette Member (Gibson 1971; Zonneveld 2008). Although these lithologies were observed within the Baldonnel Formation, a succession as thick as the Doucette Member was not recognized within the map area and could not be delineated as a separate unit.

PARDONET FORMATION

The Pardonet Formation is a medium to dark grey to dark grey-brown weathering carbonaceous limestone with lesser silty limestone, dolomitic limestone, and shale. The unit is only about 50 m thick in the east, and structural sections suggest it thickens somewhat to the west. It is commonly poorly exposed along the lower slopes; the best exposures occur in the alpine. The lower contact with the Baldonnel Formation appears to be sharp but gradational. The unit is entirely Late Triassic in age (Norian; Zonneveld et al. 2004).

The Pardonet Formation is characterized by grey to dark grey fetid, platy to fissile carbonaceous lime mudstone with lesser occurrences of lime wackestone to grainstone, which can contain crinoid and shelly debris. Limestone locally can be quite silty. The Pardonet Formation is commonly distinguished by numerous horizons of abundant bivalve remains composed of single species of *Monotis*, *Halobia*, or *Eomonotis*. These thin-shelled bivalves can be so numerous in areas that Pardonet sections display a fine crinkly or wavy bedding reflecting the compaction and superposition of numerous shell remains (Figure 18). Dark grey calcareous shale is also observed within the sequence. Dark grey to black phosphate lag deposits are recognized within the Pardonet Formation (Zonneveld 2008). In addition, it is not uncommon to observe phosphatic skeletal remains of fish or large vertebrates (Figure 19).

Figure 18. Crinkly carbonate within the Pardonet Formation composed of either stacked shells of *Monotis*, *Halobia*, or *Eomonotis*.

Figure 19. Dark grey to black phosphatised reptilian vertebrae within the Pardonet Formation.

Fernie Formation

The basal Fernie Formation represents the culmination of a profound marine transgression which may have commenced in Pardonet tims (Late Triassic). This was followed in the upper Fernie (latest Jurassic) by an influx of westerly derived coarser clastics that reflect the emergence of mountains in response to obduction of volcanic arc terranes along the western margin of ancestral North America. Although there is evidence for westerly derived clastics in the Late Devonian (Root 2001) and Early Triassic (Beranek and Mortensen 2007a), those horizons are relatively thin, and their eastward incursions affected only the westernmost edge of ancestral North America. In contrast, the Jura-Cretaceous sequences form extensive westward thickening wedges that spread as far east as Saskatchewan and Manitoba.

The Fernie Formation is some 275 to 300 m thick in the map area. Although along Williston Lake the contact with underlying Pardonet silty carbonates appears gradational (i.e., the disappearance of *Monotis* is the only manifestation of the transition to the overlying Fernie Formation), elsewhere it is believed to be an erosional unconformity (Stott 1998). Stott (1998) subdivided the Fernie Formation into three units in the vicinity of the map area. A basal Unit I composed of dark grey to dark grey-brown siltstone (Brown and Pecten beds of Stott [1998]) is followed by dark grey to black, fissile to crumbly shale, siltstone, chert and minor limestone of Unit II (equivalent to Poker Chip Shale). These are succeeded by dark siltstone (the upper unit III, equivalent in part to the Passage Beds; Stott 1998), which contains an upward increasing abundance of interbedded sandstone and coarse siltstone that grades into overlying lithologies of the Minnes Group.

The Fernie Formation in the map area encompasses Early to Late Jurassic times (Hettangian to Kimmeridgian), although current fossil control suggests numerous unconformities (Stott 1998). Units I and II are Early to Middle Jurassic in age, whereas the upper part of the Fernie Formation (Unit III) is most likely entirely Late Jurassic (Oxfordian to earliest Tithonian; Stott 1998).

The Fernie Formation is found along the west flank of Twenty Mile Ridge, along the broad syncline of the Branham Ridge area, and within several tight synclines north and northwest of Brown Hill. The poor exposure and recessive nature of the formation did not allow mapping of the various subdivisions of this formation. Outcrops of Unit I and II were observed along Williston Lake near Brown Hill, on the west flank of Twenty Mile Ridge, and at several other localities. Basal Fernie is characterized by dark grey to dark grey-brown weathering, blocky to fissile siltstone to shale and lesser slightly calcareous siltstone. Most other fine grained clastic sections of the Fernie Formation consist of crumbly to fissile dark grey to black siltstone and shale with minor fine sandstone layers. These crumbly siltstones have characteristics similar to Unit II (Poker Chip Shale).

Due to their more resistive nature, the bulk of the Fernie sections observed in the field belong to the upper unit (III). These sections comprise dark grey-brown to grey fissile shale and siltstone with interlayers of light grey to beige weathering, medium to dark grey-brown, thin to thick bedded, fine to medium or coarse grained lithic quartz arenites. Sandstone is characteristically micaceous and can contain up to 20% chert clasts. Bedding is massive to planar and commonly cross-bedded (bi-directionally), and many outcrops are highly bioturbated (Figure 20). Several 5 m thick ribs of upward coarsening sandstone occur within the middle part of the Fernie Formation on the southeast side of Branham Ridge. Some coaly partings are visible locally. Turbidite deposits are also observed in the lower part of the upper Fernie Formation. Sandstone and siltstone sections in the upper Fernie Formation typically vary between 1 and 5 m thick; sandstone becomes more prominent up-section. Shale in the lower part of the upper Fernie gives way to siltstone in the upper part, and its relative abundance decreases up-section as it is replaced by fine to coarse sandstone. The contact with the overlying Minnes Group is gradational and placed at base of the first thick section of sandstone.

Figure 20. Bioturbated sandstone and siltstone of the Fernie Formation on Williston Lake, south of Branham Ridge.

Minnes Group

The Minnes Group as defined by Stott (1998) is composed of four formations, which are, in ascending order, Monteith, Beattie Peaks, Monach, and Bickford (Figure 6). The Minnes Group can be up to 2000 m thick, is Late Jurassic to Early Cretaceous in age (Tithonian to Valanginian; Stott 1998) and reflects marine to non-marine deltaic sedimentation. Monteith and Monach formations are composed of fine to coarse sandstone and lesser fine clastics, whereas the Beattie Peaks and Bickford formations are dominated by fine clastics and form more recessive sections. Basal

Monteith sandstones and siltstones represent deeper marine deposits, which are succeeded by coarse deltaic sandstone deposits of the upper Monteith Formation. The Beattie Peaks Formation reflects a marine transgression, whereas Monach sandstones signal a return to fluvial-deltaic environments. Bickford Formation lithologies suggests marine environments.

The similarity between various units of the Minnes Group often makes the assignment of individual sections to specific formations problematic in the field. This is illustrated by the similarity between uppermost Monteith and Monach sandstones and between upper Fernie, Beattie Peaks, and middle Monteith successions.

MONTEITH FORMATION

The Monteith Formation makes up the bulk of Minnes Group exposures in the map area. The formation is approximately 450 m thick in the Branham Ridge area. Roughly 400 m of Monteith Formation was penetrated by the CNRL Dunlevy a-40-L well at the south end of Twenty Mile Ridge, and this is similar to the thickness of sections seen along the crest of the ridge. The Monteith Formation is characterized by thin to thickly bedded beige weathering, grey-brown, fine to medium grained lithic quartz arenites. These are commonly micaceous, contain up to 20% chert clasts, and are locally bioturbated. Bedding can be planar to cross-bedded, with bi-directional cross-sets indicating a marine influence. Sandstone typically makes up greater than 90% of the section. The large cliffs at Branham Ridge are composed of these sandstones.

Parts of the Monteith Formation, particularly within the middle part, contain 10 m thick sections of interbedded finer siliciclastics that include dark grey-brown siltstone and very fine sandstone. Some coaly partings were observed in these sections. These finer clastics have overall characteristics can be similar to the Beattie Peaks Formation.

The uppermost part of the Monteith Formation consists of medium to thick bedded or massive, light grey to cream or beige weathering, beige, lithic quartz arenite to quartz arenite or quartzite. These lithologies suggest fluvial environments and are very similar to sandstones developed within the Monach Formation. Grain size is quite variable, but typically this unit is medium to coarse grained sand with local granule to pebble horizons. Lithics are composed of conspicuous, chalky, white weathering feldspar clasts and mica flakes. Porosity is also reasonably well developed locally. The unit is typically cross-bedded, with some cross-sets up to 1 m thick. In addition, scours are observed at the base of some beds and contain coarser (granule to pebble clasts) lag deposits. All these features suggest fluvial environments, as described by Stott (1998).

BEATTIE PEAKS FORMATION

The Beattie Peaks Formation is a recessive unit up to 150 m thick and is composed of interlayered fine to medium sandstone and siltstone of roughly equal proportions. It is recognized on Branham and Twenty Mile ridges. The contact with underlying Monteith lithologies was not seen but is shown to be conformable (Stott 1998). Sandstones, siltstones, and minor shales in this formation, together with their interbedded relationships, are very similar to lithologies in the upper Fernie Formation or middle recessive unit of the Monteith Formation. The depositional features indicate a return to deeper marine conditions during Beattie Peaks time.

MONACH FORMATION

The Monach Formation consists of medium to thick bedded or massive lithic quartz arenite to quartz arenite or quartzite (Figure 21). These light grey to cream or beige weathering, beige sandstones are very similar to those of the uppermost Monteith Formation. These lithologies indicate a return of coarser fluvial (deltaic) environments during this part of Minnes Group deposition, (Stott, 1998). The unit is about 225 m thick along Twenty Mile Ridge, and approximately 50 to 100 m of this unit caps the top of the hill north of Branham Ridge. The contact with the underlying Beattie Peaks Formation is abrupt but conformable. Sandstones are medium to coarse grained with local granule to pebble horizons.

Figure 21. Cream to light brown or beige weathering, lithic arenites of the Monach Formation. These are medium to coarse grained and contain granule layers or lags. Bedding is very thick to massive and displays large cross-sets. This outcrop occurs on the eastern side of Twenty Mile Ridge. These sandstones are very similar to upper Monteith lithologies.

Grain size is quite variable, but typically this unit is medium to coarse grained sand with local granule to pebble horizons. Lithics are composed of conspicuous, chalky, white weathering feldspar clasts and mica flakes. Porosity is also reasonably well developed locally. The unit is typically cross-bedded, with some cross-sets up to 1 m thick. In addition, channel scours are observed at the base of some beds and contain coarser (granule to pebble clasts) lag deposits.

BICKFORD FORMATION?

A recessive notch some 50 m thick is observed along the east side of Twenty Mile Ridge between resistive sandstones of the Monach and Cadomin formations. Although no outcrops were observed in this interval, this recessive horizon may reflect the presence of Bickford lithologies. This horizon appears to be truncated southward below the Cadomin Formation, which may be a reflection of removal of the horizon by the sub-Cadomin unconformity.

Cadomin Formation

The Cadomin Formation was observed along the eastern margin of the map area and is best exposed along Twenty Mile Ridge. This unit, together with the Gething Formation, comprises the Bullhead Group and is mid-Early Cretaceous in age (Barremian to Aptian; Stott 1998). Although Gething lithologies were not observed in the map area, they probably outcrop within the syncline occupying the Dunlevy Creek valley (Legun 1984). The Cadomin is approximately 350 m thick and represents fluvial deposition (Stott 1998). It sits unconformably on top of the Minnes Group and is shown regionally to cut down into the Minnes Group in a northward direction (Stott 1998). In the map area, the Cadomin Formation is much finer grained than the typical pebble to boulder conglomerate observed south of Peace Arm. Fluvial deposits of this formation decrease in abundance northward until the formation ceases to be a mappable unit north of Graham River, where related lithologies are combined with the Gething Formation (Thompson 1989; Stott 1998).

The Cadomin Formation is characterized by thick bedded to massive, medium grey weathering, medium to very coarse grained, salt and pepper lithic quartz arenites. Thin, discontinuous horizons of granule to pebble clasts are not uncommon. Cross-bedding up to 1 m thick is also observed locally. Dark grey to grey chert and feldspar comprise approximately 20% and 10%, respectively, of clasts. Channel scours up to a few metres thick are associated up-section with finer sandstone to siltstone horizons containing root casts and coal horizons defining fining-upward channel deposits (Figure 22).

Figure 22. Fining-upward channel deposit approximately 3 m thick within the Cadomin Formation. Inset shows root casts in siltstone at the top of this channel. The thrust fault along the top of Twenty Mile Ridge occurs at the left of the photo and juxtaposes the upper Fernie Formation against the Cadomin Formation.

STRUCTURE

Rocks in the map area have undergone considerable east-west lateral shortening, which has been accommodated by folding and thrust faulting. Folding is the dominant mechanism for shortening, and the intensity and tightness increase to the west. Concentric-style folding is displayed within Jura-Cretaceous rocks, whereas folds developed within Triassic stratigraphy are decidedly chevron in nature (Figures 23 and 24). In the eastern part of the map area, broad synclines along Schooler Creek and the Adams and Aylard creeks drainages are bounded by tight anticlines or faulted anticlines along Twenty Mile Ridge, through Jones Peak, and in the Folded Hill region (Figures 2, 7). Close to tight chevron-style folding is dominant along the western part of the map area, although this is followed to the west by a broad syncline below Black Bear Ridge (Thompson 1989). This structural style (broad synclines bounded by close to tight anticlines) is particularly well developed within Cretaceous and Triassic strata north of Graham River (see Thompson's [1989] sections 2 to 6).

West-dipping monoclinal structures (or western limbs of a box fold) are observed at the mouths of Aylard and Adams creeks, along the north side of Williston Lake. Steeper structural attitudes within an otherwise flat lying to gently dipping panel are observed in the area just northwest of the Aylard Creek headwaters and may be related to monocline development (i.e., large scale "kink bands"). The chevron fold style and monoclinal structures of Triassic rocks reflect the relatively thinly interlayered nature of these sequences compared to the more competent successions within parts of the Minnes Group.

Figure 23. Faulted folds outlined by Liard and Charlie Lake formations on the south face of Folded Hill.

Figure 24. Close to tight chevron fold defined by Liard Formation sandstones. This view is to the north; this mountain is found across Schooler Creek, immediately west of Jones Peak. Note that the axial plane is dipping slightly to the east, indicating westward vergence. This attitude is also displayed in structural cross-sections through the area (Figure 8).

Generally, folds trend north-northwest. The exception occurs west of Schooler Creek and south of about 50.167° N latitude, where fold axes outline an almost north-south path. Structures plunge about 5° to 10° to the south along the southern part of the map area. This may reflect the position of the map area along the northern limit of the Deep Basin.

The series of folds that are developed in the Folded Hill area trend northward and are represented by one large anticline at the level of the Stoddart–Kindle formations (Figure 7). Folds along the eastern part of this series show westward vergence (i.e., axial planes dip steeply to the east; Figures 8 and 24). This geometry suggests some underpinning or wedging of the structural panel at a lower structural level.

A possible detachment horizon within the Toad–Grayling or Stoddart–Kindle formations would accommodate the change in fold wavelengths between stratigraphic levels. This change in wavelength with depth may reflect the difference in fold styles between the thick and relatively rigid Prophet–Debolt carbonate and overlying thinly interlayered sediments of the Triassic and Jura-Cretaceous sediments. The stratigraphic level of erosion in the south-central map area and its structural cross-sections indicate that the Prophet/Debolt carbonate is approximately 1500 to 2500 m below surface.

Several thrust faults are delineated within the map area, and the amount of stratigraphic and structural displacement on these structures is limited. Three faults are found in the Aylard Creek–Twenty Mile Ridge area. The most easterly cuts along the west side of Twenty Mile Ridge and then disappears within the core of the fold delineated along the ridge. To the west of this, along the west flank of Twenty Mile Ridge, a thrust fault loses displacement and disappears northward within Fernie lithologies. These faults probably connect southeastward with the thrust traced along the east side of Mount Gething (Legun 1984; Thompson 1989). A third thrust occurs to the west and is believed to begin at the headwaters of Aylard Creek and places rocks of the Liard Formation against those of the Baldonnel and Pardonet formations. This fault can be traced northwestward, off the current map area. The configuration of these three faults suggests a north-south transfer of displacement between the structures.

West of here, two closely spaced thrusts can be traced from Williston Lake northward to Jones Peak, after which they disappear into the core of a fold delineated by the Liard and Toad–Grayling formations. In the south, a wedge of Pardonet carbonates occupies the area between the faults. The northward interpretation of the disappearance of these faults, together with the relative position between the faults, is speculative. A thrust does occur at Jones Peak due to the juxtaposition of Liard and Baldonnel lithologies.

Cross-sections through the map area suggest that the thrusts along Aylard Creek cut down into the Prophet–Debolt. The thrust in the Jones Peak area may root westward into the top of the Prophet–Debolt, suggesting a detachment horizon within the Stoddart Formation. The amount and nature of shortening at the level of the Prophet Formation within the western part of the map area is difficult to determine. If this shortening is as great as seen at surface, it would be difficult for this thick and relatively competent horizon to have accommodated it entirely by folding. Balanced regional structural cross-sections, together with new seismic data, may shed some light on this.

Cleavage development is rare and typically occurs within tighter folds. It was observed at southern flank of Folded Hill and at a few other localities. Its development occurred within shaly horizons of the Liard, Toad–Grayling and Pardonet formations and consisted of widely spaced fracture cleavage.

DETRITAL ZIRCON GEOCHRONOLOGY

A sample of lowermost Liard Formation sandstones was taken from a section immediately west of Schooler

Creek in the north-central part of the map area to determine the distribution of detrital zircon ages within the sample. The location of this section is 56.243° N and 122.885° W. This analysis was based on growing evidence from the northern Cordillera that uplift and shortening was occurring along the western edge of ancestral North America during the Early to Middle Triassic (Beranek and Mortensen 2006, 2007a, b, 2008). One of the implications of this hypothesis is that Triassic clastics would have been sourced, in part, from the west. If this is correct, there may be regional implications with respect to the interpretation of regional Triassic sedimentation patterns.

Preliminary results (105 grains) show detrital zircon ages of 347, 358 and 395 Ma; 402 to 481 Ma; 519 to 534 Ma; 605 and 722 Ma; 882 and 886 Ma; 931 to 9994 Ma; 1007 to 1081 Ma; 1116 to 1159 Ma; 1204 to 1264 Ma; 1323 to 1397 Ma; 1402 to 1465 Ma; 1521 to 1579 Ma; 1601 to 1687 Ma; 1706 to 1788 Ma; 1813 to 1897 Ma; 1909 to 1998 Ma; 2135 to 2957 Ma and 3489 Ma.

Although no Late Paleozoic or Triassic ages were observed from this sample, the presence of middle Mississippian detrital zircons suggests a western source. No detrital zircon sources of this age would be found within the eastern parts of the Western Canada Sedimentary Basin in Triassic times or within the Innuitian orogen in the Arctic (Ross et al. 1997). Potential source areas would be uplifted sections of the distal miogeocline west of the map area, which contain thick volcanics of this age (Richards et al. 2002), and uplifted volcanic arc terranes further to the west. The lack of zircon ages younger than middle Mississippian may exclude the most westerly source area.

The distribution of detrital zircon ages is similar to the distribution in the northern Cordillera described by Beranek (2007b).

THERMAL MATURATION

Several samples were collected from throughout the map area and sent to the laboratories at the Geological Survey of Canada for determination of thermal maturation through vitrinite reflectivity (Table 1). Riediger (1997) and Riediger et al. (2004) published Rock-Eval data for samples taken from the Pardonet, Baldonnel, Liard, Toad, and Grayling formations along Williston Lake. Samples from along Black Bear Ridge (from the Pardonet and Baldonnel formations) had T_{max} values of approximately 600 °C (upper dry gas window). The data in Table 1 indicates that Baldon-

TABLE 1. VITRINITE REFLECTANCE VALUES FOR SELECT SAMPLES FROM THE MAP AREA.

Sample	Formation	Lithology	UTM E	UTM W	Latitude	Longitude	$\%Ro_R$
08FFE060	Pardonet Fm	lime wackestone	523559	6223599	56.157	-122.621	1.09
08FFE099	Baldonnel Fm	lime mudstone	517902	6219128	56.117	-122.712	1.16
08FFE119	Pardonet Fm	lime mudstone	500055	6217229	56.100	-122.999	1.03
08FFE120	Pardonet Fm	lime mudstone	499817	6217368	56.101	-123.003	0.96 1.12
08FFE122	Fernie Fm	lithic arkose	522067	6223385	56.155	-122.645	1.01
08FFE125	Monteith Fm	lithic arkose	521738	6224224	56.163	-122.650	0.81 0.96
08FFE136	Chalier Lake Frm	arkose	499913	6229627	56.212	-123.001	1.35 1.49
08FFE155	Liard Fm	arkose	507130	6233148	56.243	-122.885	0.87
08FFE178	Monteith Fm	lithic arkose	505363	6224273	56.163	-122.914	0.87
08FFE204	Monteith Fm	subarkose	526002	6236540	56.273	-122.580	0.84
08FFE209	Monteith Fm	lithic arkose	529138	6229327	56.208	-122.530	0.93
08FFE223	Cadomin Fm	lithic arkose	529256	6230669	56.220	-122.528	0.62
08FFE228	Monteith Fm	lithic arkose	527405	6232139	56.233	-122.558	0.73
08FFE263	Beattie Pks Fm	lithic arkose	527520	6231181	56.225	-122.556	0.63
08DFM083	Cadomin Fm	coal	534011	6225295	56.171	-122.452	0.68

nel and Pardonet rocks in the map area are in the middle to upper oil window and that the base of the Toad–Grayling sequence would be in the upper gas window (Figure 4). These new thermal maturation values are similar to data collected from Triassic rocks in other parts of the northern foothills (Riediger et al. 2004).

EXPLORATION

The primary exploration targets in the map area are structural plays within the Mississippian Debolt (Prophet) Formation. There are two Debolt fields at the northwest corner of the map area (Federal Debolt A and B). The wells in this area, together with the CNRL Dunlevy a-40-L well, targeted the Debolt structural culmination associated with the fold developed along Twenty Mile Ridge. These wells can be quite productive, as shown by the Talisman Husky HZ Federal d-28-H/94-B-7 well, which reported restricted flows of 21 to 25 mmcf ([5.95 to 7.08] × 10^5 m^3) per day of gross raw gas (Adams et al. 2007).

West of the map area, along the west Nabesche River, the CNRL Nabesche b-33-E/094-B-6 well was spudded in Besa River shales and encountered some 1500 m of Devonian carbonates, starting at a depth of about 850 m. The bottom of this well is reported to have penetrated into Middle Devonian Stone carbonates. Although drill-stem tests across Pine Point(?)–equivalent strata recovered fresh water, the engineering data indicate excellent reservoir characteristics.

The CNRL Dunlevy a-40-L penetrates over 800 m of siltstones and shales of the Toad–Grayling formations, which are equivalent to the Montney Formation in the subsurface further east. Interestingly, this well blew out at about the 2220 m level and experienced a gas kick at 2230 m. This horizon most likely represents a fault zone and may be related to detachment accommodating the development of the fold structure along Twenty Mile Ridge. Although engineering data from flow tests on this zone indicated limited reservoir size and low permeability, the presence of significant gas in this zone reflects the potential of this horizon and justifies the exploitation efforts the Montney Formation is receiving further east.

SUMMARY

- 1:50 000-scale mapping during the summer of 2008 covered portions of 94-B/02 and 07 on the north side of Williston Lake.
- Over 4000 m of Mississippian, Permian, Triassic, Jurassic, and Cretaceous rocks are found in the map area.
- Triassic stratigraphy comprises over three-quarters of surface exposures within the map area.
- Shortening has been accommodated primarily by folding and lesser thrust faulting.
- Surface mapping and structural cross-sections suggest the lower Toad and Grayling formations and the Stoddart Group are probable detachment horizons above the thick Prophet carbonates.
- Detrital zircon geochronology of lowermost Liard Formation sandstones returned ages as young as middle Mississippian, together with Early to Middle Devonian, Silurian, Early Ordovician, Cambrian, Proterozoic, and Archean ages.
- Thermal maturation of Pardonet carbonates reached the middle to upper oil window and the base of the Toad–Grayling sequence records upper gas window conditions.
- Exploration has historically targeted structural plays within the Mississippian Prophet Formation and its subsurface equivalent, the Debolt Formation.

ACKNOWLEDGEMENTS

The author would like to thank Duncan McLeish, Keegan Raines and Scott McGregor for assistance in the field. The logistical support and hospitality provided by the Beattie family at Wicked River Lodge is greatly appreciated. Canadian Helicopters, Vancouver Island Helicopters and Whitney Helicopters provided competent air support during the summer. The author would like to acknowledge Canfor Corporation for providing access to the Graham South Mainline road. Thanks go to Ray Jackson for use of his hunting facilities along Horseshoe Creek. The author would also like to thank Talisman Energy Ltd. and BG Canada for logistical support during the summer.

REFERENCES

Adams, C., Schwabe, M., and Riddell, J. (2007): British Columbia oil and gas exploration activity report 2006; *BC Ministry of Energy, Mines and Petroleum Resources*, Information Circular 2007-1, 37 pages.

Arnold, K.J. (1994): Origin and distribution of aeolian sandstones in the Triassic Charlie Lake Formation, northeastern British Columbia; Unpublished M.Sc. thesis, *University of Alberta,* 337 pages.

Bamber, E.W., Taylor, G.C., and Procter, R.M. (1968): Carboniferous and Permian stratigraphy of northeastern British Columbia. *Geological Survey of Canada*, Paper 68-15.

Bamber, E.W., Henderson, C.M., and Richards, B.C. (1997): Kindle Formation; *in* Lexicon of Canadian Stratigraphy, Western Canada including eastern British Columbia, Alberta, Saskatchewan and southern Manitoba, Volume 4; D. Glass (*editor*), *Canadian Society of Petroleum Geologists*, 1423 pages.

Barclay, J.E., Krause, F.F., Campbell, R.I., and Utting, J. (1990): Dynamic casting and growth faulting: Dawson Creek Graben Complex, Carboniferous-Permian Peace River Embayment, western Canada; *in* Geology of the Peace River Arch, S.C. O'Connell and J.S. Bell (editors), *Bulletin of Canadian Petroleum Geology*, Volume 38A, pages 115–145.

Beranek, L.P., and Mortensen, J. K. (2006): Triassic overlap assemblages in the northern Cordillera: Preliminary results from the type section of the Jones Lake Formation, Yukon and Northwest Territories (NTS 105I/13), *in* Yukon Exploration and Geology 2006, D.S. Emond, G.D. Bradshaw, L.L. Lewis and L.H. Weston (editors), *Yukon Geological Survey*, pages 79–91.

Beranek, L.P., and Mortensen, J. K. (2007a): Latest Permian to Middle Triassic accretions of the Yukon-Tanana, Stikine, and Quesnel Terranes to North America: new detrital zircon age data from Triassic rocks in Yukon; *Geological Society of America*, Abstracts with Programs, Volume 39, page 69.

Beranek, L.P., and Mortensen, J. K. (2007b): Investigating a Triassic overlap assemblage in Yukon: On-going field studies and preliminary detrital-zircon age data, *in* Yukon Exploration and Geology 2006, D.S. Emond, L.L. Lewis and L.H. Weston (editors), *Yukon Geological Survey*, pages 83–92.

Beranek, L.P., and Mortensen, J. K. (2008): New stratigraphic and provenance studies of Triassic sedimentary rocks in Yukon and northern British Columbia, *in* Yukon Exploration and Geology 2006, D.S. Emond, L.R. Blackburn, R.P. Hill and L.H. Weston (editors), *Yukon Geological Survey*, pages 115–124.

Buller, G.H.D.P. (2004): GanFeld: Geological field data capture; in Digital Mapping Techniques '04—Workshop Proceedings; U.S. Geological Survey Open-File Report 2004–1451.

Davies, G.R. (1997): The Triassic of the Western Canada Sedimentary Basin: tectonic and stratigraphic framework; *Bulletin of Canadian Petroleum Geology*, Volume 45, pages 434–460.

Gibson, D.W. (1971): Triassic stratigraphy of the Sikanni Chief River–Pine Pass region, Rocky Mountain Foothills, northeastern British Columbia; *Geological Survey of Canada*, Paper 70-31.

Gibson, D.W. (1993): Triassic; *in* Sedimentary cover of the craton in Canada, Stott, D.F. and Aitken, J.D. (editors), *Geological Survey of Canada,* Geology of Canada Number 5, pages 294–320.

Hunter, D.J., and Cunningham, J.M. (1991): Geology of the Burnt River and Gwillim Lake (southwest half) Areas, northeastern British Columbia (93P/5, 6); *B.C. Ministry of Energy, Mines and Petroleum Resources*, Open File OF1991-04.

Irish, E.J.W. (1970): Halfway River map-area, British Columbia; *Geological Survey of Canada*, Paper 69-11, 154 pages.

Jahans, P.C. (1993): Geology of the Pine River area, Northeastern British Columbia (93O/9, 10; P/12); *B.C. Ministry of Energy, Mines and Petroleum Resources*, Open File OF1993-22.

Kilby, W., and Wrightson, C.B. (1987a): Bedrock geology of the Sukunka River area (93P/4); *B.C. Ministry of Energy, Mines and Petroleum Resources*, Open File OF1987-07.

Kilby, W., and Wrightson, C.B. (1987b): Bedrock geology of the Bullmoose Creek area (93P/4); *B.C. Ministry of Energy, Mines and Petroleum Resources*, Open File OF1987-06.

Kindle, E.D. (1944): Geological reconnaissance along Fort Nelson, Liard, and Beaver rivers, northeastern British Columbia and southeastern Yukon; *Geological Survey of Canada*, Paper 44-16.

Lane, L.S. (2005): Foreword; Central Foreland NATMAP; stratigraphic and structural evolution of the Cordilleran foreland; *Canadian Society of Petroleum Geologists,* Bulletin of Canadian Petroleum Geology, Volume 53, pages 1–3.

Legun, A.S. (1982): Stratigraphy and sedimentology notes on the Bullhead Mountain-Peace River Canyon, Carbon Creek area, northeastern British Columbia (93O/15, 16; 94B/1, 2); *B.C. Ministry of Energy, Mines and Petroleum Resources*, Geological Fieldwork 1982, Paper 1983-1, pages 93–98.

Legun, A.S. (1983): Butler Ridge map area, Peace River District (94B/1); *B.C. Ministry of Energy, Mines and Petroleum Resources*, Geological Fieldwork 1983, Paper 1984-1, pages 123–130.

Legun, A.S. (1984): Geology of the Butler Ridge area; *B.C. Ministry of Energy, Mines and Petroleum Resources*, Preliminary Map PM57.

Legun, A.S. (1985): Geology of the West Carbon Creek area (930/15); *B.C. Ministry of Energy, Mines and Petroleum Resources*, Geological Fieldwork 1984, Paper 1985-1, pages 227–232.

Legun, A.S. (1986): Geology of the Carbon Creek area (93O/15); *B.C. Ministry of Energy, Mines and Petroleum Resources*, Geological Fieldwork 1985, Paper 1986-1, pages 155–160.

Legun, A.S. (1987a): Geology of the Carbon Creek area (93O/15); *B.C. Ministry of Energy, Mines and Petroleum Resources*, Open File 1987-21.

Legun, A.S. (1987b): A Geological update of the Carbon Creek and Butler Ridge areas (930/15,94B/l); *B.C. Ministry of Energy, Mines and Petroleum Resources*, Geological Fieldwork 1986, Paper 1987-1, pages 365–368.

Legun, A.S. (2003): Coalbed methane geology of the Peace River District; *B.C. Ministry of Energy, Mines and Petroleum Resources*, Geoscience Map GM2003-02.

Mathews, W.H. (1986): Physiography of the Canadian Cordillera; *Geological Survey of Canada*, Map 1701A.

McMechan, M.E. (1986): Mount Sir Alexander, Walker Creek, Cariboo Land Creek, British Columbia; *Geological Survey of Canada,* Open File 1229.

McMechan, M.E. (1996a): Geology, Mount Sir Alexander, West of Sixth Meridian, British Columbia; *Geological Survey of Canada*, A Series Map 1892A.

McMechan, M.E. (1996b): Geology, Walker Creek, West of Sixth Meridian, British Columbia; *Geological Survey of Canada*, A Series Map 1839A.

McMechan, M.E. (2000): Structure section and geological map of the Foothills and Front Ranges, Carbon Creek area, northeast British Columbia; *Geological Survey of Canada*, Open File 3553.

McMechan, M.E., and Thompson, R.I. (1995a): Geology, Jarvis Lakes, West of Sixth Meridian, British Columbia; *Geological Survey of Canada*, Map 1874A.

McMechan, M.E., and Thompson, R.I. (1995b): Geology, Belcourt Lake, West of Sixth Meridian, British Columbia; *Geological Survey of Canada*, A Series Map 1869A.

McMechan, M.E., and Thompson, R.I. (1995c): Geology, Wapiti Pass, West of Sixth Meridian, British Columbia; *Geological Survey of Canada*, A Series Map 1872A.

McMechan, M.E., and Thompson, R.I. (1995d): Geology, Ovington Creek, West of Sixth Meridian, British Columbia; *Geological Survey of Canada*, A Series Map 1873A.

McMechan, M.E., Thompson, R.I., Cook, D.G., Gabrielse, H., and Yorath, C.J. (1991): Structural styles, Chapter 17 in Geology of the Cordilleran Orogen in Canada, H. Gabrielse and C.J. Yorath (editors); *Geological Survey of Canada*, Geology of Canada No. 4, pages 634–650.

Moslow, T.F., and Davies, G.R. (1992): Triassic reservoir facies and exploration trends: Western Canada Sedimentary Basin; Canadian Society of Petroleum Geologists, Short Course Number 7 Notes, *Canadian Society of Petroleum Geologists – American Association of Petroleum Geologists* Conference: June 25–26, Calgary, AB, 166 pages.

Pell, J., Hammack, J.L., Fletcher, B., Harris, W.D., and Koyanagi, V. (1992): Kakwa Recreation Area geology (93H/15, 16 and 93I/1, 2); *B.C. Ministry of Energy, Mines and Petroleum Resources*, Open File 1992-10.

Pelletier, B.R. (1960): Triassic stratigraphy, Rocky Mountain Foothills northeastern British Columbia; *Geological Survey of Canada*, Paper 60-2, 32 pages.

Pelletier, B.R. (1961): Triassic stratigraphy of the Rocky Mountain and Foothills northeastern British Columbia; *Geological Survey of Canada*, Paper 61-8, 32 pages.

Pelletier, B.R. (1963): Triassic stratigraphy of the Rocky Mountain and Foothills, Peace River District, British Columbia; *Geological Survey of Canada*, Paper 62-26, 43 pages.

Richards, B.C., Ross, G.M., and Utting, J. (2002): U-Pb geochronology, stratigraphy and sedimentology of tuff in the Upper Frasnnian to Tournaision Exshaw Formation: Evidence for a Late Famenian magmatic arc, *in* Carboniferous of the World, L.V. Hills, C.M. Henderson and E.W. Bamber (editors); *Canadian Society of Petroleum Geologists*, Memoir 19, pages 158–207.

Riediger, C.L. (1997): Geochemistry of potential hydrocarbon source rocks of Triassic age in the Rocky Mountain foothills of northeastern British Columbia and west-central Alberta; *Bulletin of Canadian Petroleum Geology*, Volume 45, pages 719–741.

Riediger, C.L., Carrelli, G.G., and Zonneveld, J.P. (2004): Hydrocarbon source rock characterization and thermal maturity of the Upper Triassic Baldonnel and Pardonet Formations, northeastern British Columbia, Canada; *Bulletin of Canadian Petroleum Geology*, Volume 52, pages 277–301.

Root, K.G. (2001): Devonian Antler fold and thrust belt and foreland basin development in the southern Canadian Cordillera: implications for the Western Canada Sedimentary Basin; *Bulletin of Canadian Petroleum Geology*; Volume 49; pages 7–36.

Ross, G.M., Gehrels, G.F., and Patchett, P.J. (1997): Provenance of Triassic strata in the Cordilleran miogeocline, western Canada; *Bulletin of Canadian Petroleum Geology*, Volume 45, pages 461–473.

Stott, D.F. (1998): Fernie Formation and Minnes Group (Jurassic and Lowermost Cretaceous), northern Rocky Mountain Foothills, Alberta and British Columbia; *Geological Survey of Canada*, Bulletin 516, 516 pages.

Stott, D.F., McMechan, M.E., Taylor, G.C., and Muller, G.E. (1983): Geology of Pine Pass (Mackenzie) map area NTS 93 O, British Columbia; *Geological Survey of Canada*, Open File Report 925.

Taylor, G.C. (1979): Trutch (94G) and Ware east half (94F, E1/2) map-areas, northeastern British Columbia; *Geological Survey of Canada*, Open File Report 606.

Thompson, R.I. (1989): Stratigraphy, tectonic evolution and structural analysis of the Halfway River map area (94B), northern Rocky Mountains, British Columbia; *Geological Survey of Canada*, Memoir 425, 119 pages.

Wheeler, J.O., and McFeely, P. (1991): Tectonic assemblage map of the Canadian Cordillera and adjacent parts of the United States of America; *Geological Survey of Canada*, Map 1712A, Scale 1:2 000 000.

Zonneveld, J.-P. (2008): Triassic sedimentary framework and sequence stratigraphy, Williston Lake, British Columbia; *Canadian Society of Petroleum Geologists*, Field Trip Guidebook.

Zonneveld, J.-P., Carrelli, G.G., and Riediger, C. (2004): Sedimentology of the Upper Triassic Charlie Lake, Baldonnel and Pardonet formations from outcrop exposures in the southern Trutch region, northeastern British Columbia; *Bulletin of Canadian Petroleum Geology*, Volume 52, pages 343–375.

Zonneveld, J.-P., Gingras, M.K., and Pemberton, S.G. (2001): Trace fossil assemblages in a Middle Triassic mixed siliciclastic-carbonate marginal marine depositional system, British Columbia; *Palaeogeography, Palaeoclimatology, Palaeoecology*, Volume 166, pages 249–276.

Zonneveld, J.-P., Moslow, T.F., and Henderson, C.M. (1997): Lithofacies associations and depositional environments in a mixed siliciclastic-carbonate coastal depositional system, upper Liard Formation, Triassic, northeastern British Columbia; *Bulletin of Canadian Petroleum Geology*, Volume 45, pages 553–575.

THE ROLE OF QUATERNARY GEOLOGY IN NORTHEASTERN BRITISH COLUMBIA'S OIL AND GAS INDUSTRY: A SUMMARY

Adrian S. Hickin[1]

ABSTRACT

Quaternary geology, the field within the earth sciences that is concerned with the geological record of the last 2.6 million years, has typically received little attention from the oil and gas industry. Quaternary-aged sediments are, however, significant to the oil and gas industry for a variety of reasons. This paper discusses four aspects of Quaternary geology in northeast British Columbia that have a direct impact on the development of oil and gas resources: (1) shallow gas; (2) groundwater aquifers; (3) surficial geology; and (4) aggregate resources.

Quaternary-aged sediments host natural gas in northeast British Columbia and northwest Alberta. Gas was discovered in Quaternary reservoirs in Alberta in 1988 and has seen modest development. Several wells in British Columbia have produced from reservoirs within Quaternary sediments. These reservoirs are likely associated with the valley-fill sediments of incised paleovalleys that have little or no surface expression. The reservoirs are fluvial and glaciofluvial units underlying clay-rich till and glaciolacustrine seals. Gas in these reservoirs is rare; however, these same units commonly host water, of which some form artesian aquifers. With water demand continuing to increase, particularly where tight or shale gas plays require large volumes of water for hydraulic fracturing, groundwater aquifers may be an important water source.

Surface engineering and infrastructure development associated with the oil and gas industry require an understanding of the properties and distribution of surface materials, most of which are Quaternary deposits. Surficial geology mapping, therefore, provides important baseline data for these activities. The British Columbia Ministry of Energy, Mines and Petroleum Resources and its partners, the Geological Survey of Canada and the University of Victoria, are currently mapping regions of northeast British Columbia at the 1:50 000 scale in an effort to provide industry with this fundamental data. In addition, the Ministry's Oil and Gas Division, through the Aggregate and Surficial Mapping Program, is continuing to work with industry, government, and academic partners to identify and evaluate local sources of construction aggregate for new, quality roads into undeveloped areas and to extend the drilling season to non-winter months.

Hickin, A. S. (2009): The Role of Quaternary Geology in Northeastern British Columbia's Oil and Gas Industry: a Summary; Geoscience Reports 2009, *BC Ministry of Energy, Mines and Petroleum Resources*, pages 25–37.

[1]British Columbia Ministry of Energy, Mines and Petroleum Resources, 1810 Blanshard Street, Victoria, British Columbia

Key Words: Quaternary geology, surficial geology, surficial mapping, shallow gas, groundwater, sand and gravel, aggregate, infrastructure, roads.

INTRODUCTION

Quaternary geology typically involves the study of poorly consolidated or unconsolidated sediment that occurs above bedrock. These sediments are sometimes referred to as overburden or drift and have received little attention from the oil and gas industry, yet the distribution and character of these deposits have significant impact on the economics, safety, and marketability of British Columbia's oil and gas resources. This paper introduces some aspects of Quaternary geology that are significant to oil and gas industry in northeast British Columbia.

The Quaternary was marked by worldwide climatic deterioration and cyclic global temperature oscillation that began at the end of the Piacenzian stage of the Pliocene (2.6 million years ago). Marine oxygen isotope data from the shells of foraminifera recovered in deep ocean cores offer extensive record of global ice build-up and melt (Urey, 1947; Emiliani, 1955; Emiliani, 1966; Shackleton, 1967; Imbrie and Imbrie, 1980; Gibbard et al., 2005; Bassinot, 2007; Rohling, 2007). These data suggest that a little over 50 oscillations have occurred during which temperatures were sufficiently low to have allowed global ice sheets and glaciers to grow and retain enough water to isotopically fractionate the Earth's oceans. These oscillations, termed Marine Isotope Stages (MIS), count back from the present warm period (MIS 1; Figure 1). This implies that the Earth has experienced repeated glaciations, which have modified the landscape. Each successive event obliterated much of the

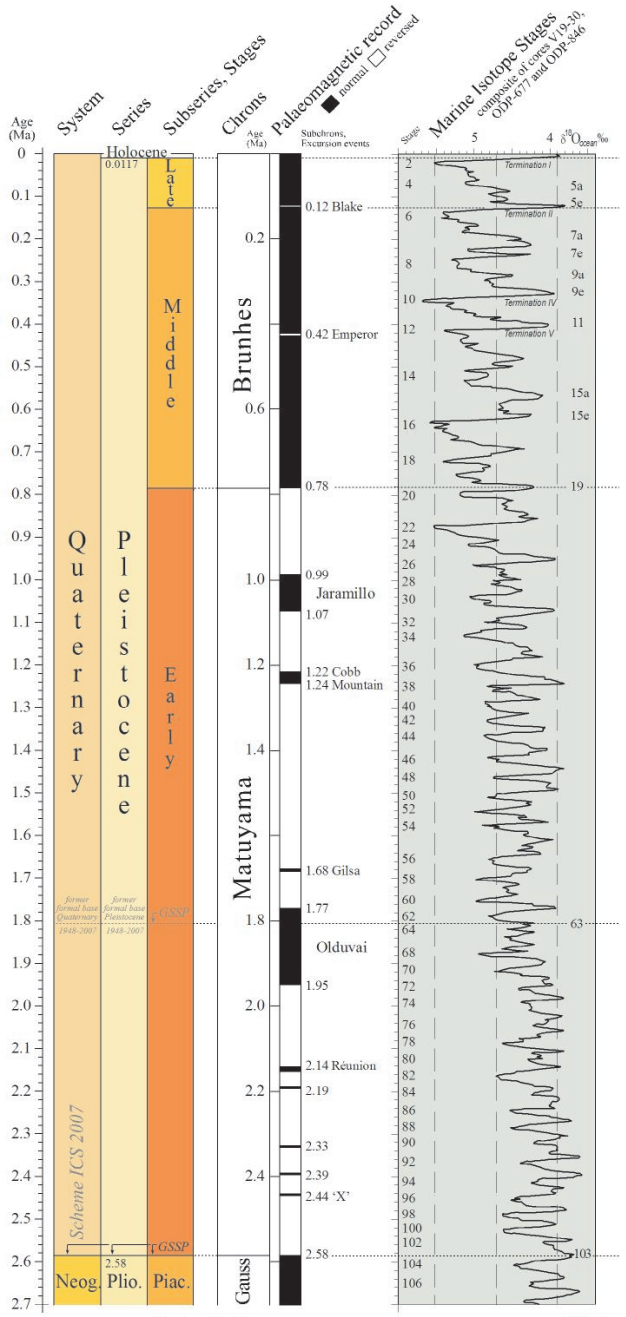

Figure 1. Quaternary geological timescale (modified from Gibbard, et al., 2005). *The Marine Isotopic Stages (MIS), on the right, show the cyclical nature of ocean isotopic fractionation associated with global temperature oscillations. Glacial conditions are inferred where dO18 values deviate to the left (oceans are enriched in 18O isotopes; even numbered MIS). Warmer interstadial or interglacial conditions are inferred where dO18 values deviate to the right (oceans enriched with light isotopes; odd numbered MIS).*

evidence of its predecessor, with the exception of rare deposits that were buried, protected, and therefore preserved. The most recent glacial event to affect northeast British Columbia is referred to in North America as the Wisconsinan glaciation, which is further divided into Early Wisconsinan cold period (MIS 4 to 5e), Middle Wisconsinan interstadial or warm period (MIS 3), and Late Wisconsinan cold period (MIS 2). Although there is some contention regarding the timing of events, it is likely that most of the surface geology in northeast British Columbia is the product of Late Wisconsinan glaciation, which occurred between 22,000 and 10,000 years ago, although it is possible that some is associated with the Early Wisconsinan (between 100,000 and 60,000 years ago) (Mathews 1978; Mathews 1980; Liverman et al. 1989; Bobrowsky and Rutter 1992; Catto et al. 1996; Bednarski and Smith 2007; Bednarski 2008a; Hartman and Clague 2008).

During the Wisconsinan, northeast British Columbia was affected by three glacial systems: (1) local montane glaciers; (2) the Cordilleran Ice Sheet; and (3) the Laurentide Ice Sheet (Catto et al. 1996). The Montane glaciers originated in high mountains as ice caps and ice fields that were drained by topographically controlled valley glaciers. The Cordilleran Ice Sheet was a continental-scale ice sheet that formed when ice accumulating in both the Rocky Mountains and the Coast Mountains merged to form a single ice mass over much of British Columbia. The ice centre was located in the Intermontane Belt in central British Columbia and reached sufficient thickness and elevation to radiate outward and flow across major mountain belts to the coast and onto the interior plains (Clague 1989; Jackson et al. 1999; Stumpf et al. 2000; McCuaig and Roberts 2002; Bednarski and Smith 2007). The Laurentide Ice Sheet occupied most of Canada and portions of northern United States at its maximum extent (Figure 2). The western sector of the Laurentide sheet advanced to the west and southwest from the Keewatin Ice Dome in the Canadian Arctic. It advanced up the regional slope, blocked major drainage routes, and caused large glacial lakes to develop along its margins. In the Late Wisconsinan, the Cordilleran and Laurentide ice sheets converged, resulting in continuous ice cover from Atlantic to Pacific Canada (Dyke and Prest 1987; Dyke et al. 2003). As climate warmed at the end of the Wisconsinan, ice sheets could not be sustained, and they eventually retreated. The Cordilleran Ice Sheet retreated into the mountains and was reduced to ice caps and fields, again, sourcing montane glaciers in the major valleys. The Laurentide Ice Sheet retreated to the east, once again blocking regional drainage and impounding large glacial lakes along its margin (Mathews 1980; Dyke and Prest 1987; Dyke et al. 2003; Bednarski 2008a). Northeast British Columbia was ice free by approximately 13,000 years ago (Wolfe et al. 2004; Wolfe et al. 2007).

QUATERNARY HOSTED ULTRA-SHALLOW GAS

Quaternary sediments in British Columbia have potential to host natural gas, particularly in buried paleovalleys, therefore these Quaternary deposits have direct economic

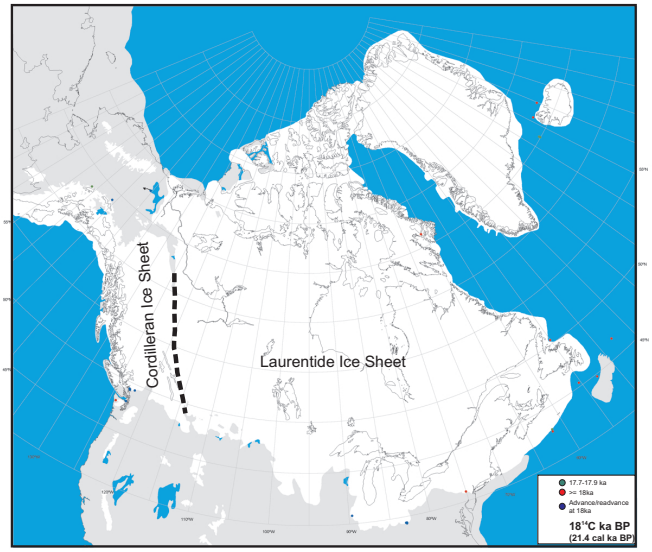

Figure 2. Maximum extent of the Laurentide and Cordilleran ice sheets (modified from Dyke et al. 2003).

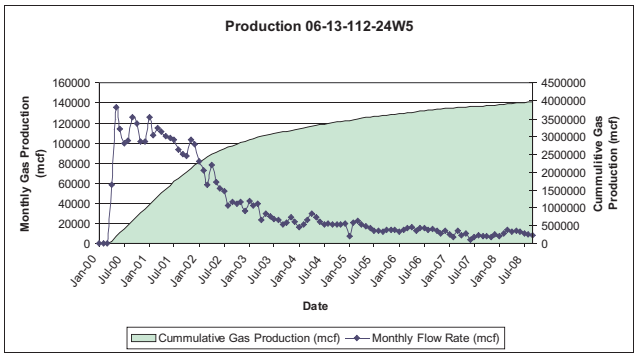

Figure 3. Natural gas production from a Quaternary reservoir in northwest Alberta (well 6-13-112-24W5) (source: IHS Accumap).

importance to the oil and gas industry (British Columbia Ministry of Energy, Mines and Petroleum Resources 2006). Gas was first discovered in Quaternary reservoirs in northern Alberta in 1988 and was brought into production in 1993 (Clare 1988; Canadian Discovery Digest 2001). The initial discovery was the result of a drilling accident during the completion of a water well 80 km west of High Level, Alberta. This well was drilled to 91 m, when a gas blow-out ignited and burned down the water drill rig (Clare 1988). Since discovery, there has been moderate success in developing Quaternary pools in the area; for example, well 6-13-112-24W5 had a cumulative production of 3.97 billion cubic feet (bcf) of gas between April 2000 and September 2008 (Figure 3). In British Columbia, three non-confidential wells (Figure 4) and one confidential well have produced from reservoirs designated as Quaternary. The reservoirs are likely hosted within the fill succession of buried paleovalleys. These pools are less than 300 m deep, are small, and have low pressure, but may be economic if developed near existing infrastructure (i.e., pipelines) or as a supplementary target in deeper wells. The valley-fill successions consist of a variety of lithologic units, including sand and gravel associated with fluvial and glaciofluvial deposits, silt and clay-rich glaciogenic diamicts (till), and sand, silt, and clay glaciolacustrine units (e.g., Figure 5). The reservoir units are likely the porous sand and gravel deposits, and the seal units are clay-rich glaciolacustrine and till units. Potential coarse-grained reservoir units can often be differentiated from fine-grained seal units in gamma logs, even behind casing, and it is recommended that exploration and development companies complete gamma logs to surface to identify these horizons (Figure 6). Source gas for these units is likely derived from the underlying bedrock. Gas may have migrated from gas-bearing bedrock incised by paleovalleys or through subcropping faults that provide a conduit for gas in bedrock units to escape into the valley-fill sediments (Figure 7).

Quaternary ultra-shallow gas was an active exploration target in British Columbia during the early part of this decade but has declined in more recent years. Identifying and mapping paleovalleys, however, remains important for other reasons, such as drilling safety and seismic processing and interpretation (Levson et al. 2006).

Inadvertent intersection of Quaternary hosted artesian aquifers or natural gas reservoirs without appropriate diverters or blowout preventers has cost the oil and gas industry millions of dollars through lost time, abandonment of wells, and destruction of equipment (Levson et al. 2006; Hickin et al. 2008). Blowouts have resulted in injury and even fatalities. These dangers prompted the British Columbia Oil and Gas Commission to issue an alert to drilling operators in 2005, warning of the potential to encountering natural gas and water in Quaternary sediments in northeast British Columbia, even while setting surface casing. Therefore, understanding the location, geometry, and stratigraphy of paleovalleys is of considerable importance for safety in the oil and gas industry. The thick packages of unconsolidated sediments of paleovalleys also present a challenge to the seismic industry. These sediments tend to reduce the propagation velocity of seismic waves relative to consolidated rock. The results are 'slow zones' that can distort later, deeper reflections. Processing can mitigate distortion if the depth and geometry of the unconsolidated zone can be determined.

Bedrock topography and drift thickness mapping and regional airborne electromagnetic surveys are initiatives that can help identify paleovalleys and thick sections of Quaternary sediments (Hickin and Kerr 2005; Levson et al. 2006). The Fontas map sheet (NTS 094I) is the only area in northeast British Columbia in which the bedrock topography has been mapped and is available as public domain data (Hickin et al. 2008), though work is being conducted in the Charlie Lake area (NTS 094A).

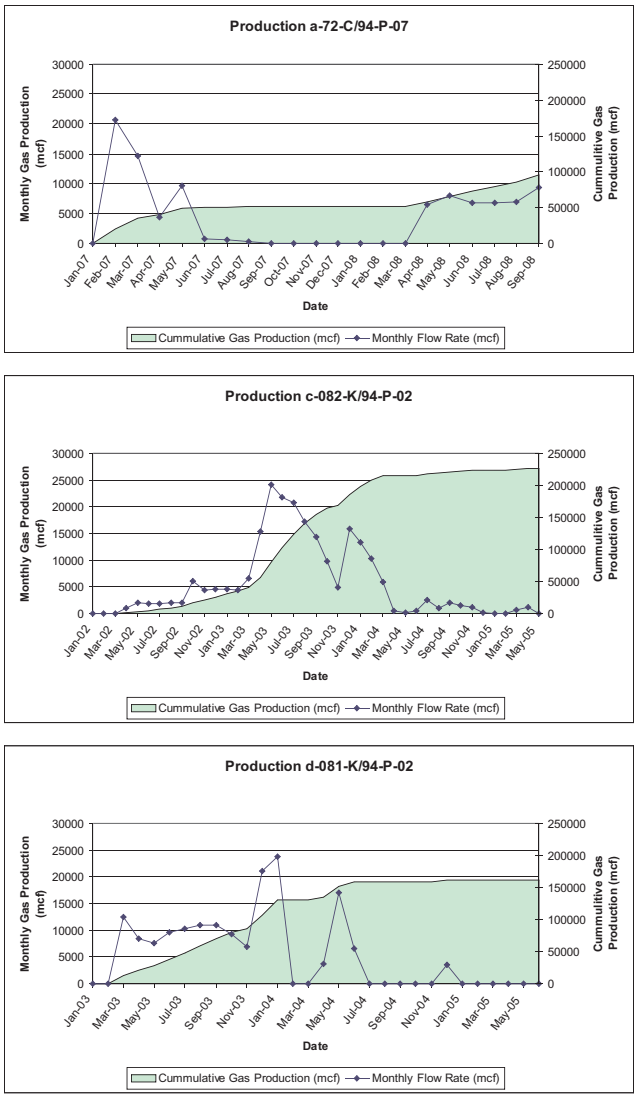

Figure 4. Natural gas production from three non-confidential wells that have been designated by the British Columbia Oil and Gas Commission as producing from Quaternary reservoirs (source IHS Accumap).

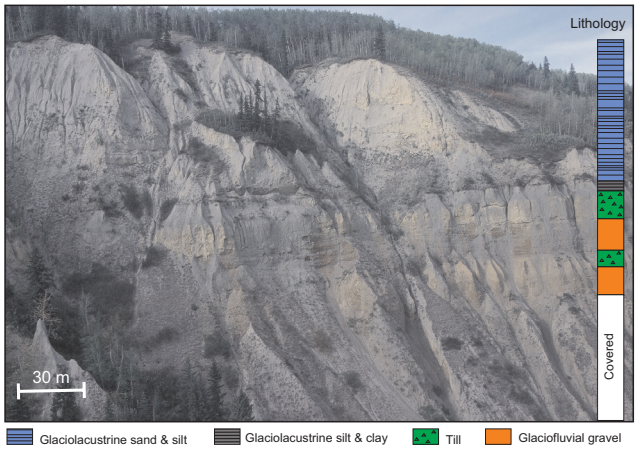

Figure 5. Incising of the Pine River into its paleovalley has revealed large sections of Quaternary valley-fill sediments.

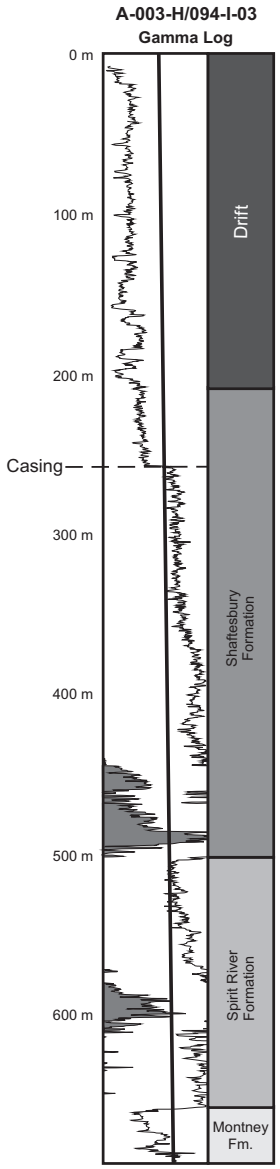

Figure 6. Example of a gamma log that shows over 200 m of Quaternary valley-fill sediments (Drift) from a paleovalley in northeast BC (from Hickin and Kerr, 2005).

GROUNDWATER AQUIFERS

Groundwater is becoming an important resource for oil and gas activity in northeast British Columbia. This is especially true in the development of shale and tight gas, relatively new unconventional natural gas plays that have become the focus of recent exploration in British Columbia (Adams et al. 2008). Though traditionally shale has been considered a source rock or reservoir seal, organic-rich silty shale is now being developed as a reservoir rock. To develop shale gas, flow is stimulated by hydraulically fracturing ("fracing") the target rock, thereby increasing its permeability and surface area. Fracing is accomplished by pumping large volumes of frac fluid (usually water based) and proppant (typically well rounded quartz sand)

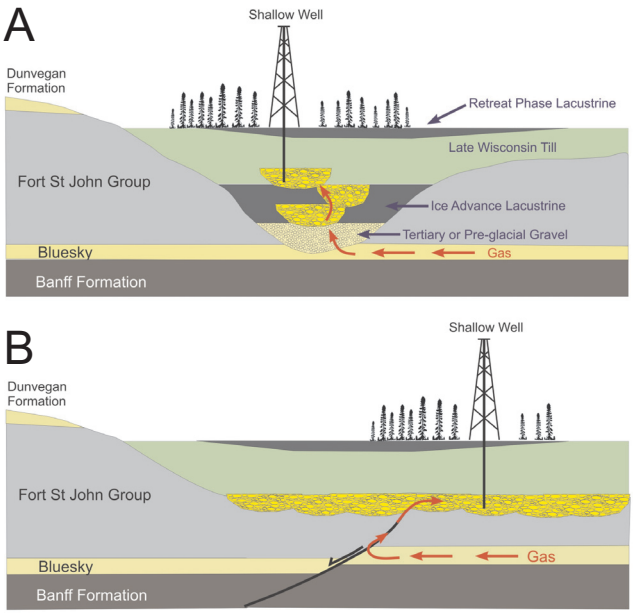

Figure 7. Two conceptual models for the emplacement of natural gas in Quaternary hosted reservoirs (Pawlowicz et al. 2004). A) The incised paleovalley has intersected a gas bearing sandstone unit, permitting the gas to migrate into channel gravel. B) Bedrock faulting provides a conduit for natural gas to migrate from gas bearing units, through the seal, to be trapped in the basal gravel units of the Quaternary sequence.

into the well bore at sufficient pressure to fracture the rock. Proppants keep the fractures open and allow liberated gas to flow back up the well bore. Surface water, deep bedrock aquifers, and Quaternary/Tertiary groundwater aquifers are the main sources of fracing water in northeast British Columbia. Surface water has environmental and competing resource considerations. Deep bedrock formations may host a significant source of saline water. Unfortunately, the geological character of deep bedrock formations, such as the Mississippian Debolt, are not suitable everywhere to host aquifers (i.e., there is insufficient porosity or permeability), consequently, these formations may not be available as a water source or for water disposal. Groundwater from Quaternary aquifers may be an important alternative water source, especially in remote areas.

The same coarse-grained units within valley-fill successions that potentially host gas, more commonly host water. The British Columbia Ministry of Environment's water well database reports 1660 water wells in the Fort St. John and Peace River South area (Alberta Plateau). Of these, 58.9% draw water from unconsolidated aquifers, 29.3% from bedrock aquifers, and 11.8% have no designation. Mean yields from wells that report data (53% of all the wells) are higher in the unconsolidated aquifers than in the bedrock (Table 1). North of the Fort St. John area, there are very little data reported, and almost all comes from around Fort Nelson. The limited data available show that unconsolidated aquifers have substantially higher yields than do bedrock aquifers. In some extreme cases, artesian Quaternary aquifers have extremely high yields that have compromised oil and gas drilling operations. Hickin et al. (2008) report water blowouts from three wells with flow rates of 83 L/s, 283 L/s, and 350 L/s from depths of 89 m, 115 m, and 150 m, respectively. Though intersecting these aquifers resulted in undesirable effects on drilling, it demonstrates that Quaternary aquifers may represent excellent source water targets for the oil and gas industry. Understanding and evaluating these aquifers is, therefore, imperative for meeting water demands in northeast British Columbia, not only for the oil and gas industry, but for residents, agriculture, and other concerned stakeholders.

SURFICIAL GEOLOGY

Surficial geology and high resolution topographic mapping provide important baseline data for oil and gas surface engineering. These data are fundamental for planning and construction of roads and pipelines, locating suitable ground for well lease development, exploring for construction aggregate, land management, and delineating terrain hazards such as unstable slopes. Surficial geology mapping is the foundation for derivative products such as gravel prospect maps and bio-terrain mapping (which delineates areas of ecological significance for wildlife, wetlands, and forest management).

TABLE 1. DESCRIPTIVE STATISTICS OF WATER WELL YIELDS FOR THE ALBERTA PLATEAU (FORT ST. JOHN AND FORT NELSON.

Statistic	Alberta Plateau						Fort Nelson			
	Bedrock		Unconsolidated		Unknown		Bedrock		Unconsolidated	
	L/s	gpm (US)	L/s	gpm (US)	L/s	gpm (US)	L/s	gpm (US)	L/s	gpm (US)
Mean	0.59	9.32	1.09	17.34	1.91	30.34	0.25	3.89	2.64	41.79
Standard Error	0.06	0.98	0.17	2.74	0.52	8.20	0.05	0.79	0.63	9.99
Median	0.38	6.00	0.50	8.00	0.79	12.50	0.19	3.00	1.42	22.50
Mode	0.63	10.00	0.32	5.00	1.26	20.00	0.19	3.00	0.25	4.00
Standard Deviation	1.11	17.53	3.68	58.35	5.28	83.64	0.21	3.37	2.96	46.86
Sample Variance	1.22	307.29	13.56	3405.18	27.85	6995.38	0.05	11.37	8.74	2196.01
Minimum	0.01	0.10	0.00	0.03	0.03	0.50	0.06	1.00	0.06	1.00
Maximum	15.78	250.00	43.16	684.00	50.48	800.00	0.95	15.00	9.47	150.00
No. Wells	323	323	453	453	104	104	18	18	22	22

Source: British Columbia Ministry of Environment water well database

Surficial mapping is done at a variety of scales for various purposes. These scales can be divided into three general categories: (1) reconnaissance (≥ 1:100,000); (2) regional (1:50 000 to 1:100,000); or (3) local (< 1:50,000). Reconnaissance mapping is typically done at 1:100,000 or 1:250,000 and is best suited for contextual purposes such as reconstructing glacial history. Context is important as it provides insight necessary to guide more focused studies. For example, understanding the location and evolution of a large glacial lake will assist aggregate exploration by directing activities to the former lake margins, where ancient deltas and beaches may have occurred, rather than expending resources exploring in the central portions of the lake basin, where fine-grained materials would dominate. Perhaps the most useful mapping for operational activities in the oil and gas industry is the regional scale, typically 1:50,000. This scale minimizes generalizations and offers enough detail to differentiate surface sediments while presenting sufficient area to be beneficial for planning. Local mapping is generally completed at 1:5,000 to 1:20,000 and is most useful for engineering or site-specific evaluations. This scale typically focuses on a limited number of surficial materials, specific properties of materials, or the evaluation of individual landforms and features (e.g., aggregate deposit, river crossing, or pad location).

Generally, northeast British Columbia has limited coverage of regional surficial geology maps despite recent resource exploration activity. The Ministry of Energy, Mines and Petroleum Resources and its partners, the Geological Survey of Canada and the University of Victoria, are currently conducting 1:50 000-scale mapping in several areas in northeast British Columbia, including portions of map sheets 93P, 94O, and 94P (Figure 8).

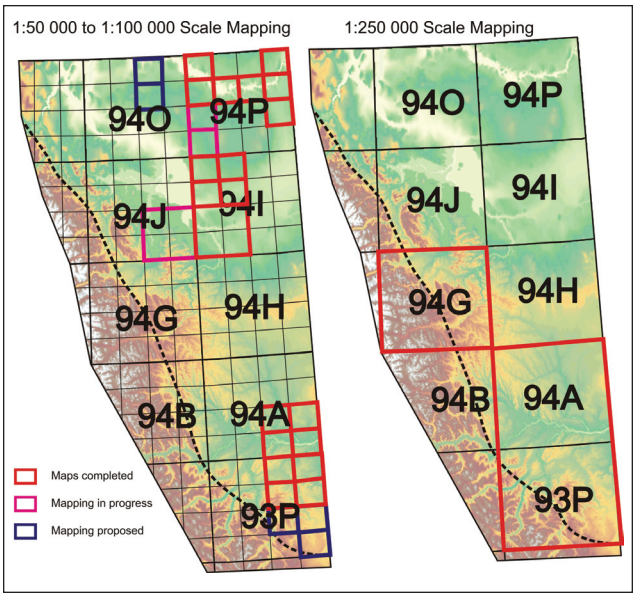

Figure 8. Index of mapping in northeast BC by the British Columbia Ministry of Energy, Mines and Petroleum Resources and its partners, the Geological Survey of Canada and the University of Victoria.

AGGREGATE

In 2003, the Province of British Columbia's Oil and Gas Development Strategy identified road infrastructure as one of the four initiatives necessary for making British Columbia one of the most competitive oil and gas jurisdictions in North America. Physical access to the land represents a challenge for oil and gas development in northeast British Columbia. Traditionally the drilling season in remote muskeg-covered areas was restricted to winter months, when ice roads can be built to bear industry traffic. Road construction is difficult in these areas because of the unfavourable terrain, poor road base, and a general lack of locally available, quality construction aggregate. To address these challenges, the British Columbia Aggregate and Surficial Mapping Program was established in 2002 with two objectives: (1) the regional assessment of aggregate resources and Quaternary geology in areas of oil and gas development; and (2) identification and evaluation of local, area-specific, aggregate resources. This program is meant to facilitate the construction and maintenance of all-season roads throughout British Columbia's traditional oil and gas region.

Conventional aggregate exploration techniques, such as aerial photographic interpretation, have had limited success in the subdued topography of northeast British Columbia. Quaternary geological expertise has, therefore, been called upon to apply new and innovative approaches and technology to locate and evaluate gravel deposits. The program has been exceptionally successful and to date has discovered 12 new deposits, some of which are now at the mining stage. Through these discoveries, the Province has realized cost savings in excess of $40 million on partnership road projects, which is more than a $30 return on investment for every dollar spent on the program. A list of published maps, articles, and theses produced as part of the program is provided in Table 2.

The program is highly collaborative with partnerships in other government agencies, academia, and industry. Contributing government partners include several municipalities, other provincial agencies, the Alberta Geological Survey, the Canadian Centre for Remote Sensing, and the Geological Survey of Canada. The program has involved collaboration with the University of Victoria, the University of Calgary, and the University of the Fraser Valley. Eight major energy companies and three consulting or contracting companies have partnered directly with the program.

In general terms, the project relies on the expertise of provincial, federal, and academic Quaternary geoscientists affiliated with the program to recognize, locate, and evaluate deposits from new and often confidential data shared by

TABLE 2. PUBLICATION FROM THE BRITISH COLUMBIA AGRREGATE AND SURFICIAL MAPPING PROGRAM.

Publications	Title	References
Aggregate Prospecting Reports	Aggregate potential of the Kimea Creek Area, northeastern British Columbia (2008-1)	Ferbey, 2008
	Aggregate potential of selected terraces along the East Kiskatinaw River, northeastern British Columbia (2006-1)	Hickin, 2006
Maps	Surficial Geology, TBD (094I/SE)	Trommelen and Levson, (in progress)
	Surficial Geology, Komie Creek, British Columbia (094P/05)	Demchuk and Levson, (in progress)
	Surficial Geology, Corvoisier Creek, British Columbia (094P/04)	Demchuk and Levson, (in progress)
	Surficial Geology, Lichen Creek, British Columbia (094/14)	Smith, 2009d
	Surficial Geology, Gunnell Creek, British Columbia (094I/13	Smith, 2009c
	Surficial Geology, Nogah Creek, British Columbia (094I/12)	Smith, 2009b
	Surficial Geology, Kyklo Creek, British Columbia (094I/11)	Smith, 2009a
	Surficial Geology, Thinahtea Lake, British Columbia (094P/09)	Bednarski, 2008d
	Surficial Geology, Pesh Creek, British Columbia (094P/08)	Bednarski, 2008c
	Surficial Geology, June Lake, British Columbia (094P/16)	Bednarski, 2008b
	Surficial Geology, Kimea Creek, British Columbia (094P/10)	Bednarski, 2007b
	Surficial geology, Etset Lake, British Columbia (094P/11)	Bednarski, 2007a
	Surficial geology, Dazo Creek, British Columbia (94I/SW)	Trommelen and Smith, 2007
	Surficial geology, Gote Creek, British Columbia (094P/12)	Bednarski, 2005b
	Surficial geology, Estsine Lake, British Columbia (094P/13)	Bednarski, 2005a
BC Government Geoscience Articles	Surficial geology and aggregate potential mapping in northeast British Columbia using LiDAR imagery	Demchuk et al., 2005
	Implementing Geomatics technology for aggregate exploration, northeast British Columbia	Kerr et al., 2005
	Northeast British Columbia Aggregate Mapping Program: a summary of selected aggregate occurrences northeast of Fort Nelson	Ferbey et al., 2005
	Bedrock topography mapping and shallow gas in Northeastern British Columbis	Hickin and Kerr, 2005
	Quaternary geology of Fort Nelson (NTS 094J/SE) and Fontas River (NTS 094I/SW), northeastern British Columbia	Trommelen et al., 2005
	Surficial mapping and granular aggregate resource assessment in northwest Alberta	Smith et al., 2005
	Surficial geology and aggregate studies in the boreal plains of northeast British Columbia	Levson et al., 2005
	Sand and gravel mapping in northeast British Columbia using Airborne Electromagnetic surveying methods	Best et al., 2004
	Quaternary geology and aggregate potential of the Fort Nelson airport area	Johnsen, 2004
	Preliminary report on Aggregate potential investigation of Fort Nelson airport area, Fort Nelson, British Columbia	Ferbey et al., 2004
	Quaternary geology and aggregate mapping in northeast British Columbia: Applications for oil and gas exploration and development	Levson et al., 2004
Consultant Reports	Sierra-YoYo-Desan Road area gravel investigation, northeastern BC	Dewer and Polysou, 2003
External Journal Paper	Using ground-penetrating radar and capacitively coupled resistivity to investigate 3-D fluvial architecture and grain-size distribution of a gravel floodplain in northeast British Columbia, Canada	Hickin et al., 2009
	Landform assemblages produced by the Laurentide Ice Sheet in northeastern British Columbia and adjacent Northwest Territories — constraints on glacial lakes and patterns of ice retreat	Bednarski, 2008a
	Mapping Quaternary paleovalleys and drift thickness using petrophysical logs, northeast British Columbia, Fontas map sheet, NTS 94I	Hickin et al., 2008
	Quaternary stratigraphy of the Prophet River, northeastern British Columbia	Trommelen and Levson, 2008
	Airborne electromagnetic mapping for buried Quaternary sand and gravel in northeast British Columbia	Best et al., 2006
	Mapping High Resistivity Buried Channel Deposits with Airborne Electromagnetic Surveys and Other Methods	Levson et al., 2006
Thesis	Landscape Evolution of the Dawson Creek map area (93P)	Hickin, PhD (in progress)
	TBD	Demchuk, MSc (in progress)
	Quaternary stratigraphy and glacial history of the Fort Nelson (southeast) and Fontas River (southwest) Map Areas (094J/SE and 094I/SW), Northeastern British Columbia	Trommelen, MSc 2007

industry partners. For example, the Program has been successful in identifying aggregate deposits from high-resolution light detection and ranging (LiDAR) data sets, which are routinely collected by the oil and gas industry. These data are the most effective tool for identifying deposits with subtle surface expression (e.g., Figure 9).

In addition to the collaborative use of industry data, the program has invested in developing innovative techniques to explore for gravel. The program has successfully employed airborne and ground-based geophysical methods to identify and evaluate prospects. Frequency domain airborne electromagnetics (EM) was successfully used to delineate a gravel deposit (Best et al. 2004; Levson et al. 2006). This method proved to be an effective tool for determining the lateral extent of the deposit and providing an estimate of the thickness, even under as much as 5 m of clay-rich till (Figure 10). Helicopter-borne frequency domain EM with a line spacing of 100 to 200 m offers high-resolution data over relatively large areas with vertical depth of penetration on the order of several tens of metres. Because gravel has

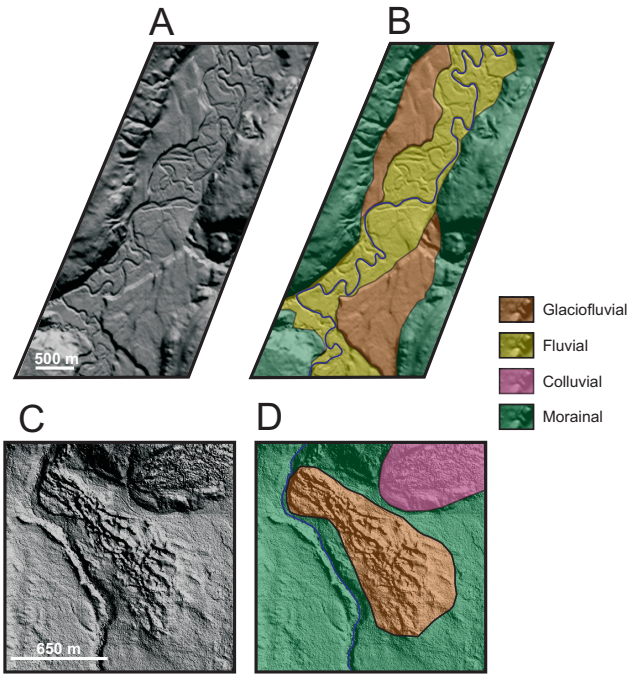

Figure 9. LiDAR is the most useful tool for mapping subtle features in northeast BC A) Digital elevation model (DEM) from LiDAR of a river floodplain and adjacent terraces along the East Kiskatinaw River (modified from Hickin, 2006). B) Interpretation of LiDAR where glaciofluvial terraces are excellent targets for aggregate deposits. C) LiDAR DEM of an esker complex in the Komie area. D) Interpretation of LiDAR where the glaciofluvial deposit is an aggregate target (Modified from Demchuk et al., 2005).

high resistivity relative to the clay-rich till and local shale, high resistivity regions correlate well with gravel deposits in northeast British Columbia. With the success of airborne EM surveys, the program looked to develop cost-effective ground-based methods to evaluate specific areas without incurring the cost of employing expensive heavy equipment. Capacitively-coupled resistivity (CCR), a relatively new variation of traditional ground-based resistivity, is routinely used by the program for rapid evaluation of potential targets (Figure 11). CCR uses capacitively-coupled dipoles towed behind a snowmobile to measure the apparent resistivity to a depth of about 5 or 6 m (Geometrics 2001). The processed data provide very high resolution 2-D resistivity pseudosections that are used to differentiate conductive fine-grained sediments from resistive granular material (Hickin et al. 2009). In addition, it has been shown that the data can discriminate sand from gravel, and resistivity distributions can even be used as a proxy for sorting. This method has been deployed on several targets to establish preliminary volumes and quality (in very general terms) of granular deposits, therefore helping to determine if additional evaluation through test pitting is justified.

CONCLUSION

Quaternary sediments in northeast British Columbia includes all of the surface materials that lies above bedrock. These materials have received little attention from the oil and gas community, as there is typically more interest in the deeper, petroleum-bearing bedrock formations. Surface materials are, however, significant to the oil and gas industry in northeast British Columbia. The simplest connection for the industry to make with Quaternary sediments is the economic implications of Quaternary natural gas reservoirs. These reservoirs occur between 100 and 300 m below surface, where gas may be hosted in the coarse-grained sand and gravel units within thick sequences that make up the valley-fill successions of incised paleovalleys. Where these units do not host gas, they may host water. Water is becoming increasingly important in the development of tight and shale gas reservoirs. These gas plays typically need huge volumes of water for hydraulic fracturing to stimulate gas flow. Quaternary hosted aquifers, therefore, may be significant sources of frac water in the absence of productive bedrock aquifers.

Surficial geology has important implications for the development of a gas field. Surface engineering, pipeline and road construction, land use planning, and development strategies are closely linked to topography and surficial material. The demand for Quaternary geology and surficial mapping continues to increase as development escalates in northeast British Columbia. Mapping is the baseline dataset necessary for responsible development and is the foundation for derivative products. The British Columbia Ministry of Energy, Mines and Petroleum Resources and its partners, the Geological Survey of Canada and the University of Victoria, are currently mapping surficial geology at a scale of 1:50 000 in two regions of northeast British Columbia.

Quality aggregate for oil and gas infrastructure devel-

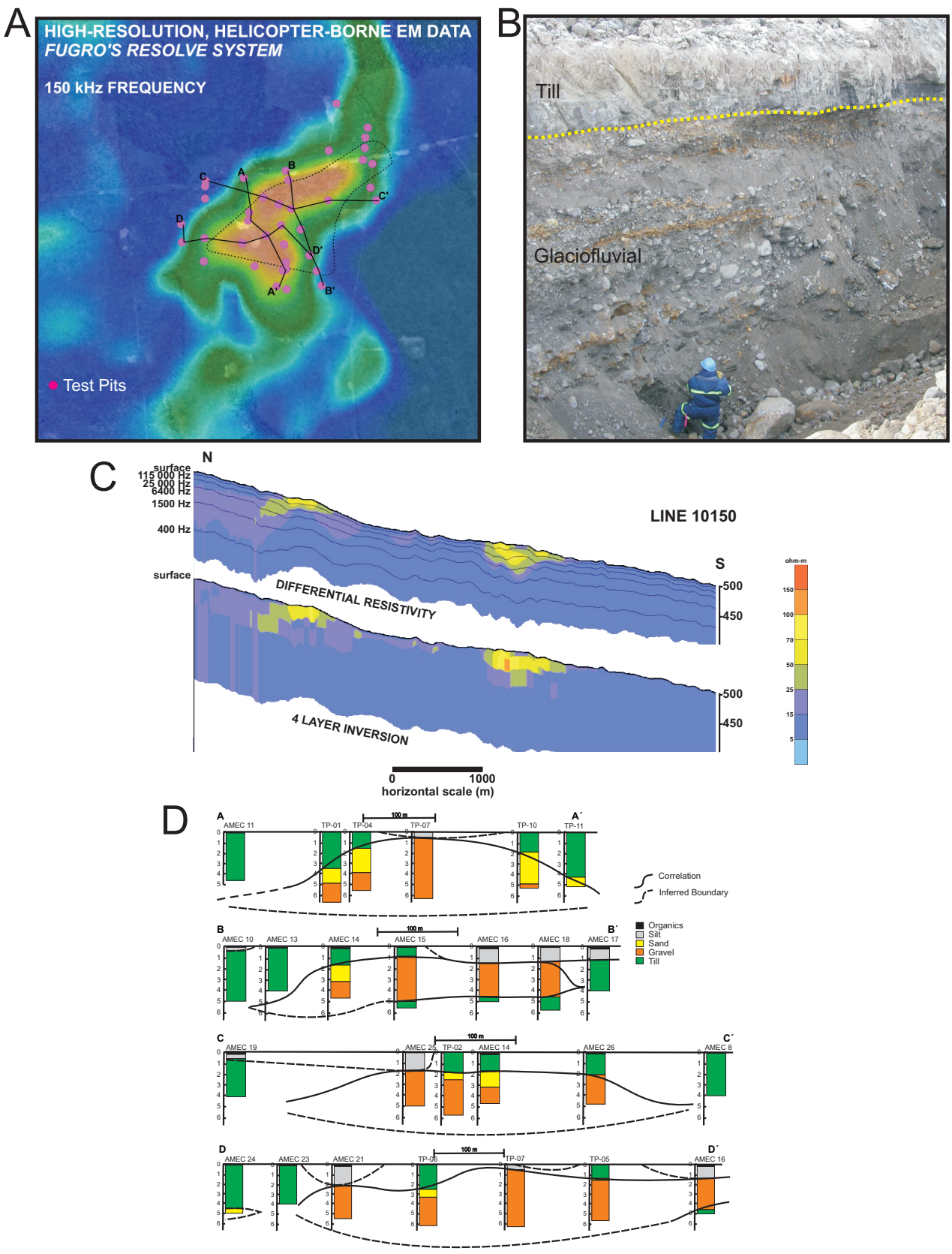

Figure 10. Airborne EM has been used by the British Columbia Aggregate and Surficial Mapping Program to identify and delineate buried aggregate (modified from Levson, et al. 2006 and Ferbey et al., 2007). A) 150 kHz depth slice with test pit locations and cross-section locations (Figure 10D). B) The deposit consists of glaciofluvial gravel under till. C) Pseudosection of EM data indicating thickness of the gravel (warm colours). D) Cross-sections of the gravel deposit, based on test pit data.

opment and maintenance has been identified as a critical limitation for road construction to gain access to the land and for establishing all-season roads that will extend the drilling season to non-winter months. Since inception in 2002, the program has experienced significant success and continues to work with partners to ensure gravel is available in high-demand areas.

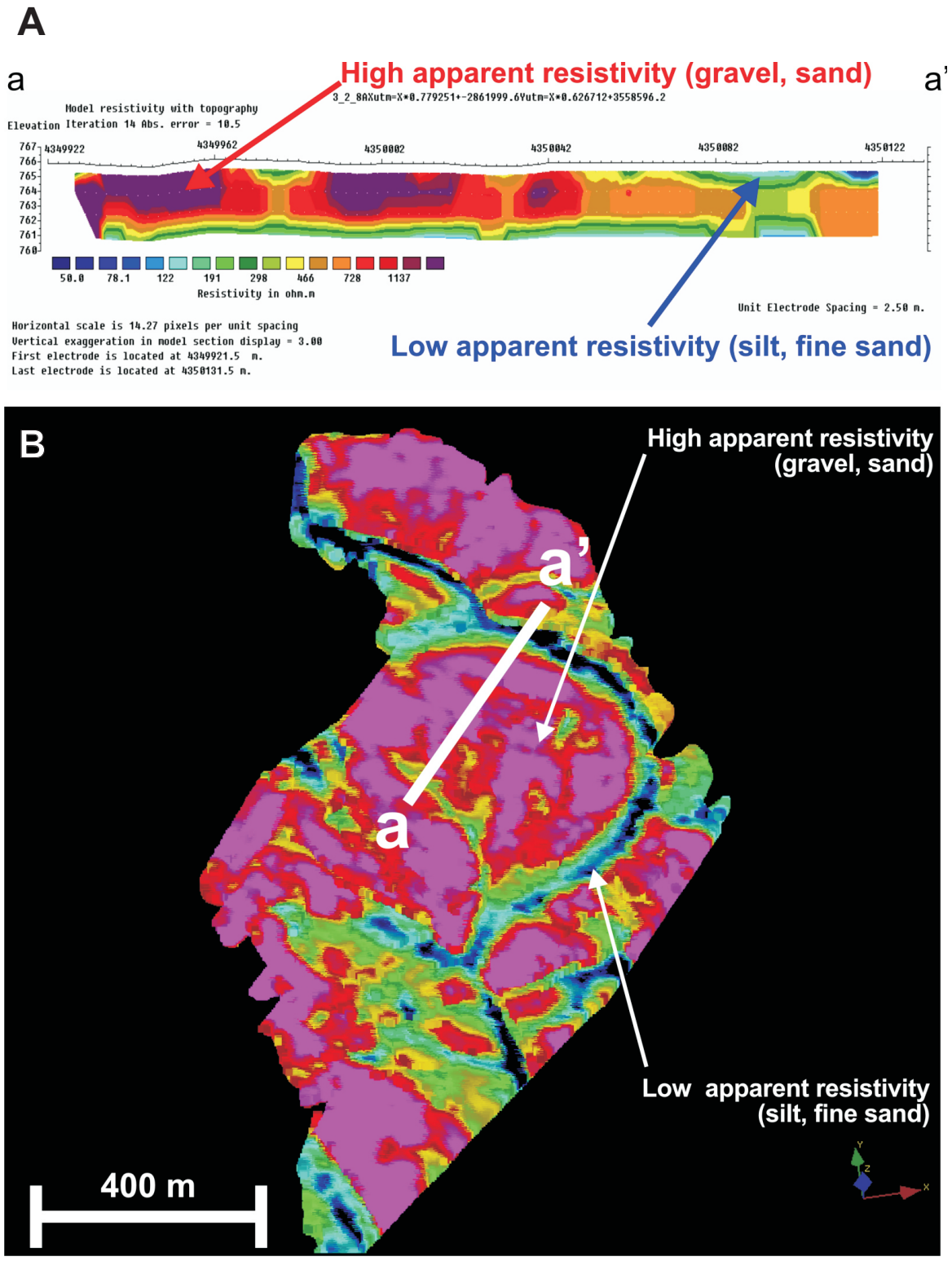

Figure 11. CCR has proven to be an effective tool for prospecting for sand and gravel. A) The 2-D psudosection (see Figure 11B) shows high resistive gravel bars and low resistivity channel deposits. B) The gravel bars can be easily differentiated from the fine-grained channel deposits in this plan view depth slice of the Halfway River floodplain approximately 0.5 m below surface.

ACKNOWLEDGEMENT

The author would like to thank the many industry, government, and academic partners whose participation and collaboration has ensured the success of the Aggregate and Surficial Mapping Program. The project has benefited from the collaborative work of Travis Ferbey, Vic Levson, Tania Demchuk, Ben Kerr, and Mel Best.

REFERENCES

Adams, C., McPhail, S., and Walsh, W. (2008): Summary of shale gas activity in northeast British Columbia 2007; *British Columbia Ministry of Energy, Mines and Petroleum Resources*, Petroleum Geology Open File 2007-1, 10 pages.

Bassinot, F.C., (2007): Oxygen isotope stratigraphy of the oceans; In Ellias, S.A., (editor): *Encyclopedia of Quaternary Science*, Elsevier,New York, Volume 3, pages 1740-1748.

Bednarski, J.M. (2005a): Surficial geology, Estsine Lake, British Columbia (094P/13); *Geological Survey of Canada*, Open File 4825, 1 map (1:50 000 scale).

Bednarski, J.M. (2005b): Surficial geology, Gote Creek, British Columbia (094P/12); *Geological Survey of Canada*, Open File 4846, 1 map (1:50 000 scale).

Bednarski, J.M. (2007a): Surficial geology, Etset Lake, British Columbia (094P/11); *Geological Survey of Canada*, Open File 5506, 1 map (1:50 000 scale).

Bednarski, J.M. (2007b): Surficial geology, Kimea Creek, British Columbia (094P/10); *Geological Survey of Canada*, Open File 5505, 1 map (1:50 000 scale).

Bednarski, J.M. (2008a): Landform assemblages produced by the Laurentide Ice Sheet in northeastern British Columbia and adjacent Northwest Territories - constraints on glacial lakes and patterns of ice retreat; *Canadian Journal of Earth Sciences*, Volume 45, Number 5, pages 593–610.

Bednarski, J.M. (2008b): Surficial geology, June Lake, British Columbia (094P/16); *Geological Survey of Canada*, Open File 5480, 1 map (1:50 000 scale).

Bednarski, J.M. (2008c): Surficial geology, Pesh Creek, British Columbia (094P/08); *Geological Survey of Canada*, Open File 5481, 1 map (1:50 000 scale).

Bednarski, J.M. (2008d) Surficial geology, Thinahtea Lake, British Columbia (094P/09); *Geological Survey of Canada*, Open File 5479, 1 map (1:50 000 scale).

Bednarski, J.M., and Smith, I.R. (2007): Laurentide and montane glaciation along the Rocky Mountain Foothills of northeastern British Columbia; *Canadian Journal of Earth Sciences*, Volume 44, Number 4, pages 445–457.

Best, M.E., Levson, V.M., and McConnell, D. (2004): Sand and gravel mapping in northeast British Columbia using airborne electromagnetic surveying methods; in Summary of Activities 2004, Ferri, F. (editor), *BC Ministry of Energy, Mines and Petroleum Resources*, pages 1–6.

Best, M.E., Levson, V.M., Ferbey, T., and McConnell, D., (2006): Airborne electromagnetic mapping for buried Quaternary sand and gravels in northeast British Columbia; *Journal of Environmental and Engineering Geophysic*s, Volume 11, pages 17-26.

Bobrowsky, P., and Rutter, N.W. (1992): The Quaternary geologic history of the Canadian Rocky Mountains; *Géographie Physique et Quaternaire*, Volume 46 (1), pages 5–50.

British Columbia Ministry of Energy, Mines and Petroleum Resources (2006): Conventional Natural Gas Play Atlas Northeast British Columbia; *British Columbia Ministry of Energy, Mines and Petroleum Resources*, 2006-1, 147 pages.

Canadian Discovery Digest (2001): Exploration Review, Sousa, Northwestern Alberta Twp 111, Rge 2 W6, Quaternary Gas; *Canadian Discovery Digest*, January/February 2001 Report, pages 25-39.

Catto, N., Liverman, D.G.E., Bobrowsky, P.T., and Rutter, N. (1996): Laurentide, Cordilleran, and montane glaciations in the western Peace River - Grande Prairie region, Alberta and British Columbia, Canada; *Quaternary International*, Volume 32, pages 21–32.

Clague, J.J. (1989): Quaternary geology of the Canadian Cordillera, Chapter 1; in Quaternary Geology of Canada and Greenland, Fulton, R.J. (editor), *Geological Survey of Canada*, pages 17–96.

Clare, S. (1988): Water well test drilling and natural gas blowout - Zama Lake south observation well project; *Alberta Environment*, 11 pages.

Demchuk, T.E. , Ferbey, T., Kerr, B.J., and Levson, V.M., (2005): Surficial geology and aggregate potential mapping in northeast British Columbia using LiDAR imagery; in Summary of Activities 2005, *BC Ministry of Energy, Mines and Petroleum Resources*, pages 51–59.

Dewer, D. and Polysou, N., (2003): Area 10 (Kotcho East) gravel investigation - Sierra-Yoyo-Desan Road area, North eastern British Columbia; *AMEC Earth and Environmental Limited*, Report No. KX04335, 13 Pages.

Dyke, A.S., Moore, A., and Robertson, L. (2003): Deglaciation of North America; *Geological Survey of Canada*, Open File 1574, [CD-ROM].

Dyke, A.S., and Prest, V.K. (1987): Late Wisconsinan and Holocene history of the Laurentide Ice Sheet; *Géographie Physique et Quaternaire*, Volume 41 (2), pages 237–263.

Emiliani, C., (1955): Pleistocene temperatures; *Journal of Geology*, Volume 63, pages 538-578.

Emiliani, C., (1966): Paleotemperature analysis of Caribbean cores P6304-8 and P6304-9 and generalized temperature curve for the past 425,000 years: *Journal of Geology*, Volume 74, pages 109-126.

Ferbey, T. (2008): Aggregate potential of the Kimea Creek area, northeastern British Columbia; BC Ministry of Energy, Mines and Petroleum Resources, Aggregate Prospecting Report, 2008-1, 16 pages, 1 map (1:50 000 scale).

Ferbey, T., Hickin, A.S., Demchuk, T.E., and Levson, V.M. (2005): Northeast British Columbia Aggregate Mapping Program: a summary of selected aggregate occurrences northeast of Fort Nelson; in Summary of Activities 2005, *BC Ministry of Energy, Mines and Petroleum Resources*, pages 65-74.

Ferbey, T., Levson, V.M., and Johnsen, T. (2004): Preliminary report on aggregate potential investigation of Fort Nelson airport area, Fort Nelson, British Columbia; *BC Ministry of Energy, Mines, and Petroleum Resources*, 41 pages.

Ferbey, T., Hickin, A.S., Barchyn, T.E., Kerr, B.J., Demchuk, T.E., Clayards, S., Levson, V.M., and Marich, A., (2007): Effective ground geophysical methods for aggregate exploration, in the lowlands of northeast British Columbia; *Canadian Quaternary Association*, Ottawa, poster presentation.

Geometrics (2001): OhmMapper TR1 Operation Manual; Geometrics Incorporated, San Jose, California, 147 pages.

Gibbard, P.L., Boreham, S., Cohen, K.M., and Moscariello, A., (2005) Global chronostratigraphical correlation table for the last 2.7 million years; *Boreas*, Volume 34, unpaginated.

Hartman, G.M.D., and Clague, J.J. (2008): Quaternary stratigraphy and glacial history of the Peace River valley, northeast British Columbia; *Canadian Journal of Earth Sciences*, Volume 45, Number 5, pages 549–564.

Hickin, A.S. (2006): Aggregate potential of selected terraces along the East Kiskatinaw River, northeastern British Columbia; *BC Ministry of Energy, Mines and Petroleum Resources*, Aggregate Prospecting Report, 2006-1, 1 Map (1:50 000 scale).

Hickin, A.S., and Kerr, B. (2005): Bedrock topography mapping and shallow gas in northeast BC; in Summary of Activities 2005, *BC Ministry of Energy, Mines and Petroleum Resources*, pages 69–75.

Hickin, A.S., Kerr, B., Barchyn, T.E., and Paulen, R.C. (2009): Using ground-penetrating radar and capacitively coupled resistivity to investigate 3-D fluvial architecture and grain-size distribution of a gravel floodplain in northeast British Columbia, Canada; *Journal of Sedimentary Research*, Volume 79, in press.

Hickin, A.S., Kerr, B., Turner, D.G., and Barchyn, T.E. (2008): Mapping Quaternary paleovalleys and drift thickness using petrophysical logs, northeast British Columbia, Fontas map sheet, NTS 94I; *Canadian Journal of Earth Sciences*, Volume 45, Number 5, pages 577–591.

Imbrie, J. and Imbrie Z., (1980): Modeling the climate response to orbital variation; *Science*, Volume 207, pages 943-953.

Jackson, L.E., Jr., Phillips, F.M., and Little, E.C. (1999): Cosmogenic 36Cl dating of the maximum limit of the Laurentide Ice Sheet in southwestern Alberta; *Canadian Journal of Earth Sciences*, Volume 36, Number 8, pages 1347–1356.

Johnsen, T., Ferbey, T., Levson, V.M., and Kerr, B. (2004): Quaternary geology and aggregate potential of the Fort Nelson airport area; in Summary of Activities 2004, *BC Ministry of Energy, Mines and Petroleum Resources*, pages 19–27.

Kerr, B., Ferbey, T., and Levson, V.M. (2005): Implementing geomatics technology for aggregate exploration, northeast British Columbia; in Summary of Activities 2005, *BC Ministry of Energy, Mines and Petroleum Resources*, pages 83–86.

Levson, V.M., Ferbey, T., Hickin, A.S., Bednarski, J.M., Smith, I.R., Demchuk, T.E., Trommelen, M., Kerr, B., and Church, A. (2005): Surficial geology and aggregate studies in the boreal plains of northeast British Columbia; in Summary of Activities 2005, *BC Ministry of Energy, Mines and Petroleum Resources*, pages 45–54.

Levson, V.M., Ferbey, T., Kerr, B., Johnsen, T., Smith, I.R., Blackwell, J., and Jonnes, S. (2004): Quaternary geology and aggregate mapping in northeast British Columbia: Applications for oil and gas exploration and development; in Summary of Activities 2004, *BC Ministry of Energy, Mines and Petroleum Resources*, pages 29–40.

Levson, V.M., Hickin, A.S., Ferbey, T., and Best, M. (2006): Mapping high resistivity buried channel deposits with airborne electromagnetic surveys and other methods; 19th Annual Symposium on the Application of Geophysics to Engineering and Environmental Problems, Seattle, pages 152–161.

Liverman, D.G.E., Catto, N.R., and Rutter, N.W. (1989): Laurentide glaciation in west-central Alberta: a single (Late Wisconsinan) event; *Canadian Journal of Earth Sciences*, Volume 26, Number 2, pages 266–274.

Mathews, W.H., (1978): Quaternary stratigraphy and geomorphology of Charlie Lake (94A) map-area, British Columbia; *Geological Survey of Canada*, Paper 76-20, 25 pages.

Mathews, W.H., (1980): Retreat of the last ice sheets in northern British Columbia and adjacent Alberta; *Geological Survey of Canada*, Bulletin 331, 33 pages.

McCuaig, S.J., and Roberts, M.C. (2002): Topographically-independent ice flow in northwestern British Columbia: implications for Cordilleran Ice Sheet reconstruction; *Journal of Quaternary Science*, Volume 17, Issue 4, pages 341–348.

Pawlowicz, J.G., Hickin, A.S., Fenton. M.M., and Paulen, R.C., (2004): Bedrock topography and drift thickness mapping of the Zama LAke area, NTS 84L: Implications for shallow gas; *Canadian Society of Petroleum Geologists*, Calgary, Poster presentation.

Rohling, E.J., (2007): Oxygen isotopic composition of seawater; In Ellias, S.A., (ed): *Encyclopedia of Quaternary Science*, Elsevier,New York, Volume 3, pages 1748-1756.

Shackleton, N.J., (1967): Oxygen isotope analyses and Pliestocene temperatures re-assessed; *Nature*, Volume 215, pages 15-17.

Smith, I.R., Paulen, R.C., Plouffe, A., Kowalchuk, C., and Peterson, R. (2005): Surficial mapping and granular aggregate resource assessment in northwest Alberta; in Summary of Activities 2005, *BC Ministry of Energy, Mines and Petroleum Resources*, pages 87–103.

Smith, I.R., (2009a): Surficial geology, Kyklo Creek, British Columbia; Geological Survey of Canada, Open File 5307, *BC Ministry of Energy,Mines and Petroleum Resources*, Map 2009-1, 1 map (1:50 000 scale).

Smith, I.R., (2009b): Surficial geology, Nogah Creek, British Columbia; Geological Survey of Canada, Open File 5306; *BC Ministry of Energy Mines and Petroleum Resources*, Map 2009-2, 1 map (1:50 000 scale).

Smith, I.R., (2009c): Surficial geology, Gunnell Creek, British Columbia; Geological Survey of Canada, Open File 5305; *BC Ministry of Energy Mines, and Petroleum Resources*, Map 2009-3, 1 map (1:50 000 scale).

Smith, I.R., (2009d): Surficial geology of Lichen Creek, British Columbia; Geological Survey of Canada, Open File 5309; *BC Ministry of Energy, Mines, and Petroleum Resources*, Map 2009-4, 1 map (1:50 000 scale).

Stumpf, A.J., Broster, B.E., and Levson, V.M., (2000): Multiphase flow of the Late Wisconsinan Cordilleran Ice Sheet in western Canada; *Bulletin of the Geological Society of America*, Volume 112, Number 12, pages 1150-1163.

Trommelen, M. (2007): Quaternary stratigraphy and glacial history of the Fort Nelson (southeast) and Fontas River (southwest) map areas (094J/SE and 094I/SW), northeastern British Columbia; *unpublished thesis*, School of Earth and Ocean Sciences, University of Victoria, Victoria, BC, 253 pages.

Trommelen, M., and Levson, V.M. (2008): Quaternary stratigraphy of the Prophet River, northeastern British Columbia; *Canadian Journal of Earth Sciences*, Volume 45, Number 5, pages 565–575.

Trommelen, M., Levson, V.M., Hickin, A.S., and Ferbey, T. (2005): Quaternary geology of Fort Nelson (NTS 094J/SE) and Fontas River (NTS 094I/SW), northeastern British Columbia; *in* Summary of Activities 2005, *BC Ministry of Energy, Mines and Petroleum Resources*, pages 105–122.

Trommelen, M., and Smith, I.R. (2007): Surficial geology, Dazo Creek, British Columbia (094I/SW); *Geological Survey of Canada*, Open File 5527, 1 map (1:100 000 scale).

Wolfe, S.A., Huntley, D.J., and Ollerhead, J. (2004): Relict Late Wisconsinan Dune Fields of the Northern Great Plains, Canada; *Géographie physique et Quaternaire*, Volume 58 (2-3), pages 9019–9032.

Wolfe, S.A., Paulen, R.C., Smith, I.R., and Lamothe, M. (2007): Age and paleoenvironmental significance of Late Wisconsinan dune fields in the Mount Watt and Fontas River map areas, northern Alberta and British Columbia; *Geological Survey of Canada*, Current Research 2007-B4, 10 pages.

Urey, H.C., (1947): The thermodynamic properties of isotopic substances: *Journal of the Chemical Society* (London), pages 562-581.

WATER POTENTIAL OF THE MISSISSIPPIAN DEBOLT FORMATION IN THE HORN RIVER BASIN, NORTHEASTERN BRITISH COLUMBIA

Elizabeth Johnson[1]

ABSTRACT

Water demand in the Horn River Basin is increasing rapidly as a result of shale gas exploration and development. The British Columbia Ministry of Energy, Mines and Petroleum Resources is studying the suitability of shallow subsurface strata, the Debolt Formation in particular, to supply the water needs of industry. There is little known of the geology or hydrogeology relative to the size of the area. The Debolt Formation subcrops against an unconformity throughout the basin. Water has been produced from the Mattson Formation in association with gas production. Drill-stem tests indicate there are highly permeable zones in the Mattson, Golata, Bluesky, and Debolt formations. The lithology and stratigraphy studies at the contact may help locate highly permeable zones in the Debolt.

Johnson, E. (2009): Water Potential of the Mississippian Debolt Formation in the Horn River Basin, Northeastern British Columbia; Geoscience Reports 2009, *BC Ministry of Energy, Mines and Petroleum Resources,* pages 39–47.

[1]British Columbia Ministry of Energy, Mines and Petroleum Resources, 1810 Blanshard Street, Victoria, British Columbia

Key Words: aquifer, groundwater, disposal, 94O, Debolt, Mattson, Golata, Scatter, Bluesky, Bullhead

INTRODUCTION

Water demands in the Horn River Basin are expected to escalate dramatically as the regional shale gas exploration and development accelerates. The British Columbia Ministry of Energy, Mines and Petroleum Resources has initiated studies to establish the availability of subsurface water sources to support industry activity. The Mississippian Debolt Formation of the Rundle Group is considered one of the most likely near-surface stratigraphic units capable of providing large volumes of water.

The Horn River Basin is located in northeastern British Columbia between Fort Nelson and the Northwest Territories border (mostly in NTS map sheets 94O eastward into 94P and southward to 94J). Located in the Fort Nelson Lowland of the Alberta Plateau, the area has very low relief (300 to 730 m above sea level), with the Etsho Plateau forming a minor upland, oriented northwest to southeast in the central region (Figure 1) (Holland 1976). There are two major drainage systems incised up to 150 m below the general level of the lowland: the Fort Nelson River and the Petitot River (which are tributaries of the Liard and Mackenzie River systems). For the most part, the study area is defined by the Devonian Slave Point reef on the east and south and the Bovie Fault on the west; the Northwest Territories border forms the northern limit.

CURRENT ACTIVITY

Recent drilling activity has increased rapidly as shale gas and tight gas exploration and development progresses (Figure 2). Currently, there are 1547 wells in the study area. This is a five-fold increase since 2000. Data from over fifty wells are confidential as they are classed as experimental schemes, and the standard period of confidentiality is extended to three years from rig release. The majority of wells along the east margin of the basin are associated with development of the Jean-Marie Formation.

The increased demand for water is primarily owed to hydraulic fracturing , the stimulation technique necessary for the economic development of tight and shale gas. To develop shale gas plays, hydraulic fracturing (herein referred to as "fracs" or "fracing") is used to create fractures in the shale that increase well-bore access to the gas trapped in the rock. Fracing requires high pressures and injection rates up to 100 MPa and 256 L/s to create fractures around the well bore. A proppant such as sand is added to the water to prevent the fractures from closing again. Substantial volumes of water are required for this process. Estimates vary by producer from 1,200 m^3 to over 2,500 m^3 of water per frac[1,2,3]. An average well may contain six to twelve fracs, so the water requirement for one well could be as low 7,000 m^3 or more than 30,000 m^3. Well configuration estimates place 3 to 8 wells

[1] Based on current industry estimates

[2] Slick water fracing of a vertical well completion can use over 5,500 m^3 (1.2 million gallons) of water, while the fracturing of a horizontal well completion can use over 16,000 m^3 (3.5 million gallons) of water. In addition, the wells may be re-fractured multiple times after producing for several years (Railroad Commission of Texas 2008)

[3] An entire frac job may take a day and uses 9,500 to 13,600 m^3 (2.1 to 3 million gallons) of water (Veil 2007)

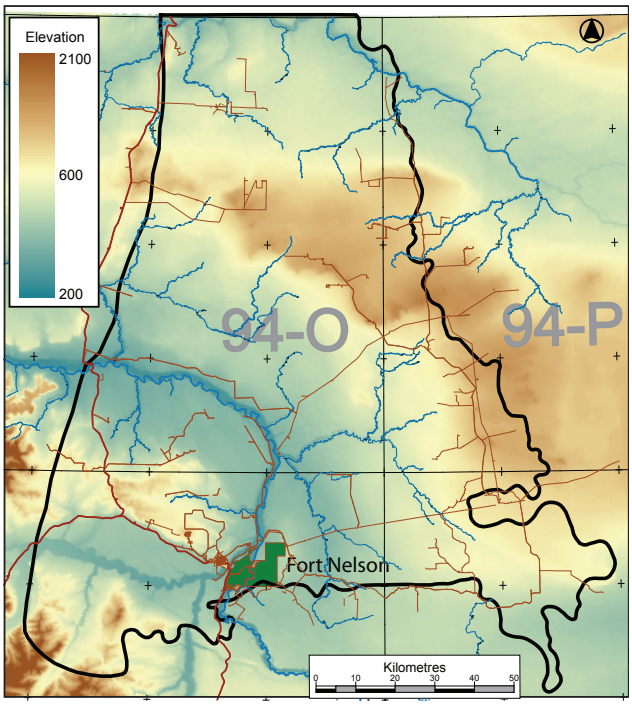

Figure 1. Topography of the Horn River Basin. The outlined area shows the geologically defined basin. Elevation in metres above sea level.

per gas spacing unit (approximately 240 ha). Producers hope to recover one quarter to one third of frac water used and recycle 100% of the return.

Industry activities initially used surface water from small lakes and borrow pits[4], which were easily accessible since much of the region is covered with small lakes, muskeg, and black spruce forests. However, an average-sized borrow pit can supply the water needs for only one or two wells. Surface water has been rejected as a long-term option as this supply is not likely to sustain prolonged industry activity and poses an environmental concern. As a consequence, subsurface water bodies being targeted include (a) fresh water from large buried valleys filled with Quaternary sediments and (b) saline waters in Mississippian Debolt Formation limestone or overlying sandstones from the Mattson, Bluesky, or Gething formations. Buried valleys are discussed elsewhere (see Hickin, this volume). This study focuses on the Debolt Formation for two reasons. First, the Debolt Formation is a possible candidate for both source and disposal water; it is a thick, continuous, locally porous calcareous unit known to contain saline water and small gas pools. Second, at present there is more data available for the Debolt than other horizons. This is an important factor as there are fifteen hundred wells with publicly released data that intersect the Debolt Formation in an area of greater than 1.3 million ha. The majority of these data are from the periphery of the Horn River Basin, especially along the eastern boundary where the target horizon is the stratigraphically lower Jean Marie Formation (Devonian).

[4]A borrow pit is the hole created when material is excavated to be used as road fill

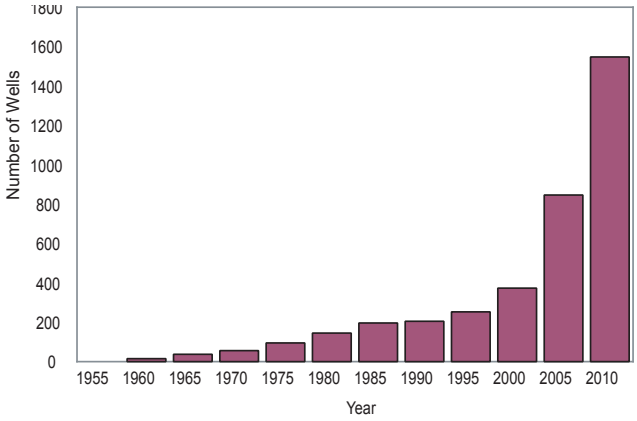

Figure 2. Increased drilling in the Horn River Basin over time.

STRATIGRAPHY

The Banff Formation forms the base for the sequence of interest. It is a 400 to 500 m thick Upper Devonian to Mississippian horizon consisting of interbedded calcareous shale and argillaceous limestones (Member B) (Glass 1997; Monahan 1999). Atop the Banff Formation is the Rundle Group, which is unconformably overlain by Cretaceous strata in much of the study area. The Rundle Group includes the Pekisko, Clausen, Debolt, Shunda, and Flett formations (Table 1). The Flett Formation in the District of Mackenzie is equivalent to Debolt in northeastern British Columbia (Richards et al. 1994). The assemblage consists of carbonate platform lithofacies with subordinate carbonate ramp lithofacies and basinal to supratidal siliciclastics. They form a shallowing upward succession over several transgressive/regressive cycles (Richards et al. 1994). At the base of the Rundle Group is the Pekisko Formation, a 25 m thick unit of clean bioclastic limestone indicative of a shelf setting. The Shunda Formation consists of argillaceous limestone and calcareous shale, and the Debolt consists of limestone with dolomite, chert, and argillaceous units (Monahan 1999). The limestone commonly has light brown mottled colouring and fine to medium granular texture and is bioclastic with crinoids, ostracods, and brachiopods.

The Debolt Formation is informally divided into lower, middle, and upper members. The Elkton forms a lower submember of the Debolt. It is capped by a distinctive argillaceous unit. The middle Debolt member has a greater argillaceous content, which is visible on gamma ray logs (Monahan 1999). Dolomites up to 60 m thick occur in the upper Debolt (Monahan 1999).

Within the geological outline of the basin, Cretaceous sediments unconformably overlie Mississippian Debolt carbonates. The surface of the Debolt is erosional and is relatively flat, with approximately 200 m total relief (Figure 3). The Debolt-Shunda-Pekisko package (Rundle Group) thins eastward (Figure 4). The upper Debolt occurs mostly in the west but has been eroded to the east.

West of the Bovie Fault, in the Liard Basin (see Figure 3 for location), Permian sediments are present, as are younger Mississippian strata such as the Mattson and Golata formations, so the elevation of the sub-Cretaceous unconformity is significantly higher than the Debolt. Figure 5 shows the thickness of sediment between this unconformity and top of Debolt and outlines the subcrop edge of the Mattson, Golata, and Fantasque formations. Wells on the map indicate the formation that subcrops against the unconformity. There are rare occurrences of these younger sediments within the basin, mostly near the Bovie fault but also along a central northeast to southwest trending features. This feature may be a splay along the Bovie Fault or related fault structures associated with the Dilly and Petitot faults (Petrel Robertson 2003).

WATER-BEARING STRATA

Little more than 100,000 m^3 of water has been produced from multiple wells in the Debolt (Flett), Mattson, and Bluesky formations (Table 2). A 15 m thick porous dolomite at the top of the Elkton has produced water in several drill-stem tests just southwest of the HRB boundary (e.g., b-6-G/94-O-7) (Monahan 1999).

Within the geologically defined basin at shallower depths (above the Banff Formation), drill-stem tests were performed in the Cretaceous sediments (10 tests) and the Mississippian Golata (1 test), Mattson (20 tests), and Debolt (61 tests) formations (Figure 6). Highly permeable formations are distinguishable from low permeability

TABLE 1. TABLE OF FORMATIONS FOR NORTHEASTERN BRITISH COLUMBIA.

ERA	PERIOD & EPOCH		N.W.T.& YUKON	NORTHERNMOST NEBC
			LIARD RIVER AREA	PLAINS
CENOZOIC	QUATERNARY		BOULDER CLAYS, SAND AND GRAVEL VARVED CLAY, SILT	BOULDER CLAYS, SAND AND GRAVEL VARVED CLAY, SILT
	TERTIARY			
MESOZOIC	CRETACEOUS	UPPER	WAPITI	WAPITI
			KOTANEELEE	KOTANEELEE
			FORT NELSON	
		LOWER	FT. ST. JOHN GROUP: SULLY	FT. ST. JOHN GROUP: SULLY
			FT. ST. JOHN GROUP: SIKANNI	FT. ST. JOHN GROUP: SIKANNI
			BUCKINGHORSE: LEPINE	BUCKINGHORSE: LEPINE
			BUCKINGHORSE: SCATTER	BUCKINGHORSE: SCATTER
			BUCKINGHORSE: GARBUTT	BUCKINGHORSE: GARBUTT
			CHINKEH	GETHING
	JURASSIC	UPPER		
		MIDDLE		
		LOWER		
	TRIASSIC	UPPER		SHROEDER CR. GROUP: BLDN.
				SHROEDER CR. GROUP: CHARLIE LAKE
		MIDDLE		SHROEDER CR. GROUP: HLFY.
		LOWER		DIABER GROUP: DOIG
				DIABER GROUP: MONTNEY
PALEOZOIC	PERMIAN		FANTASQUE	NW PART OF AREA FANTASQUE?
	PENNSYLVANIAN		MATTSON	MATTSON
	MISSISSIPPIAN	UPPER	MATTSON	MATTSON ?
			ETANDA / FLETT	RUNDLE GROUP: DEBOLT
				RUNDLE GROUP: SHUNDA
				RUNDLE GROUP: PEKISKO
		LOWER	CLAUSEN	BANFF
			YOHIN	EXSHAW

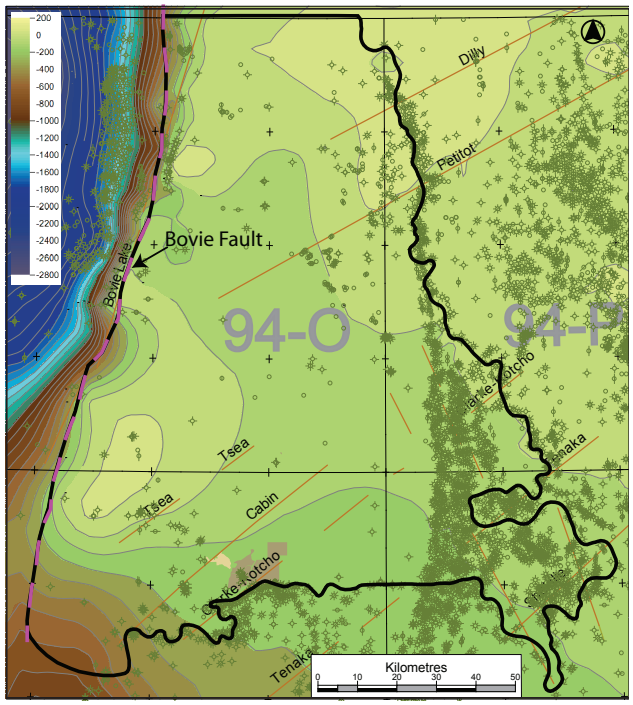

Figure 3. Elevation (in metres above sea level) of the surface of the Debolt Formation. Brown lines indicate inferred locations of regional faults.

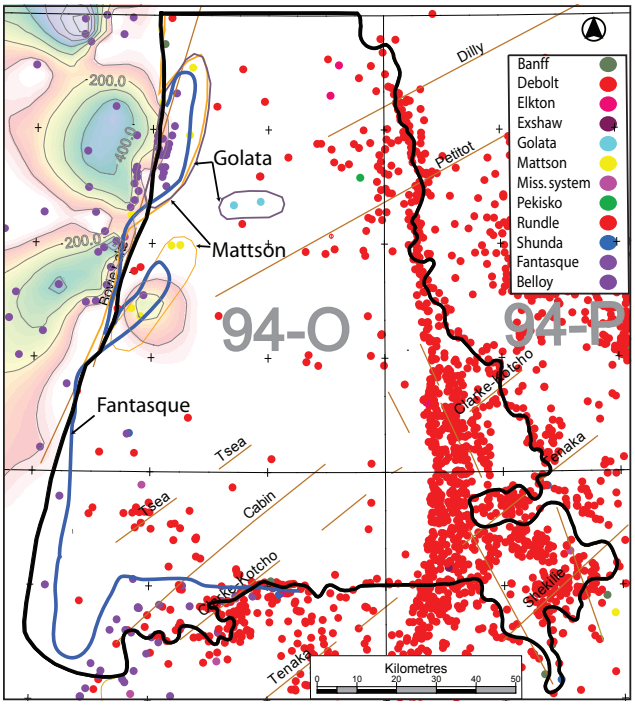

Figure 5. Kriged isopach of sediment thickness (in metres) of Paleozoic sediments younger than the Debolt Formation. Well coloration indicates the first unit intersected below the Permo Triassic unconformity. Coloured lines indicate the approximate location of the subcrop contact.

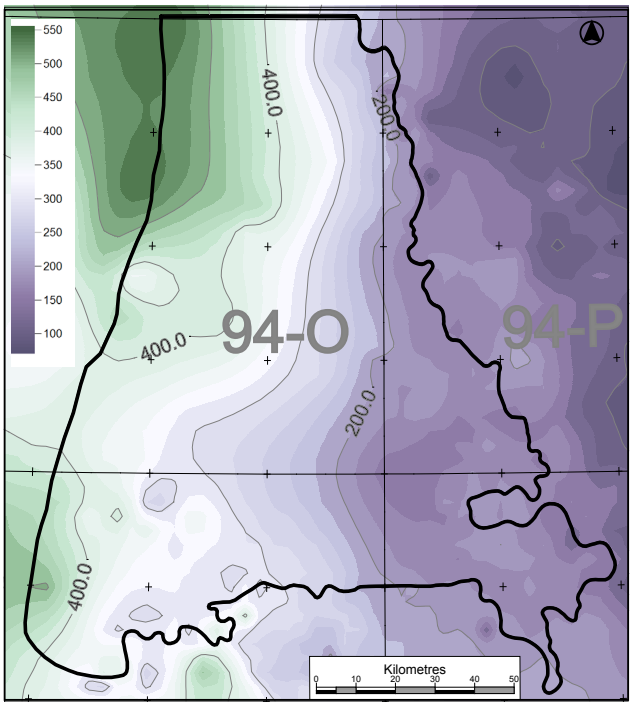

Figure 4. Isopach map for thickness (in metres) of the Rundle Group from the top of the Debolt formation to the top of the Banff Formation.

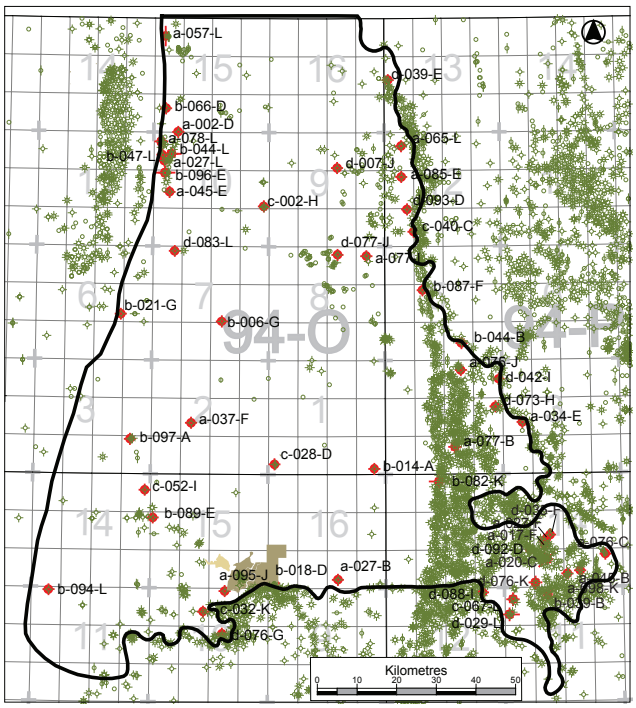

Figure 6. Locations of wells in the Horn River Basin (green dots). Wells with drill-stem tests in formations above the Banff Formation (listed in Table 3a) are indicated in red.

TABLE 2. WELLS WITH PRODUCED WATER GREATER THAN 1000 M^3.

Well ID	Water Rate First 4 mo. (m3/d)	Water Rate Last 4 mo. (m3/d)	Cum. Water Prod. (m3)	Formation	Total Prod. (hours)	Date of Last Prod. (month-year)
b-015-F/094-I-14	0.03	0.05	1455	Bluesky	14681	Oct-08
b-015-F/094-I-14	0.03	0.05	1455	Bluesky	14681	Oct-08
b-037-G/094-P-04	2.4	0.51	3717	Bluesky	37534	Oct-08
c-006-F/094-I-14	1.21	2.03	8700	Bluesky	73250	Oct-08
c-006-F/094-I-14	1.21	2.03	8700	Bluesky	73250	Oct-08
c-028-F/094-I-14	1.57	23.13	11968	Bluesky	24312	Feb-04
c-028-F/094-I-14	1.57	23.13	11968	Bluesky	24312	Feb-04
d-008-F/094-I-14	0.36	0.83	1497	Bluesky	11909	Dec-03
d-008-F/094-I-14	0.36	0.83	1497	Bluesky	11909	Dec-03
a-025-L/094-O-10	0.12	-	5506	Debolt	27204	Sep-06
a-025-L/094-O-10	0.12	-	5506	Debolt	27204	Sep-06
a-025-L/094-O-10	0.05	-	13809	Mattson	62539	Oct-08
a-025-L/094-O-10	0.05	-	13809	Mattson	62539	Oct-08
a-078-L/094-O-10	0.18	-	5848	Mattson	33754	Sep-06
a-078-L/094-O-10	0.18	-	5848	Mattson	33754	Sep-06
b-025-L/094-O-10	-	0.9	1552	Mattson	26030	Dec-04
b-025-L/094-O-10	-	0.9	1552	Mattson	26030	Dec-04
b-044-L/094-O-10	-	0.2	1674	Mattson	78000	Oct-08
b-044-L/094-O-10	-	0.2	1674	Mattson	78000	Oct-08

horizons by lower final hydrostatic pressures, smaller pressure changes, a lower rate of recovery on the second phase of the test (slope), lower salinity, and higher electrical resistance (Table 3). The Rundle Group overall has average to high permeability in drill-stem tests but has localized horizons of low permeability. The Mattson, Golata, and Bluesky also indicate average to high permeability in a small number of tests. As mentioned, upper Mississippian and Permian sediments occur mostly along the western edge of the basin boundary. The Cretaceous Bullhead Group (Bluesky Formation) occurs only along the east side with the exception of a small zone west of Fort Nelson. Salinity for the various formations is generally in the 10,000 to 20,000 ppm range. There are occurrences of fresh to slightly saline water (less than 3000 ppm) in drill-stem tests of the Bullhead Group, Scatter, and Debolt formations. A review of the water analyses for these occurrences indicates that the samples are all affected by mud filtrate. Evidence of mud filtrate includes low recovery volumes, skewed ion proportions, and physical observations.

The lithologic logs of most wells do not allow for the differentiation of subunits within the Debolt. Lithologic descriptions indicate that the Debolt is tight over broad intervals. In well D-079-G/094-O-16 (WA 6239), core analysis in the Debolt Formation from three porous horizons showed that the porosity can spike from generalized low values of 1% to 5% to high values of 10% to 28% and back to low values over short vertical thicknesses of less than a meter. In well D-090-K/094-O-07 (WA 13894), the Debolt Formation has consistently poor to no porosity through a 120 m section that is followed by a 120 m section of undifferentiated limestone averaging 3% to 5% porosity. This lower porous zone may be the lower Debolt, the Elkton submember, or (most probably) the Shunda Formation. There are many other instances, especially in the central east side of the study area, where the Shunda Formation is not differentiated from the Debolt. Similarly, the Pekisko Formation is not always identified in drill holes despite strong lateral correlation of stratigraphy from surrounding wells. A thorough review of the lithology sequence stratigraphy and a common nomenclature would be helpful to developing an integrated understanding of the porosity distribution within the basin.

The Debolt Formation is present across the basin and therefore is a prospective targets as a water source or disposal horizon. Widespread regions of very low permeability, however, may limit its utility. Thinner porous dolomite intervals in the upper, middle, and lower Debolt provide traps at the sub-Cretaceous unconformity for gas shows and small gas pools (Monahan 1999). Porosity is often increased in carbonate horizons underlying unconformities from secondary processes including (a) shallow subsurface solution by meteoric fluids and (b) increased solution by circulating fluids under a confining layer at the unconformity. Porosity is also increased with dolomite content. Careful mapping of the unconformity surface and juxtaposition of lithologies across the unconformity would be helpful in finding zones of the Debolt Formation that would yield more water.

TABLE 3A. DRILLSTEM TEST RESULTS FOR FORMATIONS ABOVE THE BANFF FORMATION.

UWID	Formation	Depth (m)	Hydro. Press. Initial (kPa)	Hydro. Press. Final (kPa)	Rate Recov. Phase 2, Test 1 (kPa/min)	Rate Recov. Phase 2, Test 2 (kPa/min)	Bore Hole Temp. (°C)	Fluid Salinity (ppm)	Resistivity of water (Ohms)	Perme-ability
d-092-D/094-I-14	Bluesky	616	6467	6322	2	1		17,729	0.419	`
a-085-E/094-P-12	Bluesky	525	6050	5963	2	2	37.8	12,638	0.475	3
a-017-F/094-I-14	Bluesky	605	5976	5748	1	1	34.6	27,400	0.240	`
c-086-A/094-I-14	Bluesky	550	6320	6414			38.0			`
a-027-F/094-I-14	Bullhead	607	6260	6150	2	4	30.0			`
a-027-F/094-I-14	Bullhead	599	6109		10	2	40.6	10,000	0.580	`
a-045-B/094-I-14	Bullhead	578	6033	6019	5	2	46.1	1,690	4.998	`
d-035-F/094-I-14	Bullhead	607	6805	6860	4	2		53,333	0.130	1
a-045-E/094-O-10	Scatter	780	8729	8687	20	10	22.8	1,583	4.880	`
b-044-B/094-P-05	Spirit River	565	5833	5833	50	25	21.1	16,791	0.363	`
d-088-I/094-I-12	Debolt	613	7102	6729			32.2			`
d-088-I/094-I-12	Debolt	613	7053	6453	2		32.2			`
a-027-B/094-J-16	Debolt	520	6322	6322	2	1	28.3	23,824	0.318	3
a-027-F/094-I-14	Debolt	700	7460	7357	40	20	36.7			`
a-034-E/094-P-03	Debolt	700	8991	8874	2	5	37.8	32,404	0.255	`
a-045-B/094-I-14	Debolt	594	6288	6288	2	1	46.1			`
a-065-L/094-P-12	Debolt	358	3813	3436				4,300	1.520	`
a-075-J/094-P-04	Debolt	638	6989	6860	8	5	36.2	20,000	0.310	2
a-076-C/094-I-14	Debolt	603	6674	6509	15	5		28,682	0.257	`
a-076-C/094-I-14	Debolt	618	6667	6681						`
a-076-C/094-I-14	Debolt	603	6674	6509	15	5		28,682	0.257	`
a-076-C/094-I-14	Debolt	618	6667	6681						`
a-077-B/094-P-04	Debolt	603	6694	6672	10	2	37.3	10,000	0.585	3
a-077-I/094-O-08	Debolt	650	6667	6529				2,310	2.550	`
a-095-J/094-J-10	Debolt	536	6481	6481	40	45	37.8	26,263	0.273	`
b-006-G/094-O-07	Debolt	528	5709	5681	5	10	28.9			`
b-006-G/094-O-07	Debolt	627	6778	6771	2	1				`
b-014-A/094-O-01	Debolt	581	6840	6709	10	10	27.8	19,000	0.310	3
b-018-D/094-J-16	Debolt	565	7474	7474	5	10	32.2	24,713	0.303	`
b-021-G/094-O-06	Debolt	555	5840	5840				1,754	4.802	`
b-039-B/094-I-14	Debolt	588	6391	6356	10	10	21.1	26,700	0.234	2
a-020-C/094-I-14	Debolt	574	6567	6223	2	1	36.7	31,787	0.227	3
b-082-K/094-I-13	Debolt	608	6440	26424	8	5	33.8	14,000	0.430	2
b-087-F/094-P-05	Debolt	707	6743	6647	2	1	33.3			`
b-089-E/094-J-15	Debolt	567	6474	6474	50					`
b-094-L/094-J-11	Debolt	1044	11232	11107	2	1	37.2	20,934	0.287	3
b-096-E/094-O-10	Debolt	724	7508	7412	1	1		10,575	0.681	`
d-093-D/094-P-12	Debolt	536	5530	5530						`
d-093-D/094-P-12	Debolt	515	5612	5612	5	2		5,760	0.990	3
b-096-E/094-O-10	Debolt	724	7508	7412	1	1		10,575	0.681	`
b-097-A/094-O-03	Debolt	347	3868	3820	2	20	12.2			`
c-028-D/094-O-01	Debolt	365	3544	4137	2		37.8			`
c-032-K/094-J-10	Debolt	589	6822	6822	10	10				`
c-040-C/094-P-12	Debolt	611	6788	6490	10	10	47.0	3,858	1.680	`
c-067-L/094-I-11	Debolt	592	6674	6571	2	1	38.0			`
d-007-J/094-O-09	Debolt	463	5281	5171	2	1				`
d-029-L/094-I-11	Debolt	557	6109	6116	2	2		30,400	0.210	`

TABLE 3A CONTINUED.

UWID	Formation	Depth (m)	Hydro. Press. Initial (kPa)	Hydro. Press. Final (kPa)	Rate Recov. Phase 2, Test 1 (kPa/min)	Rate Recov. Phase 2, Test 2 (kPa/min)	Bore Hole Temp. (°C)	Fluid Salinity (ppm)	Resistivity of water (Ohms)	Perme-ability
d-039-E/094-P-13	Debolt	301	3404	3371	1	1	29.3	8,000	0.740	3
d-042-I/094-P-04	Debolt	0	7267	7267			36.1			`
d-073-H/094-P-04	Debolt	680	7688	7564	2	1	48.9	22,732	0.307	`
d-076-G/094-J-10	Debolt	665	7308	7274						`
d-076-K/094-I-11	Debolt	594	7197	7197			35.0	24,506	0.276	`
d-077-J/094-O-08	Debolt	667	6564	6564			26.1	14,816	0.490	`
d-088-I/094-I-12	Elkton	649	7053	7164	10	15	36.7			`
a-037-F/094-O-02	Elkton	410	4854	4854			28.3			`
a-037-F/094-O-02	Elkton	399	5040	5026			28.3			`
a-045-E/094-O-10	Flett	930	10135	9832	20	30	31.1	6,190	0.949	`
a-057-L/094-O-15	Flett	1538	17633	17579	60	45	47.0			1
a-078-L/094-O-10	Flett	1092	12045	11935			45.0	15,623	0.459	`
b-044-L/094-O-10	Flett	520	5468	5378	1	1	41.7	13,470	0.460	3
c-002-H/094-O-10	Flett	805	9005	8963	20	10	33.3	20,173	0.331	`
a-002-D/094-O-15	Golata	505	5447	5323	2	2		4,000	1.240	`
c-052-I/094-J-14	Miss_sys	683	4109	4109						`
c-052-I/094-J-14	Miss_sys	598	6860	6736	5	2	52.2			`
a-027-L/094-O-10	Mattson	698	7097	6989	10	8				`
a-045-E/094-O-10	Mattson	863	9756	9632	5	5	30.0	20,314	0.311	`
a-057-L/094-O-15	Mattson	765	9134	9125	15	10	31.4	8,000	0.740	2
a-078-L/094-O-10	Mattson	770	8612	7784	5	2	40.6	9,756	0.771	`
a-078-L/094-O-10	Mattson	738	8039	7826	5	2		5180	1.348	`
a-078-L/094-O-10	Mattson	1035	11404	11342				24479	0.303	`
b-044-L/094-O-10	Mattson	396	4158	4116	10	5	18.9			2
b-047-L/094-O-10	Mattson	980	10996	10849	2	1	39.5			`
b-066-D/094-O-15	Mattson	993	11004	11004	30	20	28.9	4,480	1.370	3
b-096-E/094-O-10	Mattson	529	5447	5447			35.0			`
b-096-E/094-O-10	Mattson	530	5488	5612						`
b-096-E/094-O-10	Mattson	529	5674	5736	2	2	27.8			`
a-002-D/094-O-15	Mattson	494	5447	5447	5	2		12,497	0.582	2
b-096-E/094-O-10	Mattson	529	5674	5736	2	2	27.8			1
b-096-E/094-O-10	Mattson	530	5488	5612						`
d-083-L/094-O-07	Mattson	657	7037	6953	5	10	29.8	25,000	0.260	1
d-092-D/094-I-14	Shunda	668	7150	7205	5	4		28,983	0.187	`

TABLE 3B. SUMMARY OF DRILLSTEM TEST RESULTS BY FORMATION.

Formation	No. tests	Depth (m)	Hydrostatic Pressure Initial(kPa)	Hydrostatic Pressure Final(kPa)	Pressure Change Test1	Pressure Change Test2	Rate Recov. Phase 2, Test 1 (kPa/min)	Rate Recov. Phase 2, Test 2 (kPa/min)	Bore Hole Temp. (°C)	Fluid Salinity (ppm)	Resistivity of water (Ohms)	Permeability
Bullhead	8	585.9	6,253	6,211	3,648	1,973	4	2	37.85	20,465	1.14	Variable
Scatter	1	779.7	8,729	8,687	1,627	986	20	10	22.8	1,583	4.880	
Spirit river	1	565.4	5,833	5,833	751	213	50	25	21.1	16,791	0.363	Low
Golata	1	505.4	5,447	5,323	2,338	1,965	2	2		4,000	1.240	High
Mattson	20	642.6	7,328	7,257	2,888	1,631	8	6	30.4	13,341	0.672	Average
Debolt	51	601.7	6,404	6,738	2,207	1,092	8	6	33.3	17,700	0.758	Average
Elkton	4	464.3	5,490	5,514	2,561	1,389	15	15	31.0			
Shunda	1	667.5	7,150	7,205	3,420	3,723	5	4		28,983	0.187	Low

Additionally, there are occurrences of increased porosity from hydrothermal brecciation in Devonian carbonates where they are spatially associated with deep-seated fault structures across northeastern British Columbia. The Debolt Formation may also exhibit increased porosity from hydrothermal brecciation in association with faults like the Dilly and Petitot faults.

The Debolt Formation may not act well as a water-disposal formation. It is too shallow in some localities. The total vertical depth to the top of the Debolt Formation ranges from 280 m to more than 700 m (Figure 7). In general, areas of greatest and least depths are inversely spatially correlated with elevation. Additionally, specific locations for disposal in the Debolt need to be studied because in places the Debolt directly underlies the Quaternary sediments or subcrops against an unconformity.

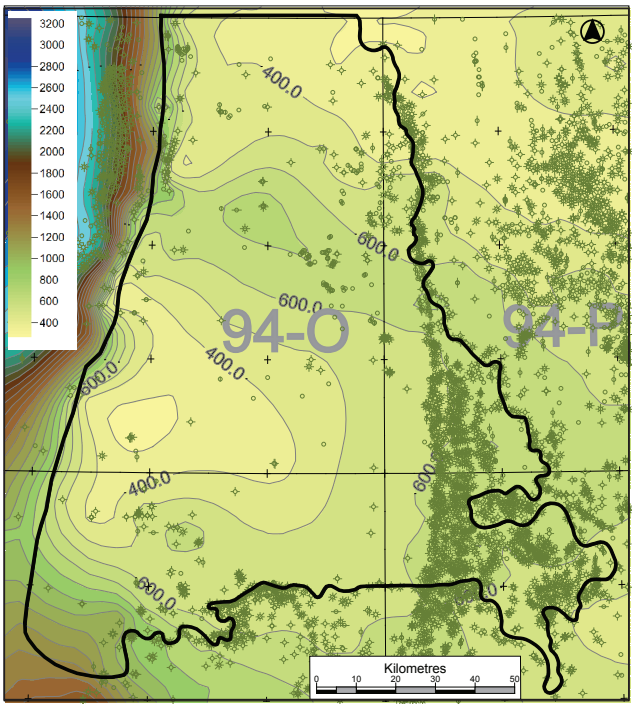

Figure 7. Total vertical depth (in metres) to the top of the Debolt Formation.

CONCLUSIONS AND RECOMMENDATIONS

Water demand in the Horn River Basin is expected to increase dramatically with increasing gas production. Cretaceous and Mississippian sandstones and limestones are considered the most likely source rocks for water in sufficient quantity to meet drilling and hydraulic fracturing requirements. Drilling has increased rapidly, but geologic knowledge is still highly limited, especially in the centre portion of the basin. The Mattson and Golata provide a potential source along the far west of the basin boundary, but the Debolt is the primary horizon of interest as it is a thick, basin-wide, porous unit. While the Debolt has good permeability in some areas, there are also broad regions of very low permeability. Knowledge of which portion of the Debolt is in contact with the unconformity, its porosity characteristics, and which formations are proximal will aid in determining zones of secondary porosity with increased permeability. Better control is needed to understand depositional and diagenetic controls on porosity and permeability.

REFERENCES

Glass, D., editor (1997): Lexicon of Canadian Stratigraphy, Volume 4: western Canada; *Canadian Society of Petroleum Geologists*, 1423 pages.

Holland, S.S. (1976): Landforms of British Columbia: A physiographic outline. 2nd Edition; *British Columbia Department of Mines and Petroleum Resources*, Bulletin No. 48, 138 pages.

Monahan, P. (c. 1999): Stratigraphy and potential hydrocarbon objectives of Mississippian to Lower Cretaceous strata in the eastern Laird Basin area; *BC Ministry of Energy, Mines and Petroleum Resources*. Access: http://www.empr.gov.bc.ca/OG/oilandgas/petroleumgeology/ConventionalOilAndGas/Documents/Report.pdf

Petrel Robertson Consulting Ltd. (2003): Exploration assessment of deep Devonian gas plays, northeastern British Columbia; *BC Ministry of Energy, Mines, and Petroleum Resources*, Petroleum Geology Open File 2003-4, Map 11. 44 pages. Access: http://www.empr.gov.bc.ca/OG/oilandgas/petroleumgeology/ConventionalOilAndGas/Documents/Deep/map11.pdf

Railroad Commission of Texas (2008): Water Use in the Barnett Shale. Access: http://www.rrc.state.tx.us/barnettshale/wateruse_barnettshale.php

Richards, B.C., Barclay, J.E., Bryan, D., Hartling A., Henderson, C.M., and Hinds, R.C. (1994): Chapter 14 - Carboniferous strata of the Western Canada Sedimentary Basin, in Geological Atlas of the Western Canada Sedimentary Basin, G. Mossop and I. Shetsen, (compilers), *Canadian Society of Petroleum Geologists* and *Alberta Research Council*, pages 221–250.

Tullier, M., Seal, J., and Weiss, S. (2007): Tight sands yield to coiled tubing fracs; *E&P*, Sept 2007, pages 109–110

Veil, J.A. (2007): Trip report for field visit to Fayetteville shale gas wells; Environmental Science Division, *Argonne National Laboratory*, ANL/EVS/R-07/4. Access: http://www.ead.anl.gov/pub/doc/ANL-EVS_R07-4TripReport.pdf

AN OVERVIEW OF GEOTHERMAL ENERGY IN BRITISH COLUMBIA

Cassandra Lee[1]

ABSTRACT

In British Columbia there is significant interest in finding ways to meet increasing demand for energy without producing additional greenhouse gases. The provincial government is also committed to becoming self sufficient in electricity generation. There is potential in British Columbia for geothermal resources to provide a clean source of energy and help the province meet these objectives.

The last major geothermal energy program by the Canadian government ended in 1986. Due to a revival of interest in geothermal, the British Columbia Ministry of Energy, Mines and Petroleum Resources and the Geological Survey of Canada are working to establish the geothermal geoscience needs of western Canada and to determine the role of government geoscience agencies in addressing these needs.

Lee, C., (2009): An Overview of Geothermal Energy in British Columbia ; Geoscience Reports 2009, BC Ministry of Energy, Mines and Petroleum Resources, pages 49–52.

[1]British Columbia Ministry of Energy, Mines and Petroleum Resources, Oil and Gas Division, Resource Development and Geoscience Branch, PO Box 9333 Stn. Prov. Govt., Victoria, BC, V8W 9N3

Key Words: geothermal, clean energy, electricity, direct use, baseload, co-production, high temperature, resource assessment

INTRODUCTION

A focus of the BC Energy Plan (BC MEMPR 2007) is to ensure energy self-sufficiency in British Columbia. Due to global climate change concerns, this must be done in a way that minimizes the release of greenhouse gases (GHGs). Geothermal energy is one option to help British Columbia meet its energy needs; it is a low GHG form of energy and previous government research has identified areas of geothermal potential in the province.

GEOTHERMAL BASICS

Geothermal energy is the heat contained within the Earth. This energy can be used either indirectly to produce electricity or directly to provide heat for buildings, agriculture (e.g., greenhouse heating), or industrial uses (e.g., pulp and paper processing). Geothermal energy can also be used on a smaller scale by GeoExchange systems, also referred to as heat pumps, in buildings and homes. The temperature, depth, and location of the resource, as well as whether fluid and permeability are present, determine the ways in which it can be used and whether development is economically feasible. Geothermal energy generates a negligible amount of greenhouse gases and has a relatively small environmental footprint.

In order to extract the heat from underground, a carrier is needed to bring it to the surface. In most cases the carrier is steam (in vapour-dominated reservoirs) or water (in fluid-dominated reservoirs), although in theory other carriers (e.g., carbon dioxide) could be used. Some sites have a reservoir of heat without permeability or an associated carrier. These reservoirs can be fractured and have water artificially added to them to act as a carrier. Such systems are referred to as enhanced geothermal systems (EGS) or hot dry rock (HDR). Abandoned mines can also be used as geothermal reservoirs. For example, water from flooded mines has been successfully used to heat several buildings in Springhill, Nova Scotia (Jessop 2008a).

When generating electricity, different types of plants are used depending on the type of resource. In the case of a vapour-dominated reservoir (or a very hot water reservoir where the water can flash to steam once the pressure is reduced), the steam can be used directly to run a turbine. If the resource is not hot enough to produce steam, then a binary plant can be used. These plants use the water from the geothermal resource to heat a secondary fluid with a lower boiling point than water; the vapour of the secondary fluid then runs the turbine.

When used to generate electricity, geothermal is a baseload resource; plants are online approximately 95% of the time (Duffield and Sass 2003). Many other alternative sources of electricity, such as wind or solar, are dependent on the weather and time of day and operate at or near their maximum capacity for limited amounts of time.

The location and depth of the resource are factors that influence the feasibility of development. For power generation, it is important that the resource is close to the power grid or the end user, as building power lines across long distances is costly. When the resource is to be used directly for providing heat, it must be used close to the source; piping water a long distance will allow it to cool. The cost of drilling increases with depth, so shallower resources are cheaper to exploit than deeper ones.

GEOTHERMAL IN BRITISH COLUMBIA

Geothermal electricity is used in many areas throughout the world (Table 1). Italy has operated a geothermal plant at Larderello for over 100 years, and New Zealand has been producing geothermal electricity for 50 years (Bertani 2006). Areas of active tectonism, young volcanic belts, radiogenic plutons, and the occurrence of hot and warm springs throughout the province indicate geothermal potential in British Columbia. Although geothermal electricity was produced in British Columbia during a test project at Mount Meager, British Columbia does not yet have commercial geothermal electricity production. This is partly because of the large, relatively inexpensive hydroelectric power resource that the province enjoys as a result of its rugged topography and abundant rainfall. Due to increasing demand for electricity, the need for electricity self-sufficiency, and the desire to reduce GHGs, British Columbia is interested in developing a larger variety of low GHG energy sources and geothermal may be able to help the province meet its energy needs (BC MEMPR 2007).

While there is not yet a study that provides a firm estimate of geothermal potential, an overview of the province's geothermal potential is illustrated in the map "Geothermal Resources of British Columbia" (Fairbank and Faulkner 1992). The map indicates 18 general areas of low, moderate and high temperature geothermal potential throughout the province. These areas include: the Garibaldi Volcanic Belt, Pemberton Belt, Harrison Lake area, Okanagan Val-

TABLE 1. COUNTRIES WITH GEOTHERMAL POWER GENERATION AS OF 2005. ADAPTED FROM BERTANI 2006.

Country	Installed Capacity (MW_e)	Annual Energy Produced (GWh/y)	Number of Units
Australia	0.2	0.5	1
Austria	1.2	3.2	2
China	28	96	13
Costa Rica	163	1145	5
El Salvador	151	967	5
Ethiopia	7.3	0	2
France (Guadeloupe)	15	102	2
Germany	0.2	1.5	1
Guatemala	33	212	8
Iceland	202	14838	19
Indonesia	797	6085	15
Italy	791	5340	32
Japan	535	3467	19
Kenya	129	1088	9
Mexico	953	6282	36
New Zealand	435	2774	33
Nicaragua	77	271	3
Papua New Guinea (Lihir Island)	6	17	1
Philippines	1930	9253	57
Portugal (Sao Miguel Island)	16	90	5
Russia	79	85	11
Thailand	0.3	1.8	1
Turkey	20	105	1
United States	2564	17917	209
Total	**8933 MW_e**	**56786 GWh/y**	**490 Units**

ley, Low Arrow Lake area, Kootenay Lake area, Southern Rocky Mountain Trench, Upper Arrow Lake area, Valemount area, Hudson's Hope area, Northeast British Columbia Thermal Anomaly, Liard River area, the Stikine Volcanic Belt, Mount Edziza area, Lakelse Lake, Gardener Canal area, King Island area and the Anahim Volcanic Belt.

The energy crisis of the 1970s prompted interest in geothermal energy. The National Geothermal Energy Program of the Department of Energy, Mines and Resources officially started in 1976. The program focused on identifying and examining Canadian resources, assessing the available technology, and responding to requests for advice. The Mount Meager Project was the National Geothermal Energy Program's largest pilot project in British Columbia and involved geophysical surveys, geological mapping, and the drilling of several drill holes. The project was able to show that there is a major geothermal anomaly in the area (Jessop 2008a). Other areas that were examined, in various levels of detail, in British Columbia were Mount Cayley, Anahim Volcanic Belt, Stikine Volcanic Belt, the town of Summerland (low temperature), Hot Springs Cove and the Western Canada Sedimentary Basin near Fort Nelson (Jessop 2008a and b).

Recent detailed summaries of what was achieved during the National Geothermal Energy Program are provided by Jessop (2008a and b). When the program ended in 1986, there was no official attempt to preserve the data. Former members of the program took it upon themselves to conserve, compile, and publicly release the data (Jessop et al. 2005).

British Columbia is the only province in Canada to have developed a Geothermal Resources Act (http://www.em.gov.bc.ca/Links/legislat.htm) that regulates leasing and drilling of geothermal resources. Nova Scotia also has legislation in place but only for low-temperature resources in abandoned mines (Jessop 2008a). The act is currently under review to ensure it can accommodate a recent increase in interest in geothermal resources in the province.

There are currently several active geothermal permits and one active geothermal lease in British Columbia. These are located in the Garibaldi Volcanic belt and the Valemount area in the Rocky Mountain Trench. Western GeoPower Corporation's South Meager project is the project which is furthest along in development. There has been a long history of interest in the geothermal potential at Mount Meager, it was one of the focuses of the National Geothermal Energy Program, and as a result there has been more research conducted in this area than for other areas in British Columbia.

Co-production with Oil and Gas Wells

British Columbia has an active oil and gas industry with a large number of producing oil and gas wells. Many oil and gas wells produce water as well as oil and gas. This water can be at very high temperatures. Currently produced water is re-injected into formations at a significant cost, and companies try to limit the amount of water produced. There is potential to use the water to generate electricity before the water is re-injected. This technology has recently been successfully tested at the Rocky Mountain Oilfield Testing Centre (RMOTC) in Wyoming, USA. The RMOTC and Ormat Technologies Inc. have been using an Organic Rankine Cycle binary power plant to produce power using produced water with an approximate temperature of 88 °C. Since the project began in September 2008, the unit has been producing between 150 and 250 gross kW of power (Nations 2008).

The British Columbia Ministry of Energy, Mines and Petroleum Resources (MEMPR) has provided support to the University of British Columbia for graduate research on this topic. Research is being conducted on the potential of electricity generation from produced water in gas fields south of Fort Nelson. "The Geothermal potential of Clarke Lake and Milo gas fields, northeastern British Columbia" (Arianpoo In Preparation) is expected to be completed for Fall 2009.

Geothermal Geoscience Workshop

Due to the renewed interest in geothermal energy in recent years, British Columbia MEMPR and Natural Resources Canada Geological Survey of Canada in cooperation with the Canadian Geothermal Energy Association (CanGEA) organized a workshop to discuss and prioritize the geothermal geoscience needs for Western Canada. It also addressed the appropriate roles of provincial and federal government agencies in addressing these needs. The workshop, entitled "Geoscience Needs for Geothermal Energy Development in Western Canada", was held in Vancouver in October 2008 and was attended by approximately 50 representatives from federal and provincial agencies, CanGEA, academia, and industry. The following is a brief summary of the findings and recommendations that resulted from the workshop. A complete summary of the workshop is available (Lebel 2009).

The workshop consisted of a series of presentations on specific topics related to geothermal geoscience; presentations were followed by break-out discussion groups on similar topics. The following three questions were presented to participants to help focus the presentations and discussions:

1. What are the key geothermal energy resources and tools?
2. What geoscience is needed to support geothermal energy development?

3. What is the appropriate role of a government geological science agency in addressing these geoscience needs?

There were four key recommendations from the participants of the workshop:

1. Develop a national geothermal resource assessment.
2. Compile regional or national geothermal related geoscience databases to support geothermal energy exploration with pre-competitive geoscience.
3. Acquire new targeted geoscience information for geothermal exploration in areas with the highest potential for development.
4. Hold other forums and undertake policy analysis to advance geothermal energy in Canada.

An important workshop discussion revolved around the appropriate role of government agencies. Participants recommended that governments be the custodians of data, have a role in interpreting data, and anticipate future geoscience needs. British Columbia MEMPR is working to satisfy this recommendation by beginning to develop a database for British Columbia geothermal information. Existing geothermal data, such as files that were submitted to British Columbia MEMPR during the federal geothermal program, are being acquired and digitized, and data from other industries, such as temperatures from oil and gas wells, that are useful for geothermal exploration are being identified and collected. The goal is to build and maintain a public web-based database of geothermal information for British Columbia.

REFERENCES

Arianpoo, N. (In Preparation): The geothermal potential of Clarke Lake and Milo gas fields, northeastern British Columbia; *University of British Columbia*, unpublished Master's thesis.

[BC MEMPR] British Columbia Ministry of Energy, Mines and Petroleum Resources (2007): The BC Energy Plan: A vision for clean leadership; *BC Ministry of Energy, Mines and Petroleum Resources*, 40 pages.

Bertani, R. (2006): World geothermal power generation 2001–2005; *Geothermal Resources Council Bulletin*, May/June 2006, pages 89–111.

Duffield, W.A., and Sass, J.H. (2003): Geothermal energy – clean power from the earth's heat; *U.S Department of the Interior and the U.S. Geological Survey, Circular 1249,* 36 pages.

Fairbank, B.D., and Faulkner, R.L (1992): Geothermal resources of British Columbia; *Geological Survey of Canada*, Open File 2526, map, scale 1:2 000 000.

Jessop, A.M., Ghomshei, M.M., and Drury, M.J. (1991): Geothermal Energy in Canada; *Geothermics*, Volume 20, No 5/6, 17 pages.

Jessop, A.M., Allen, V.S., Bentkowski, W., Burgess, M., Drury, M., Judge, A.S., Lewis, T., Majorowicz, J., Mareschal, J.C., and Taylor, A.E. (2005): The Canadian geothermal data compilation; *Geological Survey of Canada*, Open File 4887.

Jessop, A.M. (2008a): Review of National Geothermal Energy Program: Phase 1 – geothermal potential of sedimentary basins; *Geological Survey of Canada,* Open File 5690, 146 pages.

Jessop, A.M. (2008b): Review of National Geothermal Energy Program: Phase 2 – geothermal potential of the Cordillera; *Geological Survey of Canada,* Open File 5906, 146 pages.

Lebel, D, editor (*in press*): Geoscience needs for geothermal energy development in western Canada: findings and recommendations, workshop proceedings; *British Columbia Ministry of Energy, Mines and Petroleum Resources,* Open File 2009-03, 18 pages.

Nations, J. (2008): Geothermal electrical generation holds promise for older oil fields; *Rocky Mountain Oilfield Testing Center*, http://www.rmotc.doe.gov/newsevents/ormat.html.

EVALUATION OF POTENTIAL PETROLEUM SYSTEMS IN THE NECHAKO BASIN

Janet Riddell[1]

ABSTRACT

Three rock suites were assembled to evaluate components of potential petroleum systems in the Nechako region. Skeena Group sandstones collected from the north-westernmost part of the Nechako region in 2007 showed low permeability, indicating generally poor reservoir quality. Surface samples collected in 2007 and 2008 along the southeastern edge of the Nechako region of mainly Jackass Mountain Group rocks returned TOC values over 1% from 5 of 8 samples. Vitrinite reflectance data indicate that rocks in the southern part of the basin region are mainly in the oil and gas window. Three of 11 samples of sandstones from the Yalakom River area have moderate permeability and porosity values that could be sufficient for a gas reservoir. Subsurface samples collected from archived drill cuttings from oil and gas exploration wells were analysed to constrain age, stratigraphic, and structural issues raised by previous work. Results identify complexities in the structural relationship between prospective units in the Nazko River area.

Riddell, J. (2009): Evaluation of Potential Petroleum Systems in the Nechako Basin; Geoscience Reports 2009, *BC Ministry of Energy, Mines and Petroleum Resources,* pages 53–63.

[1]British Columbia Ministry of Energy, Mines and Petroleum Resources, Oil and Gas Division, Resource Development and Geoscience Branch, PO Box 9333 Stn. Prov. Govt., Victoria, BC, V8W 9N3

Key Words*:* Nechako Basin, oil and gas, petroleum, hydrocarbons, Rock-Eval, source beds, vitrinite reflectance, thermal maturity, reservoir, porosity, permeability, palynology, Skeena Group, Jackass Mountain Group, Taylor Creek Group, Nemaia Formation, Nazko River

INTRODUCTION

Three rock suites were assembled to evaluate components of potential petroleum systems in the Nechako region (Figure 1).

1. Eight outcrop samples of Skeena Group sandstones collected from the northwesternmost part of the Nechako region in 2007 were analysed for porosity, permeability, and density to assess their potential reservoir quality.
2. Fifty-five outcrop samples of sandstones, mainly of the Jackass Mountain Group, collected in 2007 and 2008 along the southeastern edge of the Nechako region were analysed for reservoir quality, source rock potential, and thermal history.
3. Thirty subsurface samples were collected from archived drill cuttings from oil and gas exploration wells drilled in 1960 and 1981 in the Nazko River valley and were analysed to constrain age, stratigraphic, and structural issues raised by previous work on cuttings (Riddell et al. 2007).

Results of reservoir quality (porosity and permeability), Rock-Eval organic chemistry, and vitrinite reflectance analyses are presented here, along with comments on some preliminary results of new palynological analyses. These results build on work done in previous years (Ferri and Riddell 2006; Riddell et al. 2007; Riddell and Ferri 2008; Brown et al. 2008) on various stratigraphic elements (Figure 2) of the Nechako region. Apatite fission track (AFT) dating, zircon U-Pb radiometric, and palynological analyses are ongoing. Those results will appear in future publications.

Northwest Nechako suite

The reservoir quality of Skeena Group rocks in the north-western corner of the Nechako region was assessed through porosity, permeability, and density measurements (Table 1) conducted by Core Laboratories of Calgary on eight samples of sandstone from south of Houston, British Columbia (Figure 1). In this region, Skeena Group outcrops are dominated by resistant, homogenous, well-sorted, greenish-grey and blocky weathering sandstones. The sandstones are generally massive or have barely discernible bedding marked by wispy black carbonaceous material. The most abundant clast type is green chert; also present are black chert, black lithic fragments, feldspar crystals, and rare pink chert. Muscovite flakes are almost ubiquitous (Riddell and Ferri 2008).

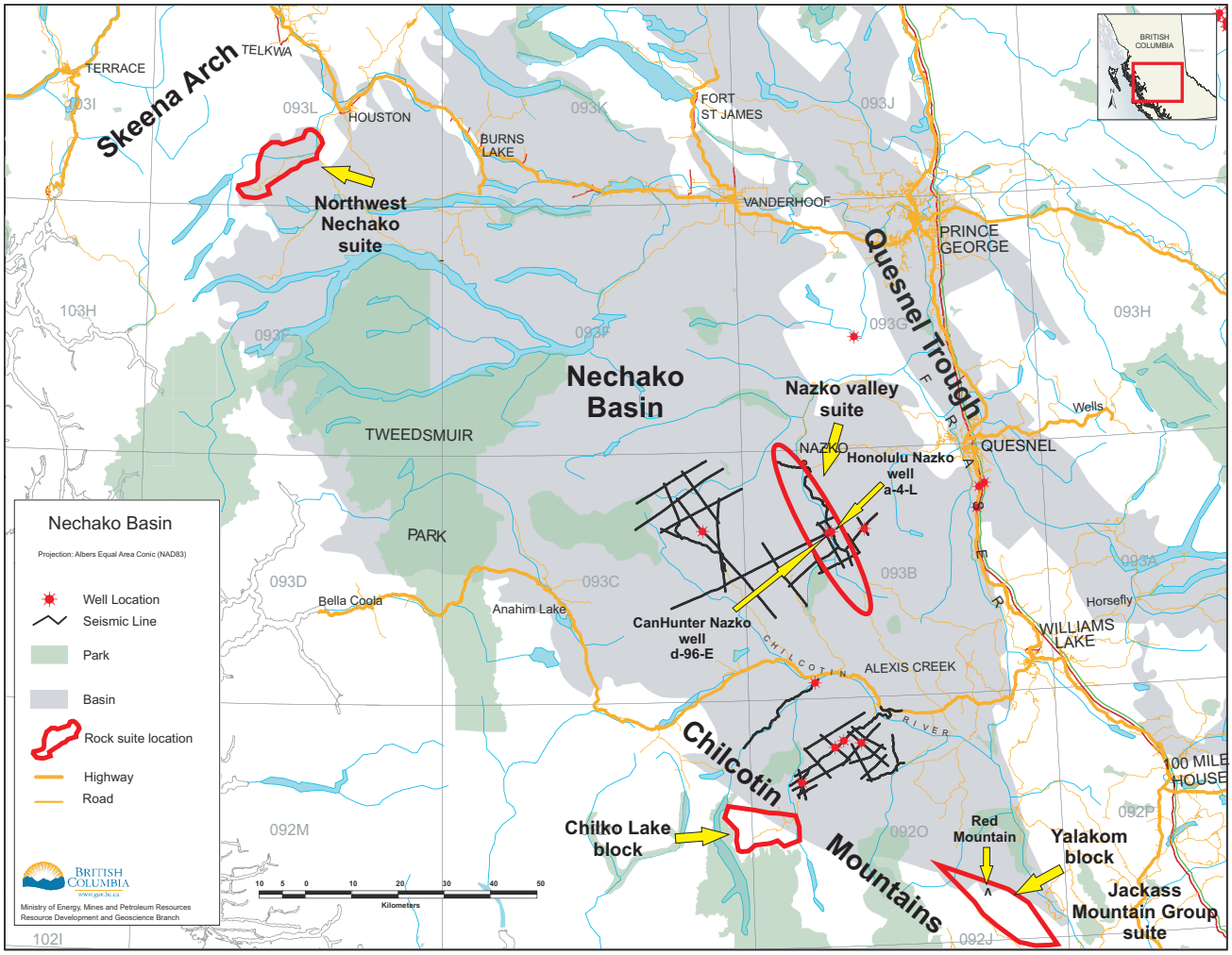

Figure 1. Location map.

RESULTS

Porosity values are mainly poor, but three samples have moderate to good porosity (5.4% to 9.9%). However, permeability values (less than 0.1 mD) for all eight samples are low.

Jackass Mountain Group suite

Regional facies patterns and basin architecture of Cretaceous Jackass Mountain Group sedimentary rocks were studied over three field seasons (2006 to 2008) by Mahoney et al. (2009). Their study focussed on the southeastern fringe of the Nechako Basin, where the Jackass Mountain Group is well exposed in two areas referred to by Mahoney et al. (2009) as the Chilko Lake and Yalakom blocks (Figure 1). The researchers collected 49 samples for analysis of reservoir quality, source bed potential, and thermal history. Most samples were from the Jackass Mountain Group, but a few samples of the Jurassic Nemaia Formation and the Cretaceous Taylor Creek Group were included.

RESULTS

Thirty hand-drilled plugs of sandstones from the Yalakom and Chilko Lake blocks (Mahoney et al. 2009) show that most samples (Table 2) have permeabilites of less than 0.01 mD; the two best samples have permeabilities of 0.12 and 0.27 mD and were collected from the Nine Mile Ridge and Madsen Creek sections in the Yalakom block. Three of the samples had moderate porosity values ranging from 5.0% to 5.7%. Brown et al. (2008) noted that pre-Late Cretaceous sedimentary rocks in the Nechako region have suffered considerable syn-depositional to very early compaction, causing destruction of primary porosity. As a result, primary depositional features such as grain size and sorting are not reliable predictors of reservoir quality. Post- depositional events such as the development of fracture permeability and of secondary porosity resulting from dissolution of minerals control the distribution of localized areas of good reservoir quality.

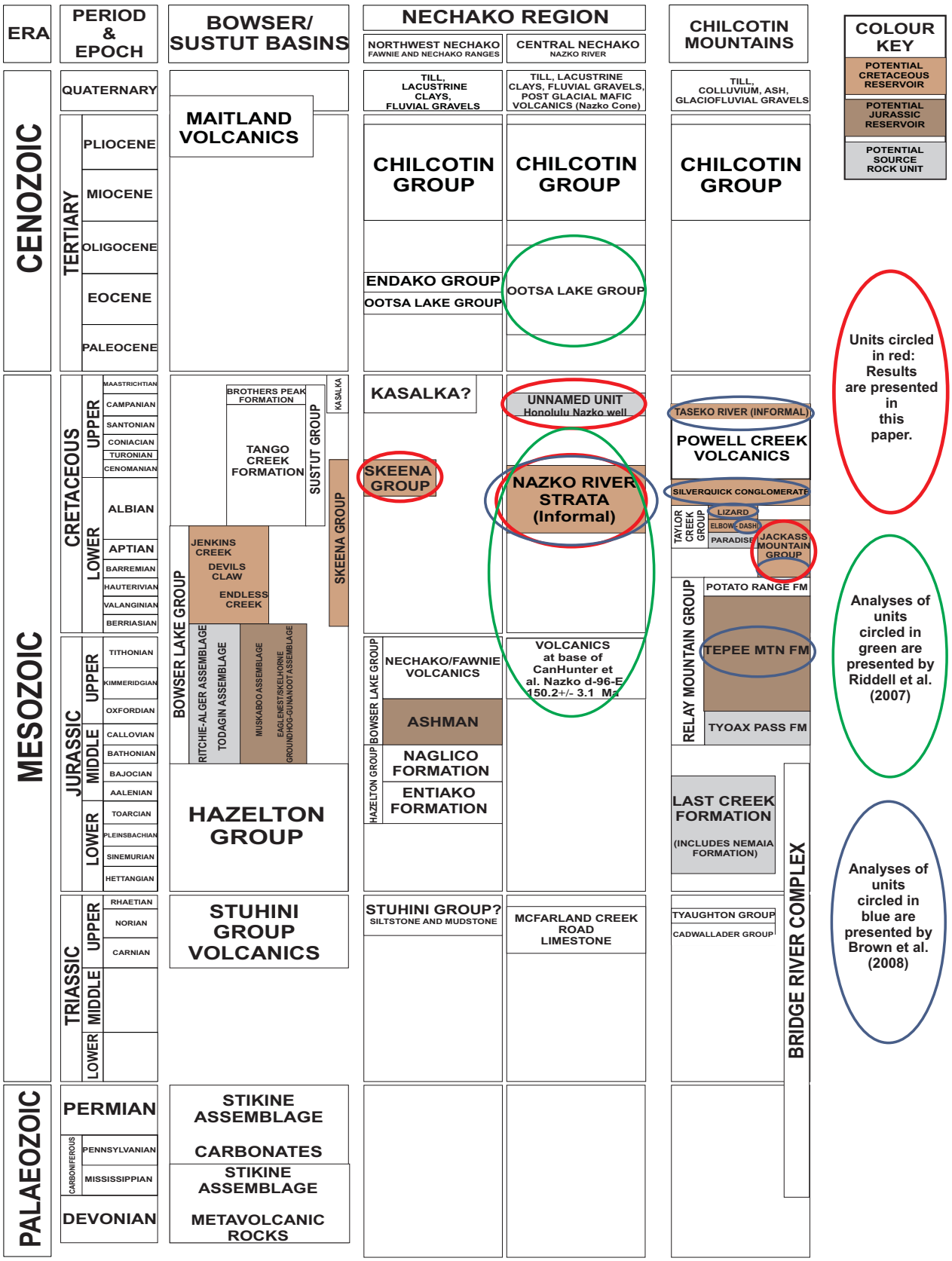

Figure 2. Nechako Basin stratigraphic correlation chart, and stratigraphic locations of samples.

TABLE 1. POROSITY AND PERMEABILITY DATA FOR SKEENA GROUP SANDSTONES FROM THE NORTHWESTERN NECHAKO REGION.

Sample	Permeability (Maximum) Kair mD	Porosity (Helium) %	Bulk density (kg/m3)	Grain Density (kg/m3)	Location Easting UTM NAD 83	Location Northing UTM NAD 83	Sandstone grain size
JR07-44	0.06	5.4	2550	2700	613738	5986834	medium
JR07-47	0.02	3.3	2600	2690	614667	5990358	medium
JR07-50	0.04	3.7	2560	2660	614576	5993426	medium
JR07-53	0.03	8.0	2510	2730	621450	5998507	medium
JR07-54	<.01	2.6	2630	2700	612559	5993131	medium
JR07-58	0.01	3.3	2610	2700	613013	5993990	fine
JR07-62	0.01	2.1	2640	2700	619260	5998870	medium
JR07-64	0.01	9.9	2420	2690	621975	5998688	medium

Mahoney et al. collected 11 samples for Rock-Eval analysis to determine source bed potential. They included shaly intervals from each of the following:

- the Beece Creek succession of the Taylor Creek Group (Schiarizza et al. 2002) from near Mount Tatlow (measured section uTCG of Mahoney et al. 2009),
- the Jackass Mountain Group on Mount Nemaia (measured section C in the Chilko Lake block of Mahoney et al. 2009),
- the Jackass Mountain Group in the Camelsfoot Range (including measured sections B and D of Mustard et al. [2008] in the Yalakom block).

Rock–Eval analyses (Table 3) provide information about the amount, quality, type, and maturity of organic carbon in the samples. A few of the samples from the Yalakom block have good to very good total organic carbon (TOC) values. Values ranging from about 2% to 11% were returned from shales within volcanic lithic sandstones of the Churn Creek facies (Schiarizza and Gaba 1997) of the Jackass Mountain Group near Red Mountain in the Yalakom block (Figure 1) and from crumbly brown shale and sand from the Madson Creek and Nine Mile Ridge sections (measured sections B and D of Mustard et al. [2008]). Rock-Eval data ratios on the two plots in Figure 3 indicate that kerogen from all sampled units is Type III (gas-prone) (Langford and Blanc-Valleron 1990; Peters 1986), which indicates that the carbon source was terrestrial plant material.

Fourteen samples were submitted for vitrinite reflectance analysis; thirteen were collected from the Yalakom block, (including 5 Red Mountain samples) and one from the Chilko Lake block. Reflectance values (Table 4) indicate maturities ranging through the oil and gas windows (Figure 4). Samples from the Red Mountain area are less mature; they are all in the oil window. The samples are plotted under the organic material Type III part of the diagram, reflecting that the Rock-Eval results from the area indicate that Type III kerogens are present.

Nazko Valley suite—archived drill cuttings

Results of previous work on archived core and cuttings from Nechako oil and gas exploration wells (Riddell et al. 2007) raised questions about the stratigraphy in the two Nazko River valley wells—Honolulu Nazko a-4-L (1960) and Canadian Hunter et al. (CanHunter) Nazko d-96-E (1981) (Figures 1 and 5). Previous sampling included only core, but not cuttings, from the Honolulu Nazko well, so in this study cuttings were submitted for palynology, thermal history (apatite fission track and vitrinite reflectance), and geochronology analyses in order to address the following issues:

- A single core sample from green shale in Honolulu Nazko a-4-L at 7364 ft (2245 m) depth (see Figure 5) produced Campanian palynomorphs (Riddell et al. 2007), indicating that a probable thrust fault is placing older (Albian-Cenomanian) over younger. A fault was proposed by the Honolulu Oil Corporation (Taylor 1961), also based on palynological analyses that indicated that "Cretaceous to Middle Upper Cretaceous" rocks occur below Lower Cretaceous strata in the well. Cuttings were submitted to find support for the Campanian date and to constrain the stratigraphic extent of the Campanian unit.
- A greenish shale unit occurs between about 2500 and 3000 m in the CanHunter Nazko (d-96-E) well (Figure 5). No age data were available for the shale, so in 2008 cuttings were submitted for palynological analyses to test whether it correlates with the Campanian green shale in the Honolulu Nazko well.
- Rock-Eval analyses by Osadetz et al. (2003) identified a 510 ft (155 m) thick interval of carbonaceous shale with good TOC and S2 values in Honolulu Nazko a-4-L between depths of 220 and 730 ft (67 and 222 m). Cuttings were submitted for palynological and vitrinite reflectance analyses to provide a better understanding of this potential source rock.

TABLE 2. POROSITY AND PERMEABILITY DATA FOR SANDSTONES (MAINLY JACKASS MOUNTAIN GROUP) FROM THE CHILCOTIN MOUNTAINS ON THE SOUTHERN FRINGE OF THE NECHAKO REGION.

Sample	Permeability (Maximum) Kair mD	Porosity (Helium) fraction	Bulk density (kg/m3)	Grain Density (kg/m3)	Area	Location Easting UTM NAD 83	Location Northing UTM NAD 83	Formation or Group	Sandstone grain size
07KM048A	<0.01	0.001	2790	2790	Chilko	421337	5713814	JMG- A	fine
07KM053C	<0.01	0.021	2710	2770	Chilko	421950	5713195	JMG- B	medium
07KM057A	<0.01	0.004	2770	2780	Chilko	422600	5712436	JMG- C	medium
07KM058B	<0.01	0.003	2830	2840	Chilko	422819	5712126	JMG- C	fine
07KM060B	<0.01	0.014	2730	2770	Chilko	419953	5713075	JMG- A	medium
07KM063A	<0.01	0.001	2820	2820	Chilko	419758	5712482	JMG- A	fine
07KM07	<0.01	0.001	2830	2830	Chilko	425453	5705048	JMG- B	fine
07KM077	<0.01	0.001	2810	2810	Chilko	424989	5705943	JMG- C	medium
07KM087	<0.01	0.008	2790	2810	Chilko	424574	5704310	Nemaia	fine
07JRG026P	<0.01	0.052	2580	2720	Yalakom	549388	5661406	JMG - F	medium
07JRG026H2	0.09	0.036	2630	2730	Yalakom	549436	5661406	JMG - F	coarse
07JRG026A2	<0.01	0.022	2640	2700	Yalakom	549566	5661291	JMG - F	medium
07JRG035B	<0.01	0.002	2830	2840	Yalakom	542640	5652417	JMG - D	fine
07JRG040A	<0.01	0.001	2770	2770	Yalakom	538625	5655828	JMG - D	fine
07JRG053B	0.12	0.057	2550	2710	Yalakom	533829	5659458	JMG - F	medium
07JRG055A	<0.01	0.031	2620	2710	Yalakom	561244	5654944	JMG - E	coarse
15MMF07	<0.01	0.024	2650	2710	Chilko	436878	5694862	Taylor Creek	fine
28MMF07	<0.01	0.022	2610	2670	Chilko	436844	5694331	Taylor Creek	medium
36MMF07	<0.01	0.02	2640	2690	Chilko	436803	5693885	Taylor Creek	medium
42MMF07	0.02	0.013	2700	2740	Chilko	436783	5693842	Taylor Creek	fine
49MMF07	<0.01	0.014	2710	2750	Chilko	436751	5693702	Taylor Creek	medium
35JBM07	<0.01	0.048	2590	2720	Yalakom	550562	5660591	JMG-E	medium
36JBM07	<0.01	0.042	2610	2720	Yalakom	549715	5661066	JMG-E	medium
37JBM07	0.06	0.045	2610	2730	Yalakom	545803	5661460	JMG-E	coarse
JBM07-47	0.27	0.05	2550	2680	Yalakom	563266	5656142	JMG-E	medium
50JBM07	<0.01	0.019	2690	2740	Chilcotin Mts.	490326	5665238	Taylor Creek	fine
58JBM07	<0.01	0.037	2650	2750	Chilko	510016	5667239	Taylor Creek	medium
07KM048A	<0.01	0.001	2790	2790	Chilko	436844	5694331	Taylor Creek	fine
07KM053C	<0.01	0.021	2710	2770	Chilko	436803	5693885	Taylor Creek	medium
07KM057A	<0.01	0.004	2770	2780	Chilko	436783	5693842	Taylor Creek	medium
07KM058B	<0.01	0.003	2830	2840	Chilko	436751	5693702	Taylor Creek	fine

- Previous Rock-Eval analyses by Osadetz et al. (2002) identified some promising TOC values from intervals where they were unexpected, specifically shaly intervals in a mainly volcanic unit near the base of the Honolulu Nazko well. These cuttings were re-examined and Rock-Eval analyses were rerun to confirm the 2002 results.
- Nineteen samples were collected from the Honolulu Nazko well cuttings for vitrinite reflectance analyses to establish a thermal maturity profile for the well.
- The age of the diorite at the base of the Honolulu Nazko well was determined to be "Cretaceous or older" by K-Ar dating done for the Honolulu Oil Company (Taylor 1961). A new sample was submitted for U-Pb zircon dating to get a more precise and reliable age.

TABLE 3. ROCK-EVAL DATA FOR ANALYSES CONDUCTED FOR THE NECHAKO PROJECT IN 2008.

Field ID	Formation	Area	Easting	Northing	TOC	S1	S2	PI	S3	Tmax	Tpeak	S3CO	PC(%)	RC%	HI	OICO	OI	MINC%
39JBM07	Taylor Creek Grp.	Mt. Tatlow	436882	5694680	0.39	0.01	0.04	0.16	0.31	607	646	0.14	0.02	0.37	10	36	79	0.1
40JBM07	Taylor Creek Grp.	Mt. Tatlow	436858	5694464	0.48	0.01	0.03	0.18	0.60	523	562	0.06	0.02	0.46	6	12	125	0.1
HFB-08-07	Jackass Mtn. Grp.	Mt. Nemaia	426045	5704835	0.16	0.01	0.03	0.17	0.28	494	533	0.04	0.01	0.15	19	25	175	0.0
HFB-08-09	Jackass Mtn. Grp.	Mt. Nemaia	425654	5704815	0.28	0.01	0.05	0.14	0.32	481	520	0.00	0.02	0.26	18	0	114	0.1
HFB-08-46	Jackass Mtn. Grp.	Nine Mile Ridge	547258	5669762	2.51	0.07	0.86	0.08	2.34	484	523	0.70	0.18	2.33	34	28	93	0.2
HFB-08-53	Jackass Mtn. Grp.	Nine Mile Ridge	555290	5672429	0.27	0.00	0.02	0.21	0.74	367	406	0.04	0.03	0.24	7	15	274	0.1
HFB-08-55	Jackass Mtn. Grp.	Madsen Creek	561982	5657241	2.02	0.01	0.14	0.08	3.93	533	572	0.32	0.14	1.88	7	16	195	0.3
HFB-08-56	Jackass Mtn. Grp.	Madsen Creek	561723	5657447	2.43	0.01	0.08	0.15	4.21	528	567	0.07	0.13	2.30	3	3	173	0.4
40EAB08	Jackass Mtn. Grp.	Red Mountain	527305	5672151	1.92	0.02	0.49	0.03	2.33	461	500	0.46	0.14	1.78	26	24	121	0.2
41EAB08	Jackass Mtn. Grp.	Red Mountain	527331	5673288	5.18	0.04	5.07	0.01	4.04	442	481	1.12	0.61	4.57	98	22	78	0.3
58EAB08	Jackass Mtn. Grp.	Red Mountain	527051	5675543	10.82	0.03	1.36	0.02	12.05	532	571	1.82	0.62	10.20	13	17	111	7.1

Depth (feet)	Section	Well	Easting	Northing	TOC	S1	S2	PI	S3	Tmax	Tpeak	S3CO	PC(%)	RC%	HI	OICO	OI	MINC%
6975	Campanian	a-4-L	471599	5835406	0.49	0.14	0.41	0.25	0.21	444	483	0.05	0.06	0.43	84	10	43	0.6
6980	Campanian	a-4-L	471599	5835406	0.45	0.08	0.30	0.21	0.23	446	485	0.04	0.04	0.41	67	9	51	0.3
8685	Nechako Volcanics?	a-4-L	471599	5835406	0.06	0.01	0.03	0.30	0.46	414	453	0.03	0.02	0.04	50	50	767	0.2
8700	Nechako Volcanics?	a-4-L	471599	5835406	3.55	13.77	26.98	0.34	0.28	391	430	0.06	3.40	0.15	760	2	8	0.1
8705	Nechako Volcanics?	a-4-L	471599	5835406	3.92	15.42	29.72	0.34	0.27	385	424	0.17	3.77	0.15	758	4	7	0.1
8710	Nechako Volcanics?	a-4-L	471599	5835406	6.27	22.83	50.06	0.31	0.29	400	439	0.08	6.07	0.20	798	1	5	0.2
8715	Nechako Volcanics?	a-4-L	471599	5835406	7.69	25.79	64.05	0.29	0.31	412	451	0.13	7.48	0.21	833	2	4	0.1
8720	Nechako Volcanics?	a-4-L	471599	5835406	5.74	20.22	46.65	0.30	0.25	405	444	0.04	5.56	0.18	813	1	4	0.2
9575	Nechako Volcanics?	a-4-L	471599	5835406	0.59	3.60	2.08	0.63	0.33	299	338	0.06	0.49	0.10	353	10	56	1.1
9580	Nechako Volcanics?	a-4-L	471599	5835406	3.32	13.75	24.63	0.36	0.42	312	351	0.02	3.20	0.12	742	1	13	0.4
9585	Nechako Volcanics?	a-4-L	471599	5835406	0.06	0.09	0.12	0.43	0.26	327	366	0.07	0.03	0.03	200	117	433	0.4
9915	Nechako Volcanics?	a-4-L	471599	5835406	0.27	0.11	0.22	0.35	0.45	312	351	0.04	0.05	0.22	81	15	167	0.4
9920	Nechako Volcanics?	a-4-L	471599	5835406	1.72	7.91	9.20	0.46	0.93	296	335	0.02	1.45	0.27	535	1	54	0.3
9925	Nechako Volcanics?	a-4-L	471599	5835406	3.93	16.22	19.50	0.45	3.88	410	449	0.96	3.12	0.81	496	24	99	0.6
9930	Nechako Volcanics?	a-4-L	471599	5835406	2.31	10.24	11.46	0.47	2.11	407	446	0.78	1.90	0.41	496	34	91	0.4
9935	Nechako Volcanics?	a-4-L	471599	5835406	0.06	0.06	0.13	0.31	0.34	319	358	0.08	0.03	0.03	217	133	567	0.2

Standard criteria for rating potential source rocks (Peters 1986)

Rating	Total organic carbon (TOC) wt. %	S1 mg HC/g rock	S2 mg HC/g rock
Poor	0 - .5	0 - .5	0 - 2.5
Fair	.5 - 1	.5 - 1	2.5 - 5
Good	1 - 2	1 - 2	5 - 10
Very good	2+	2+	10+

TOC: Total Organic Carbon (weight per cent), a measure of the amount of organic carbon. S1: the amount of hydrocarbons that can be distilled from one gram of rock (mg/g rock). S2: the amount of hydrocarbons generated by pyrolitic degradation of the kerogen in one gram of rock (mg/g rock). S3: milligrams of carbon dioxide generated from a gram of rock during temperature programming up to 390 °C. S1, S2, and S3 are measures of the quality of the generative potential of the source rock. T_{max} is the temperature at which the maximum amount of S2 hydrocarbons is generated and is an indication of thermal maturity. HI and OI are calculated from S2, S3, and TOC analytical data and are plotted to provide an indication of kerogen type (see Figures 3 and 6).

RESULTS

- The new cuttings yielded Campanian palynomorphs in the Honolulu Nazko well at about 7025 and 7530 ft (2140 and 2295 m), which supports the Campanian age (Riddell et al. 2007) for the greenish shale from drill core at 7364 ft. The new suite also produced Albian to Cenomanian palynomorphs at about 6425 and 6680 ft (1958 and 2036 m), which tightens the depth constraints on the probable thrust fault to between 6680 and 7025 ft (2036 to 2140 m) depth.
- Cuttings from the green shale unit at 2265 to 2805 m in the Can Hunter Nazko well (d-96-E) yielded only Albian to Cenomanian palynomorphs (telephone communication, Arthur Sweet 2009), so a correlation with the Campanian interval 7115 to 8595 ft (2168 to 2620 m) in the Honolulu Nazko well (a-4-L) is shown to be invalid.
- The cuttings of the shaly intervals in the volcanic unit near the base of the Honolulu Nazko well (a-4-L) had distinct waxy or petroleum odours and greasy, clumpy textures. The Rock-Eval reruns (Table 3) essentially reproduced the 2002 results of Osadetz et al., confirming that labelling or lab errors were not responsible for the original anomalies. The samples contain Type I and Type II kerogens (Figure 6). The samples are currently undergoing further examination to eliminate the possibility that the Rock-Eval results are an artifact of contamination by drilling materials.
- Preliminary palynological work indicates a Cenomanian or possibly Turonian age for the 450 ft (137 m) thick shale section from 250 to 700ft (76 to 213 m) in the Honolulu Nazko well. A mainly lacustrine depositional environment is indicated by the abundance of algal botryococcous (Arthur Sweet, telephone communication 2009) through most of the interval. Brackish water

TABLE 4. VITRINITE REFLECTANCE DATA. SURFACE SAMPLES ARE FROM JACKASS MOUNTAIN GROUP SANDSTONES FROM THE CHILCOTIN MOUNTAINS ON THE SOUTHERN FRINGE OF THE NECHAKO REGION. SUBSURFACE SAMPLES ARE FROM THE HONOLULU NAZKO WELL (A-4-L).

Sample ID	Sample type	Depth	Vitrinite Reflectance % Ro	Area	Location Easting UTM NAD 83	Location Northing UTM NAD 83	Formation
Field samples							
013JRG07	outcrop	Surface	**0.85**	Yalakom	549597	5662551	Jackass Mtn Gp
52JBM08	outcrop	Surface	**0.78**	Chilko	452262	5711849	"
53JBM08	outcrop	Surface	**1.05**	Yalakom	515269	5676521	"
56JBM08	outcrop	Surface	**1.25**	Yalakom	512925	5677117	"
HFB-08-48	outcrop	Surface	**0.86**	Yalakom	546066	5669559	"
HFB-08-53	outcrop	Surface	**1.27**	Yalakom	555290	5672429	"
HFB-08-55	outcrop	Surface	**1.19**	Yalakom	561982	5657241	"
HFB-08-56	outcrop	Surface	**0.84**	Yalakom	561723	5657447	"
32MMF08B	outcrop	Surface	**1.15**	Yalakom	506737	5681481	"
40EAB08	outcrop	Surface	**0.81**	Red Mtn.	527305	5672151	"
41EAB08	outcrop	Surface	**0.57**	Red Mtn.	527331	5673288	"
42EAB08	outcrop	Surface	**0.68**	Red Mtn.	526845	5675565	"
50EAB08	outcrop	Surface	**0.60**	Red Mtn.	527267	5673367	"
58EAB08	outcrop	Surface	**0.51**	Red Mtn.	527051	5675543	"
Subsurface samples							
Honolulu Nazko a-4-L well	cuttings	350 – 390'	**0.43**	Nazko Valley	471599	5835540	Late K shale
"	cuttings	400 – 440'	**0.44**	"	"	"	"
"	cuttings	450 - 490	**0.46**	"	"	"	"
"	cuttings	500- 540'	**0.47**	"	"	"	"
"	cuttings	550 -590'	**0.49**	"	"	"	"
"	cuttings	600 – 640'	**0.49**	"	"	"	"
"	cuttings	650 -690'	**0.50**	"	"	"	"
"	cuttings	700 – 740'	**0.51**	"	"	"	"
"	cuttings	1010 –1100'	**0.53**	"	"	"	Albian-Cenomanian
"	cuttings	1110 -1200'	**0.52**	"	"	"	"
"	cuttings	1710 -1800'	**0.60**	"	"	"	"
"	cuttings	2240 -2310'	**0.57**	"	"	"	"
"	cuttings	2670 -2690'	**0.54**	"	"	"	"
"	cuttings	3020 -3060'	**0.61**	"	"	"	"
"	cuttings	4010 –4080'	**0.64**	"	"	"	"
"	cuttings	4870 -4890'	**0.57**	"	"	"	"
"	cuttings	6110 -6140'	**0.60**	"	"	"	"
"	cuttings	7180 -7300'	**0.62**	"	"	"	Campanian shale
"	cuttings	7430 -7470'	**0.69**	"	"	"	Campanian shale

and fully marine dinoflagellates are present among the dominantly terrestrial assemblage in the 350 to 400 ft (107 to 122 m) interval, indicating the presence of one or more near-shore marine tongues in the part of the section. Vitrinite reflectance values in this interval range between 0.43% and 0.51% Ro, which are below the oil window.

- New reflectance values for 19 new samples of cuttings from Honolulu Nazko a-4-L are listed in Table 4. The reflectance values range from 0.43% to 0.69%, showing a modest increase in maturity with depth. Samples below 1100 ft (335 m) are in the oil window. The plot of reflectance values against depth for Honolulu Nazko a-4-L contrasts with those of five other Nechako region oil and gas exploration drillholes, all of which show greater maturity increases with depth. Figure 7 illustrates the significant difference in slope between the Honolulu Nazko a-4-L (yellow squares) maturity/depth relationship and those of the other Nechako oil and gas exploration wells. It is interesting that the back-stepping breaks in the plot for the CanHunter d-96-E well (red circles) which seem to indicate post-burial thrust faulting, are not apparent in the Honolulu Nazko a-4-L well, although their wellhead locations are separated

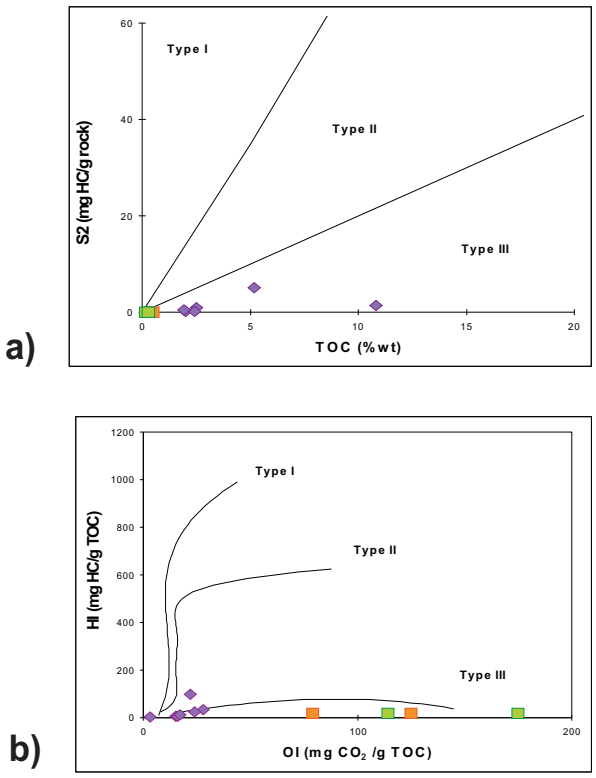

Figure 3. Kerogen classification diagrams of Rock-Eval data from surface samples collected in 2007 and 2008 from the Yalakom and Chilko Lake areas of Mahoney et al. (2009) on the southeastern fringe of the Nechako region. *Purple diamonds represent samples of Jackass Mountain Group from the Yalakom block, green squares are Jackass Mountain Group samples from the Chilko Lake block, and orange squares are Taylor Creek Group samples from the Chilko Lake block. These graphs give an indication of the kerogen type; Type I is very oil-prone, Type II is oil-prone, Type III is gas-prone. These surface samples fall in the Type III (gas-prone) fields. a) S2 versus TOC (total organic carbon); (Langford and Blanc-Valleron 1990); b) HI (hydrogen index) versus OI (oxygen index); (Peters 1986). See Table 3 for definitions of S2, S3, and TOC. HI and OI are calculated from S2, S3, and TOC values. HI = (S2/TOC) × 100 (mg HC/g C_{org}); OI = (S3/TOC) × 100 (mg HC/g C_{org}). c) HI (hydrogen index) versus Tmax.*

by only 1500 m. Also, the maturity values are generally lower (Figure 8) in the Honolulu Nazko well than they are in the CanHunter Nazko well.

- A cuttings sample from the diorite at the bottom of the Honolulu Nazko well has produced a U-Pb date from zircon of about 170 Ma (Middle Jurassic) (Paul O'Sullivan, written communication 2009). Some phases of the Stag Lake suite near Burns Lake (Whalen and Struik 1997) and the Spike Peak stock at Tatla Lake (MacIntyre et al. 2001) have similar ages.

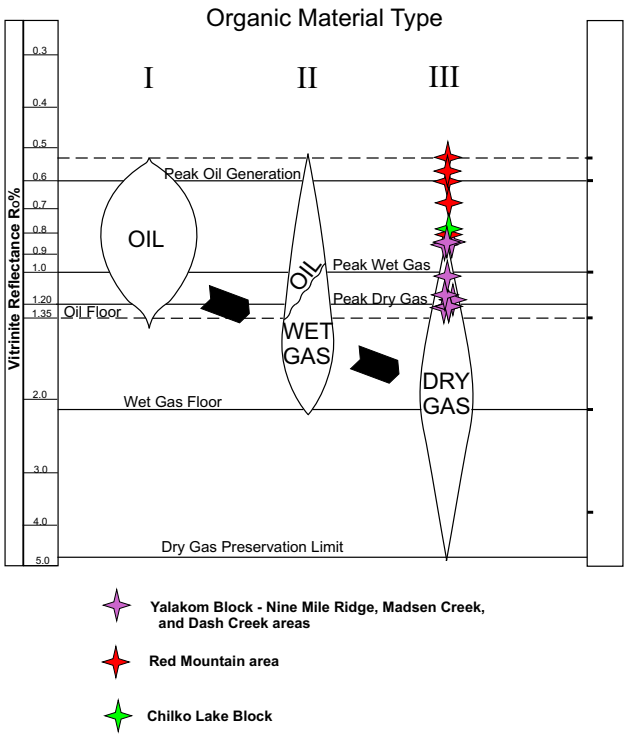

Figure 4. Thermal maturation (Ro) values from vitrinite reflectance data for the Jackass Mountain Group suite, Chilcotin Mountains. *The values are plotted under Organic Material Type III, because Rock-Eval data for the area indicate that the kerogen in these rocks is gas-prone (Type III). The diagram is adapted from Dow (2000). Most of the samples have maturity levels in the range of the oil floor to the peak dry gas zone. The exception is the Red Mountain area, where the samples are undermature for gas generation.*

CONCLUSIONS

- Low permeability (<0.06 mD) values in 5 of 8 samples indicate poor reservoir potential in Skeena Group sandstones from the area south of Houston, British Columbia.
- Jackass Mountain Group sedimentary rocks are exposed along the southeastern fringe of the Nechako region. Vitrinite reflectance thermal maturity data indicate that most samples from the Yalakom block are in the oil to dry gas windows. Six of 9 samples from shale intervals in the Red Mountain and Madsen Lake areas in the Yalakom block yielded TOC values over 1%. Ratios of H, C, and O indicate that the kerogens present are Type III (gas-prone). Three of the 11 sandstone samples from the Yalakom block have moderate permeability and porosity values that could be sufficient for a gas reservoir.
- A potential source bed at 220 to730 ft (67 to 222 m) depth in the upper part of the Honolulu Nazko well contains Type II kerogens. Palynological data indicate it is Cenomanian or possibly Turonian, and formed in a mainly lacustrine environment. There is evidence of

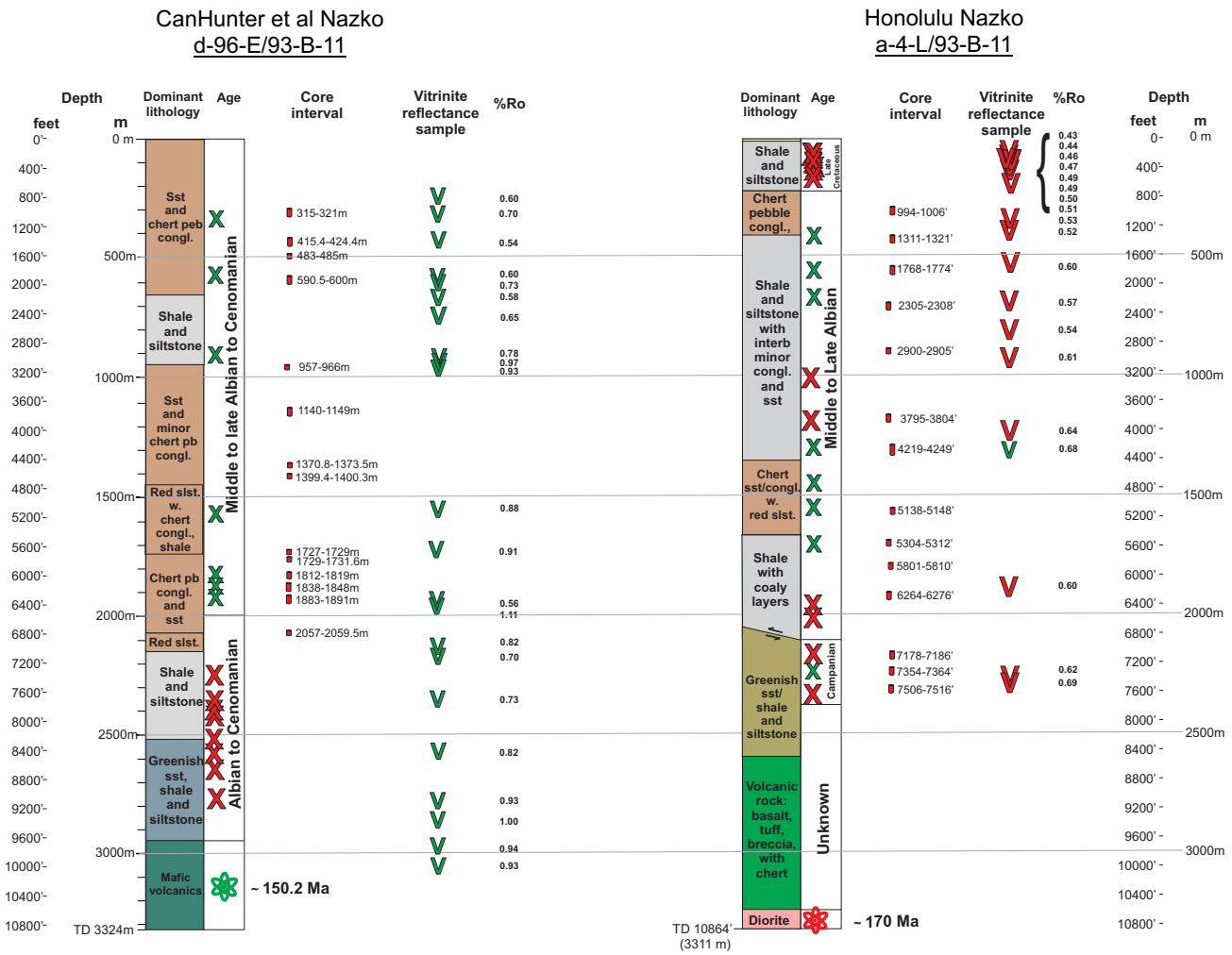

Figure 5. Stratigraphic columns of the two oil and gas exploration wells in the Nazko River valley: Honolulu Nazko (a-4-L), drilled in 1960, and CanHunter Nazko (d-96-E), drilled in 1981. *Locations of new analyses (palynology, vitrinite reflectance, and zircon for radiometric age) are marked in red. Results from samples marked in green were reported by Riddell et al. (2007). Palynology samples are marked with Xs; vitrinite reflectance samples are marked with Vs; radiometric U-Pb dates are marked with the atom symbol.*

some marine deposition in the 350 to 400 ft (107 to 122 m) interval. It is thermally undermature in this location but could form a good source bed if it is buried deeper elsewhere in the region.

- New palynogical data strengthen the Campanian age estimate for the green shale interval in the Honolulu Nazko well and extend its known stratigraphic extent to 7025 to 7530 ft (2140 to 2295m).
- The wellheads of the two Nazko River wells are only 1500 m apart, but there are significant differences between the stratigraphy of each. The Honolulu Nazko (a-4-L) well is at a lower thermal maturity and shows a lower thermal gradient than CanHunter Nazko (d-96-E) well. The CanHunter Nazko well lacks the Late Cretaceous shale sequence near the top and the Campanian section at the base. The thermal gradient, as indicated by vitrinite reflectance and apatite fission track analyses (Riddell et al. 2007), in the CanHunter Nazko well shows significant back-stepping, which suggests thrust faulting. Back-stepping is not apparent in the thermal gradient of the Honolulu Nazko well, neither in the vitrinite reflectance data nor in the thermal alteration index (TAI) of the palynological samples (Riddell et al. 2007). The thrusting that placed the older Albian-Cenomanian rocks over the Campanian in that well must predate the thermal history of the well section recorded in these samples.
- The differences between the two wells implies that, despite their important similarities (both have a 2000 to 2500 m thick Albian-Cenomanian sedimentary section and a Jurassic basement), there are significant differences in their structural and thermal histories. The nature and orientation of a structure or structures between the two wells is a question to be addressed by current interpretations of data from new seismic (Hayward and Calvert 2009) and magnetotelluric (Spratt and Craven 2009) projects.

a)

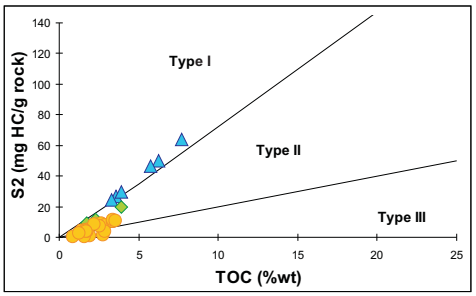

b)

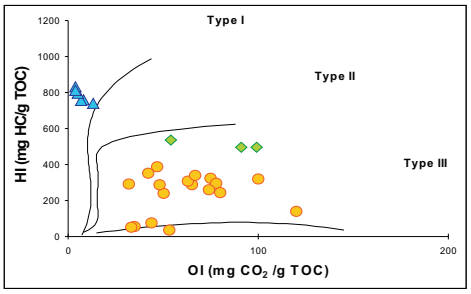

Rock-Eval samples from the Honolulu Nazko well

Late Cretaceous interval, 220 to 730 ft (67 to 222m)

Rerun samples from the volcanic unit, 6975 to 9935 ft (2125 to 3028 m)

Samples with a petroleum odour

Samples with a waxy odour

Figure 6. Kerogen classification diagrams of Rock-Eval data from subsurface drill cuttings from the Honolulu Nazko well (a-4-L/93-B-11). *Blue triangles and green diamonds represent rerun samples (results in Table 3) from shaly intervals in the volcanic unit between 6975 and 9935 ft. The green diamond samples have a distinctive wax crayon smell and fall along the Type I to Type II kerogen boundary zone. Yellow dots (values from Osadetz et al. 2003) are from the Late Cretaceous shale unit between depths of 220 and 730 feet (67 and 222 m). They have Type II and Type III kerogens. See the caption for Figure 2 for explanation of the diagrams.*

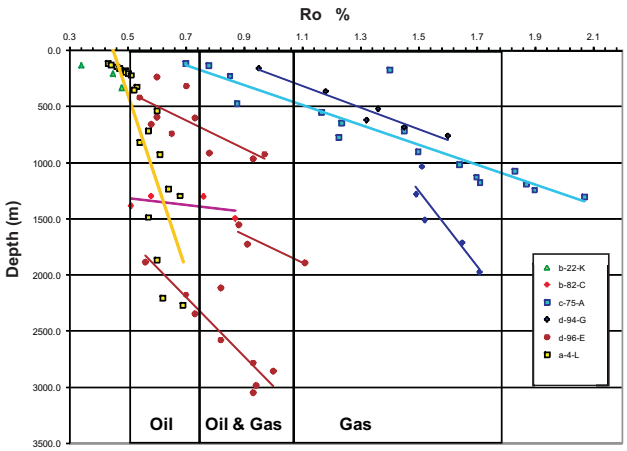

Figure 7: Vitrinite reflectance plotted against depth for Nechako region oil and gas exploration wells. *Data for the Honolulu Nazko well (a-4-L) (yellow squares) are presented in Table 4. Data for the other wells are from Riddell et al. (2007).*

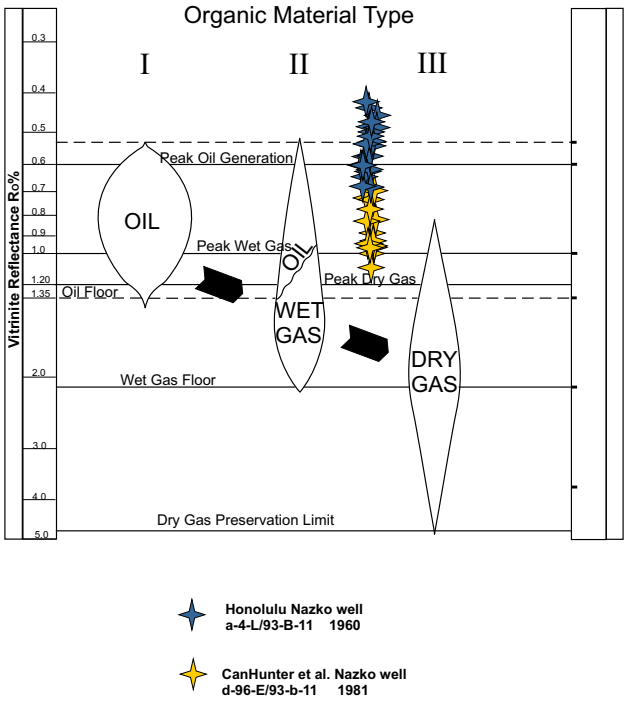

Figure 8. Thermal maturation (Ro) values from vitrinite reflectance data (from Table 4) for the Honolulu Nazko well (a-4-L) (blue crosses). *Data for the CanHunter Nazko well are from Riddell et al. (2007). The maturity range is distinctly lower in the Honolulu Nazko well than in the CanHunter Nazko well. The Honolulu Nazko well is undermature for gas generation. The CanHunter Nazko (d-96-E) well (yellow crosses) values range between the middle of the oil window and the peak dry gas zone. This diagram is adapted from Dow (2000).*

ACKNOWLEDGEMENTS

I am most grateful to members of the Jackass Mountain Group sedimentology project—Peter Mustard, Brian Mahoney, Jim Haggart, Kate MacLaurin, Rusty Goodin, Elizabeth Belford, and Michelle Forgette—for their hard work in the field while drilling, collecting, and carrying samples. Their fieldwork was supported by Geoscience BC. I would like to thank Krista Boyce, Julito Reyes, Kirk Osadetz, and Arthur Sweet of GSC Calgary for their work on the Rock-Eval, vitrinite reflectance, and palynological analyses. Core Labs of Calgary provided prompt analysis of the reservoir samples. Thanks to Filippo Ferri and Vic Levson of the BC Ministry of Energy, Mines and Petroleum Resources and Art Sweet of GSC Calgary, and Justine Pearson.

REFERENCES

Brown, D., Simpson, J., Daniels, H., and Riddell, J. (2008): Petrographic analyses of potential reservoir units of the Nechako region of British Columbia; *British Columbia Ministry of Energy, Mines and Petroleum Resources,* Petroleum Geology Open File 2008-09, 110 pages.

Dow, W.G. (2000): Geochemical analysis of outcrop samples from Tingmerkpuk 1998 project; *State of Alaska Department of Natural Resources*, Division of Geological and Geophysical Surveys, Raw Data File 2000-3, 64 pages.

Ferri, F., and Riddell, J. (2006): The Nechako Basin project: new insights from the southern Nechako Basin; *in* Summary of Activities 2006, *British Columbia Ministry of Energy, Mines and Petroleum Resources*, pages 89–124.

Hayward, N., and Calvert, A.J. (2009): Preliminary first-arrival modelling constraints on the character, thickness, and distribution of Neogene and Eocene volcanic rocks in the southeastern Nechako Basin, south-central British Columbia (NTS 092N, O, 093B, C); *in* Geoscience BC Summary of Activities 2008, *Geoscience BC,* Report 2009-1, pages 151–156.

Langford, F.F., and Blanc-Valleron, M.M. (1990): Interpreting Rock-Eval pyrolysis data using graphs of pyrolizable hydrocarbons vs. total organic carbon; *American Association of Petroleum Geologists* Bulletin, Volume 74, pages 799–804.

Mahoney, J.B., Haggart, J.W., MacLaurin, C.I., Forgette, M.M., Goodin, J.R., Balgord, E.A., and Mustard, P.S. (2009): Regional facies patterns in the northern Jackass Mountain Group, northern Methow Basin, southwestern British Columbia (NTS 092O); *in* Geoscience BC Summary of Activities 2008, *Geoscience BC*, Report 2009-1, pages 183–192.

MacIntyre, D.G., Villeneuve, M.E., and Schiarizza, P. (2001): Timing and tectonic setting of Stikine Terrane magmatism, Babine-Takla lakes area, central British Columbia; *Canadian Journal of Earth Science*, Volume 38, pages 579–601.

Mustard, P.S., Mahoney, J.B., Goodin, J.R., MacLaurin, C.I. and Haggart, J.W. (2008): New Studies of the Lower Cretaceous Jackass Mountain Group on the Southern Margin of the Nechako Basin, South-Central British Columbia: Progress and Preliminary Observations; *in* Geoscience BC Summary of Activities 2007, *Geoscience BC,* Report 2008-1, pages 135-144.

Osadetz, K.G., Snowdon, L.R., and Obermajer, M. (2003): Rock-Eval/TOC data from eleven northern British Columbia boreholes; *Geological Survey of Canada*, Open File 1550.

Peters, K.E. (1986): Guidelines for evaluating petroleum source rock using programmed pyrolysis; *American Association of Petroleum Geologists,* AAPG Bulletin, Volume 70, pages 318–329.

Riddell, J., and Ferri, F (2008): Nechako Project update; *in* Resource Development and Geoscience Branch, Geoscience Reports, *British Columbia Ministry of Energy, Mines and Petroleum Resources*, pages 67–78.

Riddell, J., Ferri, F., Sweet, A., and O'Sullivan, P. (2007): New geoscience data from the Nechako Basin Project; *in* The Nechako Initiative – Geoscience Update; *British Columbia Ministry of Energy, Mines and Petroleum Resources*, Open File 2007-1, pages 59–98.

Schiarizza, P., and Gaba, R.G, compilers (1997): Geology of the Taseko-Bridge River area [map], *in* Geology and mineral occurrences of the Taseko-Bridge River area (NTS 092O/2, 3; 092O/1; 092J/15, 16), *British Columbia Ministry of Energy, Mines and Petroleum Resources*, Bulletin 100, 1:100,000 scale.

Schiarizza, P., Riddell, J. Gaba, R.G., Melville, D.M., Umhoefer, P.J., Robinson, M.J., Jennings, B.K. and Hick, D. (2002): Geology of the Beece Creek-Nuit Mountain Area, B.C. (NTS 92N/8, 9, 10; 92O/5, 6, 12); *British Columbia Ministry of Energy, Mines and Petroleum Resources,* Geoscience Map 2002-3, 1:100 000 scale.

Spratt, J.E., and Craven, J.A. (2009): Preliminary images of the conductivity structure of the Nechako Basin, south-central British Columbia (NTS 092N, O, 093B, C, F, G) from the magnetotelluric method; *in* Geoscience BC Summary of Activities 2008, *Geoscience BC,* Report 2009-1, pages 175–182.

Taylor, N.W. (1961): A report on the Nazko River and Puntzi permit areas – Interior Plateau, central British Columbia; *British Columbia Ministry of Energy, Mines and Petroleum Resources, Petroleum Resources Branch*, Assessment Report No. 935, Honolulu Oil Corporation, 19 pages.

Whalen, J.B., and Struik, L.C., 1997. Plutonic rocks of southeast Fort Fraser map area, central British Columbia; *in* Current Research 1997-A; *Geological Survey of Canada*, pages 77–84.

POSSIBLE USE OF WATER ISOTHERMS TO MEASURE POROSITY AND RELATED PROPERTIES OF SHALES.

Barry Ryan[1] and Douglas Wells[2]

ABSTRACT

A variable but important component of the gas resource of shale is held in meso- and microporosity. As depth increases, this gas resource component becomes more important and can exceed the resource component held by adsorption on the total organic carbon. This paper introduces a new process to estimate shale porosity on cuttings at surface in a way that is minimally stressful on the shale matrix. The procedure relies on the principles outlined in the Kelvin-Laplace equation, which predicts the way porous media release water as the relative humidity of the surrounding air decreases. Water is lost from successively smaller pores as relative humidity decreases. The weight loss versus relative humidity plot (a water isotherm) therefore can provide information on pore-size distribution and total porosity.

Ryan, B. and Wells, D. (2009): Possible use of Water Isotherms to Measure Porosity and Related Properties of Shales; Geoscience Reports 2009, *BC Ministry of Energy, Mines and Petroleum Resources,* pages 65–80.

[1]Consultant, bryan@islandnet.com

[2]British Columbia Ministry of Energy, Mines and Petroleum Resources, Oil and Gas Division, Resource Development and Geoscience Branch, PO Box 9333 Stn. Prov. Govt., Victoria, BC, V8W 9N3

Key Words: Water isotherms, shale porosity, gas saturation, shale gas.

INTRODUCTION

Shale gas is the new frontier for exploration of unconventional gas. As an example of the interest, land sales largely for the opportunity to explore for shale gas in northeastern British Columbia (Horn River Basin) raised about $1 billion in 2007. Interest is high because shale with some total organic carbon (TOC) content is moderately common in the geological rock column. These shales contain small amounts of gas, in part held by adsorption on organic matter and in part held in shale microporosity. Shale is therefore both a source and reservoir rock for methane.

The ability of shale to retain gas (because of its very low permeability) makes it an enormous potential resource; however, this is also a liability in terms of turning the resource into a reserve. The amount of TOC required to convert a "normal" shale into one capable of producing shale gas is small. Productive shales contain TOC contents that range from 1% to 10%. This is the weight percent TOC measured today and is considerably less than the amount present during early maturation of the shale. As organic carbon matures and expels gases, such as methane and carbon dioxide, its volume decreases. A weight percent TOC of 6% at a rank of 0.35% (vitrinite reflectance) is reduced to about 2% TOC when rank increases to 2% based on the difference in moisture and volatile matter contents at the two ranks. As well as expelling methane, the TOC expels heavier gases such as ethane and propane, which are cracked to methane at ranks greater than about 1.3%. The decrease in TOC volume as rank increases may translate into post-depositional porosity of up to 9% to add to original depositional porosity (Figure 1). All porosity is available to be charged by methane generated during TOC maturation that is in excess of that retained by adsorption on the TOC. This includes methane generated by cracking heavier gases in the oil rank window.

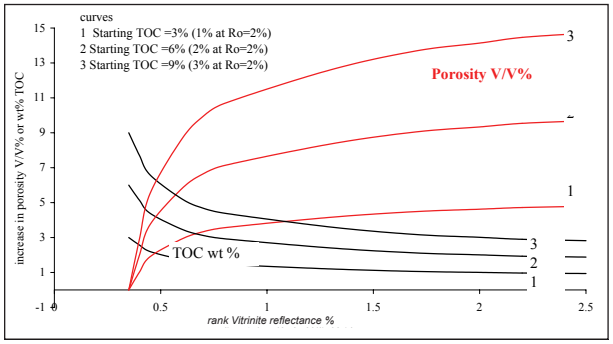

Figure 1. Volume decrease of TOC as rank increases and resulting increase in secondary porosity V/V% - secondary porosity.

In simple terms, for shale to be gas charged, there has to be a balance between the thermal maturity and the ratio of porosity to TOC (Figure 2). There are a lot of variables, so Figure 2 is only a schematic representation. In terms of total resource, the ratio of free gas in porosity to adsorbed

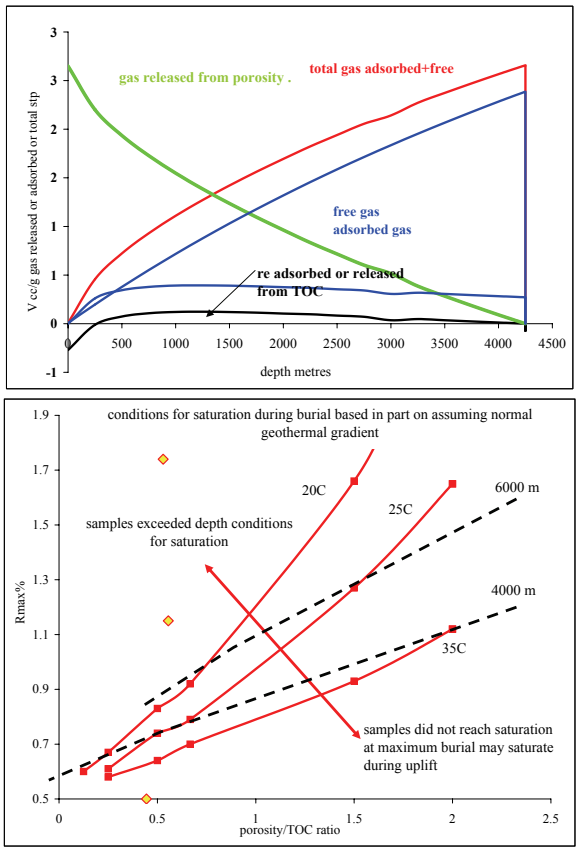

Figure 2. Schematic relationship of ratio porosity/TOC to rank for gas-filled porosity.

gas on TOC will increase with depth. This is because the rate of increase in adsorption capacity of TOC with depth is less than the rate of increase in capacity of porosity to store gas with depth. Porosity, size distribution of porosity, and degree of water saturation are very important properties in estimating the resource potential of shale, assuming there is sufficient TOC to charge the porosity.

Shale porosity can become gas saturated in two ways. First, the excess thermogenic gas generated by the TOC during maturation pushes water out of porosity through interconnected small pores by overcoming hydrostatic pressure plus capillary pressure. Excess gas can also remove water vapour to a degree that depends on the partial pressure of water in the gas phase. This requires a substantial excess of methane greater than that required to fill the porosity at existing pressure and temperature conditions.

Water occupies porosity as free water and as water adsorbed on TOC and kaolinite. Shales contain a high proportion of clay (usually kaolinite), so there is the possibility that some water is held in porosity by adsorption on these clay particles. Under burial conditions, it is possible that excess methane can reduce relative humidity (RH) in porosity enough that water adsorbed on kaolinite is removed in the vapour phase and the adsorption sites (volume) are then filled by methane. It is unlikely that water adsorbed on kaolinite can be removed during uplift or by biogenic methane that has to access microporosity from external fractures.

Measuring shale porosity is difficult. As the definition of shale implies, it has meso- or microporosity, and differentiating between connected porosity and total porosity is a challenge. Total porosity, which may be greater than connected porosity, is difficult to measure and probably not important for estimating free gas volumes unless diffusion of free gas through pore walls is considered. Another major problem when measuring porosity is that most techniques are applied to samples at surface, not at in-situ temperature and pressure.

Techniques for measuring connected porosity involve infusing mercury or inert gases into dry samples. Mercury infusion under high pressure may not measure the microporosity of interest, which is the connected porosity available for methane molecules. Methane and helium molecules are approximately spherical, with a significant difference in molecular size (CH_4 = 4.3 A° [angstroms]; He = 0.98 A°). Therefore, using an inert gas such as helium may overestimate methane porosity. Water molecules (2.8 A°) are closer in size to methane molecules and might be a better candidate for measuring porosity available to methane. Geophysical logs provide various measurements of porosity and water saturation, but there is always a desire to confirm results with measurements on samples at surface.

This paper describes an alternative method of estimating shale porosity. It involves drying samples by progressively reducing RH to determine volume loss of water and associated weight decrease of samples.

Porosity is calculated using

$$Ø = [(SG_{dry} - SG_{wet})/(SG_{dry} - 1)] \times 100$$

where

Ø = porosity (volume percent)

SG_{dry} = specific gravity of sample with pore water removed (g/cm^3)

SG_{wet} = specific gravity of the sample with pore water included (g/cm^3)

SG_{wet} is determined using Archimedes' Principle. Samples are weighed and have only surface water removed. The weight loss of the sample after drying to zero RH and dry weight at zero RH provide enough data to calculate SG_{dry}.

The initial assumption is that sample porosity is totally filled with water and that decrease in weight as RH decreases is directly related to removal of water from porosity. Samples are maintained at atmospheric temperature and pressure as RH is reduced. The resulting plot of weight loss versus decreasing RH is a water isotherm. Water isotherms were used in the past to investigate porosity and water retention in coals (See Ryan 2006 for references on the subject).

If porosity is not totally filled with water, then it is possible, using He pycnometry, to measure SG_{dry} to estimate porosity and degree of gas saturation as described later.

BACKGROUND

Gas isotherms are used extensively to study adsorption, pore-size distribution, and diffusion characteristics of solids. Generally, inert gases such as helium, nitrogen, and argon are used, with non-inert gases such as carbon dioxide used less frequently. There is also literature that describes the use of water isotherms to investigate properties of coal, building materials, soil, and organic compounds. Many of these studies are aimed at understanding how these materials hold water, pore-size distribution, and porosity determination. For example, Allardice and Evans (1978) described water isotherms on coal; Likos and Ning (2002) used water isotherms to investigate water adsorption on clays; Carmiet and Roels (2002) used water isotherms to study moisture uptake and porosity of building materials. Studies in these areas have applicability to measurement of porosity in shale cuttings and help provide an understanding of pore-size distribution.

Why construct a water isotherm to measure porosity? It is possible to dry a sample either by heating or putting it in a desiccator at zero RH and weighing the sample before and after drying. Unfortunately this does not address the initial problem—differentiating between water on the surface of shale cuttings and water held in porosity (pore water). Also, drying by increasing temperature may damage samples, rendering the results invalid.

This study uses shale cuttings wet-screened to a particular mesh size; consequently, the first problem is to differentiate between surface water and pore water. Water isotherms make this possible because surface moisture evaporates from samples at higher RH values than does pore water. For most porous rocks, there will not be a distinct break point in the weight loss versus RH curve, as large pores or grain fractures will hold water with about the same tenacity as grain surfaces. Because of the meso- to microporosity in shale, the weight loss versus RH curve shows a distinct break point that separates surface water from pore water (Figure 3).

Many authors divide water isotherms into two main fields: the over-hygroscopic field at high RH, which probably represents surface water, and the hygroscopic field at lower RH, which probably represents water held mainly by capillary force in meso- and micropores (Grunewald 2007). The break in slope in the RH versus weight plots separates these two fields. There does not appear to be a consistent definition of over-hygroscopic water, but one interpretation is that it is surface water adhered to a surface with a tenacity that is related to the liquid–solid contact angle. Water with

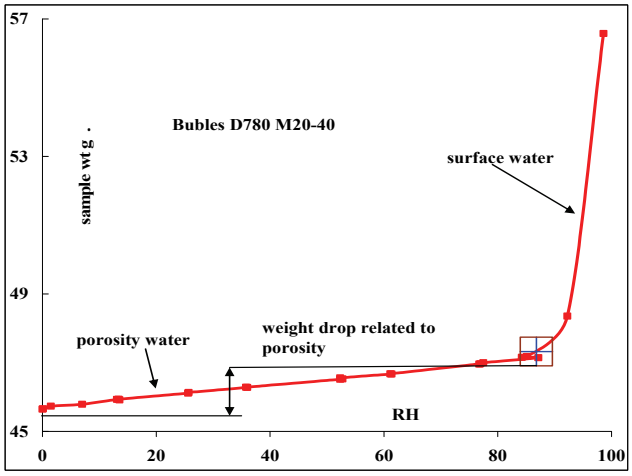

Figure 3. A water isotherm for shale cuttings (20 to 40 mesh size) illustrates the break between surface and pore moisture (Sample Bubles D780).

low contact angles on hydrophilic surfaces will be dried at lower RH than will water with larger contact angles on hydrophobic surfaces.

It is difficult to separate, in the hygroscopic field, water held by capillary forces in small pores from water adsorbed onto clays. A number of papers discuss adsorption of water by clays. Likos and Lu (2002) studied water adsorption on suspended mixtures of smectite and kaolinite at varying values of RH. Curves generally have an inflection point at about 85% RH, which Likos and Lu interpreted as the change from molecular adsorption to capillary condensation. They were studying fine grains of clays in a slurry, so the inflection point could alternatively be the break point between surface moisture and adsorbed moisture (hygroscopic to over-hygroscopic). They did document the adsorption ability of kaolinte at decreasing RH and found that there was about a 2.5% weight loss when RH changed from about 85% to 0%. This would correspond to an apparent porosity of about 6.5% for a sample composed of 100% kaolinite. Shales are not 100% kaolinite, and the ability of a kaolinite slurry to adsorb water is probably much greater than that of kaolinite as a component of solid rock. Is the volume occupied by water adsorbed on kaolinite available to be occupied by methane gas? Aggressively drying a sample in a laboratory would remove this water and influence the calculation of porosity. Calculated porosity might be higher than that available for free gas with a high relative humidity.

Equilibrium moisture content of coal is a laboratory measurement designed to provide an estimate of the moisture-holding capacity of coal. The measurement is done in an atmosphere with 97.6% RH controlled by a saturated solution of KSO_4. This RH value was chosen probably because coal is hydrophobic, and therefore surface moisture is removed at relatively high values of RH compared to rocks that are variably hydrophilic and might retain surface moisture at lower values of RH.

Two water isotherms were constructed for a sample of high-volatile B bituminous coal. Coal of this rank usually has equilibrium moisture (EQ) in the range of 6% to 10%, and the two sample splits have EQ moisture of 6.33% and 6.58%, which agrees with the commercial laboratory EQ moisture analysis made on coal from the same area. The break points in both graphs are at about 98% RH (Figure 4), illustrating the difference in wettability of hydrophobic coal and of hydrophilic shale. Based on the comparison of coal and shale water isotherms, the break point in slope varies based on the degree of hydrophobicity, which is a measure of surface wettability. Careful measurements may indicate subtle variations in wettability, which is closely related to relative permeability.

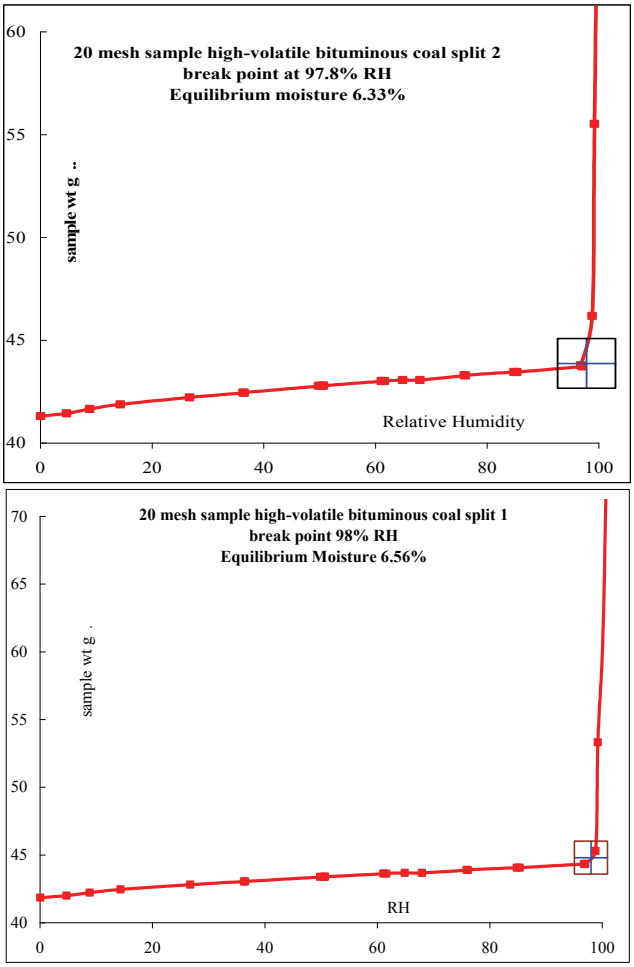

Figure 4. Water isotherms on two samples of high-volatile B coal indicate break points at about 98% RH.

Attempts to do EQ measurements on shales using ASTM (American Society for Testing and Materials) procedures may not produce meaningful results, because the reported water content may include surface moisture. It is probable that surface water is retained by shale until RH values are reduced to about 85%, depending in part on sample size and maybe grain size. An indication of the RH values separating over-hygroscopic from hygroscopic fields is evident in data from Grunewald (2007) (Figure 5).

KELVIN EQUATION AND PORE-SIZE DISTRIBUTION

The part of a water isotherm that covers the hygroscopic range provides information about cumulative volume of connected pores, distribution of pore sizes, and capillary pressure. Capillary force is an attractive force between liquids and solids that manifests as surface tension and contact angles between solid and liquid. An example of surface tension and capillary pressure is the ability of liquid in a small tube placed in a vessel to rise, against the force of gravity, above the liquid in the vessel. The liquid height is proportional to the diameter of the tube. As the diameter decreases, the liquid height in the tube increases. Thus, surface tension will work against the inclination of water molecules to evaporate when RH of the surrounding gas phase is less than 100%. The effect increases as pore diameter decreases and depends on RH, not on total pressure.

Relative humidity is reduced above a concave meniscus because surface tension forces reduce the ability of water to evaporate. This has the effect of producing a relationship between the radius of the meniscus or pore throat size and the RH below which water will evaporate from the pore and above which water will remain in the pore. The Kelvin equation (also referred to as the Kelvin-Laplace equation) relates pore radius to RH. It also incorporates surface tension, universal gas constant, and temperature (in Kelvin). An explanation of the development of the Kelvin equation and how it relates to analysis of pore-size distribution is given by many authors (for example, Grunewald 2007).

There are a number of forms of the Kelvin equation. The standard form relates pore radius to surface tension and RH:

$$\ln(RH) = -2\sigma/(R_c \rho RT)$$

where

ln = natural logarithm

σ = surface tension (N/m)

Rc = Kelvin mean radius of pore (m)

ρ = density of liquid (g/cm^3)

R = universal gas constant ($JK^{-1}mol^{-1}$)

T = temperature (K)

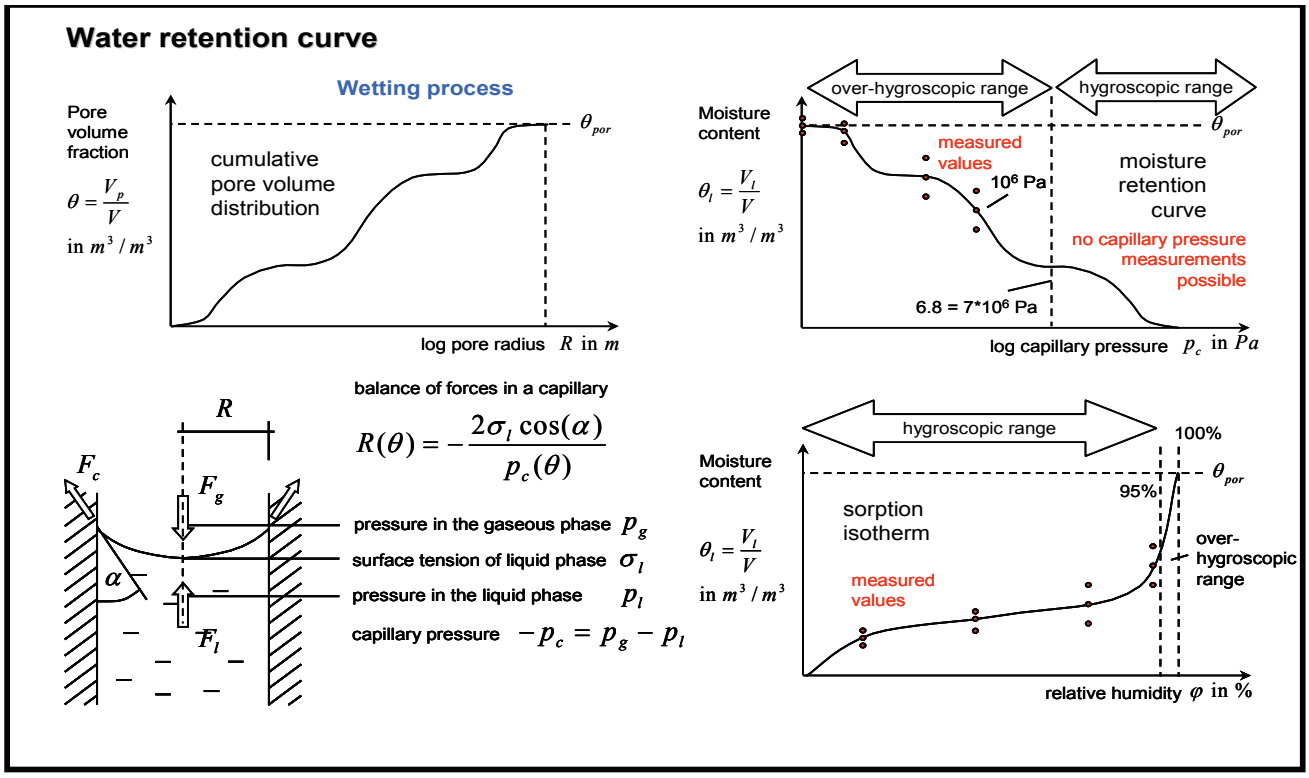

Figure 5. Hygroscopic and over-hygroscopic fields (Grunewald 2007).

Alternatively the Kelvin equation from Wang and Fredlund 2003 can be written as

$RTln(RH) = \sigma V[1/Rc - (P - P_{sat})]$

where

R = universal gas constant ($JK^{-1}mol^{-1}$)

T = temperature (K)

ln = natural logarithm

σ = surface tension (N/m)

V = molar volume (m^3/mol)

Rc = Kelvin mean radius of pore (m)

P = vapour pressure (N/m^2)

Psat = saturated vapour pressure (N/m^2)

Shang et al. (1994) and Prost et al. (1998) use the Kelvin-Laplace equations in the following form:

$ln(RH) = [(V)/(RT)]2(\sigma/R_k)$

where

ln = natural logarithm

V = molar volume (m^3/mol)

R = universal gas constant ($JK^{-1}mol^{-1}$)

T = temperature (K)

σ = surface tension (N/m)

R_k = R_c – t where R_c = actual pore radius and t = adsorbed film thickness

Another form is this:

$P_c = \rho RTln(RH)$

where

P_c = capillary pressure (MPa)

ρ = density of liquid (g/cm^3)

R = universal gas constant (JK-1mol-1)

T = temperature (K)

ln = natural logarithm

Or

$R_c = -2\sigma[\cos(\alpha)/P_c]$

where

R_c = Kelvin mean radius of pore (m)

σ = surface tension (N/m)

α = contact angle. The angle α is close to 0, so cos(α) is assumed to be 1

P_c = capillary pressure (Pa)

Molar volume of water = 1.8×10^{-5} m^3/mol

Surface tension = 0.0728 N/m^2

T (degrees Kelvin at stp) = 298 K

R (universal gas constant) = 8.314 $JK^{-1}mol^{-1}$

Figure 6 indicates the relationship between RH, capillary pressure, and pore-size distribution predicted by the Kelvin equation. The equation is used in material sciences and in soil sciences, where it is applied to the drying effect of decreased humidity on soils composed of compacted particles with surface water contained in the interstices (Wang and Fredlund 2003). A number of authors have used the Kelvin-Laplace equation and capillary pressure to document pore-size distribution. Dabous et al. (1976) measured pores sizes ranging from 0.4 to 200 μ in coal core using measurements of capillary pressure and the relationship $R_c = -2\sigma \times \cos(\alpha)/P_c$. Prost et al. (1998) used water isotherms to differentiate between water held external to quartz grains from water held in the pores in grains. Pore sizes are 3 to 6 μ (0.003 to 0.006 mm) and 18 to 32 μ (0.018 to 0.032 mm). This falls in the mid range of macropores (0.0001 to 0.1 mm) as used in geological literature. Water is extracted from these pores at 2 distinct RH values.

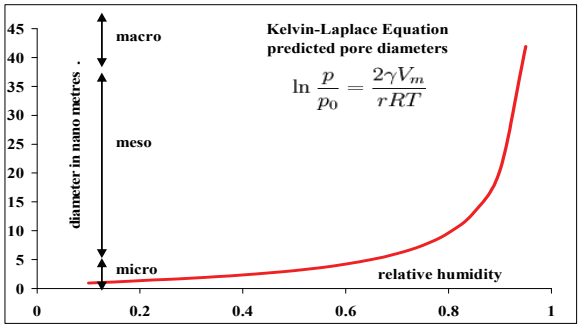

Micro metres = mm (10^{-6} metres) nano metres = nm (10^{-9} metres)
Angstroms = A (10^{-10} metres)

	Nano metres		Angstroms	
	from	to	from	to
Micro pores	0.2	2	2	20
Meso pores	2	50	20	500
Macro pores	50	10000	500	100 000
20-40 mesh grain Dia	6.4*10 5			
40-60 mesh grain Dia	3.4*10 5			
ratio (grain diameter 20-40m)/(macro pore)			128000	640

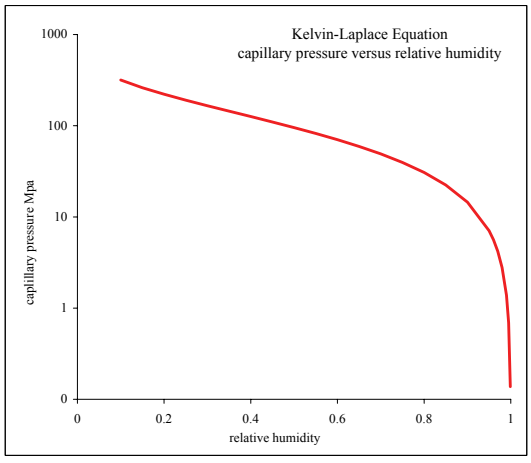

Figure 6. Relative humidity versus pore size (top) and versus capillary pressure (bottom) as predicted by the Kelvin-Laplace equation.

The Kelvin equation provides a value for the Kelvin radius, which is probably an underestimate of the pore size holding moisture at any RH value. It appears that for rocks with mainly meso- and micro-porosity, water isotherms will provide a good way of differentiating between surface water on grains and pore water filling mesoporosity (averaging 0.00001 mm). For samples with porosity in the macropore range, there is confusion between grain surface water and pore water.

In the ideal case, the Kelvin equation provides a pore-size distribution (Figure 6). In general it is difficult to classify the pore-size distribution in a sample. Water escaping from a sample composed of variable connected pore sizes will be forced to travel through both narrow and wide pore throats. The smaller pore throats will tend to control water escape, therefore a water isotherm cannot be used to clearly provide a pore-size distribution.

Inflection points in an isotherm represent minima or maxima in the rate of change in water loss. A plot of δV/δ(RH) versus RH displays these inflection points as maxima or minima, indicating that they represent preferences for particular pore sizes in the pore-size distribution.

FRENKEL-HALSEY-HILL EQUATION

Frenkel (1946), Halsey (1948), and Hill (1952) developed the Frenkel-Halsey-Hill (FHH) equation, which helps demonstrate the state of adsorbed water versus RH rather than pore-size distributions versus RH.

The equation is

$(q/q_m)^n = A/\ln(RH)$

where

q/q_m = relative saturation = RH
n = a power term
ln = natural logarithm
A = $e_o/(X_m^n RT)$
e_o = potential for adsorption
X_m = film thickness (m)
R = gas constant ($JK^{-1}mol^{-1}$)
T = temperature (K)
RH = $[(1 - Ø)/Ø][\rho r/\rho wq]$
Ø = porosity %
ρ = density of rock or water (g/cm^3)

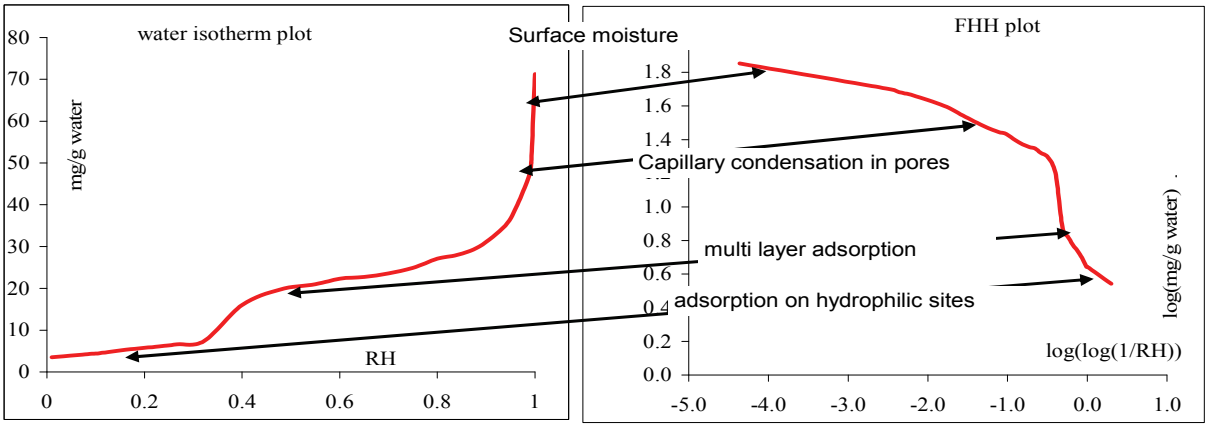

Figure 7. The Frenkel-Halsey-Hill equation demonstrates the relationship between RH and the ways water is held in pores.

The equation can be rewritten as

$\ln[\ln(1/RH)] = \ln(A) - n[\ln(RH)]$

or

$Ln(RH) = \ln(A)/n - Ln[\ln(1/RH)]/n$

They showed that for intermediate values of RH:

$\log(1/RH) = k/w^r$

where

w = water content; k and r are constants

In this form the equation provides a useful plot for differentiating four domains of water retention (Figure 7):

Domain 1 = Monolayer adsorption (adsorption on hydrophilic sites).

Domain 2 = Multilayer adsorption.

Domain 3 = Water held capillary condensation. (capillary condensation in pores).

Domain 4 = External surface water (surface moisture).

Porosity is defined by the water represented by domain 3. Water represented by domains 1 and 2 is probably adsorbed on clays and might not be occupying porosity available for free gas.

The FHH plot demonstrates the way a solid retains water; it does not predict pore sizes. The water retention method is closely related to pore size. Prost et al. (1998) used the FHH equation to break out these four domains of water retention in quartz and Al_2O_3 pastes. Shang et al. (1994) found that the FHH equation fits water desorption isotherms well and is capable of tracking capillary condensation and adsorption processes. They used cuttings and core samples and found that cuttings could be used despite the increase in external surface area.

CAPILLARY PRESSURE

Capillary pressure is the pressure required to initiate fluid movement through pore throats of a particular size. It is dependent on pore size, RH, surface tension, and temperature. Capillary pressure increases as temperature and surface tension increase and decreases as pore size and RH increase. At a particular capillary pressure, there is a value of RH above which the liquid in a pore is stable and below which water will tend to evaporate. This is the equilibrium RH value associated with the specific capillary pressure. At a fixed temperature, capillary pressure increases exponentially as RH decreases and this, in effect, defines the irreducible water content of a porous solid. Irreducible water is found wetting pores and can only be removed by evaporation at very low RH.

Maturation of TOC during burial generates gas in excess of that retained by adsorption. This gas fills pores as temperature and pressure increase with depth of burial. Capillary pressure in pores is fixed mainly by pore size, though it decreases somewhat as surface tension decreases with increasing temperature. Relative humidity in pores increases as temperature (and therefore depth) increases. For pores to survive gas filled, or for gas saturation to increase by displacing water, gas pressure must overcome hydrostatic pressure plus capillary pressure. This is increasingly difficult as pores get smaller but is probably easier as depth increases.

The potential for shale porosity to be gas overpressured is in part dependent on the ratio of porosity to TOC and on rank, as these two parameters define the ability of shale to have excess gas available to move water out of the porosity. As an example, a pore diameter of 0.001 mm has a capillary pressure of about 2.9 MPa, which corresponds to a depth of about 300 m, based on a normal geothermal gradient.

Capillary pressure increases exponentially as pore sizes decrease during burial and compaction. While maturity of TOC is increasing, secondary porosity also is increasing, and excess gas is produced, which may force water out

of pores. As compaction and burial progress, pore sizes decrease, as does the amount of excess gas generated by TOC for each incremental increase in rank. At this stage, capillary pressure increases because of decreased pore size, and external water tries to re-enter pores. Pore pressure also increases because of increasing temperature and decreasing pore volume, making it difficult for water to re-enter small pores. Compaction, increase in temperature, and generation of excess gas all increase the gas pressure in pores. This more than counters the increase in capillary pressure, which will tend to force water back into gas-filled pores.

As TOC matures it produces methane, which under geological conditions will remain as a gas or in solution in water. Once water surrounding TOC is gas saturated, any further gas generated will remain, partially filling the porosity at a pressure that is hydrostatic plus capillary. The percent of porosity that is gas filled may be small, but because water is incompressible, some water will be forced out of the porosity. Generally, rough calculations using plausible values of TOC, porosity, and cumulative gas generated indicate that it is difficult for excess gas to provide sufficient overpressure during burial to overcome hydrostatic and capillary pressure and force all the water out of the porosity. It will force out some water because gas in excess of adsorbed gas is nearly always generated. During uplift, as hydrostatic pressure decreases, pore overpressure may develop and work to force water out of pores. In this case, hydrostatic pressure may appear to be normal, but once new fracture surfaces are developed during completion of the well and pressure is reduced during gas production, there may be a rapid expulsion of water and gas from the porosity as pore gas pressure is able to overcome capillary pressure.

Capillary pressure, acting on a pore of fixed size, increases with temperature and therefore depth. However, the RH value separating evaporation from adsorption increases with temperature so that the net affect is that the capillary pressure acting on liquid in a pore at equilibrium does not change as temperature increases. It is therefore possible to estimate the degree of overpressuring in shale that excess TOC gas must generate in order to push water out of micropores and into fractures.

During uplift, if there is a dry gas phase (biogenic gas with low RH) in fractures, then excess gas can remove water from pores by evaporation and effectively erode water from shale porosity working inwards from fractures. Water in contact with methane will become saturated with methane in solution. Methane in solution that comes in contact with TOC surfaces will adsorb onto TOC surfaces. It is therefore possible for the TOC in shale to be adsorption saturated, but harder for the porosity to become gas saturated.

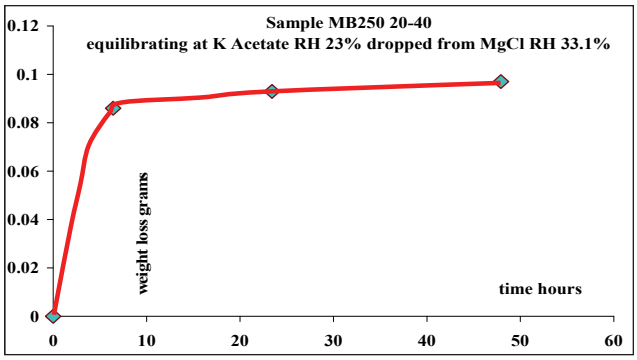

Figure 8. The graph of weight loss over time at a set relative humidity is similar to a desorption curve.

IMPLICATIONS FOR DIFFUSION

The weight loss of a sample is not dependent on the time for which it is held at a particular RH value, as long as an equilibrium time of about one day has elapsed; rather it is dependent on the RH value (Figure 8). The weight loss versus time plot is very similar to a desorption curve for methane, and consequently, it is possible to use the equivalent of sorption time to comment about the diffusivity, or micropermeability, of a sample.

Permeability in shale is often very low, and if the rock is not fractured into small blocks, then diffusion may be the process that limits gas production. There is probably not a single diffusion coefficient in effect. Some gas molecules move to grain boundaries, accessing larger connected pores (a weight loss versus time plot at a higher RH step), and some gas molecules move to grain boundaries, accessing smaller connected pores, and experience a slower diffusion (as measured by a weight loss versus time plot at a lower RH step). It therefore becomes possible to construct time versus water loss plots for different initial and final RH values. This is equivalent to constructing desorption curves, each one providing a sorption time constant for a different component of the gas resource represented by the fraction of porosity associated with the RH step.

WATER FILM THICKNESS

Film thickness or wettability on grain boundaries provides information on physical characteristics of rock that influence relative permeability of gas flow along fractures. It is possible to estimate the thickness of the wetting surface by using dry sample weight and average grain diameter to estimate total surface area of all grains (TS). At each RH above the break in slope separating surface water from pore water, the weight of water is equivalent to identifying a volume of water, which, when divided by TS, provides the thickness of the water layer. The rate at which this thickness decreases as RH decreases (towards RH at break point) is a measure of hydrophobicity, which affects the relative per-

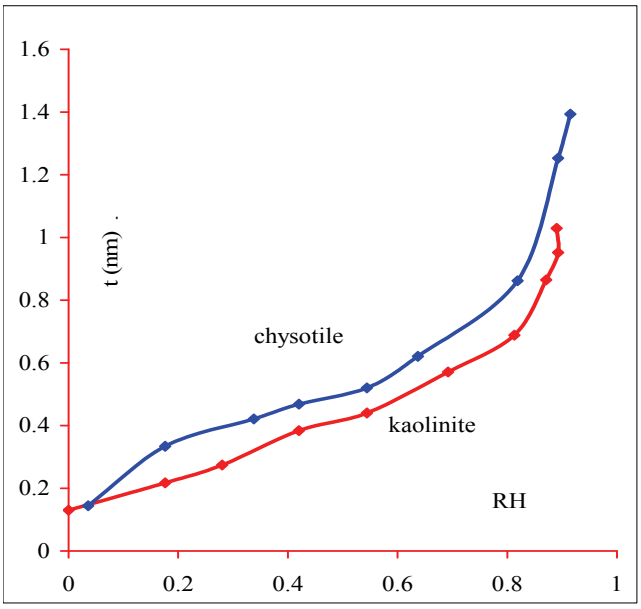

Figure 9. The thickness (t) of the water film on a mineral grain is a function of relative humidity (RH). Data from Hagymassy et al. (1969).

meability of gas. It is possible to estimate water film thickness on dispersed grains using an equation developed by Hagymassy et al. (1969) (Figure 9). Data from Hagymassy et al. (1969) and Prost et al. (1998) suggests that the water film thickness decreases rapidly at RH values greater than about 85% on grains of kaolinite and that below 86% RH, the decrease is much slower. This is equivalent to an external expression of a water isotherm that is measuring water loss from internal pores.

SAMPLE PREPARATION AND ANALYSIS PROCEDURE

Sample porosity is measured using moderately coarse shale cuttings that have been kept water-saturated (with formation water if possible) since retrieval. The assumption is made that at atmospheric pressure, free gas is completely replaced by water in all pores. Samples are wet-screened to a number of size fractions. In this case samples were separated into size fractions greater than 20 mesh, 20 to 40, 40 to 60, 60 to 100, and less than 100 mesh. Size fractions are kept water-saturated prior to analysis.

Most of the samples analysed in this study were screened to 20 to 40 mesh. At this size, a single grain is over 20 000 mesopore diameters wide. A water-soaked sample weighing about 50 g is placed in a modified desiccator (Figure 10), which holds two such samples. Modifications to the desiccator include replacing the domed top with a flat top; inserting a small fan (the type found in laptop computers); and drilling an insert tunnel so that the RH probe can be inserted into the desiccator. A number of chemicals that

Figure 10: A desiccator with a relative humidity meter inserted. The desiccator contains two samples above a dish containing a salt solution that maintains a specific humidity.

provide relative humidity control points at about 10% RH steps are used (Table 1).

A series of saturated salt solutions are placed in the desiccators in sequence to decrease RH from 100% to 0%. The first solution is a saturated solution of KSO_4, and the final compound is dried $CaCl_2$. Samples are weighed once RH has stabilized at the RH value maintained by each solu-

TABLE 1. SALT SOLUTIONS USED TO CONTROL RELATIVE HUMIDITY OF SAMPLES.

Sequence for relative humidity control	
saturated solutions	humidity %
Water	100
potassium sulfate	97.6
potassium chloride	85.1
sodium chloride	75.7
sodium bromide	59.1
magnesium nitrate	54.38
potassium carbonate	43.2
magnesium chloride	33.1
potassium acetate	23.11
lithium chlorite	11.3
baked calcium chloride	0

tion. It takes about 1 to 2 days for sample weights to equilibrate at each new RH value as defined by a new saturated salt solution. Samples have to be weighed quickly when periodically removed from desiccators because they will either lose or gain weight, depending on whether RH in the desiccator is greater or less than ambient room RH.

SAMPLING CONSTRAINTS

The first problem during construction of a water isotherm for measuring porosity is to differentiate between surface water and water that is held in porosity. This is critical when using cutting samples. All RH versus weight plots for shale samples have a distinct break point that occurs at

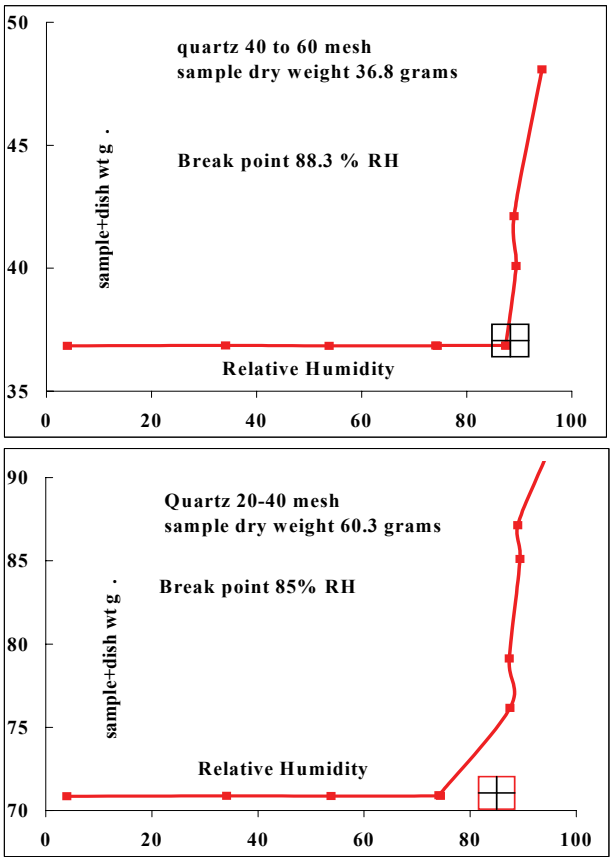

Figure 11. Water isotherms of quartz grains screened to 20 to 40 mesh and 40 to 60 mesh.

about 86% RH (Figure 3). The RH value of 86% appears to separate removal of surface water from pore water, based on the fact that the same break point is seen in water isotherms on screened quartz grains (Figure 11). Samples of quartz grains screened to 20 to 40 mesh and 40 to 60 mesh were analysed, and both have zero porosity below a RH value of about 86% (no decrease in weight as RH decreases below 86%).

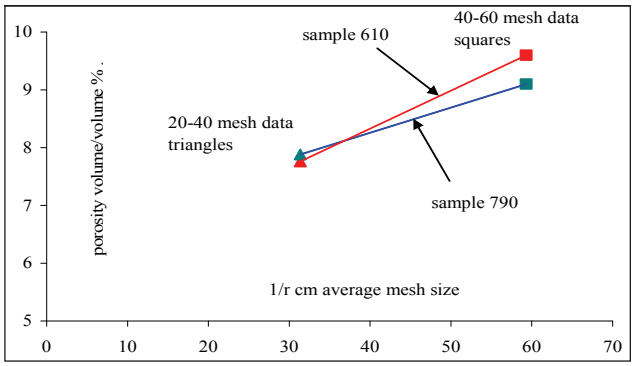

Figure 12. Relationship of porosity to mesh size of shale cuttings. Mesh size decreases to the right.

A correlation between particle size and porosity is expected. As grains get smaller, there is better access to porosity, especially non-connected porosity. This effect is related to the ratio of surface area to grain volume (1/radius). As grain size increases (1/radius approaches zero), porosity measurement converges on true connected porosity, which will be a minimum value. Smaller grain size samples will have higher estimated porosities (Figure 12), and this is probably a surface-area effect. By screening samples to a constant grain size, relative porosities should be valid, but all values will need to be corrected for absolute connected porosity. There should also be a correction based on the compressibility of the solid to correct porosity measured at surface to actual porosity at depth, but that is outside the scope of this paper.

IMPLICATIONS FOR TOTAL ORGANIC CARBON (TOC)

The small amount of organic material in shales adsorbs water as well as methane. The amount and mechanism of water adsorption is indicated by water isotherms. Generally water retained at 50% RH on coal is considered to be mono-layer adsorbed (Mahajan and Walker 1971). This water will be extracted at low values of RH and may influence porosity calculations, as will water adsorbed on kaolinte. It is unlikely that this water will ever be removed to provide porosity for free gas, because it would require low values of RH or very high capillary pressures to force it out. In a gas-saturated shale, there is a portion of porosity that has strongly adsorbed water (or irreducible water), which should not be considered part of a porosity calculation. This water is removed only when samples are dried by decreasing RH to values approaching zero. Present calculations of effective porosity may be too high, and therefore calculated values of the degree of effective gas saturation may be too low and resource estimates too high.

Identification of water adsorbed by TOC may be possible by using the shape of water isotherms to partition equilibrium moisture between capillary, condensed, multi-layer adsorbed, and mono-layer adsorbed water. Once this relationship is established, if the rank of the TOC material is known, then it is possible to estimate the amount of TOC based on the amount of water removed in the RH range 10% to 0%.

DETAILS OF POROSITY AND APPARENT DEGREE OF SATURATION CALCULATIONS

Calculation of porosity requires the specific gravity of sample with water-filled pores (SG_{wet}) and skeletal specific gravity with no water in pores (SG_{dry}). The procedure is documented in Table 2 and is as follows:

1. Split sample into two subsamples.
2. For one subsample, remove surface water (dry to 86% RH) and weigh sample (Table 2; a1).
3. Use Archimedes' principle (water immersion) to measure subsample volume at 86% RH and calculate SG_{wet} (Table 2; a2 a6).
4. Second subsample, dry to 86% RH weight then weigh again at 0% RH (Table 2; a3 and a4).
5. Use the SG_{wet} value from first subsample and wet weight second subsample to calculate 86% RH volume of second subsample (Table 2; a7).
6. Calculate water-filled volume of second subsample (Table 2; a2, a3).
7. Calculate SG_{dry} of second subsample using dry weight and dry volume (Table 2; a9).
8. Calculate porosity from RH data using

   $Ø = (SG_{dry} - SG_{wet})/(SG_{dry} - 1) \times 100$

   Ø = porosity, volume %,

   1 = assumed SG of water filling all pores (Table 2; a10).
9. Calculate porosity using He pycnometry data (Table 2; a11).
10. Calculate total pore volume using SG_{wet} RH 86% and SG_{dry} He Pycnometry (Table 2; a12).
11. Using porosity from RH 86% to 0% and porosity using He pycnometry, calculate apparent % gas saturation (Table 2; a13) as described in detail below.

TABLE 2. METHOD FOR CALCULATING CONNECTING POROSITY AND DEGREE OF SATURATION.

	Calculation of degree of saturation and porosity		
	Sample 1 is saturated with water then put in the desicator		
	Sample 2 is put into the desicator as received		
	The water saturated SGwet is measured on sample 1		
	the wieght loss is measured on sample 2 from 86% RH to 0%RH		
	The SGdry is measured using He pycnometry		
	Calculation of porosity and % saturation Example Calculation		
a1	sample 1 water saturated weight at 86% RH	60	
a2	Sample 1 water saturated volume at 86% RH	24	
a3	Sample 2 wet wt 86% RH	56.00	
a4	Sample 2 dry wt 0% RH	55.00	
a5	SGdry by He injection	2.65	
a6	sample 1 water saturated SGwet	**2.5**	a1/a2
a7	Sample 2 wet volume	**22.4**	
a8	weight water filled pore volume sample 2	**1.00**	(a3-a4)
a9	SGdry sample 2 from RH 86% and RH 0% SGwet sample 2 from 86% RH and 0% RH	**2.57**	a4/(a7-a8)
a10	Porosity calculated using RH data	**4.46**	(a9-a17)/(a9-1)*100
a11	porosity calculated using He SGdry	**9.09**	(a5-a6)/(a5-1)*100
a12	total pore volume in sample 2	**2.08**	(a11/100*a4/a5/(1-a11/100)
a13	gas saturation	**51.82**	(a12-a8)/a12*100

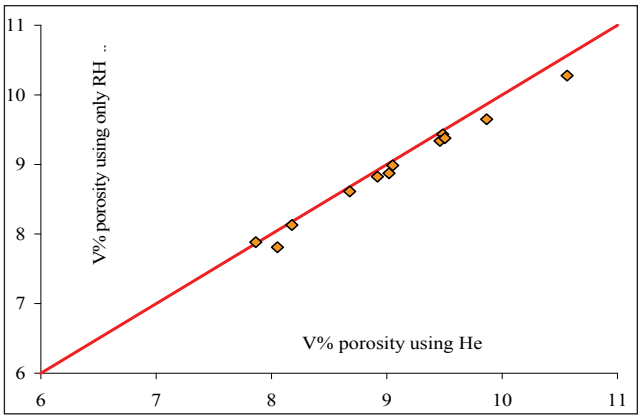

Figure 13. Plot of porosity V, (volume %) calculated using only desiccator data against porosity calculated using He pycnometry and desiccator data.

There are two ways of calculating porosity for samples that are completely water saturated. One uses only data from the desiccator, the other uses He Pycnometry and desiccator data. For the data presented here, the two methods produce similar estimates of porosity (Figure 13). Using the split-sample approach provides a way to calculate degree of gas saturation of the porosity as it exists in the samples under atmospheric conditions for samples not fully water saturated.

Shale porosity at depth may be partially or completely gas filled or water filled. Physical measurement of the degree of gas saturation in porosity at surface is difficult. As a sample is retrieved, pressure decreases and gas escapes from porosity and is replaced by water. This process might be slow if the porosity is composed of meso- or micropores with restricted inter-connecting throats, and larger fragments may still preserve evidence of the degree of gas saturation. The degree of gas saturation at surface will be different than that at depth. Gas expands as pressure decreases, whereas the water volume changes very little. If a sample is crushed to a finer size and a water isotherm measured, then the weight of water loss from 86% RH to 0% RH may help determine degree of saturation when compared to data from a second sample that is completely water saturated.

It is possible to estimate degree of saturation using a combination of He Pycnometry and RH data if samples are not 100% water saturated (i.e., gas saturation > 0%). The procedure requires two sub-samples, one as-received (sample 2, Table 2) and one water-saturated (sample 1, Table 2). The SG of sample 1 is measured at 86% RH (= SG_{wet} sample 1). Sample 2 is put into the desiccator as-received, and the weight at 86% RH and at 0% RH are measured. SG_{dry} is measured using He Pycnometry on sample 1, and the total porosity is calculated using SG_{dry} (1) and SG_{wet} (1). The pore volume in the second sample 2 is calculated using its dry weight with SG_{dry} and total porosity calculated from sample 1. This volume is compared to the weight loss (= water volume) when drying sample 2 to calculate the percent gas saturation (Table 2). The validity of the estimate depends on the history of sample 2 since it was collected during drilling operations.

During uplift gas expands in porosity and will force water out. Rock decompresses and this may increase porosity and tend to pull water in. Once at or close to surface, if the sample is wet, water will tend to displace gas in the porosity because of capillary pressure. There are many uncertainties in estimating degree of gas saturation in porosity for samples brought to surface. Water in pores is in contact with methane and may be a mixed gas on the external side of the throat. This means that there is a concentration gradient for methane in solution in the water and there will be diffusion movement of methane out of the pores despite the effect of capillary pressure to trap gas in pores.

Using He pycnometry to calculate SG_{dry} may result in values that are too high because the He molecule is smaller than the methane molecule and may access additional sites. If this is the case, then the calculated total porosity will be too high, as will the percent gas saturation. This could result in a significant overestimation of resource.

In cases where percent gas saturation is high, it is possible that RH is very low, and this could mean that the ability of the TOC to adsorb methane is increased. A number of studies indicate that adsorption of low- and medium-rank coals increases if they are dried below equilibrium moisture. Resource estimates on gas-saturated shales may be too low because they use isotherms measured on water equilibrated samples (100% RH) to estimate the adsorbed gas component of the resource.

An alternative approach that uses water chemistry to estimate percent gas saturation may be possible. The chemistry of formation water can be measured to provide a fingerprint that is very different from surface water. For rock that is partially saturated with formation water, if dried at surface and then washed in a known volume of pure water it is possible to calculate the amount of formation water contained in the porosity by changes in the chemistry of the wash water.

SAMPLES

Cuttings samples were provided by a number of companies. They were kept saturated with formation water when possible until ready for preparation. Hudson Hope Gas provided 24 cuttings samples of the Lower Cretaceous Moosebar Formation intersected in hole b-43-A/94-B-1 (WA report number 21477) over a depth range of 250 to 490 m. Petro-Canada provided samples from three holes: Bubbles C-25-G/94-G-8 (WA report number 21577), PC Town d-36-C/94-G-1, and PC West Beg C-046-C094-G-01, each covering part of the interval from 350 to 800 m.

TABLE 3. SUMMARY ANALYTICAL DATA: SPECIFIC GRAVITY AND POROSITY CALCULATIONS. UNITS ARE AS FOLLOWS: DEPTH, M; RH, %; DRY WT AND WT LOSS, G; GAMMA RAY, COUNTS/SEC; SG, G/CM^3.

Hole	B-43-A/94-B-1											
depth	RH break point	dry wt	86%-0% wt loss RH	Gamma ray counts	SGdry He	SGwet measured	SGdry calc from SGwet measured	SGwet calc using SGdry He	porosity using SGdry He and Sgwet calc	porosity V% using SGdry calc from SGwet measured	V% Porosity using SGwet measured and plot	EQ 86%RH
250	85.5	47.919	0.921	90.95	2.6532			2.573	4.85			
260	86.2	52.191	1.139	94.79	2.6551			2.564	5.48			
270	84.4	54.262	1.338	90.77	2.6677			2.565	6.17			
280	86	48.151	0.759	93.43	2.661			2.594	4.03			
290	89.3	49.398	0.892	91.68	2.666			2.589	4.59			
300	89.5	45.239	0.761	93.65	2.6659			2.594	4.29			
Hole	C-025-G/094-G-08											
610	86.4	45.444	1.596	134	2.6834	2.558	2.706	2.538	8.61	8.68	8.8	
670	86.9	48.439	2.061	129	2.6916	2.589	2.776	2.518	10.28	10.56	9	
720	86.6	48.237	1.853	135	2.7112	2.564	2.728	2.550	9.43	9.49	8.2	
750	86.9	47.7	1.74	145	2.7062	2.572	2.728	2.553	8.98	9.05	7.5	
780	90	45.646	1.814	140	2.6873	2.581	2.754	2.524	9.65	9.86	9.2	
790	86.3	48.246	1.844	137	2.6947	2.570	2.734	2.536	9.34	9.46	8.7	
Hole	PC west Beg c-46-C/94-G-1											
350		41.99	1.64	122	2.6498	2.528	2.688	2.495	9.38	9.50	9.502	3.759
410		32.25	1.032	116	2.6744	2.536	2.667	2.542	7.88	7.86	7.863	3.101
450		44.66	1.42	76.7	2.6643	2.613	2.754	2.534	7.81	8.05	8.052	3.082
Hole	PC town d-36-C/94-G-1											
370		27.27	0.993	120.32	2.6744	2.567	2.722	2.526	8.87	9.02	9.05	3.513
380		24.38	0.808	91.64	2.6701	2.549	2.687	2.534	8.13	8.18	8.177	3.208
410		31.73	1.156	78.96	2.6562	2.537	2.687	2.510	8.82	8.92	8.92	3.515

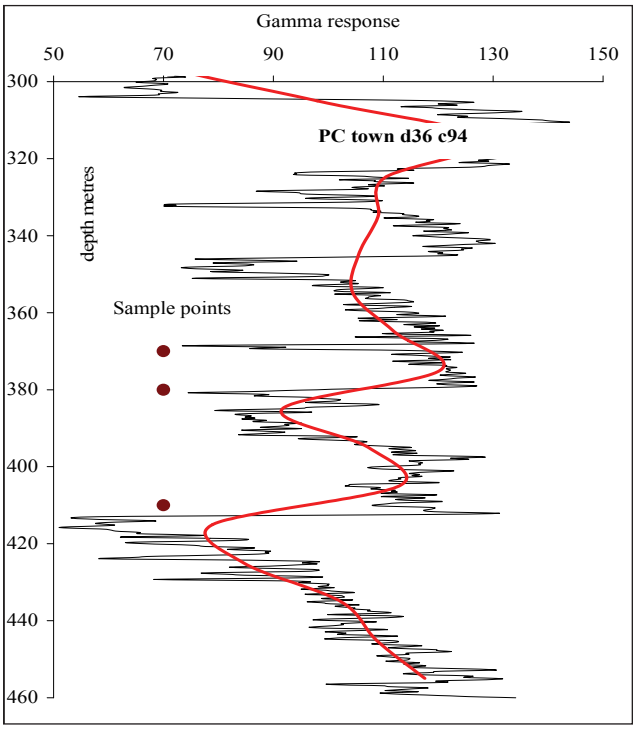

Figure 14. Example of gamma log with smoothing and sample points.

After a measurement protocol was established, 12 samples were analysed. Six samples from hole b-43-A/94-B-1; six samples from hole C-25-G/94-G-8; three samples from hole PC Town d-36-C/94-G-1; and three samples from hole PC West Beg C-046-C094-G-01. All samples represent 10 m intervals (Table 3). Samples were generally collected to represent the maximum range in gamma readings from geophysical logs (Figure 14).

DISCUSSION

Porosity values measured for the 12 samples range from 4 volume % to over 10 volume % (Table 3). They are in the range of what is expected, but at present there is no independent way to verify these values. Some general comments can be made about the data. Calculation of porosity using a weight at a low (but not zero) RH may provide a means of correcting for water adsorbed on kaolinite. Water isotherms may provide information on pore-size distribution; however in this study there do not appear to be different segments in the water isotherm plots with varying slopes indicating different amounts of water held in pores of various sizes. The SG_{dry} value measured using He pycnometry is generally lower than the value calculated from

desiccator data (Figure 15). This is because samples were not maintained at exactly 0% RH during shipment for He pycnometry.

Gamma counts usually respond to K, U, or Th. These data have a poor correlation with K and therefore must be responding to U or Th. Porosity, SG_{dry}, and Al content all increase as gamma counts increase (Figure 16). The correlation of increased gamma with higher SG_{dry} and Al_2O_3 content (low SiO_2 content) reflects the higher SG of clay minerals compared to quartz. The increase in SG_{dry} values increase with Al_2O_3/SiO_2 ratios. This indicates that the higher SG values of clay minerals compared to quartz are influencing SG_{dry} values more than variable amounts of TOC, which has low SG and which tends to increase in content as Al_2O_3/SiO_2 ratio increase. There is no relationship of porosity to %K, so that illite is not effecting porosity estimation by adsorbing large quantities of water. It is not clear whether gamma counts correlate with estimated porosity, because there are clearly two populations of data.

Trace element contents of shales provide information on depositional environment and on the potential to retain TOC. Major oxide chemistry, on the other hand, can provide indications of potential porosity and fracability. The basic chemistry of the samples indicates a low CaO content and high SiO_2 content compared to average shale (Figure 17). The figure also shows data from the Barnett Shale estimated from mineral content data (Jarvie 2006), data estimated from mineral composition data in Ross and Bustin (2008), and average illite and kaolinite compositions in terms of the three oxide parameters. Figure 17 also includes an estimate of the relationship of total clay content to Al_2O_3/SiO_2 ratio (estimated from data in Ross and Bustin [2008],), which allows the clay content of samples in this study to be estimated.

Porosity is influenced by mineral composition, burial history, and rock properties. In this study, porosity increases as Al_2O_3/SiO_2 ratio increases (Table 4), indicating either a positive relationship of kaolinite (i.e., negative correlation to silica content) or an adsorption effect by kaolinite. Ross

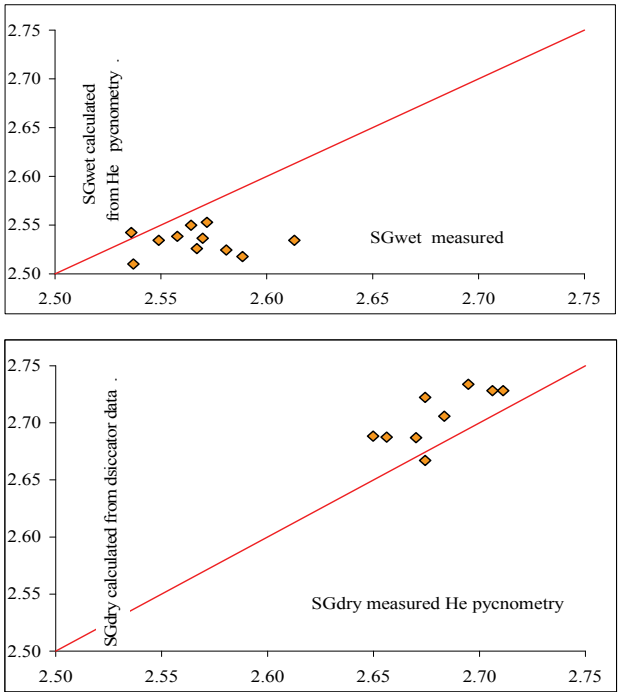

Figure 15. Comparison of SG_{dry} data determined using He pycnometry and calculated from desiccator data and similar comparison for SG_{wet}. Units for SG (specific gravity) are g/cm³.

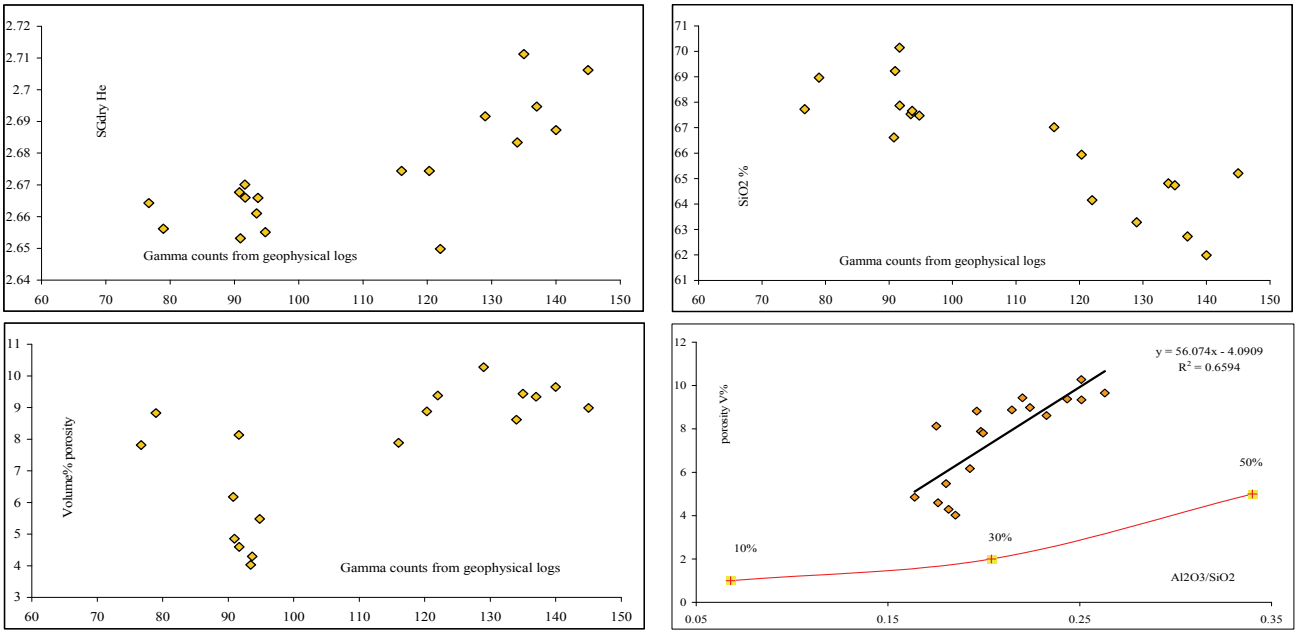

Figure 16. Plot of SG_{dry} (g/cm³) measured using He pycnometry versus gamma counts from geophysical logs.

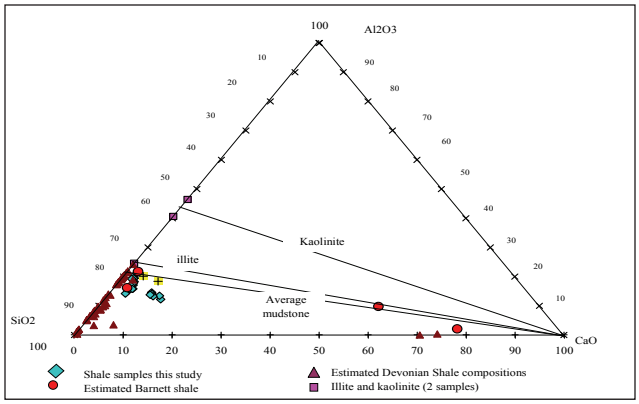

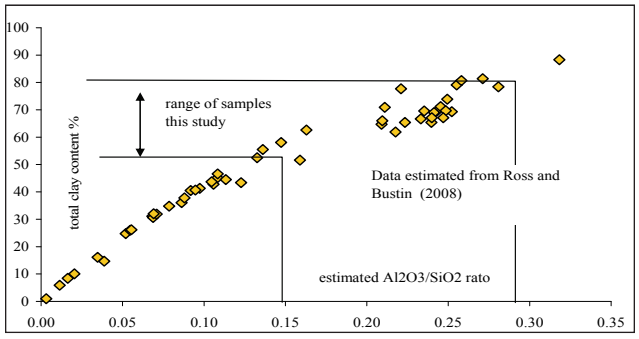

Figure 17. Major oxide chemistry of samples compared to average shale from Clarke (1924).

and Bustin (2008) report a negative correlation between silica content and porosity in Devonian Muskwa and lower Besa River mudrocks in northeastern British Columbia (Figure 18). They provide a table of mineral content data from which major oxide chemistry can be estimated assuming mineral compositions of quartz, kaolintie, illite, and calcite and making the assumption that these four minerals account for most of the rock. Once this is done, it is possible to estimate the relationship of porosity to silica content and of porosity to TOC for the samples (Figure 18). The porosity data from this study are plotted in Figure 18 and fall along the same trend of increasing porosity with decreasing silica content.

Low silica content is preferred for high porosity and potentially high free-gas content; however, rocks with high silica content are easier to fracture. The amount of TOC tends to increase as silica content decreases. A compromise has to be made in terms of preferred high silica content for ease of fracture stimulation during well completion and preferred low silica content for potentially higher gas content. Ease of fracturing is related to Poisson's ratio and Young's modulus. These two rock parameters are not independent—Young's modulus increases as Poisson's ratio decreases. Rock property constants *lambda* (incompressibility) and *mu* (rigidity) are derived from Young's modulus and Poisson's ratio (Goodway et al. 2006). Figure 19, which is a simplified version of a plot of *lambda* versus *mu* from Goodway et al. (2006), illustrates the fracture potential of rocks and the preferred values of *mu* and *lambda*. The figure also shows a trend in porosity and *lambda* and *mu* values for common rock-forming minerals.

TABLE 4. LINEAR CORRELATION OF SOME ROCK CHEMISTRY AND WATER ISOTHERM DATA. UNITS: POROSITY, VOLUME%; SG, G/CM^3; GAMMA RAY, COUNTS/SEC.

	Al_2O_3/SiO_2	porosity	SG dry	K_2O	gamma	P_2O_5
Al_2O_3/SiO_2	1.00					
porosity	0.81	1.00				
SG dry	0.58	0.57	1.00			
K_2O	0.44	0.54	-0.22	1.00		
gamma	0.82	0.66	0.78	0.06	1.00	
P_2O_5	-0.58	-0.79	-0.50	-0.25	-0.52	1.00

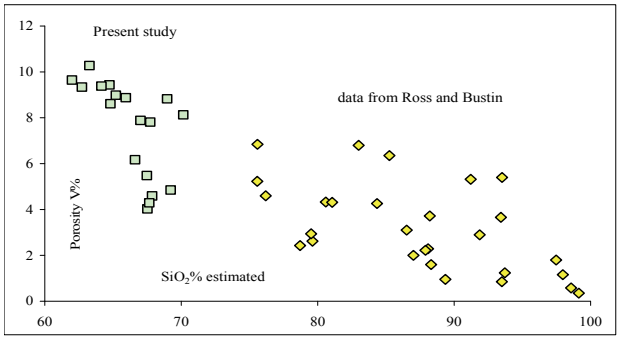

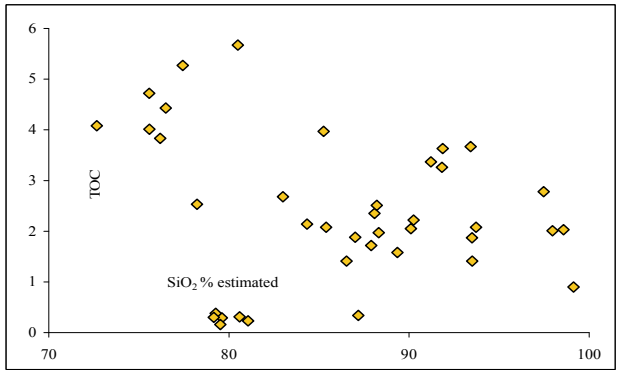

Figure 18. Estimated relationships of porosity and TOC to silica content (data from Ross and Bustin 2008).

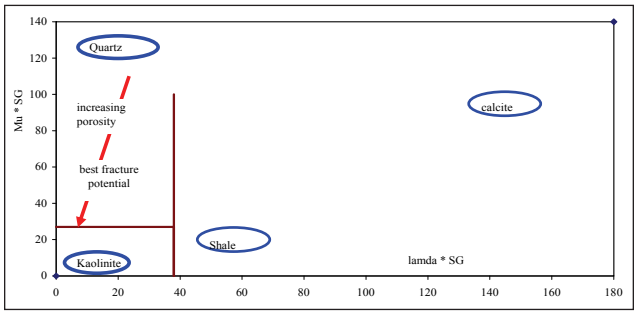

Figure 19. Relationship of fracture potential to rock properties; figure is a simplified version of a figure in Goodway et al. (2006) Lambda (incompressibility), Mu (rigidity), SG specific gravity.

CONCLUSIONS

- It is possible, using water isotherms, to measure porosity of shale cuttings. This is important because cuttings are much more readily available than core samples.
- The water isotherm approach to remove water is much less stressful on samples than using heat to dry samples or high-pressure mercury injection of gases of different ionic size.
- The water isotherm method allows for differentiation of surface water from pore water and makes it possible to use cuttings for porosity determination. However, there are indications that a correction must be made to the connected porosity measurement based on the grain size of the cuttings.
- The method provides information on the degree of hydrophobicity, which relates to relative gas permeability.
- It is possible to obtain information about pore-size distribution.
- A careful analysis of the time it takes for moisture to escape samples at each RH step should provide information on gas escape rate, whether it is described as diffusion or flow based on micropermeability.
- Combining the water isotherm approach with He pycnometry provides a way of estimating gas saturation.

The next stage for this study is to partner with industry so that core can be collected for porosity measurements and can provide samples for comparative analysis of porosity using crushed core samples as proxy for cuttings. In addition, consideration should be given to redesigning the desiccators and attaching dedicated humidity meters with continuous digital readout.

REFERENCES

Allardice, D.J., and Evans, D.G. (1978): Moisture in coal; in Analytical Methods for Coal and Coal Products; Volume 1, *Academic Press*, New York.

Carmiet, J., and Roels, S. (2002): Description of moisture capacity of building materials; Building Physics, 2002 6th Nordic Symposium.

Clarke, F.W. (1924): The data of geochemistry; *US Geological Survey* Bulletin 770.

Dabbous, K.K., Reznik, A.A., Mody, B.G., Fulton, P.F., and Taber, J.J. (1976): Gas–water capillary pressure in coal at various overburden pressures; *Society of Petroleum Engineers*, paper 5348.

Frenkel, J. (1946): Kinetic theory of liquids. London, UK; *Oxford University Press*.

Goodway, B., Varsek, J., and Abaco, C. (2006): Unconventional seismic methods for gas resource plays; 8th Annual Unconventional Gas Conference, Canadian Society of Unconventional Gas, Calgary, November 2008.

Grunewald, J. (2007): Research Associate Professor @ Syracuse University Building Environmental Modeling and Simulations; MAE 300 Spring 2007, 246 Link Hall Tuesday 6:30 p.m. – 9:30 p.m. internet at Kein Folientitel.

Hagymassy, J., Brunauer,S., and Mikhail, R.S.H. (1969): Pore structure analysis by water vapour adsorption t-curves for water vapour; *Journal of Colloid and Interface Science*, Volume 29(3), pages 485–491.

Halsey, G. (1948): Physical adsorption on non uniform surfaces; *Journal of Chemical Physics*, Volume 6(10), pages 931–937.

Hill, T.L. (1952): Theory of physical adsorption; *Advances of Analysis*, Volume 4, pages 212–258.

Jarvie, D.M. (2006): Comparison of producing and prospective shale gas plays in the U.S.A. and Canada; Humble Geochemical Services, 8th Annual Unconventional Gas Conference; Canadian Society of Unconventional Gas, Calgary, November 2008

Likos, W.J., and Ning, L (2002): Water vapour sorption behaviour of smectite-kaolinite mixtures; *Clays and Clay Minerals*, Volume 50, Number 5, pages 553–561.

Mahajan, O.P., and Walker Jr., P.L. (1971): Water adsorption on coals; *Fuel*, Volume 50 (3), pages 308–317.

Prost, R., Koutit, T., Benchara, A., and Huard, E. (1998): State and location of water adsorbed on clay minerals: consequences of the hydration and swelling-shrinkage phenomena; *Clay and Clay Minerals*, Volume 46, Number 2, pages 117–131.

Ross, D.J.K., and Bustin, M.R. (2008): Characterizing the shale gas resource potential of Devonian–Mississippian strata in the Western Canada sedimentary basin: Application of an integrated formation evaluation; *AAPG Bulletin*, Volume 92, Number 1, pages 87–125.

Ryan, B. (2006): A note on moisture in coal: Implications for coalbed gas and coal utilization;Resource Development and Geosciences Branch, *BC Ministry of Energy, Mines and Petroleum Resources*. Summary of Activities 2006.

Shang, S., Horne, R.N., and Ramey Jr., H.J. (1994): Experimental study of water vapour adsorption on geothermal reservoir rocks; *Stanford Geothermal Program*, Report Number SGP-TR-148.

Wang, Y. H., and Freeland, D. G. (2003): Towards a better understanding of the role of the contractile skin; Proceedings of the 2nd Asian Conference on Unsaturated Soils, April 15-17, Osaka, Japan, pages 419–424.

NOTE ON DESORPTION RESULTS OF COMOX FORMATION COALS FROM THE QUINSAM AREA, VANCOUVER ISLAND, BRITISH COLUMBIA

Douglas Wells[1] and Barry Ryan[2]

ABSTRACT

This paper presents desorption and gas chemistry data from a small-scale study of gas content of coals from the Quinsam area, Vancouver Island, British Columbia. Seven coal samples from two holes in the Comox Formation were taken from depths ranging from 245 to 333 m. Desorption data are compared to pre-existing isotherms and indicate near-saturated conditions. Gas contents range from 2.61 to 4.80 cm^3/g on a mineral-matter-free basis. Gas chemistry data display a high proportion of methane gas.

Wells, D. and Ryan, B. (2009): Note on Desorption Results of Comox Formation Coals from the Quinsam Area, Vancouver Island, British Columbia; Geoscience Reports 2009, *BC Ministry of Energy, Mines and Petroleum Resources,* pages 81–88.

[1]British Columbia Ministry of Energy, Mines and Petroleum Resources, Oil and Gas Division, Resource Development and Geoscience Branch, PO Box 9333 Stn. Prov. Govt., Victoria, BC, V8W 9N3

[2]Consultant; bryan@islandnet.com

INTRODUCTION

In the summer of 2008, Hillsborough Resources Limited undertook a drilling program to further delineate the coal resource available for underground mining on the Quinsam North property on Vancouver Island. As part of this program, two holes were chosen to provide coalbed methane (CBM; also referred to as coalbed gas or CBG) data on the coals of this area. Canister tests, which provide estimates of the amount and composition of gas adsorbed in coal, may be a part of a coal exploration program because results affect considerations of mining safety, ventilation, and greenhouse gas emissions. These data are also a starting point for a realistic CBM resource estimate.

The canister tests discussed in this paper were performed by the authors on behalf of the British Columbia Ministry of Energy, Mines and Petroleum Resources and at no cost to the company. In this situation, the company gets data at no cost but loses the right to keep it confidential for an extended period, because the government is obliged to make the information public. Obviously this applies only to data collected by the authors and not to other aspects of the exploration program.

This paper presents gas content and composition data collected from seven canister tests of samples from two holes drilled by Hillsborough. Sample depths range from 245.9 to 333.5 m, and gas contents range from 2.61 to 4.80 cm^3/g on a mineral-matter-free basis (mmfb).

REGIONAL GEOLOGY

The Cretaceous Nanaimo Group sediments were deposited during a period of subsidence in the Georgia Basin east of current Vancouver Island. Over 5 km of sediment accumulated by the close of the Cretaceous (England and Bustin 1995). These sediments overlie Triassic weathered crystalline volcanic basement known as the Karmutsen Volcanics. The Nanaimo Group is cut by northwest-trending, southwest-verging thrusts that are indirectly dated as Eocene. These thrusts shorten the basin by up to 30% (England and Calon 1991). Six subbasins are contained within the Georgia Basin: from north to south, they are Quatsino Sound, Suquash, Comox, Alberni, Nanaimo, and Cowichan. The Comox and Nanaimo subbasins are the largest and contain the Comox and the Nanaimo Coalfields, respectively. In the literature, the use of the terms “basin”, “subbasin”, “coalfield”, and “deposit” is inconsistent. In this paper, it is convenient to refer to the Quinsam area within the Comox Coalfield of the Comox subbasin. The Comox subbasin lies within the Georgia Basin.

LOCAL GEOLOGY

The Quinsam area is located in the northwestern corner of the Comox Coalfield (Figure 1). The coal measures are contained in the Comox Formation of the Nanaimo Group. These coal measures correlate with coals that occur further south in the Cumberland and Tsable River areas of the Comox Coalfield. Only the basal half of the coal-bearing section has been preserved at Quinsam. The Quinsam area is a discrete body separated from the rest of the Comox

Coalfields by a basement rock topographic high. The Karmutsen Formation underlies the coalfield and consists of basalt, gabbro, volcanic breccia, skarn, and granodiorite. These rocks are folded and faulted and display an erosional contact with the overlying sediments. Paleotopography of the basement rocks strongly influences the distribution of the coal measures. The Comox Formation is divided into three members (Benson, Cumberland, and Dunsmuir; Table 1) in the Quinsam area. The Benson, which is largely conglomeratic, forms the base of the section. It is conformably overlain by and interfingers with the Cumberland. The Dunsmuir overlies the Cumberland. The Cumberland Member contains sandstones, mudstones, and two coal zones of mineable thickness in the Quinsam area. The Dunsmuir Member contains conglomerates to mudstones and multiple thin coal seams.

The structure of the Comox Formation in the Quinsam area consists of a generally northeast dipping (8° to 12°) monocline over the basement. Smaller-scale, asymmetric synclines verging southwest and displaying steeper dips (up to 60°) occur in the northeastern portion of the Quinsam area. Other minor folds and buckles are common throughout. The Quinsam area has undergone brittle, thick-skinned deformation characterized by moderate to steep faults. Three major sets of faults are mapped in the area. Bedding plane shear is common in the coal zones of the Comox Formation producing both slickensided and pulverized coals. A more detailed description of local geology is available in Kenyon et al. (1991) and Gardner (1999).

Seven coal zones occur at Quinsam: from shallowest to deepest, they are the No. 5, No. 4, No. 4B, No. 3 (Dunsmuir Member), No. 2, No. 1 Rider, and No. 1 (Cumberland Member). Some of the zones split into individual plies within a varied spatial distribution. The No. 1 zone ranges from 2.5 to 4.5 m thick in the area and is at a depth of approximately 330 m at drill location B (Figure 1). The No. 2 zone averages approximately 1 m thick and is at an approximate depth of 320 m at drill location B. The No. 3 zone was not intersected in either hole A or B. The No. 4 zone is at a depth of 245 m in drill hole A and at 290 m in drill hole B and is less than 1 m thick.

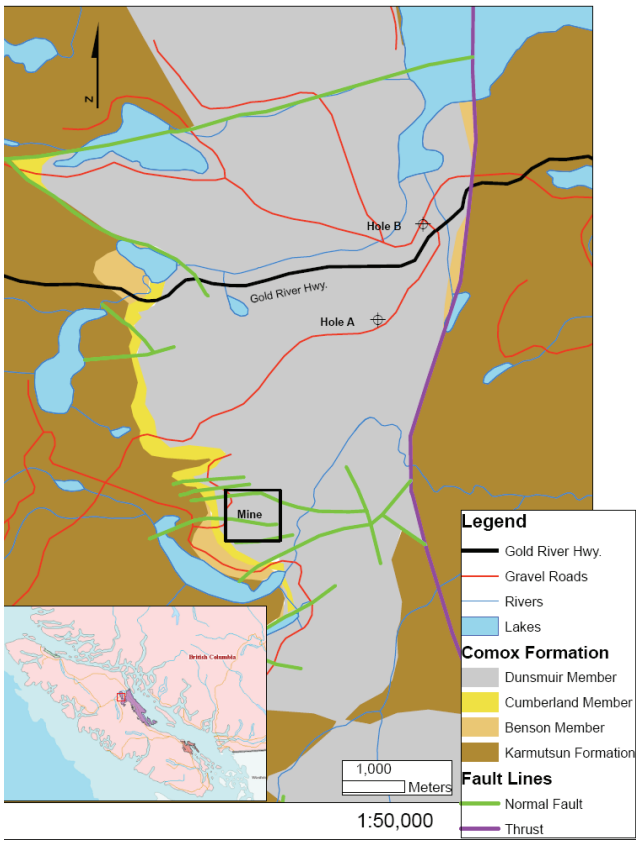

Figure 1. Geological map of the Quinsam area, showing drill locations in this study. *Geological layers modified from Cathyl-Bickford (1991).*

TABLE 1. GEOLOGICAL FORMATIONS OF THE QUINSAM AREA. (MODIFIED FROM CATHYL-BICKFORD 1991).

Quaternary	Pliestocene and Recent	Drift	Till, Gravel, Sand, Silt, Clay
	Unconformity		
Cretaceous	Santonian	Nanaimo Group Comox Formation	
		Dunsmuir Member	Sandstone; Minor conglomerate; Shale and Coal
		Cumberland Member	Siltstone; Shale and Coal
		Benson Member	Conglomerate; Minor red shale
	Unconformity		
Triassic	Ladinian to Carnian	Vancouver Group Karmutsen Formation	Fine-Grained basalt and Basalt breccia

PREVIOUS CBM DATA

CBM information on the coals of Vancouver Island is limited. Before this study, Ryan and Dawson (1994a) collected samples from two drill holes in the Quinsam Coalfield to provide information for underground coal mining. The holes intersected the No. 1 seam at 106 m and the No. 3 seam at 142 m. Gas contents were 1.0 cm^3/g on a dry ash-free basis (dafb) for No. 1 seam and 1.0 to 1.6 cm^3/g (dafb) for No. 3 seam. An adsorption isotherm suggests the seams were undersaturated at this depth. In 2004, eight samples were collected from four holes drilled as part of a coal exploration program west of Quinsam Mine (Ryan et al. 2005). The samples ranged from 134 to 156 m in depth and consisted of high ash content coal with interlayered mudstone. Gas contents ranged from 1.1 to 2.1 cm^3/g (mmfb). In 2006, Ryan (personal communication) desorbed three samples from the Quinsam area. The samples were collected between 192 m and 205 m depth, and gas contents ranged from 2.83 to 2.86 cm^3/g (mmfb). The adsorption isotherms

produced in 1994 and desorption data from 2004 and 2006 (Figure 4) are discussed in this study.

Some data are available from other areas of the Comox Coalfield. In 1996, Ryan (1997) collected and desorbed 13 samples from the Tsable River area. Sample collection depths ranged from 127 to 377 m, and gas contents ranged from 2.4 to 6.5 cm^3/g (dafb). No gas composition analysis was performed. Ryan (2002) collected 12 samples from three holes in Comox Formation coals in the Courtenay area as part of Priority Ventures' appraisal of CBM potential in the area. Samples were collected from depths of 237 to 513 m and range in gas content from 3.5 to 11.5 cm^3/g (dafb). The methane concentrations ranged from 9% to 93%.

Very little data are available prior to these studies. In 1984, Novacorp drilled 14 holes, five of which intersected the Douglas coal seam. A number of authors reported that samples were desorbed, but the information was never published. Cathyl-Bickford et al. (1991) cite a number of references that indicate a range of 5 to 12 cm^3/g (basis unknown) in the Douglas coal seam.

PROCEDURES

Methods used to acquire desorption data in this report were developed by Ryan and Dawson (1994b). These methods evolved from those outlined by Kissel et al. (1973). A spreadsheet designed by Ryan (2002) was used in this study to handle data input and manipulation. Manipulations included all necessary corrections, such as changes in temperature and atmospheric pressure, and curve fitting. Gas contents are reported on a dry, ash-free basis (dafb) and on a mineral-matter-free basis (mmfb). The conversion from dafb to mmfb can be performed in a number of ways. This study uses a normative calculation known as the Parr formula, widely used in North America. The Parr formula requires both ash and sulphur content:

mineral matter % = 1.08(ash %) + 0.55(sulphur %)

Samples were collected directly from wireline core upon reaching the surface after drilling. Samples were quickly placed in air-tight canisters capable of holding up to 40 cm of core (Figure 2); any space not filled with sample was filled with inert argon gas to inhibit sample oxidation. Canisters were maintained at approximately 23 °C, and any deviation from this was recorded and corrected for. Gas was bled off the canisters and into a manometer to measure volumes of gas lost over time. As gas comes out of the canisters, it displaces fluid in a tube of known volume. Both the manometer and the canisters were constructed by Barry Ryan. These data were entered into a spreadsheet that calculates cumulative gas, desorption rates, and canister pressure. Data were corrected to both standard temperature and pressure.

Desorbed gas is lost from a sample before it is sealed in a canister. There are a number of ways to estimate the amount of lost gas. In this study, the USBM direct method was used (McCulloch et al. 1975). The amount of desorbed gas was plotted against the square root of time for the first initial measurements. Cumulative gas as a function of time was plotted about a straight line that was projected back to the time when the sample was halfway up the hole during wireline haul-up. Lost times (time from sample halfway up the hole to being sealed in a canister) ranged from 6 to 12 minutes and average about 8 minutes in this study. Lost gas over this time averaged 6.7% of the total gas desorbed. This method does not account for free gas (gas compressed in the pores of the coal), only lost desorbed gas. Free gas is not estimated by canister tests—it is released in unknown quantities from the sample before they are sealed in canisters (Ryan 2002).

The measurements were made with the manometer over a period averaging 60 days in this study. When the amount of cumulative gas levelled off and less than 0.05 $cm^3/g/day$ was bled off the canisters, the measurements were considered insignificant and the process was stopped. The remaining gas was estimated by fitting a desorption curve and projecting the data to infinite time. The curve used was developed and discussed by Airey (1968) and is based on experimental data. The curve is manually fitted to the data by adjusting variables. This has proved to be the most efficient way of curve fitting (Ryan 2002). The amount of remaining gas averaged 0.27 cm^3/g and comprised an average of 11.7% of the total gas desorbed.

The natural logarithm of the gas desorption rate was also plotted as a function of time. This plot acts as a check of errors in the data. Any errors are immediately apparent because an invalid data point lies well outside the trend.

When the process of measuring cumulative gas is finished, the volume of dead space in the canisters (the amount of space in the canister not occupied by sample) must be measured. This is accomplished by a method developed by Ryan and Dawson (1994b) using the same manometer used to measure cumulative gas. By raising the reserve liquid container in the manometer, a hydraulic head is created, which forces gas back into the canister. The manometer is then used to measure this pressure from the canister. Using the volume of gas as read on the manometer and the height of the hydraulic head, the volume of dead space is calculated.

One sample was subjected to gas analysis to provide information on gas composition. Four gas samples were taken from sample #7 (depth of 333 m) of hole B. The gas samples were extracted from the canister via the manometer during cumulative gas measurements. A 50 cc syringe was used to gather gas from the system; the gas was injected into nonreactive bags to be sent to Loring Labs for analysis using a Shimadzu 9A gas chromatograph. One sample was

taken early in the first hour of desorption, another sample was taken the 20th hour, a third sample was taken after five days, and the last sample was taken on the 25th day of desorption. This allows gas compositions to be compared over the duration of the desorption process.

DATA

Figure 2. Example of typical core sample.

TABLE 2. COAL CHEMISTRY AND GAS RESULTS.

Hole	Canister	Depth to Top metres	Seam	Wieght arb grams	Moisture arb %	Ash db %	Mineral Matter db %	Lost Gas cm^3/g	Desorbed Gas cm^3/g	Remaining Gas cm^3/g	Total Gas arb cm^3/g	Total Gas dafb cm^3/g	Total Gas mmfb cm^3/g
A	1	245.9	No. 4	2312	4.38	27.49	32.47	0.05	2.05	0.36	2.46	3.61	3.90
A	2	246.3	No. 4	2459	4.70	15.82	19.95	0.07	2.10	0.40	2.57	3.23	3.41
B	3	290.7	No. 4	2107	6.18	16.05	18.75	0.30	2.51	0.11	2.92	3.75	3.89
B	4	291.3	No. 4	2190	9.35	28.91	32.68	0.29	1.21	0.02	1.52	2.45	2.61
B	5	319.2	No. 2	3246	5.84	49.96	56.34	0.10	1.42	0.24	1.75	3.96	4.63
B	6	332.2	No. 1	2583	6.53	29.57	32.15	0.19	2.28	0.48	2.94	4.60	4.80
B	7	333.5	No. 1	2755	6.61	33.05	35.84	0.12	1.96	0.34	2.41	3.99	4.19

arb As received basis
db Dry basis
dafb Dry ash free basis
mmfb Mineral matter free basis

TABLE 3. GAS COMPOSITION RESULTS.

Hole: B
Canister: 7
Depth: 333 metres

Sample	A	B	C	D
% Total Gas Desorbed	10.0	40.7	62.7	78.0
% Air	82	80	74	72
Mole Fraction (Air Free Basis)				
N_2	0.0000	0.0000	0.0000	0.0000
CO_2	0.0015	0.0013	0.0009	0.0009
H_2S	0.0000	0.0000	0.0000	0.0000
CH_4	0.9884	0.9874	0.9860	0.9845
C2	0.0097	0.0104	0.0120	0.0139
C3	0.0004	0.0005	0.0006	0.0007
iC4	trace	0.0004	0.0005	trace

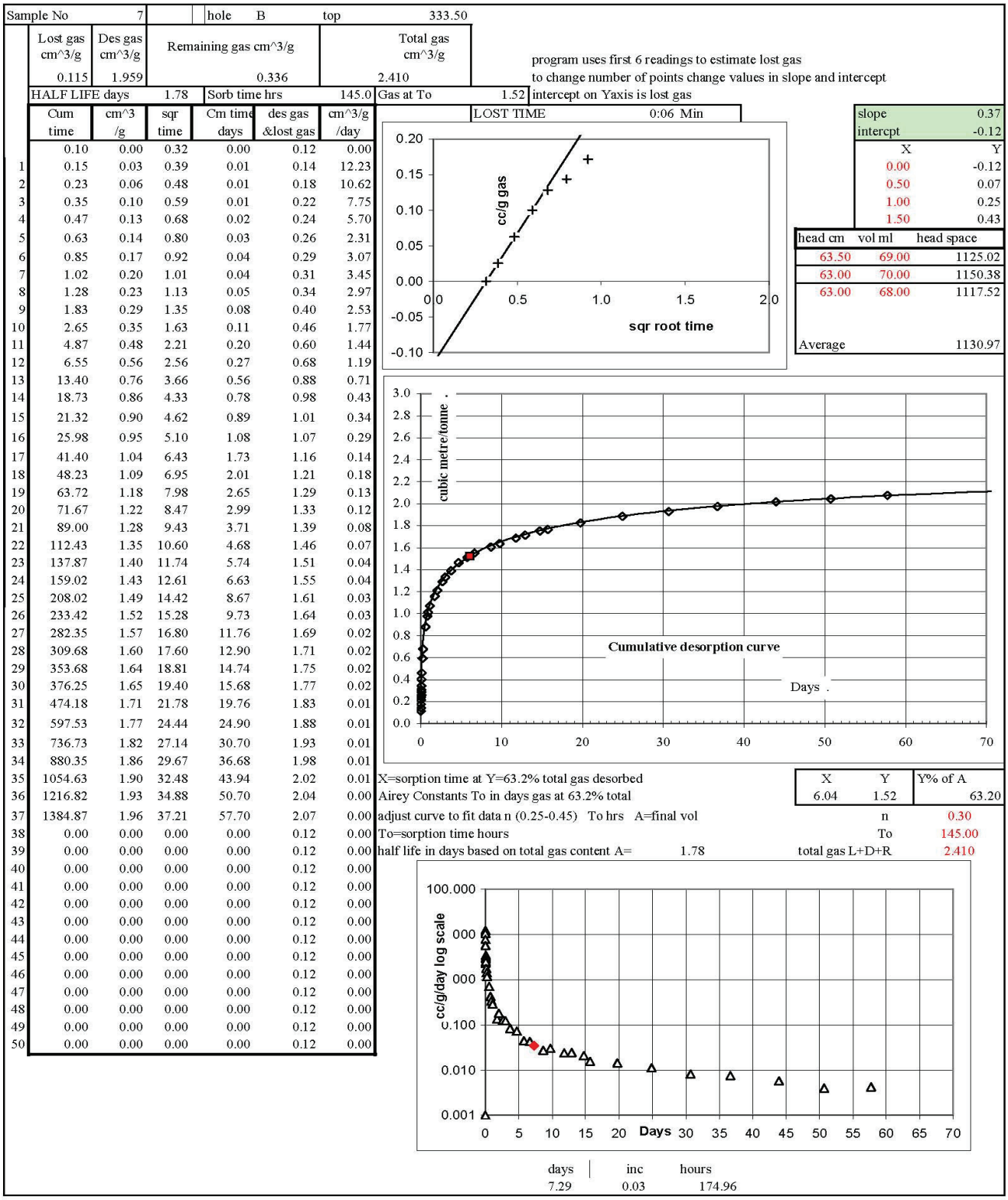

Figure 3. Example of data sheet used in calculating gas contents.

DISCUSSION

Gas contents of the samples ranged from 2.61 to 4.80 cm^3/g (mmfb); the average was 3.92 cm^3/g (mmfb). Collection depths of samples range from 245.9 to 333.5 m; 294 m is the average depth.

Ryan et al. (2005) report a gas resource of 14.4 billion cubic feet for the Quinsam area of the Comox Coalfield. This estimate is based on a coal resource estimate of 112 million tonnes and an average gas content of 4 cm^3/g (mmfb). Given the average depth to the coal seams in the Quinsam area, new data support the estimate of average gas content and therefore also the resource estimate from Ryan et al. (2005).

Gas contents are plotted as a function of depth in Figure 4. Desorption data from previous studies performed in the Quinsam area are also shown (Ryan 2004, 2006). Desorption data are compared to two isotherms (from Ryan and Dawson 1994a) that are based on adsorption data from two samples from the Quinsam area. The data follow the same general trend of the isotherms, though at a slightly lower gas content. The two isotherms displayed show the theoretical maximum adsorbed gas content for Quinsam coals at two different pressure gradients: 0.009805 and 0.007000 MPa/m.

Our estimate of whether or not the coals are gas saturated depends on our estimate of the pressure in the coal at depth. The two isotherms shown are based on two different estimates of pressure gradients. This shows that with a lower, subhydrostatic pressure gradient of 0.007000 MPa/m, the coals are nearly saturated. With a hydrostatic pressure gradient (due to an interconnected water column) of 0.009805 MPa/m, the coals are undersaturated. Subhydrostatic pressures are common in sedimentary formation waters and can be the result of several different hydrogeological phenomena. One possible phenomena is explained in the steady-state model of Toth (1972). This model explains general characteristics of regional groundwater flow and states that in areas of groundwater recharge, subhydrostatic pressures generally occur. Given the shallow regional dip of the Comox Formation towards the Georgia Strait and the shallow depth to the seams, it is possible that the seams experience a subhydrostatic pressure.

When considering pressure gradients at shallow depths (maximum sample depth 333 m), the depth of the water table plays a significant role. Hydrostatic pressure will change with water table depth. One must consider the water table depth over the time since the coals started developing gas.

When coals are saturated, it means that gas occupies all available adsorption surfaces. When this occurs, there is the potential for free gas development. Any gas that develops in the coals past the adsorption capacity of the coal has the potential to fill pore spaces. For gas to fill the pore space it must overcome hydrostatic and capillary pressures to force water out of the pore space. Free gas is not measurable via desorption; however, it is often noticed during drilling when an overpressured seam is encountered. The two holes drilled in this study did not encounter any significantly overpressured seams.

Excluding canister 5, ash contents range from 15.82% to 33.05%; the average is 25.15%. Ash content of Canister 5 is 49.96%, increasing the average ash content to 28.69%. These are ash contents of only the 40 cm sample taken for desorption tests and are not the ash content of the whole seam from which the samples were collected. These data were used for a correction to estimate the amount of gas per unit of clean coal in each canister. The 40 cm samples might not be representative of the entire seam, because they might have higher proportions of rock splits.

Four gas samples were taken from canister 7 to provide estimates of methane content. These data are not sufficient to provide a reliable estimate of the composition of all the gas in the Quinsam area. All samples contained high levels of nitrogen and (probable) oxygen contamination. Gas released from coal often contains some nitrogen, which tends to preferentially release before methane. When the coal is brought to surface and placed in a canister, air (oxygen and nitrogen) contamination is introduced. Proportions of oxygen to nitrogen will change in the canister over time because of oxidation. An effort was made to minimize the amount of air (head space) in the canisters. This was accomplished both by flooding the canisters with inert argon gas as well as by physically minimizing air space with a PVC pipe sleeve. This sleeve fits tightly into the canister and is placed around the coal before inserting the coal in the canister. Despite these efforts, minor air contamination is expected. When taking samples for gas composition analysis, there is another risk of air contamination from space in hoses of the manometer and from potential minor air space in both the end of the syringe and the gas sample bag nozzle.

The percentage of air in the samples decreased from 82% to 72% over the desorption process. The remaining 18% to 28% of the gas that came off the samples was made up of approximately 99% methane (Table 3). The lesser fraction of the gas consisted of ethane, propane, and CO_2. There was no H_2S in any sample.

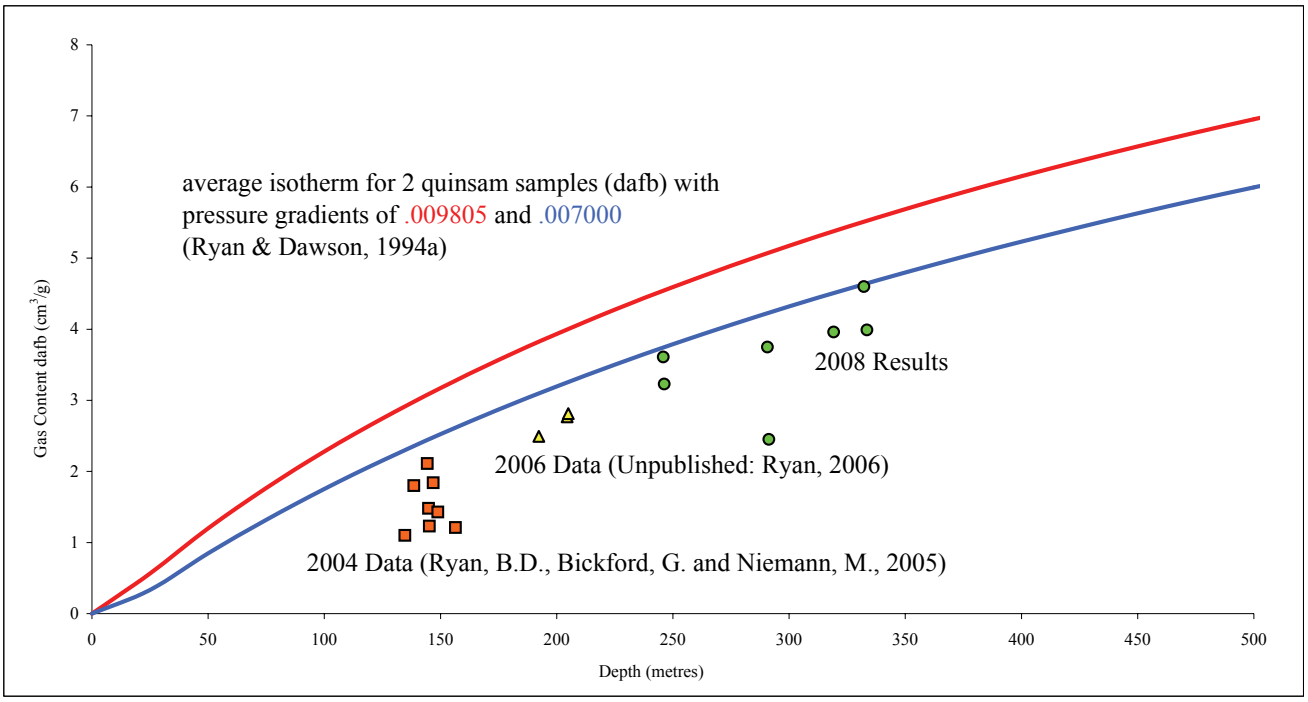

Figure 4. Coal adsorption isotherms and desorption results as a function of depth.

CONCLUSIONS

Results from this study support estimates of gas content in the Quinsam area made by previous studies and agree with a resource estimate of 14.4 billion cubic feet. Coals are nearly saturated at a depth averaging 294 m using a subhydrostatic gradient of 0.00700 MPa/m, and gas contents are 3.92 cm^3/g (mmfb) on average. Maximum gas content observed was 4.80 cm^3/g (mmfb) at a depth of 332 m. Likely due in part to contamination, the percentage of air in the gas samples was high; however, on an air-free basis, the gas was 99% methane.

ACKNOWLEDGEMENTS

This study benefitted from cooperation with Hillsborough Resources Ltd./Quinsam Coal Corporation and knowledgeable contributions from Steve Gardner and Gwyneth Cathyl-Bickford.

REFERENCES

Airey, E.M. (1968): Gas emissions from broken coal: An experimental and theoretical investigation; *International Journal of Rock Mechanics and Mineral Sciences*, Volume 5, pages 475–494.

Cathyl-Bickford, C.G. (2001): Lithostratigraphy of the Comox and Trent River formations in the Comox coalfield, Vancouver Island (92F/7, 10, 11, 14); *B.C. Ministry of Energy, Mines and Petroleum Resources*, Paper 2001-1, pages 363–370.

Cathyl-Bickford, C.G. (1991): Coal geology and coalbed methane potential of the Comox and Nanaimo coalfields, Vancouver Island, British Columbia; *in* Coalbed Methane of Western North America, *Rocky Mountain Association of Geologists*, pages 155–162.

England, T.D.J., and Calon, T.J. (1991): The Cowichan fold and thrust system, Vancouver Island, southwestern British Columbia; *Geological Society of America Bulletin*, Volume 103, pages 336–362.

England, T.D.J., and Bustin, R.M. (1995): Geology of the Georgia Basin; *Geological Association of Canada/Mineralogical Association of Canada,* Annual Meeting, Victoria BC, Field Guide Number B3.

Gardner, S.L. (1999): Coal resources and coal mining on Vancouver Island; *British Columbia Ministry of Energy, Mines and Petroleum Resources,* Open File 1999-8.

Kenyon, C., Cathyl-Bickford, C.G., and Hoffman, G. (1991): Quinsam and Chute Creek coal deposits (NTS 92F/13, 14); *British Columbia Ministry of Energy, Mines and Petroleum Resources*, Paper 1991-3.

Kissel, F.N., McCulloch, C.M., and Elder, C.H. (1973): The direct method of determining methane content of coalbeds for ventilation design; *U.S. Bureau of Mines*, Report of Investigations, 7767.

Ryan, B.D., Bickford, G., and Niemann, M. (2005): Cumulative coal thickness and coalbed gas potential in the Comox coal basin, Vancouver Island; *in* Summary of Activities 2005, *BC Ministry of Energy*, *Mines and Petroleum Resources*, pages 157–175.

Ryan, B.D., and Dawson, F.M. (1994a): Coalbed methane desorption results from the Quinsam coal mine and coalbed methane resource of the Quinsam coalfield, British Columbia, Canada (92F/13,14); *in* Geological Fieldwork 1993, Grant, B. and Newell, J.M. (editors), *BC Ministry of Energy, Mines and Petroleum Resources*, Paper 1994-1, pages 215–224.

Ryan, B.D., and Dawson, F.M. (1994b): Coalbed methane canister desorption techniques; *in* Geological Fieldwork 1993, Grant, B. and Newell, J.M. (editors), *BC Ministry of Energy, Mines and Petroleum Resources*, Paper 1994-1, pages 245–256.

Ryan, B.D. (2002): A note on desorption results of Comox Formation coals, Courtenay area, Vancouver Island, British Columbia; *BC Ministry of Energy, Mines and Petroleum Resources,* Geological Fieldwork 2001, paper 2002-1, pages 63–73.

Ryan, B.D. (1997): Coalbed methane in the Comox Formation, Tsable River Area, Vancouver Island; *BC Ministry of Energy, Mines* and Petroleum Resources, Paper 1997-1, pages 353–364.

Ryan, B.D. (1992): An equation for estimation of maximum coalbed methane resource potential; *BC Ministry of Energy, Mines and Petroleum Resources*, Geological Fieldwork 1991, Paper 1992-1, pages 393–396.

Toth, J. (1972): Properties and manifestations of regional groundwater movement; Proceedings of the 24th International Geological Congress, Montreal, Section 2, pages 153–163.

McCulloch, C.M., Levine, R.J., Kissel, F.N., and Deul, M. (1975): Measuring the methane content of bituminous coalbeds; *United States Department of the Interior,* Report of Investigations 8043.

GEOCHEMISTRY OF THE FRACTURE-FILLING DOLOMITE AND CALCITE CEMENTS IN MIDDLE DEVONIAN DUNEDIN FORMATION: IMPLICATION FOR THE STRATA DOLOMITIZATION MODEL.

Sze-Shan Yip[1], Hairuo Qing[1] and Osman Salad Hersi[1]

ABSTRACT

Coarsely crystalline saddle dolomite and blocky calcite cements in the dolomitized reservoir of the Dunedin and Stone formations of northeast British Columbia have been studied over the last two decades. Vitrinite reflectance study, and isotopic composition and fluid inclusion geochemical analyzes supported that these two crystalline phases were precipitated during the Latest Devonian to Early Carboniferous from modified Devonian seawater. Coarsely crystalline saddle dolomite has been interpreted to be the product of hydrothermal dolomitization. Hydrothermal dolomitization and secondary porosity creation are therefore interpreted to have occurred during the Latest Devonian to Early Carboniferous.

Recent core investigation identified three sets of fractures within the strata that cross-cut the two coarsely crystalline cement phases. These fractures are filled with dolomite, filled with calcite and remaining open. Geochemical analyzes have shown similarities between coarsely crystalline saddle dolomite and fracture-filling dolomite. Similarities were also found between coarsely crystalline calcite and fracture-filling calcite. Petrological observation and geochemical analytical results suggest the fracturing-filling dolomite was precipitated at the same time as or immediately after its void-filling, coarsely crystalline saddle dolomite counterpart, and that fracture-filling calcite was precipitated at the same time as or immediately after its void-filling, coarsely crystalline blocky calcite counterpart. High dip angles measured from both dolomiteand calcite- filled fractures indicate that the dominant compression direction was from top to bottom. These findings help to put an additional and essential time constraint on the relative timing of hydrothermal dolomitization.

Yip, S., Qing, H. and Hersi, O. S. (2009): Geochemistry of the fracture-filling dolomite and calcite cements in Middle Devonian Dunedin Formation: Implication for the strata dolomitization model.; Geoscience Reports 2009, *BC Ministry of Energy, Mines and Petroleum Resources,* pages 89–95.

[1]Department of Geology, University of Regina. Regina, Saskatchewan S4S 0A2, Canada

INTRODUCTION

The Middle Devonian carbonate play type has upwards of 2.35 trillion cubic feet (Tcf) of remaining undiscovered gas in place within northeastern British Columbia (National Energy Board 2000). Investigating the sedimentology, diagenetic evolution, fractures, and geochemical and fluid inclusion attributes of the strata provides a renewed opportunity for expanding our knowledge of the dolomite reservoirs in northeastern British Columbia. Coarsely crystalline saddle dolomite, calcite, and cemented-filled fractures in the Middle Devonian Stone and Dunedin formations are the focus of this study (Figures 1 and 2).

GEOLOGICAL MODEL AND PROBLEMS

A development model for dolomite reservoirs in the study area has been proposed by Morrow et al. (1990). Maturation of organic-rich Devonian Besa River shale occurred during the Late Paleozoic to Early Mesozoic. Hydrocarbons were expelled and migrated laterally and downward into the permeable dolomitized strata. Intense deformation during the Tertiary Laramide orogeny has resulted in further fracturing and additional permeability development; anticlinal folding and thrust faulting also occurred during that time. Fluid inclusion microthermometric analysis by Aulstead (1987) showed that the homogenization temperatures of primary inclusions in saddle dolomite are between 150 and 215 °C with a mean of around 185 °C, which corresponds to the geothermal temperature during the Late Devonian to Carboniferous in southernmost Yukon (adjacent to 94N map area; Morrow and Aulstead 1995). Fractures that are filled with dolomite cement were found by Davies and Smith (2006). The fractures were interpreted to be shear microfractures.

Collaborative diagenesis studies on the Stone and Dunedin formations between the British Columbia Ministry of Energy, Mines and Petroleum Resources (MEMPR) and the University of Regina were initiated in 2007. Nineteen diagenetic phases have been identified from core and petrological investigation (Figure 3). Core investigation in Janu-

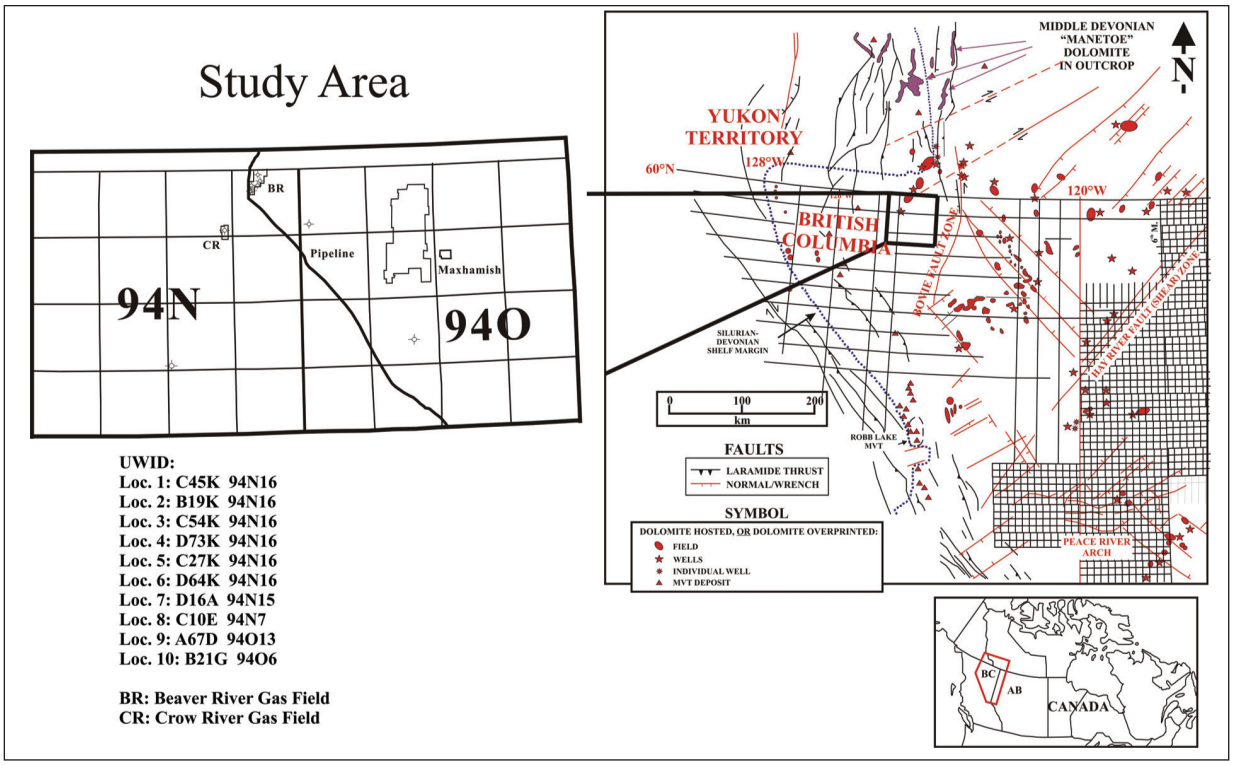

Figure 1. Geographic map of northeast British Columbia and the study area and list of studied wells.Geographic map modified from Davies and Smith (2006).

SYSTEM	SERIES/STAGE		SOUTHERN YUKON	94O SUB-SURFACE	94K SUB-SURFACE	94B SURFACE AND SUB-SURFACE
DEVONIAN	UPPER FAMENNIAN					
	UPPER FRASNIAN		Besa River Shale	Besa River Shale	Muskwa	Besa River Shale
					Besa River Shale	
	MIDDLE GIVETIAN				Waterways	
					Slave Point	Slave Point
					Watt Mountain	Watt Mountain
					Muskeg	
	MIDDLE EIFELIAN		Nahanni / Dunedin	Dunedin	Keg River / U. Chinchaga	Keg River
					Detrital Break	
			Arnica	Stone	L. Chinchaga	Stone
	LOWER EMSIAN	DALJEAN	Detrital Break			
		ZLICHOVIA				
	LOWER SIEGENIAN	PRAGIAN				
	GEDINNIAN	LOCHOVIAN	Muncho-McConnell	Muncho-McConnell	Muncho-McConnell	Muncho-McConnell

Figure. 2. Stratigraphic chart of the Middle Devonian strata in northeast British Columbia and adjacent Yukon subsurface (Modified from Nadjiwon 2001).

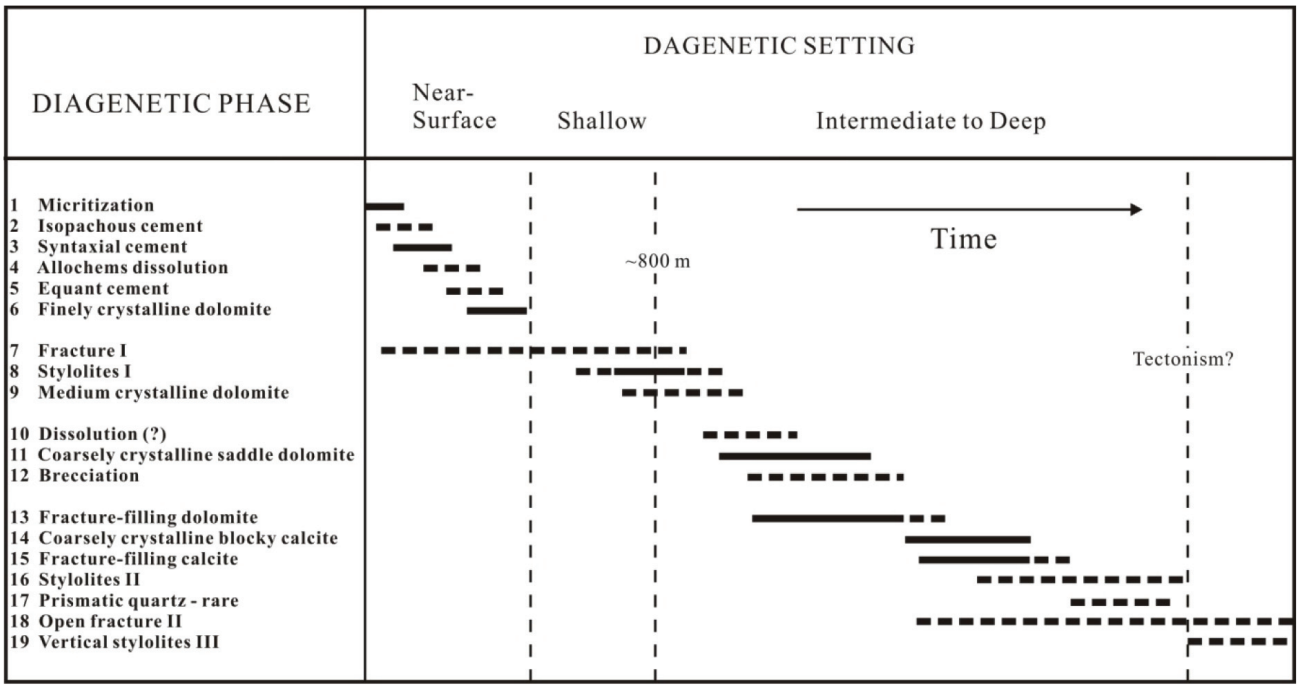

Figure 3. Summary of diagenetic paragenesis of the Middle Devonian Stone and Dunedin formations. Diagenetic phases were identified from petrological and petrographic investigation. They were record by their first appearance and cross-cutting relationship with other phases. Diagenetic phase 1 being the first phase that precipitated or formed immediately after sedimentation. Diagenetic phase 11 – Coarsely crystalline saddle dolomite, 13 – Fracture-filling dolomite, 14 – Coarsely crystalline blocky calcite, 15 – Fracture-filling calcite and 18 – Open fracture II are discussed in this report. Diagenetic phase 1 to 9 and other phases are described and interpreted in the first author's thesis-in-preparation.

ary 2009 has identified three sets of fractures in the strata (Figure 4). These fractures were found filled with dolomite, filled with calcite, or remaining open. Dolomite-filled fractures are suggested to have developed before coarsely crystalline saddle dolomite precipitation (Davies and Smith 2006). Calcite-filled fractures have not been reported in the literature. These fractures are crucial geological records in studying dolomitized carbonate reservoirs, because they are the diagenetic phases that directly cross-cut saddle dolomite. They provide important information on the fluid temperature and isotopic composition of the diagenetic fluid that flowed through the strata, in which pin down a time constraint on the relatively timing of dolomitization. As a result, stratal dolomitization models can further be refined.

RESULTS

Structure

Structural measurements of dolomite- and calcite-filled fractures were plotted in Figures 5 and 6. Dolomite-filled fractures show bimodal strike orientation towards east and west. Dip directions are oriented north and south. Dip angles are dominantly 60° to 90°. Calcite-filled fractures show diffused to bimodal strike orientation towards northeast and southwest. Dip directions are oriented northwest and southeast. Dip angles are predominantly from 50° to 90°. The core axis was assumed to be vertical because no record was available.

Oxygen and Carbon Isotopes

Stable oxygen and carbon isotope results are summarized in Table 1. $\delta^{18}O$ and $\delta^{13}C$ cross-plots are presented in Figure 7. Coarsely crystalline, nonplanar-e, saddle dolomites show oxygen isotope ratios from -10.01 to -16.63 ‰ V-PDB and carbon isotope ratios from -1.51 to -9.02 ‰ V-PDB. Medium crystalline, fracturing-filling dolomite shows oxygen isotope ratios from -9.09 to -14.28 ‰ V-PDB and carbon isotope ratios from +1.05 to -7.71 ‰ V-PDB. Coarsely crystalline, blocky calcites show oxygen isotope ratios from -9.80 to -15.50 ‰ V-PDB and carbon isotope ratios from -1.71 to -11.23 ‰ V-PDB. Medium crystalline, fracture-filling calcites show oxygen isotope ratios from -11.61 to -13.49 ‰ V-PDB and carbon isotope ratios from -1.74 to -10.63 ‰ V-PDB.

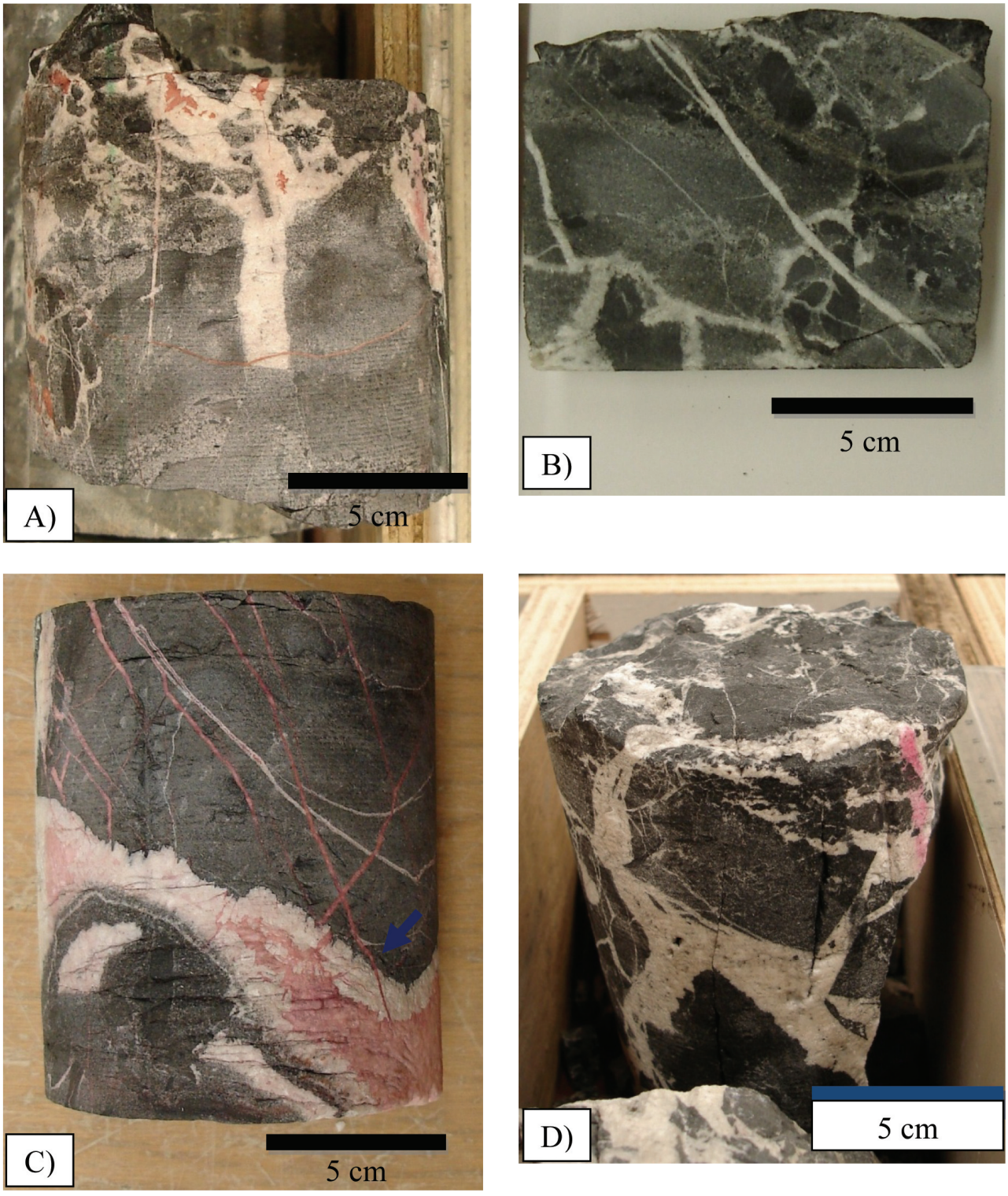

Figure 4. Core photos from D-16-A/94-N-15. A) Stained core photo showing the cross-cutting relationship between coarsely crystalline saddle dolomite, coarsely crystalline blocky calcite, dolomite-filled fracture, and calcite-filled fracture. 3798.0 m. B) Dolomite-filled fracture. 3810.9 m. C) Dolomite- and calcite-filled fractures as shown by Alizarin Red S staining. Notice calcite-filled fractures cut into saddle dolomite at the lower right corner (arrow). 3815.0 m. D) Open to partially open fracture post-dating coarsely crystalline saddle dolomite and blocky calcite. 3783.7 m.

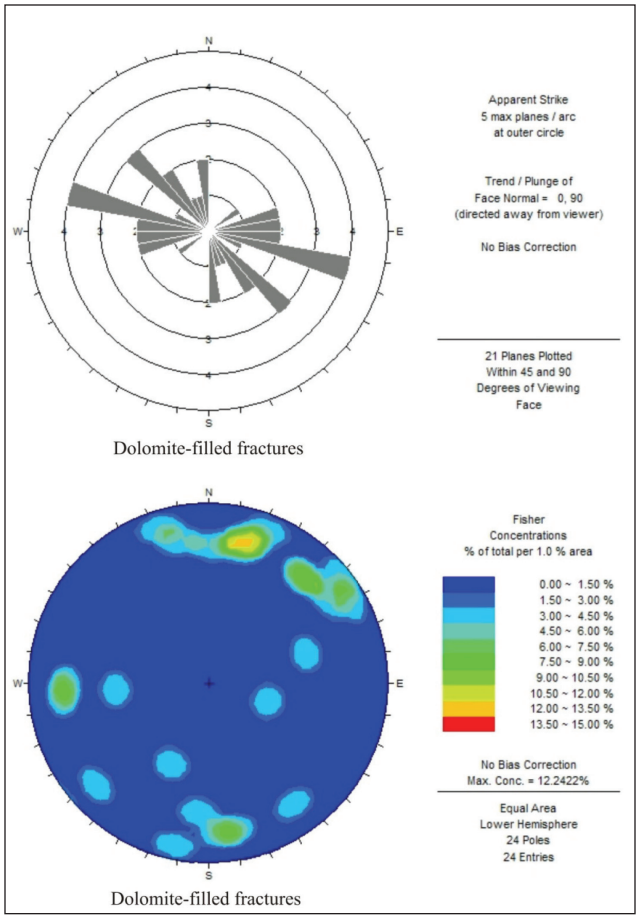

Figure 5. Structural data measured from well D-16-A/94-N-15, 3764.0 to 3818.0 m. Top: Strike orientation of dolomite-filled fractures. Bottom: Lower hemisphere stereoplots of structural data showing bimodal dipping directions towards SW and NE.

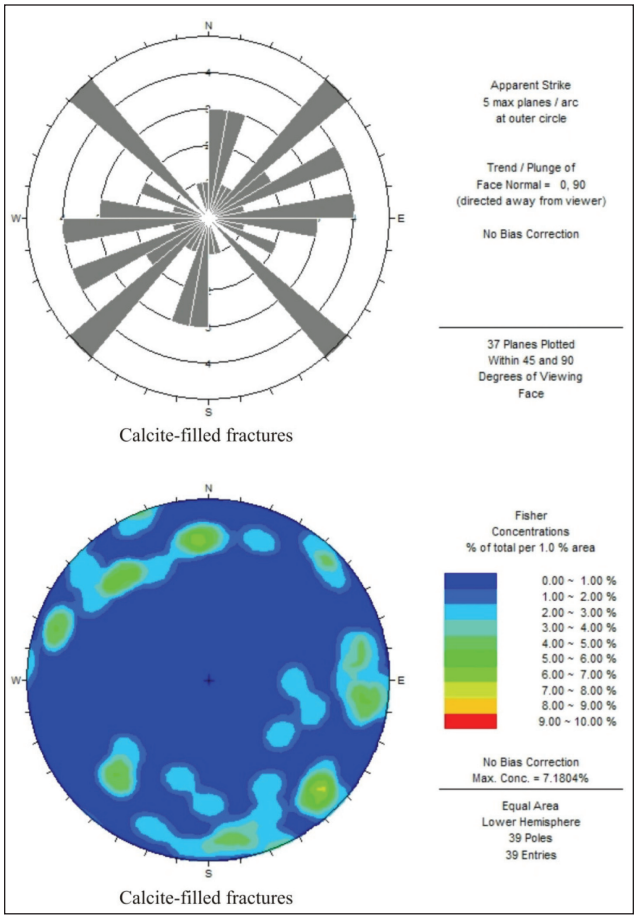

Figure 6. Structural data measured from well D-16-A/94-N-15, 3764.0 to 3818.0 m. Top: Strike orientation of calcite-filled fractures. Bottom: Lower hemisphere stereoplots of structural data showing bimodal dipping directions towards SE and NW.

TABLE 1. SUMMARY OF STABLE OXYGEN AND CARBON ISOTOPE ANALYTICAL RESULTS FOR SAMPLES FROM THE STONE AND DUNEDIN FORMATIONS.

Diagenetic Phase (Number of Samples)	$\delta^{18}O$ (Mean; ‰, V-PDB)	$\delta^{13}C$ (Mean; ‰, V-PDB)
Coarsely crystalline, nonplanar-e, saddle dolomite (n=13)	-12.47	-3.25
Medium crystalline, fracture-filling dolomite (n=19)	-11.54	-2.53
Coarsely crystalline, blocky calcite (n=10)	-13.26	-6.95
Medium crystalline, fracture-filling calcite (n=11)	-12.87	-6.58

Fluid Inclusion Microthermometry

Fluid inclusion microthermometric data of two samples collected from the Dunedin Formation in well D-16-A/94-N-15 are presented in Table 2. Homogenization temperatures (T_h) measured from coarsely crystalline saddle dolomite are from 191 to 228 °C (mean = 209 °C; n = 7); melting temperatures (T_m) are from -17.0 to -16.8 °C (mean = 16.9; n = 2). Homogenization temperatures measured from coarsely crystalline calcite are from 165 to 196 °C (mean = 186 °C; n = 19); melting temperatures are from -18.5 to -13.2 °C (mean = 16.0; n = 8). Homogenization temperatures measured from fracturing-filling dolomites are from 185 to 208 °C (mean = 199 °C; n = 21); melting temperatures are from -16.0 to -16.1 °C (mean = -16.1; n = 2). Homogenization temperatures measured from fracturing-filling calcites are from 176 to 195 °C (mean = 188 °C; n = 9); melting temperatures are from -20.8 to -15.1 °C (mean = -17.8; n = 5).

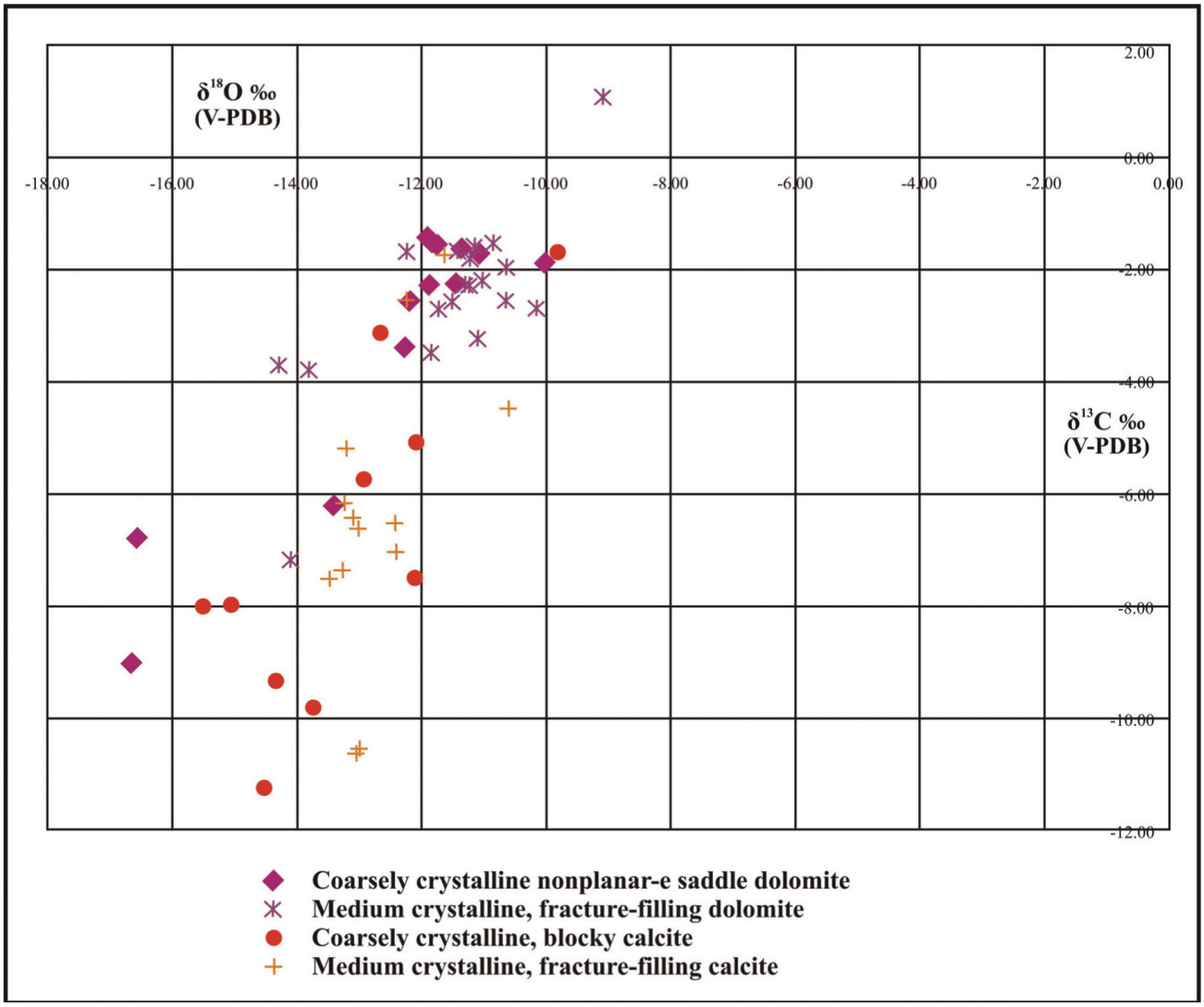

Figure 7. Oxygen and carbon isotope cross-plot for saddle dolomite, fracture-filling dolomite, blocky calcite, and fracture-filling calcite.

SUMMARY

This report summarizes the recent geochemical analysis of an ongoing graduate research project. Three sets of fractures have been identified. One fracture set is filled with dolomite, one fracture set is filled with calcite and one set is open. Coarsely crystalline saddle dolomite in the matrix is being compared with fracture-filling dolomite, and coarsely crystalline calcite in the matrix is being compared with fracture-filling calcite. Oxygen isotope analyses and fluid inclusion microthermometric studies have shown similarities between the coarsely crystalline saddle dolomite and the fracture-filling dolomite. Both phases are depleted in $\delta^{18}O$, and the majority of the values are from -10 to -13 ‰ V-PDB. Homogenization temperatures are predominantly from 195 to 205 °C. These indicate that the two dolomite phases were precipitated under similar conditions. Similarities were also found between the coarsely crystalline calcite and fracture-filling calcite. $\delta^{18}O$ analytical results of both phases are from -12 to -16 ‰ V-PDB (Figure 7). Homogenization temperatures are predominantly from 174 to 195 °C. These suggest that the two calcite phases were precipitated under similar conditions.

Petrological observation and geochemical analytical results suggest that 1) the fracture-filling dolomites were precipitated at the same time as or immediately after their void-filling, coarsely crystalline saddle dolomite counterparts; 2) fracture-filling calcites were precipitated at the same time as or immediately after their void-filling, coarsely crystalline calcite counterparts.

High dip angles (70° to 90°) measured from both dolomite- and calcite-filled fractures indicate that the dominant compression direction was from top to bottom. The preliminary interpretation is that these fractures were developed in deep burial settings. Ongoing fracture mapping will help to determine whether these fractures were developed by tectonic activity or by hydrostatic pressure during massive fluid flow (Davies and Smith 2006).

TABLE 2. SUMMARY OF FLUID INCLUSION MICROTHERMOMETRIC DATA FOR TWO SAMPLES FROM WELL D-16-A/94-N-15.

Well ID (Depth)	Diagenetic Phase	Occurrence (inclusions measured)	Size (μm)	Vapor (%)	Tm-first (range °C; n)	Tm-HH (range °C; n)	Tm-H_2O (range °C)	Tm-H_2O (mean °C; n)	Th-final (range °C)	Th-final (mean °C; n)
D16A 94N15 3764.3 m	Coarsely-crystalline saddle dolomite	Random (7)	1 – 3	5 – 7	-55 (1)	-25 (2)	-16.8 – -17.0	-16.9 (2)	191 – 228	209 (7)
D16A 94N15 3764.3 m	Coarsely-crystalline blocky calcite	Random (2)	3 – 5	5 – 6	-53 (1)	-23 (2)	-15.1 – -14.8	-15.0 (2)	188 – 191	190 (2)
		Random (1)	9	5	<-49 (1)	-24 (1)	-14.0	-14.0 (1)	196	196 (1)
		Cluster (5)	4 – 13	6 – 10	-	-25 (2)	-18.5 – -16.0	-17.5 (5)	188 – 199	193 (5)
		Random (2)	8 – 14	5 – 6	-	-22 (1)	-15.5 – -13.2	-14.4 (2)	186 – 191	189 (2)
		Random (3)	9 – 20	6	<-46 (1)	-23 (1)	-14.8 – -14.5	-14.7 (3)	165 – 166	166 (3)
		Random (3)	5 – 6	6	-52 (1)	-23 (1)	-16.3 – -15.3	-15.8 (3)	174 – 193	182 (3)
		Random (3)	4 – 9	5 – 6	<-46 (1)	-23 (2)	-18.5 – -18.2	-18.4 (2)	184 – 194	188 (3)
D16A 94N15 3816.8 m	Fracture-filling dolomite	Random (3)	2 – 3	5	-56 (1)	-25 (1)	-16.0	-16.0 (1)	202 – 207	205 (3)
		Random (2)	2	5	-	-	-	-	206 – 208	207 (2)
		Random (3)	2	5	-	-	-16.1	-16.1 (1)	197 – 198	198 (3)
		Random (7)	2 – 4	5	-55 (3)	-24 (1)	-	-	185 – 212	200 (7)
		Random (3)	2 – 3	5 – 6	-	-	-	-	186 – 194	189 (3)
		Cluster (3)	3 – 4	5 – 6	-56 (1)	-26 (2)	-	-	194 – 204	197 (3)
D16A 94N15 3816.8 m	Fracture-filling calcite	Random (1)	10	5	-53 (1)	-24 (1)	-17.3	-17.3 (1)	187	187 (1)
		Random (1)	4	5	-54 (1)	-25 (1)	-20.8	-20.8 (1)	179	179 (1)
		Random (2)	6	5	-53 (1)	-24 (1)	-19.3	-19.3 (1)	193 – 195	194 (2)
		Random (1)	5	6	-53 (1)	-24 (1)	-16.3	-16.3 (1)	176	176 (1)
		Random (2)	5	6	-53 (1)	-24 (2)	-15.1	-15.1 (1)	191 – 193	192 (2)
		Random (1)	7	6	-52 (1)	-23 (1)	-	-	189	189 (1)
		Random (1)	7	6	-	-23 (1)	-16.6	-16.6 (1)	192	192 (1)

Tm-first: first (antarcticite) melting temperature (observed antarcticite melting temperature).
Tm-HH: hydrohalite melting temperature (observed hydrohalite melting temperature).
Tm-H_2O: ice melting temperature (observed ice melting temperature).
Th-final: final homogenization temperature (from liquid + vapor → liquid)

REFERENCES:

Aulstead, K.L. (1987): Origin and diagenesis of the manetoe facies, southern Yukon and Northwest Territories, Canada; Unpublished M.Sc. thesis, University of Calgary, 143 pages.

Davies, G., and Smith, L.B. (2006): Structurally controlled hydrothermal dolomite reservoir facies: an overview; American Association of Petroleum Geologist Bulletin, Volume 90, pages 1641–1690.

Morrow, D.W., and Aulstead, K.L. (1995): The Manetoe dolomite—a Cretaceous-Tertiary or a Paleozoic event? Fluid inclusion and isotopic evidence; Bulletin of Canadian Petroleum Geology, Volume 43, pages 267–280.

Morrow, D.W., Cumming, G.L., and Aulstead, K.L. (1990): The gas-bearing Devonian Manetoe facies, Yukon and Northwest Territories; Geological Survey of Canada Bulletin, Volume 400, 54 pages.

Nadjiwon, L.M. (2001): Facies analysis, diagenesis and correlation of the middle Devonian Dunedin and Keg River formations, northeastern British Columbia; Unpublished M.Sc. thesis, University of Waterloo, 167 pages.

National Energy Board (2000): Northeast British Columbia natural gas resource assessment 1992–1997; Calgary: National Energy Board. Cat. No. NE23-85/2000E. 10 pages.

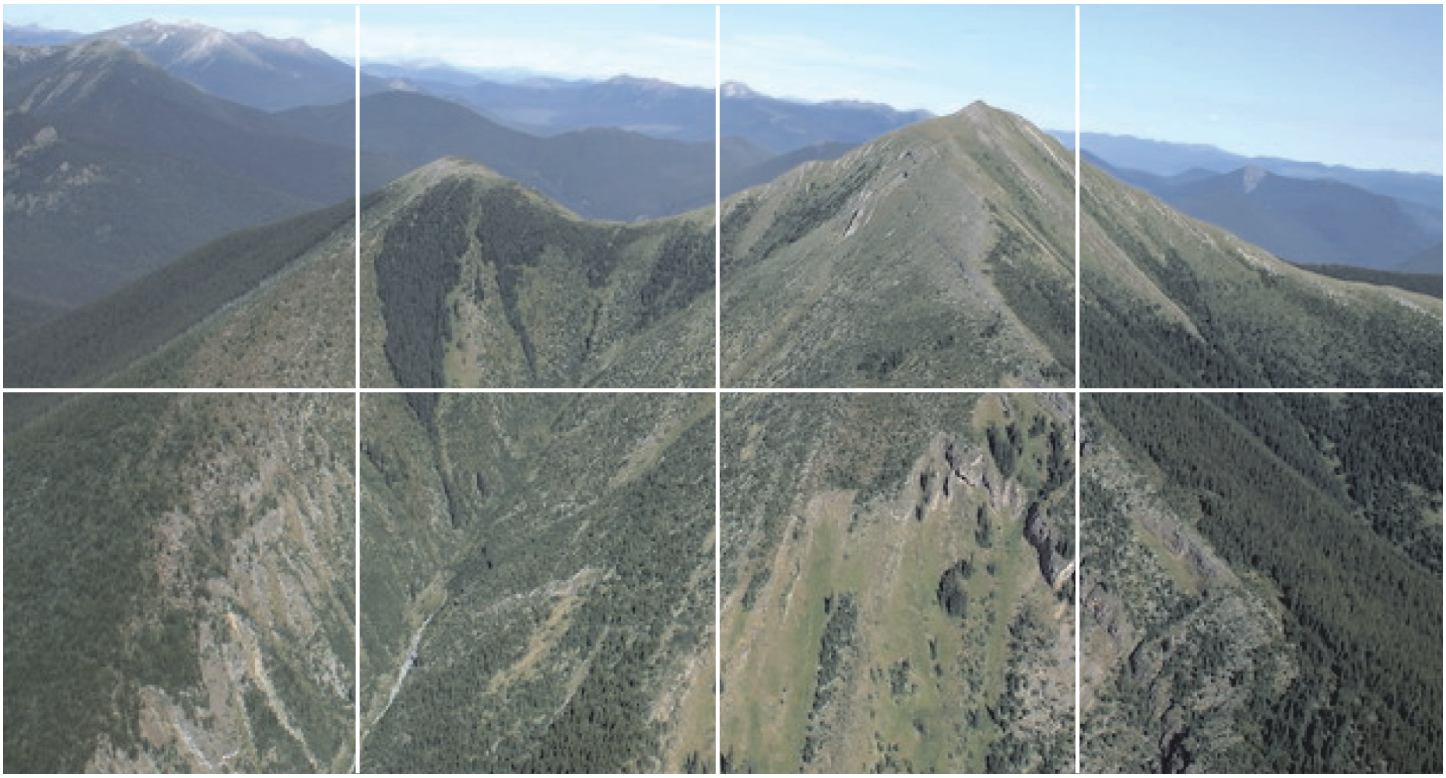

BRITISH COLUMBIA
The Best Place on Earth